The Mcm2-7 complex is the eukaryotic replicative helicase.

by

Matthew L. Bochman

Bachelor of Science, Juniata College, 2003

Submitted to the Graduate Faculty of

Arts and Sciences in partial fulfillment

of the requirements for the degree of

Doctor of Philosophy

University of Pittsburgh

2008

UNIVERSITY OF PITTSBURGH

ARTS AND SCIENCES

This dissertation was presented

by

Matthew L. Bochman

It was defended on

September 4, 2008

and approved by

Karen Arndt, PhD, Associate Professor, Biological Sciences

Jeffrey Brodsky, PhD, Professor, Avinoff Chair of Biological Sciences, Biological Sciences

Linda Jen-Jacobson, PhD, Professor, Biological Sciences

Sanford Leuba, PhD, Assistant Professor, Cell Biology & Physiology

Michael Trakselis, PhD, Assistant Professor, Chemistry

Dissertation Advisor: Anthony Schwacha, PhD, Assistant Professor, Biological Sciences

The Mcm2-7 complex is the eukaryotic replicative helicase.

Matthew L. Bochman, PhD

University of Pittsburgh, 2008

Replicative helicases are essential enzymes in DNA replication that separate duplex DNA into single strands to be used as templates by polymerases. The identity of these helicases in prokaryotes and viruses has been known for some time, but there is controversy in defining the eukaryotic replicative helicase. Fifteen years of *in vivo* work and comparison to other helicases suggests that the minichromosome maintenance proteins two through seven (Mcm2-7 complex) play this role, but *in vitro* DNA unwinding has never been demonstrated. In order to address this dilemma, I analyzed the biochemical activities of the *Saccharomyces cerevisiae* Mcm2-7 complex and the contributions of its conserved ATPase motifs to these activities. My findings indicate that Mcm2-7: 1) binds single-stranded DNA with high affinity in an ATP-dependent manner, 2) has six distinct active sites that differentially contribute to its biochemistry, and 3) is sensitive to anionic conditions *in vitro*. Elucidation of these characteristics led to the discovery that Mcm2-7 helicase activity is stimulated by large anions, and I was able to demonstrate *bona fide in vitro* DNA unwinding for the first time. The culmination of this work is the view that the Mcm2-7 complex is the true eukaryotic replicative helicase and the emerging view that Mcm2-7 ATPase active sites have evolved specialized functions within the complex.

TABLE OF CONTENTS

LIST OF TABLES

LIST OF FIGURES

PREFACE

In the Disney cartoon "DuckTales," Scrooge McDuck amasses his vast fortune by following advice given to him by his father, "Scrooge my boy…you have to learn to work smarter, not harder." When I heard that for the first time in 1988, it seemed like a good idea to me, and that maxim served me well all the way through college. Unfortunately, sage wisdom from cartoons can only take you so far. When I showed up for grad school at Pitt, it quickly became obvious that everyone here was smarter than me, so "working smarter" just wasn't going to cut it anymore. That only left me with one option – try working harder.

By working in a place of great thinkers and great experimentalists, trying to keep pace with everyone here has pushed me to be my best, and I want to thank everyone for that simple fact. It hasn't been a one-man battle though; I've had plenty of help along the way:

Obviously, Tony Schwacha deserves a lot of credit for shaping me into the biologist that I've become. Carl Sagan once wrote something along the lines of "grad students are like gunslingers, you never know when one is going to challenge you for fastest gun in the west." Well, there's no doubt about it – Tony is still the fastest gun in 560 Crawford…at least after he's had his coffee. He's got an undeniably keen mind, a unique perspective, and he attacks scientific problems by unconventional means. If even a little of that has managed to rub off on me, I'll

count myself lucky. Aside from being the master of the Mcm ATPase assay, Tony also manages to attract good people to the lab, and it has been my pleasure to work with all of them.

I really need to thank my committee (and various past and present members of their labs) for everything they've helped me with over the years: Karen Arndt (Peggy Shirra, Maggie Braun, Marcie Warner, and Dan Sheidy to name a few); Jeff Brodsky (Mike Morrow, Jen Goeckeler, Sheara Fewell, Craig Scott, Nancy Kaufmann, Christine Wright, and Shruthi Vembar); Linda Jen-Jacobson (Lisa Engler, Paul Sapienza, and Steve Hancock); Sanford Leuba; and Michael Trakselis.

I've got to thank plenty of other people in the Department too. While she was here, Susan Gilbert took me under her wing and was a great help with my early work. Bob Duda, James Conway, and Tom Harper taught me everything I know about electron microscopy, and Bob is always ready to help with just about everything else. Craig Peebles has freely given me advice, experimental ideas, reagents, and bits of equipment on numerous occasions. I also need to acknowledge the Hatfull, Hendrix, Oke, and Pipas Labs for use of equipment and reagents over the past half decade.

I should probably take the time to thank my parents now before my mom throws a fit for not being mentioned sooner. She was pretty disappointed when I didn't include her in the acknowledgements section of any of my papers, especially after I told her that she couldn't be a co-author either. So here you go mom, you get top billing after all the scientists! Many thanks to my dad as well for keeping me humble, donating rhubarb for pies, and only asking, "How much is this going to cost me?" after I told him I wanted to go to grad school. As for the rest of the family, thanks for everything!

I'd like to thank my friends, many of whom have been mentioned above for helping me with science and the rest who have shown up as guest stars on the Dr. Yeti blog. That second list includes, but isn't limited to, Amanda, Parry, Mala, Jared, Dave Hayes, and the Brothers Brown. If I've missed anyone, please forgive me; I'll owe you a beer.

Last but not least, I want to thank Julia. She's had to endure my shenanigans more than anyone else in recent years, and I apologize for doing all the things that make her brain want to explode. She's been my friend, fishing partner, pie maker, paper reviewer, camping buddy, and better half for a long time already and hopefully a long time to come. I like to say that she's my better two-thirds because I think she picks up more than half of my slack, but then she thinks I'm calling her fat…

Enough of my ramblings; let's get on with the show!

1.0 INTRODUCTION

The replicative helicase is the major molecular motor in a DNA replication fork that not only helps propel the replication machinery along a chromosome, but is often a key target of regulation and a linchpin for the assembly and stability of a large number of accessory replication factors. Although the replicative helicase is reasonably well understood in many bacterial and viral systems, the identity and mechanism of the eukaryotic replicative helicase, the Mcm2-7 complex, has proven to be a complex and controversial journey. This introduction compares Mcm2-7 to the better-studied prokaryotic DnaB helicase (with additional insights gleaned from bacteriophages and mammalian viruses), and reviews the biochemistry of the related Mcm467 subcomplex and archaeal MCM complex.

1.1 REPLICATIVE HELICASES

1.1.1 The function of the replicative helicase

As first noted by Watson and Crick [1, 2], the replication of a DNA double helix likely occurs by dissociation of its duplex structure into component single strands, which then serve as templates for the assembly of new and complementary strands. A direct prediction of this model would be that an enzyme, later termed DNA polymerase [3], would function to assemble the necessary

precursor dNTPs into the complementary sequence. As rapidly became clear through both the study of *Escherichia coli* DNA polymerase by the Kornberg lab (reviewed in [4]), as well as the subsequent study of a wide variety of DNA polymerases from diverse sources [5, 6], replicative DNA polymerases lack the ability to dissociate double-stranded DNA (dsDNA) into single strand templates. Some polymerases that primarily serve to repair DNA damage solve this problem by using an attached 5'–>3' exonuclease to degrade the non-template strand (originally described for *E. coli* Pol I, [7]; reviewed in [8]). However, DNA polymerases that specialize in the replication of a duplex genome usually require a specialized molecular motor that uses NTP hydrolysis to separate the DNA double helix into single-stranded DNA (ssDNA), which is a suitable template for DNA replication. These molecular motors are known as replicative helicases.

1.1.2 *E. coli* DnaB, the paradigm of a replicative homohexameric helicase

Genetic analyses of DNA replication in *E. coli* lead to the identification of *dnaB*, the gene later shown to encode the replicative helicase. These genetic screens were conducted to isolate conditional mutations that would block the incorporation of toxic nucleotide analogs into genomic DNA and led to the identification of a variety of accessory factors in DNA replication (reviewed in [4]). Subsequent analyses of these mutants allowed them to be grouped into one of two classes: 1) mutants that immediately blocked DNA replication when shifted to non-permissive conditions (fast stop mutants) 2) mutants that when shifted to non-permissive conditions would finish the current cycle of DNA replication, but were unable to begin a new round of replication (slow stop mutants). Additional analysis demonstrated that fast stop mutants were specifically defective in replication fork progression (elongation), while slow stop mutants

were specifically defective in starting new DNA replication (initiation). The *dnaB* gene proved unique in this analysis, since both a slow stop and a fast stop phenotype are demonstrated by different alleles of this gene [9], indicating an essential role of DnaB in both the initiation and elongation phases of DNA replication.

The biochemical demonstration that DnaB has ATP-dependent DNA unwinding activity fundamentally explained its function [10-12]. However, the subsequent ability to reconstitute both the initiation and elongation reactions biochemically from purified components has provided a wealth of mechanistic information concerning the role of DnaB and its partners [13]. In prokaryotes, initiation involves the loading of the replicative helicase at specific DNA sequences called origins; this requires prior loading of a specific protein to the origin called the initiator protein (DnaA in *E. coli*). It is believed that DnaA uses ATP binding and hydrolysis to locally unwind the dsDNA at the origins [14], likely by polymerizing into a helical filament that opens the DNA by locally generating negative super coiling [15]. The replicative helicase is then loaded by a molecular matchmaker (DnaC in *E. coli*) that uses nucleotide binding and hydrolysis to open the toroidal DnaB structure to allow passage of ssDNA into the central channel of the helicase (reviewed in [16]). Localized DNA unwinding by the replicative helicase promotes the self-assembly of additional replication factors which culminates in the loading of the DNA polymerase. Thus, the limiting step in prokaryotic replication is the loading of the replicative helicase at origins, a process controlled in multiple ways by regulating the expression, activity, and origin accessibility of DnaA [13].

1.1.2.1 Helicases as part of the replication fork

The relationship between DnaB and the rest of the replication fork has been illuminated by the isolation and study of a macromolecular assembly called the DNA polymerase III holoenzyme

(reviewed in [17]). This complex not only contains two (possibly three [18]) molecules of DNA polymerase, (one for both lagging and leading strand synthesis) but also a factor that keeps the polymerase from falling off of the DNA (the beta clamp), a protein complex that reversibly loads the clamp onto DNA (gamma complex), a protein that coordinates the two polymerases (tau), a special RNA polymerase that functions to generate primers for use by DNA polymerase (primase), and the replicative helicase. In this complex, DnaB is physically involved in keeping the leading and lagging strand polymerases together. In addition, both the replicative helicase and DNA polymerase work synergistically to translocate the holoenzyme along DNA [19, 20]. The original studies on fork progression were largely unable to demonstrate if this synergy was due to the individual enzymatic activities of each component or if it was due to stabilizing interactions between the two proteins. However, recent work confirms that synergism is due to the activities of the polymerase and helicase [21], since this cooperativity can be observed in a heterologous system (phage T4 polymerase and T7 helicase) that likely precludes the possibility of protein-protein interactions.

1.1.2.2 Biochemical activities of DnaB

From the beginning, the *E. coli* DnaB helicase has been a very tractable biochemical system [13]. The ~52 kDa subunits exist as monomers in solution at low concentrations but form trimers as concentration increases [22]. Hexamers are formed in the presence of Mg^{+2} over a range of DnaB concentrations, and this hexameric oligomerization has been confirmed by a variety of techniques: sedimentation [22, 23]; cross-linking [23, 24]; electron microscopy [25-27]; and gel filtration [24]. Oddly, ring-shaped complexes with both three-fold and six-fold symmetry have been observed via EM [25, 26]. Although the x-ray crystal structure of *E. coli* DnaB has yet to be solved, structures of *Bacillus stearothermophilus* DnaB (unliganded and in complex with the

helicase binding domain of the DnaG primase; [28]), the bacteriophage SPP1 DnaB homologue G40P [29], and the N-terminal domain of *Mycobacterium tuberculosis* DnaB [30] have shed light on this discrepancy. These helicases have a unique double-layered ring structure in which the N-termini of the six subunits form a three-fold symmetric triangular "collar" sitting atop a six-fold symmetric hexagonal C-terminal base (Figure 1). The three-fold symmetry of the collar arises from the N-terminal domains of each subunit assuming one of two alternating conformations (*cis* and *trans*), relative to that subunit's C-terminal domain, around the ring. Although no atomic level structures exist for DnaB bound to nucleotide cofactors or DNA, sedimentation studies have shown that occupancy (apo, ATP, or ADP) of the ATPase active sites affects the global conformation of the hexamer, which in turn affects ssDNA binding affinity (see below; [31]).

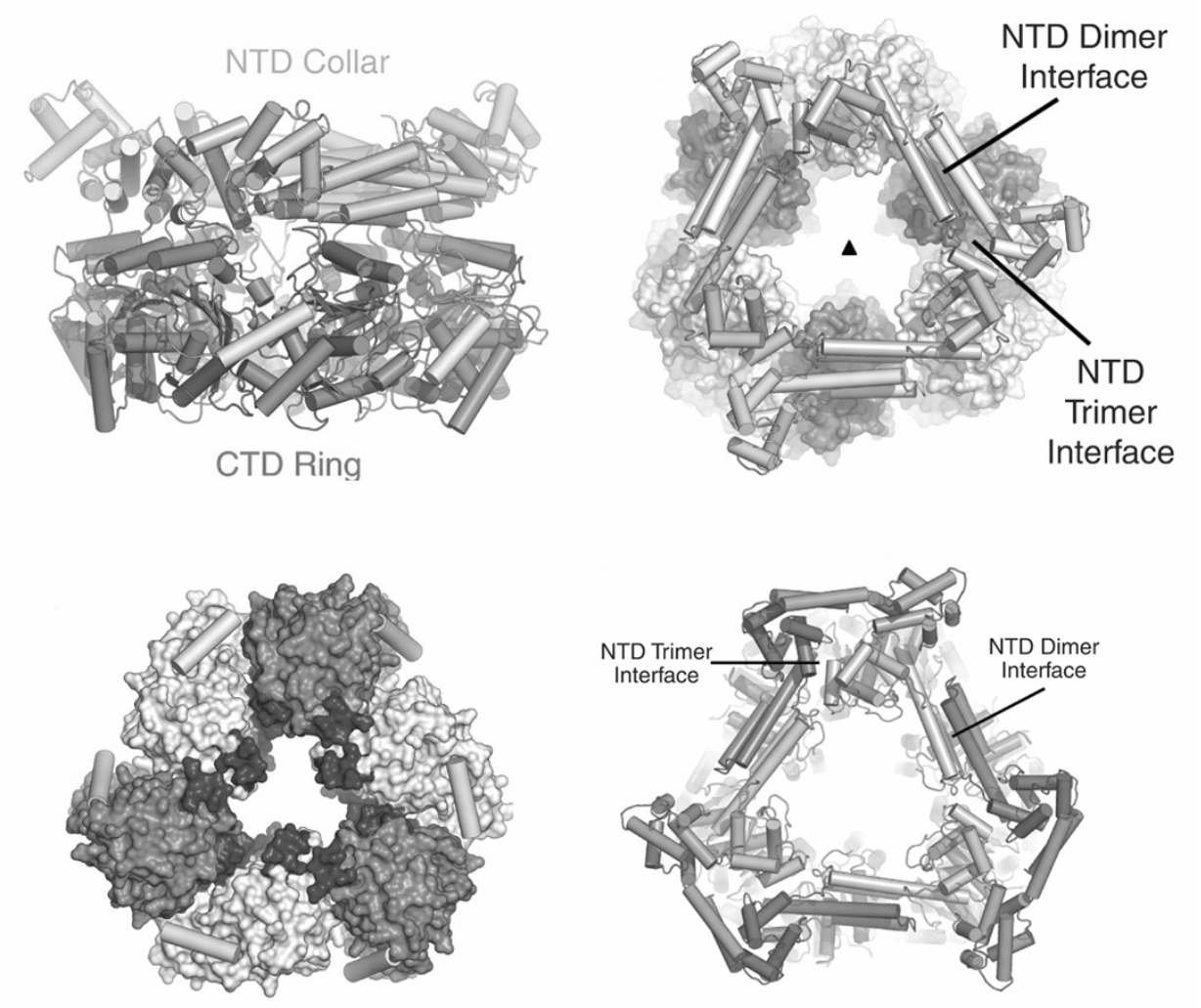

Figure 1. Crystal structure of the *B. stearothermophilus* DnaB.

The side (top left) and top (top right) views of *B. stearothermophilus* DnaB. The six-fold symmetric CTD ring (bottom left) and three-fold symmetric N-terminal collar (bottom right) are shown individually for clarity. These images are from [28]. Reprinted with permission from AAAS.

Sequence analysis of *E. coli* DnaB predicts that it contains an ATP/GTP binding domain [32, 33] in the central "β domain" [34] of the protein. As an NTPase, DnaB isn't as promiscuous as other hexameric helicases [35]. While ATP is generally considered the preferred substrate, CTP and GTP are just as effective as fuel for the helicase [10]. On the other hand, UTP, dATP, and ATP analogues are poorly hydrolyzed. The ATPase activity of DnaB can be stimulated (up to ~50-fold) by a wide variety of DNA substrates [11], and the C-terminal "γ domain" influences both this DNA-dependent stimulation and stimulation of the basal ATPase level of the protein [34]. Nucleotide binding by the hexamer was found to saturate with all six active sites filled, but there is heterogeneity in the binding [36]. The first three nucleotides are bound with high affinity, the subsequent three with low affinity, and there is negative cooperativity among the six binding sites. However, all six nucleotide binding sites do have ATPase activity [37]. Kinetic studies of nucleotide binding at the active sites indicated that binding occurs by a (minimally) four step process which most likely involves the formation of the DnaB/nucleotide complex followed by conformational changes in the active site itself and/or the entire hexamer [38].

Early work by Arai and Kornberg [11] demonstrated that DnaB possesses both ss- and dsDNA binding activity. As might be expected from the discussion of NTPase activity (above), NTPs stimulate the basal levels of DnaB/ssDNA binding ~2-fold, but dNTPs actually decrease the ability of the hexamers to bind ssDNA. Further stimulation of ssDNA binding (>6-fold over basal levels) was observed with the poorly hydrolyzable nucleotide analogues ATPγS and GTPγS. Although base composition of the ssDNA substrate does affect levels of binding, all probes tested had a minimum length requirement of 10 nt, and Mg^{+2} must be present for DnaB binding. Unlike ssDNA binding, dsDNA binding is not nucleotide-dependent and does not require Mg^{+2}.

Subsequent work on DnaB/ssDNA binding was exhaustively carried out by Bujalowski and colleagues. It was found that a single DnaB complex interacts with ~20 nt of ssDNA (40mers were bound by two DnaB hexamers) through a single site on one subunit in the hexamer [39, 40]. This was the first strong evidence that ssDNA was not extensively wound around the outside of the complex (*i.e.*, simultaneous binding by all six subunits) and suggested that it may pass through the central channel of the hexamer [39]. FRET was later used to demonstrate ssDNA passage through the center of the toroid [41]. Interestingly, ssDNA binding is salt-dependent, with anions probably being released by the protein upon formation of the ternary complex, and ssDNA binding causes extensive conformational changes in the hexamer [40]. An inherent preference for binding poly(dA) sequences was also observed.

The effect of ATPase active site occupancy was also revisited. It was found that in the apo-state, DnaB hexamers have a very low affinity for ssDNA ("closed" conformation); in the ATP-bound state (approximated by AMP-PNP in this case), the affinity toward ssDNA is increased by ~4 orders of magnitude ("tense" conformation); and in the ADP-bound state, DnaB assumes an intermediate ("relaxed") conformation with a ssDNA binding affinity ~3 orders of magnitude less than the tense state [42]. A stopped-flow kinetic study of ssDNA binding with DnaB complexes pre-formed in the tense state demonstrated that DnaB/ssDNA binding occurs minimally by a three step process (*i.e.*, initial binding followed by two conformational changes) with an association rate (10^4 $M^{-1}s^{-1}$; [43]), that is significantly lower than a diffusion controlled reaction (10^7-10^8 $M^{-1}s^{-1}$; [44]). Importantly, this study also indicated that ssDNA does not need to be threaded through the central channel of the DnaB hexamer because transient and local opening of the ring likely follows formation of the DnaB/ssDNA collision complex [43]. Many of these ssDNA binding characteristics, as well as the effect of other replication factors (*e.g.*,

single-stranded binding protein (SSB) and DnaC) on DnaB/ssDNA binding, have been independently verified by other groups using various techniques (*e.g.*, see [34]).

Finally, as the prototypical prokaryotic helicase, the ability of DnaB to translocate along [12] and unwind DNA has been extensively investigated [13]. *In vitro*, this activity requires a forked DNA substrate (with a preference for long ssDNA tails) and proceeds with a 5'–>3' polarity [10]. Further, as the sum of its biochemical properties (hexamerization, ATPase activity, and DNA binding), helicase activity should minimally require the DnaB domains that can hexamerize, hydrolyze ATP, and bind ssDNA (*i.e.*, the central β and C-terminal γ domains; [34]). It was found however, that the full length DnaB protein was necessary for DNA unwinding [34], underscoring the importance of the N-terminal α domain which forms the triangular collar in the aforementioned crystal structures [28-30].

When DnaB binds to DNA forks, there is a >6-fold preference for binding to the 5' arm than the 3' arm [10, 45, 46], consistent with its 5'–>3' directionality, but two hexamers binding in opposite orientations to both arms of a single probe have been observed [45, 46]. Binding to the 3' arm is not thermodynamically stable, and the structural necessity of that arm for DNA unwinding indicates that DnaB works via the steric exclusion model (Figure 2A). In fact, single turnover kinetics of unwinding seemed to indicate that the hexamer translocating in the 5'–>3' direction on the 5' arm of the fork transiently interacts with the 3' arm, perhaps using it as a kind of "fulcrum" to mechanistically aid the movement of the helicase on the opposite strand [47]. The kinetics of unwinding also revealed that only one base pair of dsDNA is unwound per ATP hydrolyzed [48]; this efficiency is typical of helicases as a whole [49]. The rate of unwinding at room temperature was quite fast (~300 bp/sec) and increased with both increasing temperature

[48] and decreasing stability of the duplex region of the fork (*i.e.*, G+C bp content) [47], but processivity of the isolated hexamer was only moderate [48].

Work by the O'Donnell lab expanded the known repertoire of DnaB's enzymatic activities [50]. It was found that the hexamer could accommodate dsDNA within its central channel and translocate along it. This translocation did not involve DNA unwinding and generated ample force to displace proteins that were tightly bound to the duplex DNA. Further, when a synthetic Holliday junction was used as the DNA probe, DnaB could encircle dsDNA and drive branch migration. As such, it was suggested that DnaB could be involved in removing protein roadblocks from chromosomes and in DNA recombination *in vivo* [50, 51]. The T7 helicase gp4 was also found to have branch migration activity [50], so it is unclear if the phage replicative helicase could also be involved in DNA recombination or if these are intrinsic biochemical activities of hexameric helicases only displayed under obligatorily synthetic *in vitro* conditions. Additional studies by Kaplan and O'Donnell demonstrated DnaB translocation along 3 strands of DNA (indicating that it could convert the invading strand of a D loop into a daughter lagging strand for DNA replication) and the ability of head-to-head hexamers to act as dsDNA pumps (Figure 2C) to unwind DNA [52].

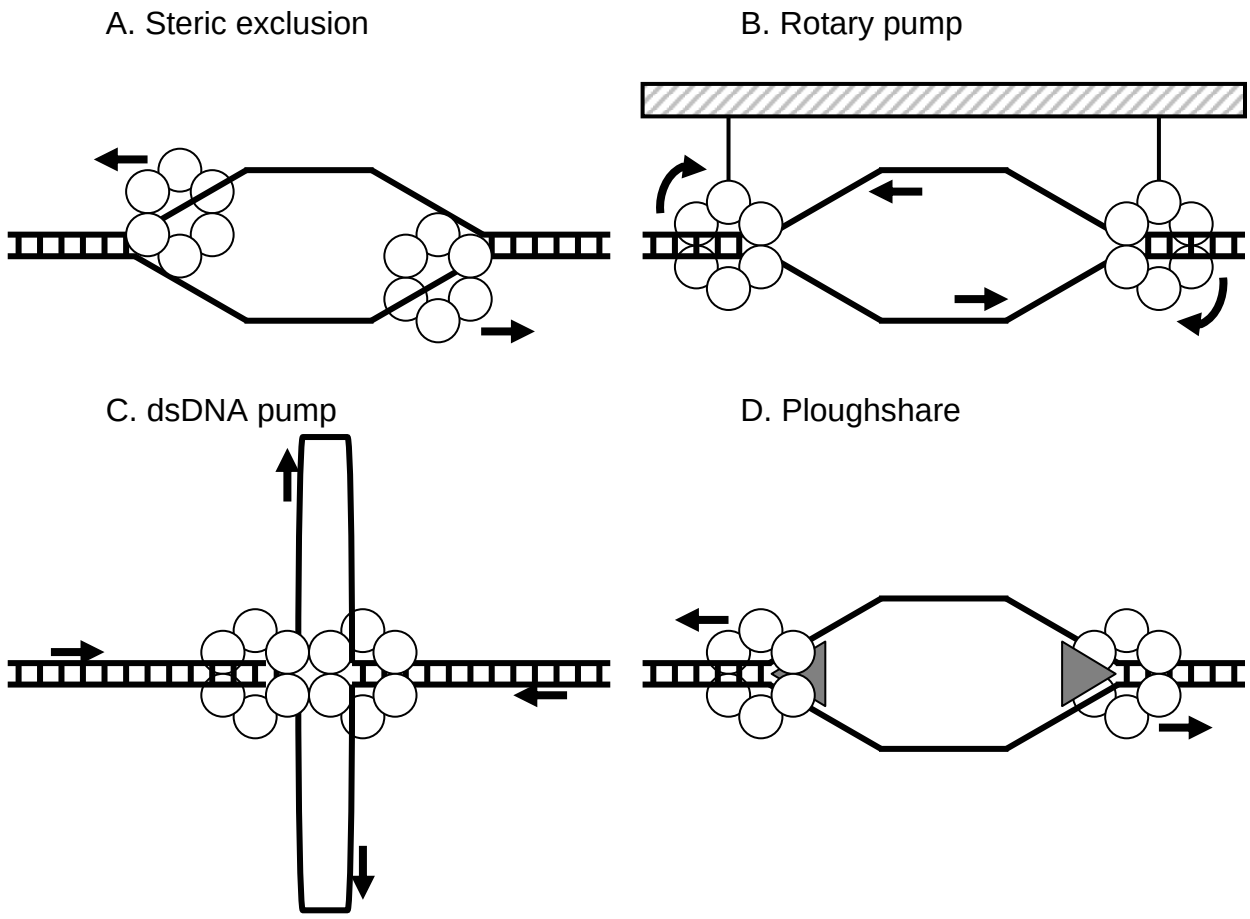

Figure 2. Putative models of helicase action.

This figure was adapted from [53]. A) In the steric exclusion model, the helicase encircles and translocates along one strand of ssDNA and unwinds the duplex DNA by exclusion of the other strand. B) In the rotary pump model, the helicases load at origins and translocate away from them where they are eventually anchored (to the hatched rectangle in this schematic). They then rotate in opposite directions causing the unwinding of the DNA double helix at the origin. C) In the dsDNA pump model, two helicases form a head-to-head complex and pump dsDNA towards the origin where it is extruded as single-strands. D) In the ploughshare model, the helicase encircles dsDNA, and, after local melting of the DNA duplex at the origin, "drags" a separate rigid protein (grey triangle) that acts as a wedge to separate the DNA strands. In A), the helicase is initially loaded onto ssDNA; in B-D) it is loaded onto dsDNA. Arrows indicate the direction of DNA and/or helicase movement.

1.1.3 Structural biology of hexameric helicases

More recently, structural investigation of DnaB [28-30] as well as several other replicative helicases (*e.g.*, [54, 55]) has provided insights about how these enzymes actually function (reviewed in [35]). All of these proteins are homohexameric toroids, with six ATP binding and hydrolysis sites formed at dimer interfaces with a central channel believed to encircle and bind ssDNA. The ATPase active sites are formed from catalytically essential amino acid residues from each dimer, with one dimer typically contributing canonical Walker A and B ATPase motifs, and the other subunit frequently providing a catalytically essential arginine [33]. In some helicases, the ATP binding sites are also required for hexamer oligomerization (*e.g.*, SV40 large T-antigen [56] and Bovine Papilloma Virus E1 protein [57]), whereas, in other helicases, nucleotide dependent oligomerization is not observed (*e.g.*, DnaB [28]). The distinction between these two types of oligomerization appears to correlate with the *in vivo* function of the helicase; helicases that require ATP for oligomerization tend to bind to and oligomerize around the DNA prior to initiation, whereas those the lack nucleotide-dependent polymerization tend to require an additional loading factor that likely is needed to transiently open the toroidal structure to facilitate DNA strand passage [16].

Helicases usually bind ssDNA in a nucleotide dependent manner. Though the internal surfaces of the central channel are often quite positively charged and likely contribute to DNA binding [35, 58, 59], a specific nucleotide-dependent DNA binding surface has been identified [55, 58]. A β sheet domain was found adjacent to the α helices that form the bulk of the ATPase domain. This β domain forms a hairpin (Figure 3), with positively charged residues at or near the tip that protrude into the central channel of the hexamer, and constitutes the main nucleotide

dependent DNA binding surfaces. Evidence suggests that nucleotide occupancy of the adjacent ATP binding domain is capable of causing significant conformational changes in the position of this hairpin (~17 Å in SV40 TAg; [54]). The simultaneous or sequential movement of such hairpins while interacting with DNA suggests possible mechanisms for helicase translocation and unwinding.

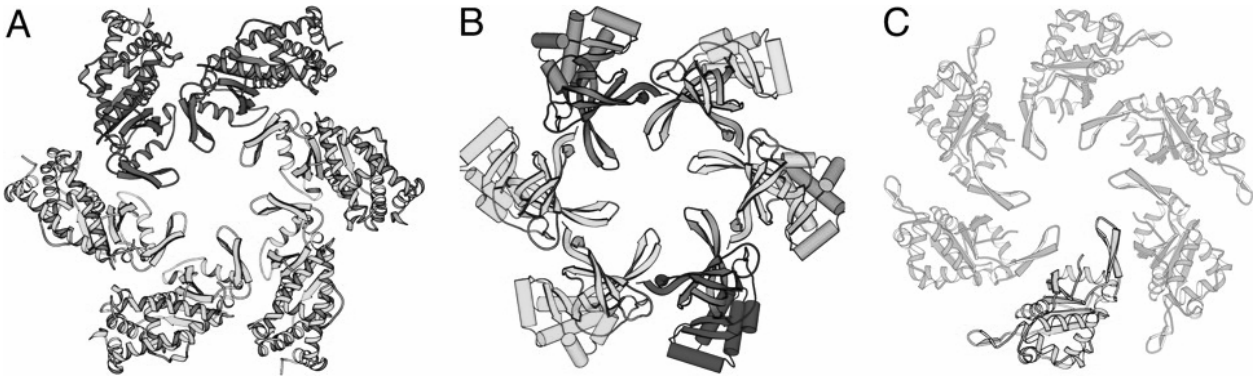

Figure 3. The β-hairpin fingers in the central channels of replicative helicases.

A) SV40 TAg [60]. B) Archaeal MCM [58]. C) Papilloma virus E1 [61]. This image is reprinted, with modifications, from [62] following the Rights and Permissions guidelines for *PNAS* as described (see: http://www.pnas.org/site/misc/rightperm.shtml#reprint).

1.1.4 How do hexameric helicases unwind DNA?

Since DNA unwinding is an inherently dynamic process, static crystal structures of helicases have not provided a reliable mechanism that explains the coupling between nucleotide binding/hydrolysis and DNA unwinding. Although several models are possible (Figure 2), biochemical evidence is largely consistent with a model that hexameric helicases unwind duplex DNA by binding one of the two strands within the central channel, while excluding the other (steric exclusion model, [63]). Translocation of the helicase along the bound strand displaces the unbound strand. Further, the directionality of this process suggests that nucleotide binding and hydrolysis within the complex are likely to be highly ordered and obligatorily coupled to translocation, possibly by virtue of the β-hairpin (Figure 3). On this point, structural information has yet to provide a consistent answer. In the cases in which the structure of co-crystals between hexameric helicases and nucleotides have been solved, a variety of nucleotide occupancies have been observed (reviewed in [35]), which has lead to very different models for the unwinding mechanism. With the T7 helicase, only a specific subset of active sites are populated with nucleotide at any given time [64, 65], leading to the suggestion that occupancy is based on a binding-change model predicting that nucleotide occupancy of one site alters the affinity of nucleotide at other sites within the hexamer. In contrast, the nucleotide occupancy of SV40 TAg is "all-or-nothing," suggesting simultaneous ATP binding and hydrolysis at all six sites [54]. This predicts an "iris-type" mechanism in which the diameter of the central channel changes based on the apo-, ADP-, and ATP-bound states. Finally, with the BPV E1 helicase, nucleotide binding also appears to differ between binding sites [55]. In this case, a ternary complex between the helicase, DNA, and nucleotide was analyzed, and a strong correlation was noted

between the occupancy of the active site (ATP, ADP, or empty) and the number of hydrogen bonds between the β hairpin of the respective subunit and DNA. While this elegant "staircase model" for helicase/DNA is appealing, its general applicability to other systems is unknown.

1.2 THE MCM PROTEINS

In sharp contrast to the prokaryotic and viral helicases discussed above, the identification and characterization of the eukaryotic replicative helicase, the Mcm2-7 complex, and its role in the replication fork is at a relatively early stage of study. Unlike any other known hexameric helicase, the eukaryotic helicase is a true heterohexamer formed from six unique subunits (historically numbered 2–>7, below). The Mcms are the focus of the remainder of this chapter.

1.2.1 Discovery of the Mcms

Unlike the case with *E. coli* [4], the use of genetics in eukaryotes to identify mutations that block incorporation of nucleotide precursors into DNA has not been successful; such mutations tend to represent specific defects in cell cycle regulation [66, 67]. Moreover, both *Saccharomyces cerevisiae* and *Schizosaccharomyces pombe*, the ideal eukaryotic genetic systems for such a screen, each lack the ability to incorporate exogenously added dNTP precursors (*e.g.*, they lack thymidine kinase) and an efficient means to transport them into the cell[a]. Instead, genes involved in DNA replication (specifically the *MCM* genes) were first identified by Bik Tye and

[a] These shortcomings have since been overcome; see (Vernis *et al*., 2003; Hodson *et al*., 2003).

her collaborators through the isolation of mutations specifically defective in plasmid segregation (also known as minichromosome maintenance, MCM) [68]. Of the original 16 complementation groups only *MCM2, 3, 5,* and *10* turned out to be replication factors (Mcm10p is not part of the replicative helicase but loads subsequent to it [69]); most of the rest have since been shown to correspond to genes required for chromosome segregation. The genes that would later become known as *MCM4* (originally *CDC54*) and *MCM7* (originally *CDC47*) were isolated as cell cycle division mutants [66, 67], while *MCM6* was originally isolated as *mis5* in *S. pombe* in the Yanagida lab [70]. To simplify the nomenclature, it was proposed by Julian Blow in 1996 to standardize the naming of these six genes as *MCM2* through *7* [71].

The deduction that these genes were directly involved in DNA replication was made by thorough work with both yeast and *Xenopus* systems. Hennessy and Botstein, who had isolated a tight cold-sensitive allele of *MCM4*, demonstrated a direct DNA replication defect at non-permissive conditions [67]. It was then shown that "replication licensing factor," a purified fraction from *Xenopus* egg extract that was needed for *in vitro* DNA replication, was in fact composed of the Mcm2-7 proteins [72].

Comparative bioinformatics of these genes from a variety of organisms demonstrated that they were paralogous with one another, and defined six unique gene families in all eukaryotes that have been examined (Figure 4) [73]. Through the subsequent availability of complete genomic sequences from all three kingdoms of life, it was shown that while prokaryotes lack *MCM* homologues, the archaea contain one (usually) or more MCM genes [74, 75]. Interestingly, sequence analysis has revealed that a *Bacillus cereus* prophage encodes a Mcm-like protein (that also has homology to eukaryotic primase) [76], and archaeal virus BJ1 which was found in a hypersaline lake in Inner Mongolia, China, encodes a hypothetical protein gp35

with homology to Mcm2 [see: http://www.ncbi.nlm.nih.gov/entrez/viewer.fcgi?val=CAL92457]. Further analysis has demonstrated that all Mcm proteins are AAA+ ATPases, a group that commonly forms toroidal hexamers with conserved Walker A, Walker B, and arginine finger ATPase motifs [33, 77]. Although no structural data concerning the Mcm ATPase active sites exists, the evolutionary relatedness of the Mcms to other AAA+ proteins predicts that the active sites are formed *in trans* with the Walker A and B motifs provided by one subunit and the arginine finger provided by the neighboring subunit [77, 78].

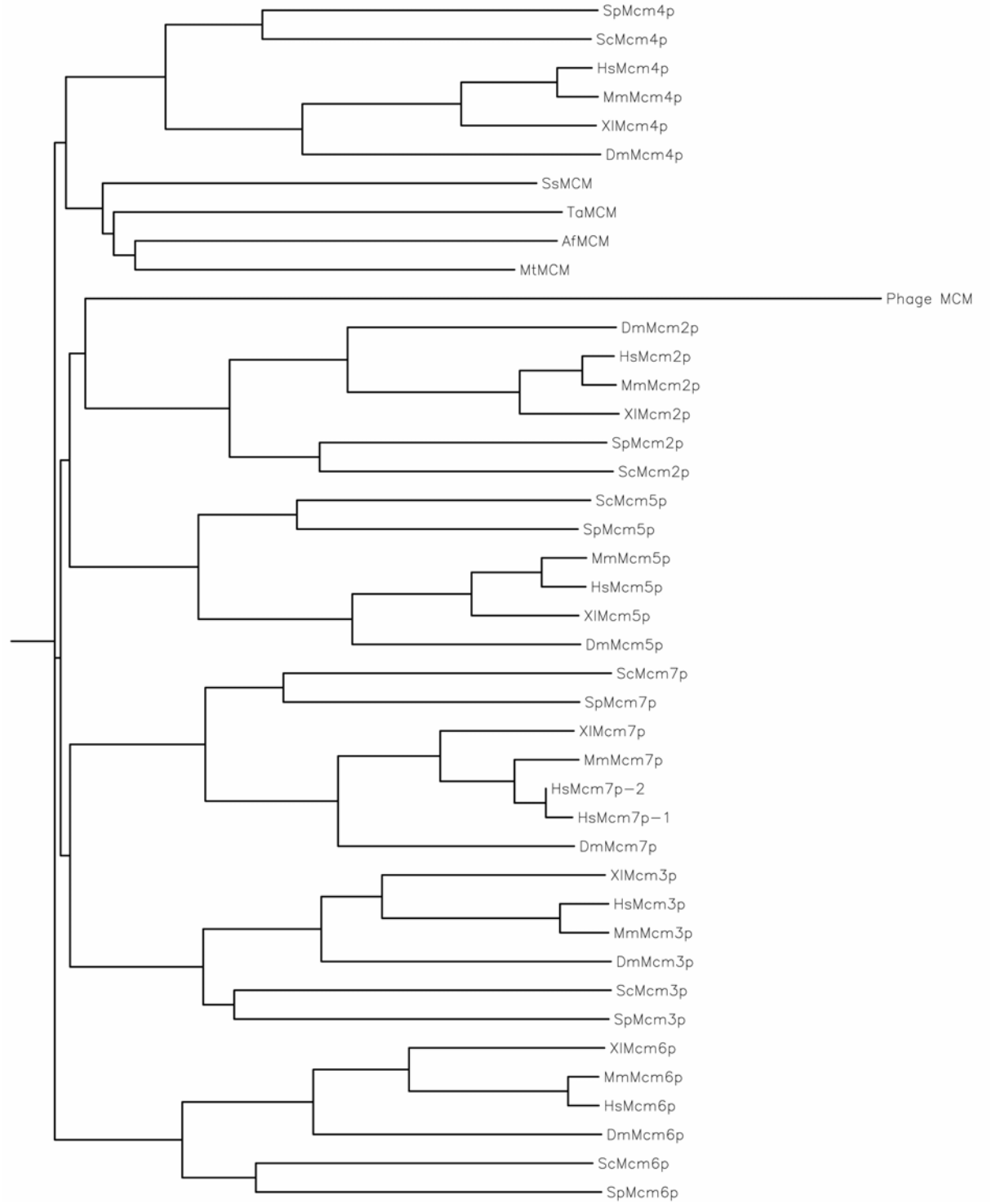

Figure 4. Phylogenetic tree of archaeal and eukaryotic Mcms.

The proteins were aligned using CLUSTALW [79], and the tree was generated using the Phylogeny Inference Package (http://seqtool.sdsc.edu/CGI/BW.cgi#!). Af, *Archaeoglobus fulgidus*; Dm, *Drosophila melanogaster*; Hs, *Homo sapiens*; Mm, *Mus musculus*; Mt, *Methanothermobacter thermoautotrophicus*; Phage; *Bacillus cereus* prophage [76]; Sc, *S. cerevisiae*; Sp, *S. pombe*; Ss, *Sulfolobus solfataricus*; Ta, *Thermoplasma acidophilum*; Xl; *Xenopus laevis*.

1.2.2 *In vivo* role of the Mcms in both the initiation and elongation phases of DNA replication

Unlike the case of prokaryotic DNA replication that can and does occur concurrently with cell division [13], in eukaryotes, DNA replication (S phase) and chromosome segregation (M phase) are mutually exclusive temporal events. However, even though the synthesis of new DNA only occurs in S phase, the process is - in some manner - set up in the preceding G1 phase (as hinted at through cell fusion experiments by Rao and Johnson [80-83]). The biochemical interpretation of these observations has since been worked out. The initiation of DNA replication, culminating in the loading of the Mcm2-7 complex to form the pre-replicative complex (pre-RC), occurs in G1, while DNA unwinding, recruitment of additional replication factors, and the commencement of elongation occurs in S-phase (Figure 5; reviewed in [84]). The critical event at the G1/S transition that triggers subsequent elongation is phosphorylation of the replication complex by two kinases; the cyclin dependent kinases and the replication-specific kinase Cdc7/Dbf4. As the temporal regulation of eukaryotic DNA replication has been discussed extensively elsewhere (see [84] and references therein), I will instead discuss evidence suggesting a role of the Mcm2-7 complex in pre-RC formation and DNA unwinding.

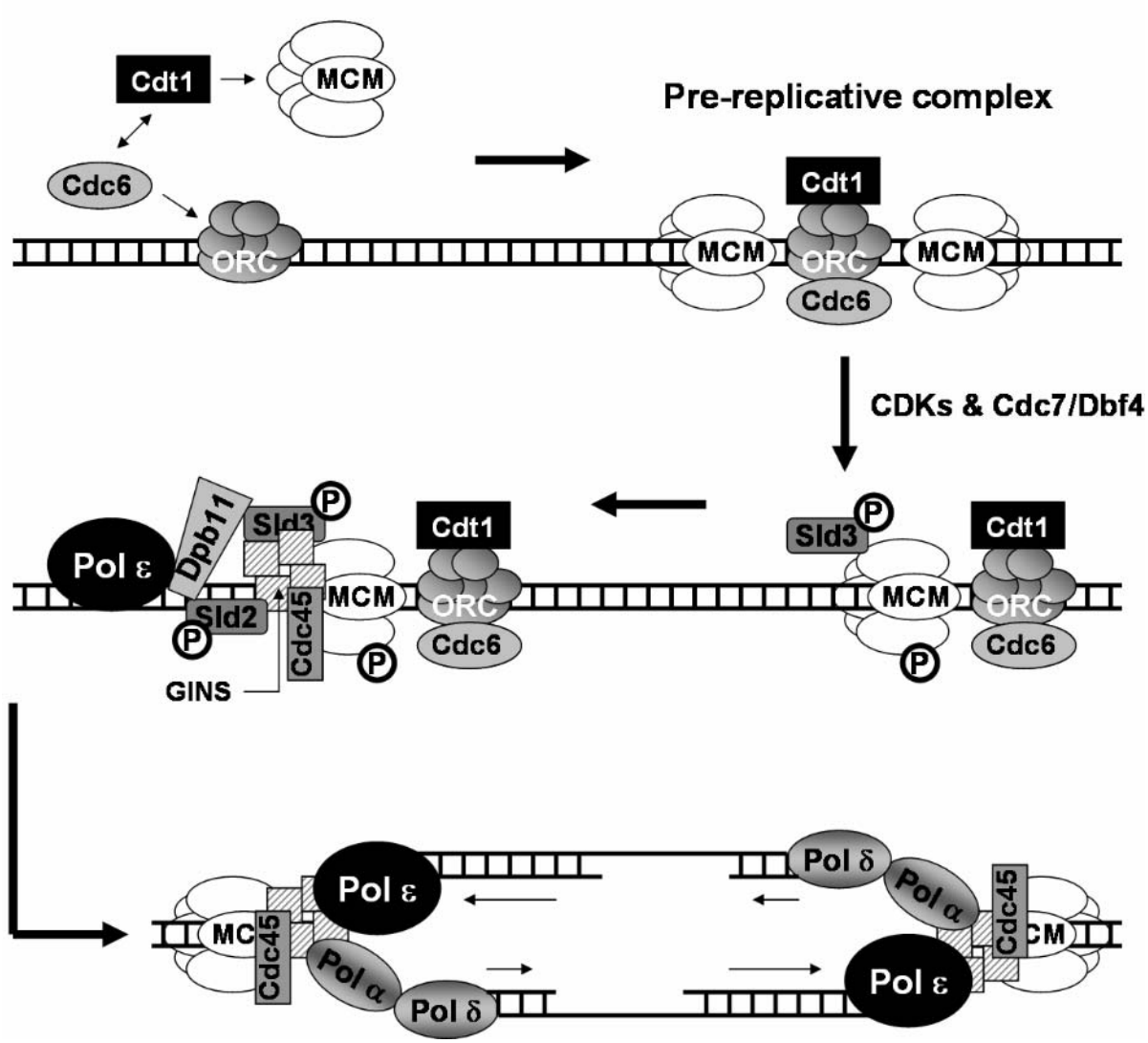

Figure 5. The initiation and elongation phases of eukaryotic DNA replication.

After the G1/S-phase boundary CDK/Cdc7 phosphorylation event and before bi-directional replication, the recruitment of replication factors around only one Mcm2-7 hexamer is shown for convenience. Though not discussed in the main text, Dpb11, Sld2, and Sld3 have been included because they are important for loading Cdc45, the GINS complex, and polymerases [84]. Several other important proteins (*e.g.*, Mcm10) have been omitted for the sake of simplicity. Phosphorylation is denoted as a P within a circle.

1.2.2.1 The role of the Mcms in pre-RC formation

Much of our information concerning the role of the Mcms in initiation comes from studies in *S. cerevisiae*, an organism with well-defined replication origins [85]. Through the use of chromatin immunoprecipitation (ChIP) to examine the binding of specific proteins to defined genomic regions *in vivo*, results indicate that all six of the Mcm subunits specifically localize to replication origins during G1, and then subsequently lose origin localization during S phase (reviewed in [73, 84]). This basic result has been further substantiated at the genomic level of all *S. cerevisiae* origins of replication (>400 origins, [86]). Moreover, through the use of temperature sensitive degron alleles of the *MCM*s, inactivation of any Mcm subunit during G1 results not only in loss of origin association of the entire Mcm2-7 complex, but causes a block in the ensuing loading of additional DNA replication factors and a block to bulk DNA replication upon entry into S-phase [87]. Evidence from yeast also indicates that the Mcm2-7 complex is pre-formed in the cytoplasm, transported into the nucleus, and presumably loads into the pre-RC as a readymade heterohexamer [88].

The localization of the Mcms to origins of replication depends upon prior binding of the origin recognition complex (ORC), as well as the activity of the Cdc6 and Cdt1 proteins (Figure 5; reviewed in [84]). It is believed that the main function of assembling the pre-RC is to simply load the Mcm2-7 complex, since in various *in vitro* systems, ORC, Cdc6 and Cdt1 can be removed after Mcm loading without a loss of subsequent DNA replication [89, 90]. More recent work by the Bell lab has shown that ATP hydrolysis by Cdc6 is activated by origin-bound ORC and is required to load Mcm2-7 [91]. Though ATP hydrolysis by ORC itself is not necessary for loading a single Mcm2-7 complex, it is required for loading multiple complexes [92].

1.2.2.2 Involvement of Mcms during elongation

Similar to initiation, the Mcms have an obligatory role in the elongation phase of DNA replication. Upon entry into S-phase, it has been shown via ChIP analysis of cell cycle-synchronized yeast that, concomitant with the loss of origin association during S-phase, the Mcms co-localize with DNA polymerase ε to flanking genomic regions with similar kinetics [93]. In addition, inactivation of any of the *MCM* degron alleles during S-phase causes an immediate loss of fork progression [87]. Although both Cdc45 and the GINS complex (Figure 5; Appendix C) are also directly required for fork progression [93-97], neither of these factors have the ATPase motifs characteristic of motor proteins, strongly suggesting that the Mcm2-7 complex provides the driving force for fork progression.

1.3 THE MCM HELICASES

Attempts to biochemically prove that Mcm2-7 was involved in DNA unwinding uncovered unexpected complications. Early work with the archaeal MCM proteins demonstrated that they have robust ATP-dependent helicase activity [59, 98-100]. In contrast, the situation in eukaryotes is more complicated. Ishimi *et al.* [101] found that a subcomplex of three specific human Mcm proteins (Mcm467) had a relatively weak DNA unwinding activity, while the Mcm2-7 complex containing all six subunits lacked *in vitro* helicase activity. This basic observation was confirmed in several other systems [102-104]. Although these observations initially cast some doubt as to the actual involvement of the Mcm2-7 complex during DNA replication, DNA unwinding has been recently observed with a *Drosophila* complex that contains Mcm2-7 and five other replication factors [105]. Why has the verification of the

Mcm2-7 complex as the eukaryotic replicative helicase posed such a problem? As a step towards addressing this question, a biochemical comparison of the archaeal MCM complex, the Mcm467 subcomplex, and the Mcm2-7 complex concerning the shared properties of all replicative helicases (ring-shaped architecture, NTPase activity, DNA binding, and helicase activity) is presented below.

1.3.1 Structural biology of the Mcm complexes

1.3.1.1 Archaeal MCMs

Sequencing and analysis of the first archaeal genomes occurred in the mid-to-late 1990s, and it quickly became apparent that the archaeal DNA replication machinery was much like that found in eukaryotes [106, 107]. Significantly, all archaea sequenced so far contain at least one homologue of the eukaryotic Mcms: Crenarchaea have a single homologue; Euryarchaea often encode only one homologue but have been found with up to four copies (reviewed in [74, 108]). Archaeal MCM complexes have been studied both *in vivo* [109, 110] and extensively *in vitro*. These *in vitro* observations are discussed at length below.

To date, the MCM complex from crenarchaeon *Sulfolobus solfataricus* and euryarchaeon *Methanothermobacter thermoautotrophicus* have been most widely studied. Gel filtration and glycerol gradient centrifugation suggested that the *S. solfataricus* MCM (SsoMCM) protein forms homohexamers in solution [59, 111]. However, recombinant *M. thermoautotrophicus* MCM (MthMCM) appeared to form dodecamers [98-100, 112]. The dodecomeric oligomerization seems to be a physical property corresponding to MthMCM itself and not all euryarchaeal MCMs, because the MCMs from the euryarchaeons *Archaeoglobus fulgidus*

(AfuMCM; [113]) and *Thermoplasma acidophilum* (TacMCM; [114]) each form single hexamers.

Atomic resolution structural data confirmed the solution studies and highlighted additional differences between SsoMCM and MthMCM. While no one has successfully crystallized a full-length MCM to date, the structures of the N-terminal domains of both SsoMCM [115] and MthMCM [58] have been solved in recent years. SsoMCM was found to form toroidal homohexamers with a narrow central channel that could accommodate ssDNA [115], while MthMCM formed a head-to-head dimer of hexamers (*i.e.*, a dodecamer) with a central channel wide enough to hold dsDNA [58].

Electron microscopy (EM) further complicated the MthMCM story. The original low resolution micrographs seemed to indicate a stacked double-ring dodecomeric structure of the full length protein [98], but a three-dimensional reconstruction of similarly negatively stained particles unexpectedly revealed single heptameric rings [116]. A separate 3-D reconstruction by the Onesti lab unambiguously demonstrated a hexameric arrangement, although only as a single ring [117]. The discrepancy between single and double hexamers could simply be an effect of the protein concentration (high for crystallography and much lower for EM) shifting the equilibrium from doubles to singles, but the hexamer vs. heptamer situation was more difficult to explain. In the end, it was shown that the oligomeric state of MthMCM was sensitive to NaCl concentration, temperature, and the presence or absence of various concentrations of Mg^{+2}, nucleotide (including transition state analogs), and DNA [118-120]. Altering these parameters led to the independent observation by several groups of single and double hexamers and heptamers, as well as MCM rings containing a gap. Occasionally, helical filaments of MthMCM proteins were also observed [116, 121], but these are most likely biochemical artifacts.

1.3.1.2 Mcm467

When Ishimi first purified Mcm467 from HeLa cells, it was apparent that the ~600 kDa complex is comprised of a dimer of Mcm4, 6, and 7 heterotrimers [101]. This basic observation was confirmed in a variety of other systems – mouse [122], *S. pombe* [123], and *S. cerevisiae* [104]. Despite the fact that the ATP active sites of Mcm467 are most likely formed at subunit interfaces, mutations in the Walker A box of Mcm6 (K401A,S402A) or Walker B boxes of Mcm4 (D572A,E573A) and/or Mcm6 (D459A,E460A) have no effect on gross complex formation [122]. The existence of double hexamers of Mcm467 has been implicated by EMSAs (see below; [103]), but EM studies have only revealed ring-shaped single hexamers [124-126].

1.3.1.3 Mcm2-7

Co-immunoprecipitation assays in *S. pombe* first demonstrated that all six Mcm2-7 subunits stably interact [127]. Subsequent gel filtration analysis of the *S. pombe* [127, 128], *S. cerevisiae* [102, 104], and *Xenopus* [129] Mcm2-7 complexes showed that they were large (~600 kDa) heterohexamers comprised of one copy of each subunit. Often, gel filtration analysis indicated that the size of Mcm2-7 was larger than the molecular weight calculated from the individual Mcm proteins, suggesting that the complex adopted something more complex than just a globular conformation. Indeed, it was observed early by EM that Mcm2-7 existed in solution as a ring-shaped complex with an empty central channel [127].

While structural characterization of Mcm2-7 has lagged behind the beautiful work done on the archaeal MCMs and even the simple work on Mcm467, a good deal is known about how the subunits may knit themselves together into a heterohexamer. Schwacha and Bell were the first to propose a Mcm2-7 subunit arrangement for full heterohexamers (produced *in vivo* by baculovirus-infected insect cells) that consisted of a Mcm467 trimer stacked on top of a Mcm235

trimer such that each subunit contacted four other subunits (Figure 6A; [104]). This model was followed by work using recombinant *S. cerevisiae* Mcm subunits produced in *E. coli* to reconstitute heterohexamers [102] and *in vivo* protein cross-linking followed by co-immunoprecipitation (co-IP) of human Mcms [130]. Each study proposed an alternative ring-shaped Mcm2-7 architecture in which each subunit contacted only 2 neighboring subunits (Figure 6B).

An important fact that came to light about the Mcm2-7 complex by study of the heterohexamer and various Mcm subcomplexes is that the Mcm2-7 toroid contains at least one "weak spot." Of the six Mcm dimer combinations needed to form the hexamer [102], the active site formed between Mcm2 and Mcm5 is structurally unique. Unlike the other Mcm dimers, physical interaction between *S. cerevisiae* Mcm2 and Mcm5 has never been demonstrated, and these two subunits in isolation do not appear to stably interact *in vitro* [102] nor following co-expression in insect cells (Figure 6C; **Chapter 4**). Further, this weak spot in Mcm2-7 architecture seems to be conserved across many species. In *S. pombe*, the association of Mcm2 with Mcm4 and 6 *in vivo* is labile [131], and in humans, no other Mcm subunits were found to co-IP with Mcm5 following *in vivo* protein-protein cross-linking [130]. A recent study has also found that an Mcm binding protein (Mcm-BP) can substitute for Mcm2 and oligomerize with Mcm3-7 in humans [132]. Mcm5 is more tightly associated with complexes containing Mcm-BP instead of Mcm2, and the Mcm complex as a whole is more stable with Mcm-BP than Mcm2.

Taken together, these results indicate that the Mcm2/5 interface may represent a gap in the Mcm2-7 ring and that Mcm2-7 can assume an open or "lock-washer" conformation. Similar structures have been observed for other hexameric complexes involved in nucleic acid metabolism. A crystal structure of the SV40 TAg origin binding domain shows that it assumes

an open ring structure with an axial rise for binding origin DNA [133-135]. Dynamic light scattering indicates that RecA can form hexamers in a closed toroid or lock-washer state *in vitro* [136]. Additionally, the Rho transcription terminator can transition from a lock-washer to closed ring conformation [137].

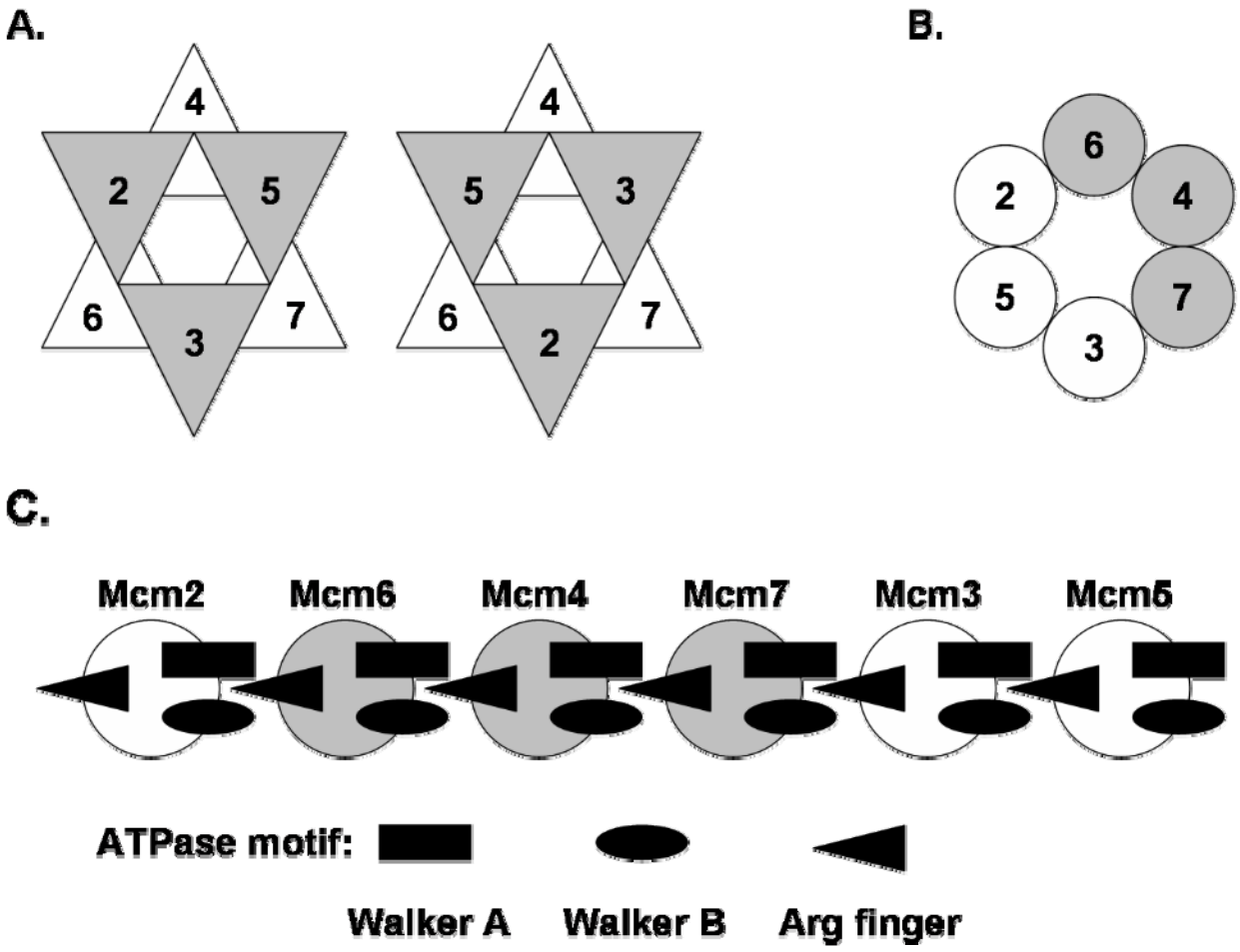

Figure 6. Models of Mcm2-7 subunit architecture.

A) The two possible models predicted by Schwacha and Bell [104] in which each Mcm subunit contacts four other subunits. B) The model first predicted by Davey *et al* [102] in which each Mcm subunit contacts only two neighboring subunits. Although no direct structural proof yet exists, the model in B) is generally accepted as true. Subunits thought to be catalytic are grey; regulatory subunits are white. C) The linear arrangement of Mcm subunits predicted by dimer association studies and the ATPase motifs comprising each active site.

1.3.2 The Mcms are AAA+ ATPases

1.3.2.1 Archaeal MCMs

Hexameric helicases unwind DNA via conformational changes brought on by the binding and hydrolysis of (d)NTPs [35]. Both double [138] and single hexamers [139] of MthMCM can hydrolyze ATP, and this activity is stimulated ~4-fold by the presence of closed circular ssDNA [98, 140] and closed circular dsDNA [98, 141]. However, there is at least one report of inhibition of ATPase activity by higher concentrations of circular ssDNA [98]. Linear ssDNA was just as effective as circular, but linear ssRNA had no stimulatory effect on MthMCM ATPase activity [142]. Like all AAA+ ATPases, the Walker A box was essential for ATP hydrolysis [98], and various deletion constructs indicate that both the N- [98] and C-termini [141] influence the ATPase activity of the central AAA+ domain.

The ATPase activity of the SsoMCM is slightly more cryptic than the MthMCM. Most studies have found no stimulation of ATP hydrolysis in the presence of DNA [59, 111, 143, 144], but one group has reported mild DNA-dependent stimulation [145]. Additionally, a SsoMCM deletion construct missing the extreme C-terminal HTH domain, which already had ~2-fold greater ATPase activity than wild type, was also further stimulated by DNA [143]. Unlike typical AAA+ proteins, a Walker A motif mutation in SsoMCM (K346A) only reduced hydrolysis instead of completely eliminating it [111]. Several SsoMCM DNA binding mutants (discussed in **Section 1.3.3.1**) retained wild type (or slightly greater than wild type) levels of ATPase activity as well [59]. Significantly, there are two reports that the C-terminal half of SsoMCM, which largely forms dimers and thus only a single active site, displays as much ATPase activity as the full wild type hexameric complex [143, 144].

An elegant study by Moreau *et al* investigated the ATPase active site architecture of SsoMCM [146]. Like other AAA+ ATPases [77], it was observed that the active sites were formed *in trans* by neighboring subunits [146]. Interestingly, SsoMCM contains multiple *trans* acting motifs that are similar to highly divergent AAA+ proteins (*e.g.*, SV40 TAg and Mg chelatase). Mutant subunit doping experiments also demonstrated that SsoMCM can tolerate up to three inactive ATPase sites, suggesting a semi-sequential mode of hydrolysis rather than the all-or-none model of TAg activity [54].

1.3.2.2 Mcm467

Mcm467 ATPase activity has been investigated by many groups. It was originally observed that the complex could weakly hydrolyze ATP, and this activity was stimulated by various forms of DNA and even tRNA [101]. These basic observations – little to no stimulation by dsDNA, intermediate stimulation by circular ssDNA, and the highest (~5-fold) stimulation by linear ssDNA – have been repeated in a variety of systems [122, 123, 147, 148]. The DNA-dependent stimulation was also sequence-dependent. Stimulation of ATPase activity was greatest with substrates containing poly(dT) tracts [123, 147], much decreased by poly(dA) or (dC), and absent with poly(dG) [147]. However, one partially contradictory report exists in which it was observed that both strands (A-rich and T-rich) corresponding to the *S. cerevisiae* origin ARS1 are equally stimulatory [148].

An incomplete examination of the AAA+ ATPase motifs of murine Mcm467 revealed that multiple mutations are necessary to decrease ATPase activity [122]. Mcm467 complexes containing Walker B box mutations (DE->AA) in either Mcm4 or Mcm6 have no effect on hydrolysis individually, but complexes containing both Walker B mutants displayed a significant reduction in activity. Further, a Walker A mutant (KS–>AA) Mcm6 subunit caused a slight

decrease in ATPase activity. The importance of Mcm7 was tested using recombinant *Xenopus* Mcm467; a Walker A mutation reduced ATPase activity of the complex by ~6-fold [129].

1.3.2.3 Mcm2-7

Lee and Hurwitz were the first to describe a weak ATPase activity for the *S. pombe* Mcm2-7 complex [128]. This work was followed by an exhaustive study of the *S. cerevisiae* Mcm2-7 complex and the effects of Walker A box K–>A (KA) mutations on ATPase activity [104]. It was found that wild type Mcm2-7 has three kinetically distinct ATP binding/hydrolysis modes: high affinity/low activity, medium affinity/medium activity, and low affinity/high activity. Further, adenosine nucleotides are preferred, and the β-phosphate is critical for binding.

A single KA mutant subunit in the Mcm2-7 complex reduces ATPase activity 6-20-fold, but double and triple mutant hexamers sort into two groups [104]. Complexes that have two or more KA mutations in the Mcm2, 3, or 5 subunits retain wild type or greater than wild type levels of ATPase activity; multiple KA mutant complexes of the Mcm4, 6, or 7 subunits are highly impaired for hydrolysis. It was therefore suggested that Mcm4, 6, and 7 have catalytic roles within the Mcm2-7 complex while Mcm2, 3, and 5 have regulatory roles with regard to ATPase activity. The effects of single and double KA mutant hexamers have since been confirmed *in vitro* in the *Xenopus* system for Mcm6 and 7 [129].

Studies of isolated Mcm dimer pairs demonstrated that the Mcm3/7 dimer had as much activity as the full Mcm2-7 heterohexamer [102, 104]. It was also shown via an arginine finger mutation in Mcm3 and a Walker A box mutation in Mcm7 [102] that they formed a classic AAA+ ATPase active site [77, 78]. No large scale work has yet been done concerning the

effects of mutations in the Walker B and arginine finger motifs on the Mcm2-7 hexamer, and this forms the basis for Specific Aim 2 (below).

1.3.3 DNA binding activity

1.3.3.1 Archaeal MCMs

Before a helicase can unwind DNA, it must first be bound to/around it. Therefore, the DNA binding activity of the archaeal MCMs has been extensively analyzed. EMSA assays were originally used to demonstrate that MthMCM can bind a 30mer ssDNA substrate in a Mg^{+2}-dependent manner [98]. High levels of binding were also seen with AMP-PNP, but decreased when ATPγS or ATP were used in the assay. Binding levels also decreased when the N-terminus was deleted from the protein.

The publication of the N-terminal MthMCM crystal structure [58] explained these previous observations. The N-terminus of the protein, which does not contain the AAA+ ATPase domain, was able to oligomerize into a double hexamer, and each subunit contained a β-hairpin "finger" that pointed towards the central channel running through the complex. These fingers contain positively charged residues that were shown to be important for dsDNA binding. This, coupled with the fact that the central channel itself is highly positively charged, argued that DNA binding occurs in the center of the MthMCM toroid. It was also later shown by mutation of the protein that oligomerization of MthMCM into hexamers [140] or double hexamers [139] is not obligatory for ssDNA or dsDNA binding. Making a *BOB1* (P62L) mutation (see **Section 3.4.3**) in MthMCM slightly decreased ssDNA binding and significantly decreased dsDNA binding (~30% and 80%, respectively) as assayed by EMSAs [138]. Regardless, the affinity of

wild type MthMCM for DNA is high (K_d = ~130 nM; [149]) and similar to other hexameric helicases [35]. Like other helicases, MthMCM can also weakly bind RNA [142].

EMSAs were also used to probe DNA binding by the AfuMCM complex [113]. ssDNA, dsDNA, forks, and bubble substrates were all bound by AfuMCM, and this binding was not dependent on ATP or Mg^{+2}. Structure specific binding was observed with the highest affinity binding corresponding with bubble-containing substrates, then forks, and the lowest affinity for blunt duplexes. The data also suggested cooperative binding between two hexamers on the bubble substrates.

DNA binding by SsoMCM was first demonstrated by the Pisani lab [59, 150]. It was found by EMSAs that SsoMCM binds ssDNA with higher affinity than blunt dsDNA [59]. Structural specificity was also observed: forked DNA substrates were bound with higher affinity than partial dsDNA probes containing a poly(dT) bubble or a 5' ssDNA tail [150]; both forks and bubbles were preferred over simple ssDNA probes [59, 151]. At lower protein concentrations, faster migrating bands were observed, especially with the bubble and fork substrates, suggesting that SsoMCM subcomplexes or single subunits can bind DNA [150]. Similar results were later obtained with dsDNA probes [115].

Soon after, the same group surveyed the effects of alanine substitution mutations on positively charged residues predicted to point towards the central channel of the SsoMCM hexameric complex [59]. While most of the mutations (K129A, H146A, and K194A) abolished binding to all of the tested substrates, the K134A mutation had no effect on ssDNA binding, a marginal effect on bubble binding, but almost completely abolished dsDNA binding. These specialized roles in DNA binding have implications for mechanisms of DNA unwinding (see **Section 1.3.4.1**).

This early work was followed by an elegant study of SsoDNA binding by McGeoch *et al*. [145]. Structure-aided sequence alignments suggested that SsoMCM contains an N-terminal β-hairpin finger like that found in the MthMCM (Figure 3B; [58]), but also an additional predicted β-hairpin motif within the AAA+ domain like that found in SV40 TAg [54, 60] and E1 [61]. To determine the roles of the hairpins in DNA binding, alanine substitution mutations were made in each separately and in combination [145]. EMSA assays (in the absence of nucleotide) demonstrated that the N-terminal mutation reduced affinity for forked DNA ~10-fold, and the C-terminal mutation reduced affinity ~3-fold. Mutating both β-hairpin fingers together, however, completely abrogated DNA binding. The results were similar with ss- and dsDNA substrates but were in stark contrast to the N-terminal hairpin mutant of MthMCM that was completely defective for DNA binding [58]. The existence of at least two DNA binding regions of SsoMCM was also later verified using domain deletion constructs [115, 143, 144].

Recently, it was convincingly demonstrated by fluorescence resonance energy transfer (FRET) that SsoMCM hexamers bind to the 3' tail of forked DNA probes and then slide with a 3'–>5' polarity towards the duplex region of the fork [145]. SsoMCM loads such that the AAA+ domain is near the ss/dsDNA junction of the fork and the N-terminus is closer to the end of the 3' tail. Single molecule FRET has confirmed these findings but also indicated that interaction of the 5' tail of a fork substrate with the surface of the SsoMCM hexamer increases the stability of the MCM/DNA interaction [151].

1.3.3.2 Mcm467

DNA binding by Mcm467 has been investigated via EMSAs by a number of labs. DNA binding was originally observed with the murine proteins after cross-linking to a radiolabeled ssDNA

37mer [122]. At the time, it was unclear if the binding was ATP-dependent since mutations in the Walker A box of Mcm6 or Walker B boxes of Mcm4 and/or 6 had little to no effect. However, it was quickly determined with *S. pombe* Mcm467 that ssDNA binding (to 41mer and 50mer probes) is ATP-dependent by both EMSAs and filter binding [128]. This activity only requires ATP binding however, as the nonhydrolyzable ATPγS stimulates ssDNA binding too.

The substrate specificity of Mcm467/DNA binding has since been investigated. Lee and Hurwitz observed stable gel shifts of dsDNA with a 3' tail, weak binding to a DNA duplex with a 5' tail (corresponding to the 3'–>5' directionality of helicase activity; **Section 1.3.4.2**), and the appearance of two shifted species with a forked probe after cross-linking [103]. This yeast work was then further extended with the mouse Mcm467 [147]. It was shown that a single hexamer of Mcm467 binds to an 80mer ssDNA probe (despite being long enough to theoretically thread through two hexamers), single hexamers weakly bind dsDNA, and dsDNA substrates containing large ssDNA bubbles in their middles are bound by two Mcm467 complexes. Using a DNA fork probe, two shifted species were once again observed as well. Finally, regardless of the structure of the substrate, a preference for polypyrimidine tracts and little to no binding of poly(dA) substrates was seen (dT>dC>dG>dA). Given the role of the Mcms at origins of replication, which often contain T-rich sequences ([152-155]), this sequence specificity is not surprising.

1.3.3.3 Mcm2-7

Assaying *in vitro* DNA binding by the Mcm2-7 complex has either been largely unsuccessful or simply ignored by the replication field. Prior to the recent work in the Schwacha lab [126], no reports exist concerning this biochemical activity. The analysis of Mcm2-7 DNA binding forms the basis for Specific Aim 1 (below).

1.3.4 Helicase activity

1.3.4.1 Archaeal MCMs

From the beginning, it was clear that euryarchaeon MCM complexes have robust and processive 3'–>5' directed helicase activity [98, 113, 114]. As expected from investigation of its ATPase activity, DNA unwinding by MthMCM is dependent on ATP and Mg^{+2} [141] with the Walker A K341E mutant being completely devoid of the activity [98]. Various segments of the MthMCM N-terminus have also been found to be important: N-terminal deletions lack helicase activity [98]; the *BOB1* mutation caused a ~10-fold decrease in activity [138]; and the β–α–β helix-2 insert in the AAA+ ATPase domain was absolutely necessary for DNA unwinding [141]. Formation of double hexamers is also needed for full helicase activity as single hexamers have ~10-fold less activity [139], and subcomplexes and single subunits lack the activity altogether [140]. There is very little MthMCM substrate specificity; blunt, singly-tailed, and forked substrates were all unwound. DNA/RNA hybrids can also be unwound as long as the helicase traverses along the DNA strand [142]. However, TacMCM absolutely requires a probe with both 3' and 5' ssDNA tails, not just a 3' overhang [114].

The SsoMCM complex displays similar DNA unwinding characteristics. It too is a 3'–>5' helicase [143] with activity on a variety of circular, linear, and tailed substrates [59, 111, 143, 145]. This activity was ATP-dependent (ATP>dATP>ATPγS>all other NTPs and dNTPS) [111, 143] and required hydrolysis; AMP-PNP, ADP, and the transition state analogue ADP-AlF_4 failed to support DNA unwinding [143]. As such, truncations of SsoMCM that contain the AAA+ domain retain helicase activity, but usually at reduced levels [143, 144]. Similarly, the Walker A K346A mutant SsoMCM complex cannot unwind DNA [111, 143]. However, ssDNA

binding mutants either reduce (N-terminal β-hairpin finger mutant, [145]) or eliminate (K129A, H146A, K194A, [59]; or C-terminal β-hairpin finger mutant, [145]) helicase activity. The exception to this is the K134A mutation which selectively inhibits dsDNA binding; it has little effect on fork unwinding [59] suggesting that ssDNA binding is more important for this activity.

It should also be noted that the interplay between the archaeal MCM complexes and various other replication factors and chromatin-associated proteins has begun to be fleshed out. The Cdc6 homologues in archaea have been shown to have variable (either no, inhibitory, or stimulatory) effects on MCM helicase activity depending on the model organism [150, 156-160]. Similar effects on DNA unwinding have been found with transcriptional initiation and elongation complexes, the TrpY transcriptional repressor [161], and chromatin binding proteins [162].

1.3.4.2 Mcm467

Ishimi was the first to report helicase activity from Mcm proteins when he observed low processivity 3'–>5' unwinding of a blunt duplex substrate by the Mcm467 complex isolated from HeLa cells [101]. This activity could only be fueled by ATP or dATP and depended upon hydrolysis since ATPγS, AMP-PNP, and the other NTPs did not activate DNA unwinding. This was further underscored (using mouse Mcm467) by the observation that Walker A and B motif mutations in the AAA+ core of Mcm4 or 6 reduce (Mcm4DE–>AA or Mcm6KS–>AA) or eliminate (Mcm6DE–>AA) unwinding [122]. The (d)ATP/hydrolysis-dependent, directionality, and low processivity characteristics were later confirmed for the *S. cerevisiae* [63] and *S. pombe* [128] proteins.

The same group later determined that using a forked substrate instead of blunt duplex DNA stimulated Mcm467 helicase activity [103]. ssDNA tails shorter than 30 nt were

ineffective, but the increased efficiency of unwinding correlated with increasing tail length up to 60 nt. Interestingly, a 5' biotin-streptavidin complex could substitute for a 5' ssDNA tail on a fork substrate suggesting that the DNA strand not bound by Mcm467 simply needs to be sterically excluded from the central channel of the complex for unwinding (Figure 2A). Further, the addition of *E. coli* SSB to helicase reactions increased the processivity of excess amounts of Mcm467 from ~200 bp to ~600 bp, ostensibly by the SSB stabilizing newly unwound ssDNA and preventing reannealing.

A similar result was obtained with murine Mcm467 and the human SSB analogue RPA; processivity increased from ~350 bp to ~450 bp with a marked increase in efficiency as well [147]. The length dependence (~50 nt) on ssDNA tails for high stimulation of unwinding was also seen, and poly(dT) tails were preferred 10-fold over any other sequence. Unwinding of bubble substrates was observed, especially when the bubbles contained 3' poly(dT) tracts.

Like the archaeal MCMs, the yeast Mcm467 complexes can translocate along ss- [163] or dsDNA [52, 63, 163], but dsDNA translocation requires a 3' ssDNA tail for efficient loading. However, unlike the archaeal MCM complexes, Mcm467 translocation does not generate sufficient force to displace streptavidin bound to a biotinylated nucleotide [163]. The complex also uses a "pump in ring" mechanism to drive branch migration of a synthetic Holliday junction substrate [63]. If the Holliday junction probe includes two 3' ssDNA tails on opposite arms, two Mcm467 hexamers can translocate to the center of the junction and simultaneously melt the two duplexes via a pumping mechanism [52].

1.3.4.3 Mcm2-7

Thus far, *in vitro* helicase activity from the isolated Mcm2-7 complex has never been observed [101, 102, 104, 129]. Interestingly, Mcm2-7 has been purified as part of an 11 protein super-

complex (containing Cdc45 and the GINS tetramer; CMG complex) from *Drosophila* that does unwind DNA [105]. This activity was ATP-dependent, had 3'–>5' directionality, and had a similar processivity to Mcm467 [103, 105]. Recombinant CMG complexes have been made with the baculovirus system using the *Drosophila* (Botchan, personal communication) and human (Hurwitz, personal communication) proteins. These behave similarly to CMG purified from *Drosophila* cells and absolutely require all 11 proteins for helicase activity. Despite these promising results, Cdc45 and the GINS complex do not contain ATPase domains, thus even if the CMG complex was found to be the eukaryotic replicative helicase, it is likely that Mcm2-7 is still the workhorse of the complex. Attempting to discover why Mcm467 displays *in vitro* helicase activity while Mcm2-7 does not is addressed in Specific Aim 3 (below).

1.4 SPECIFIC AIMS

Mcm2-7 is almost certainly the elusive eukaryotic replicative helicase, and as such, a vitally important piece of cellular machinery. Despite this, relatively little work has been done to investigate its known and putative biochemical activities. The goal of my thesis work has been to remedy this situation.

1.4.1 Aim 1 – Analysis of the DNA binding activities of Mcm2-7 and Mcm467

DNA binding is an inherent activity of helicases. Because demonstration of Mcm2-7 helicase activity has proven so difficult, my goal was to investigate an upstream activity – DNA binding – in hopes of discovering why Mcm2-7 might fail to unwind DNA *in vitro*. The Mcm467

subcomplex was used as a basis of comparison because it has classically been easier to manipulate experimentally and previously characterized as both a DNA binder and unwinder. The results of these experiments are presented in Chapter 3.

1.4.2 Aim 2 – Initial characterization of Mcm Walker B and arginine finger mutants

The contribution of the Walker A motif of each of the Mcm2-7 subunits has been investigated previously. However, it is unclear whether the six evolutionarily divergent Mcm subunits form six equivalent ATPase active sites typical of a homohexamer or if the active sites themselves have also diverged. An analysis of the *in vivo* and *in vitro* effects of Walker B and arginine finger motifs of the Mcm2-7 complex was carried out to address this question. The results are presented in Chapter 4.

1.4.3 Aim 3 – Analysis of Mcm2-7 helicase activity

Research involving Mcm2-7 has always been stymied by the complex's lack of detectable helicase activity *in vitro*. It was my hope that the investigation of other biochemical activities (above) would shed light on why Mcm467 unwinds DNA while Mcm2-7 apparently does not. Further, if only the Mcm4, 6, and 7 subunits are necessary for helicase activity, then what do Mcm2, 3, and 5 do? My findings on these topics are presented in Chapter 5.

2.0 MATERIALS AND METHODS

2.1 NUCLEOTIDES, OLIGONUCLEOTIDES, DNA, AND OTHER REAGENTS

Radiolabeled nucleotides were purchased from PerkinElmer Life Sciences or MP Biomedical, and unlabeled ATP was obtained from GE Healthcare. Oligonucleotides (oligos; Table 1) were purchased from Integrated DNA Technologies (Coralville, IA). Polynucleotide substrates were purchased from GE Healthcare or Sigma. Circular single- and double-stranded M13mp18 DNA was bought from Bayou Biolabs (Harahan, LA). Nucleotide and DNA concentrations were calculated from absorbance at 260 nm. All other reagents were of the highest available purity.

Table 1. Oligonucleotides used.

Oligo # (length (nt))		Sequence (5'–>3')
3	(44)	GGTGTTTGTTGTATTAACCAGTTTGATAAAATGAGTGATTCTAC
96	(27)	GACGGAGCTCACACGGTTATTCAGGCG
105	(21)	GGAGACTTCAAATCATCATAC
233	(85)	TTTTTTTTTTTTTTTTTTTTTTTTTTTTTTTTTTTTTTTTGGTTGGCCGATCAAGTGCCCAGTCACGACGTTGT AAAACGAGCCC
235	(90)	CACTCGGGCTCGTTTTACAACGTCGTGACTGGGCACTTGATCGGCCAACCTTTTTTTTTTTTTTTTTTTTTTTT TTTTTTTTTTTTTTTT
283	(26)	CACAGGCAATACCGTCAGTTTACCAC
285	(27)	GAGGTACATACATAAACATACGCGCAC
306	(20)	GTCCTGAGATCAACTCCGGT
354	(26)	GCTATGCGGTGTGTGGCGTGTTTCCC
372	(29)	CATCCCCATTGCTGCTGCTTCCAGGCAAC
373	(29)	GTAGGGGTAACGACGACGAAGGTCCGTTG
374	(29)	CGATGTGGTCGCTGTTGCTAAAGTTTCAG
375	(29)	GCTACACCAGCGACAACGATTTCAAAGTC
389[b]	(70)	CTGGCACGTTCAGGTCCATCCGGCCG(XYZ)8ATTAGAGCTAATTCCAGGCA
390	(66)	CCAGGCAACGCGTACTAGCGCGC(XYZ)8TCGTTGTATAAAACATACG
391	(71)	CATACGTCGATGTGGTCGGGCCC(XYZ)8GTTAAAAAAGTTTCAGATAAGA GG
392	(56)	CTGGCACGTTCAGGTCCATCGCTGCTGGGCCCGCTGCTAAAGTTTCAGATAAGAGG
455[c]	(90)	*GGGCTCGTTTTACAACGTCGTGACTGGGCACTTGATCGGCCAACCTTTTTTTTTTTTTTTTTTTTTTTTT TTTTTTTTTTTTTTTT
510	(85)	ACCTGTCGTGCCAGCTGCATTAATGAATCGACTGCTCTCACATATAGCTACATATCCGACGCGACCACTCA CAATCACAGTTAAC
770	(15)	TTTTTTTTTTTTTTT
771	(20)	TTTTTTTTTTTTTTTTTTTT
772	(25)	TTTTTTTTTTTTTTTTTTTTTTTTT
773	(30)	TTTTTTTTTTTTTTTTTTTTTTTTTTTTTT
774	(35)	TTTTTTTTTTTTTTTTTTTTTTTTTTTTTTTTTTT
775	(40)	TTTTTTTTTTTTTTTTTTTTTTTTTTTTTTTTTTTTTTTT
776	(50)	TTTTTTTTTTTTTTTTTTTTTTTTTTTTTTTTTTTTTTTTTTTTTTTTTT
777	(60)	TTTTTTTTTTTTTTTTTTTTTTTTTTTTTTTTTTTTTTTTTTTTTTTTTTTTTTTTTTT
778	(80)	TTTTTTTTTTTTTTTTTTTTTTTTTTTTTTTTTTTTTTTTTTTTTTTTTTTTTTTTTTTTTTTTTTTTTTTTTTT TT
806	(23)	GTTAACTGTGATTGTGAGTGGTC
826	(50)	TGTCTAATCCCGAAAGGCCCTGCCACTGAAATCAACACCTAAAGCATTGA
869	(22)	GTAATACGACTCACTATAGGGC
870	(20)	AATTAACCCTCACTAAAGGC
887	(20)	TAATACGACTCACTATAGGG
888	(20)	ATTAACCCTCACTAAAGGGA

[b] (XYZ)8 = eight XYZ codons of random sequence where the ratio of A:T:C:G is 25:25:25:25 (X), 31:19:19:31 (Y), and 0:39:39:22 (Z).

[c] * denotes sites of biotinylation.

2.2 BUFFERS

The recipes for the buffers below are preceded by descriptions using the following format: **abbreviation**, name, method in which the buffer is used. When the major salt concentrations were varied, this is denoted in the text as the abbreviation followed by the molar concentration (*i.e.*, S/0.15 = S buffer containing 150 mM KCl).

1. **1DS**, 1-D Sample Buffer, two-dimensional gel electrophoresis
   (2.85 g urea, 1 mL 10% Triton X-100, 250 µL Beta-mercaptoethanol, 250 µL Ampholytes, H_2O to 5 mL; warm in 30°C water bath to dissolve urea. Store 500 µL aliquots at -70°C.)

2. **A**, Acetate Buffer, coupling apyrase to beads
   (100 mM NaOAc, pH 4.0, 500 mM NaCl, 10% glycerol)

3. **B**, Blocking Buffer, coupling apyrase to beads
   (200 mM glycine, 10 % glycerol, 50 mM Tris-HCl, pH 8.0)

4. **B1**, Bead Buffer, coupling DNA to magnetic beads
   (5 mM Tris-HCl, pH 7.5, 0.5 mM EDTA, 1 M NaCl, 100 µg/mL bovine serum albumin (BSA; NEB))

5. **B2**, Binding Buffer, double filter binding assay and Mcm dialysis
   (25 mM potassium-HEPES, pH 7.4, 50 mM KCl, 10 mM MgOAc, 50 µM ZnOAc, 100 µM EDTA, 10% glycerol, 0.02% Nonidet P-40 (NP-40), 1 mM dithiothreitol (DTT))

6. **B3**, Bead Binding Buffer, magnetic bead binding assay
   (25 mM sodium-HEPES, pH 7.4, 50 mM NaCl, 10 mM MgOAc, 50 µM ZnOAc, 100 µM EDTA, 10% glycerol, 0.02% NP-40, 1 mM DTT, 100 µg/mL BSA)

7. **C**, Coupling Buffer, coupling apyrase to beads
   (100 mM $NaHCO_3$, pH 8.3, 500 mM NaCl, 10% glycerol)

8. **EB**, Extraction Buffer, rescue of integrated plasmids from yeast
   (0.5 M NaCl, 0.2 M Tris-HCl (pH 7.6), 0.01 M EDTA, +/- 1% SDS)

9. **H**, H Buffer, ATPase assays
   (2x stock = 47.6 g K^+HEPES, 20 mL 0.2 M EDTA, 20 mL 0.2 M EGTA, 4.3 g MgOAc, 400 mL glycerol, pH to 7.6 with 10 N KOH, MilliQ H_2O to 2 L)

10. **LC**, Lower Chamber Buffer, two-dimensional gel electrophoresis

(9.8 mL 10% H_3PO_4, H_2O to 1 L; Degas for 30 min and store in a tightly capped container.)

11. **PBS**, Phosphate Buffered Saline, co-immunoprecipitation
(8g NaCl, 0.2g KCl, 1.44g Na_2HPO_2, 0.24g KH_2PO_4, adjust pH to 7.4, MilliQ H_2O to 1 L)

12. **S**, S-Buffer, gel filtration chromatography
(25 mM K^+HEPES (pH 7.4), 100 mM KCl, 5 mM MgOAc, 50 μM ZnOAc, 10% glycerol, 100 μM EDTA, 0.2% NP-40, 1 mM DTT)

13. **SL**, 10x Stop-Load Buffer, loading dye for helicase assays
(0.25% Bromphenol Blue, 0.25% Xylene Cyanol, 1% SDS, 100 mM Na_2EDTA (pH 8.0), 25% Ficoll (type 400)).

14. **SO**, Sample Overlay Buffer, two-dimensional gel electrophoresis
(2.7 g urea, 125 μL Ampholytes, Bromphenol blue to taste; warm in 30°C water bath to dissolve urea. Store 500 μL aliquots at -70°C.)

15. **TBE**, Tris/Borate/EDTA Buffer, native PAGE gels
(90 mM Tris base, 90 mM boric acid, 2 mM EDTA; adjust the pH to 8.0)

16. **TBS**, Tris buffered saline, double filter binding
(8 g NaCl, 0.2 g KCl, 3 g Tris base, pH to 7.4 with HCl, MilliQ H_2O to 1 L)

17. **TBST**, TBS + Tween-20, western blots and array south westerns
(10x stock = 200 mL 1 M Tris-HCl (pH 7.6), 80 g NaCl, 50 mL 20% Tween-20, MilliQ H_2O to 1 L)

18. **TG**, Tris-Glycine buffer, native gradient gel electrophoresis
(10x stock = 0.25 M Tris, 1.92 M glycine; pH to 8.8 or 6.8)

19. **UC**, Upper Chamber Buffer, two-dimensional gel electrophoresis
(4 g NaOH, H_2O to 1 L; degas for 30 min and store in a tightly capped container.)

2.3 PROTEIN PURIFICATION

Hexameric Mcm2-7 and Mcm467 complexes were expressed and purified as described [104]. Briefly, all *S. cerevisiae* Mcm2-7 protein preparations were expressed in baculovirus-infected insect cells and contained a C-terminal His_{10} epitope tag on Mcm4 and 7 with the other subunits

being untagged. They were purified through metal affinity, gel filtration and ion exchange chromatography. The presence of individual Mcm subunits were either directly visualized following separation by SDS-PAGE (for Mcm6, 3, and 5) or using Western blot analysis with subunit-specific antibodies (Santa Cruz anti-Mcm2 (sc-6680) and anti-Mcm7 (sc-6688) and anti-Mcm4 monoclonal antibody (AS6.1)). Mcm subcomplexes were purified similar to the hexameric complexes and were made using specific mixtures of recombinant baculoviruses that each encode the desired Mcm subunits, with one Mcm subunit containing a C-terminal His_{10} tag to facilitate metal chelate chromatography. SV40 large T-antigen was expressed in insect cells and purified as a C-terminal His-tagged protein; details are available upon request. All of the proteins were dialyzed against B2 buffer containing 100 mM potassium chloride and protease inhibitors. Protein concentrations were quantified using a Fuji FLA-5100 laser imager on SDS-PAGE-separated protein bands stained with Sypro orange (see below; Molecular Probes, Eugene OR) using known amounts of BSA as a standard; protein concentrations unless otherwise noted are in pmol or nM of hexamer. *mcm* genes containing the Walker A (KA), Walker B (DENQ), or arginine finger (RA) alleles were completely sequenced to verify the constructs and used to make Mcm complexes in a manner identical to the wild type complexes [104].

2.3.1 Sypro orange staining

Sypro orange binds to negatively charged molecules, so SDS-PAGE gels were run until the SDS front, which migrates with or slightly ahead of the dye front, exited the gel. Gels were separated from the glass casting plates and placed into a small plastic dish containing MilliQ H_2O. They were washed briefly with two changes of MilliQ H_2O to remove SDS from the surfaces of the gels. The water was decanted, and 50 mL of 1x Sypro orange in 7.5% acetic acid was added to

the plastic dish. This was sufficient to stain ≤ 3 gels; larger numbers of gels were divided between several containers. The gel dishes were wrapped in aluminum foil (Sypro is photosensitive) and incubated on a rocking platform for ≥ 1 hr at room temperature. Prior to scanning with the Fujifilm FLA-5100, the gels were briefly rinsed with MilliQ H_2O or 7.5% acetic acid. To decrease background staining, especially when staining was allowed to proceed overnight, the gels were incubated in 7.5% acetic acid in the dark for ≥ 1 hr at room temperature. This did not appear to affect levels of protein staining. Staining solution can be used more than once, but the best results come from fresh stain.

2.4 *IN VITRO* PROTEIN CHARACTERIZATION

2.4.1 Co-immunoprecipitation

Mcm subunit association following the final step in purification was verified by co-immunoprecipitation of the complex using AS6.1 (anit-Mcm4), followed by verification of individual Mcm subunits in the precipitate. Briefly, two pmol of either Mcm2-7 or Mcm467 were incubated with AS6.1 and 30 μL of 1x PBS-equlibrated GammaBind Plus beads (GE Healthcare) for ≥ 2 hours at 4°C, washed extensively with buffer B2, resuspended in SDS-PAGE loading buffer, and separated by electrophoresis. A more detailed protocol is presented below.

Small aliquots (30 μL of the resin for every reaction) of GammaBind Plus sepharose beads were prepared before each experiment by washing the resin extensively in several changes of 1x PBS buffer (pH 7.4). To conjugate the beads with the anti-Mcm antibody, the resin was spun down for 2 sec in a microfuge, and the buffer was removed. The beads were resuspended

in 500 μL antibody (usually anti-Mcm4, AS6.1) that had been diluted 50% with PBS, and the suspension was rotated on a rotisserie overnight at 4°C. For "mock" controls, the beads were washed as above, but PBS was added instead of antibody.

Before the immunoprecipitation, the beads were spun down as above, the antibody was pipetted off, and the resin was washed 3x with PBS. The beads were then washed once with a large volume of B2 buffer, spun down, and resuspended to a 50% slurry with B2. 60 μL aliquots were made and 2 pmol Mcm complex were added per aliquot. The reactions were incubated at 4°C for ≥2 hr on a rotisserie. Finally, the aliquots were spun down, the buffer removed, and washed with 500 μL B2. As much buffer as possible was removed, and the beads were resuspended in 15 μL 2x SDS loading dye to release the proteins. The samples were boiled and run on a 10-well 7% SDS-PAGE gel at 200 V for ~1hr.

To quantitate, the gels were stained with Sypro orange. Generally, ~60% of the input was pulled down with the beads. If washed properly, virtually no Mcms stuck to the naked beads (mock control). Westerns were performed to probe for the presence of the co-migrating subunits (Mcm2,4,7) as described in **Section 2.3**. The same gel was either stripped and re-probed using the three separate antibodies, or the sample was run in triplicate.

The limiting factor to getting Mcms to stick to the beads didn't seem to be the amount of antibody or the incubation time, but rather the volume of beads used. However, using anymore than 30 μL would necessitate TCA precipitation of proteins later to fit everything in the wells.

2.4.2 Gel filtration chromatography

Briefly, a 1 mL glass column was packed with Sephacryl 300 HR (Sigma) equilibrated in buffer S/0.15 and calibrated with standard molecular weight markers including blue dextran (2,000

kDa), thyroglobulin (669 kDa), apoferritin (443 kDa), β-amylase (200 kDa), and BSA (66 kDa). Small samples of purified protein (20-25 μL; approximately 10 μg) were subjected to analytical gel filtration chromatography run by gravity flow at room temperature. Twenty-one μL fractions were collected and analyzed by SDS-PAGE and staining with Sypro orange. A detailed protocol is presented below.

To prepare the Sephacryl 300 HR (S300) resin, it was warmed to room temperature, gently resuspended, and poured (~2 mL) into a 10 mL plastic column. The ethanol that the resin is stored in was drained off, and the beads were gently resuspended in 2 mL of room temperature S/0.15 buffer. The buffer was drained off, and the resin was washed several more times as before. The S300 was then resuspended to ~50% in S/0.15.

To prepare the long column, a short length of the tip of a 1 mL glass pipet was scored with a metal file and snapped off so that a syringe cap would fit snugly. The top of the pipette was similarly trimmed down such that a round gel loading tip could reach the 0 mL mark. A small plug of silanized glass wool was then inserted into the top of the pipette and forced into tip with compressed air. A piece of Tygon® tubing (~2 inches) was placed on top to act as a reservoir.

The glass pipette was prepared for the addition of resin by running 1 mL of S/0.15 through it, capping the bottom, and filling it with S/0.15 to the bottom of the reservoir. The resin slurry was then added to the reservoir and allowed to slowly settle into the pipette. As needed, additional resin was added to bring the column volume up to ~1 mL. Several bed volumes of S/0.15 were allowed to drip through the column to help pack the resin. Complete packing of the S300 took several days and was often left to settle over the weekend. The column was always

stored in buffer when not in use, with a syringe cap plugging the bottom and a binder clip sealing the reservoir on top.

The column was calibrated by first finding the void volume. To do this, a small amount of blue dextran was dissolved in S/0.15, and 25 µL was loaded and allowed to enter the column. The dye was then flushed through the column with small volumes of S/0.15 to determine how much was needed to elute the blue dextran peak. That volume of buffer (generally 400-500 µL) corresponds to the void volume. Next, a 40 µL cocktail of protein standards (10 µL each of 8 mg/mL thyroglobulin, 10 mg/mL apoferritin, 1 mg/mL β-amylase, and 1 mg/mL BSA) was loaded and allowed to enter the column. This was chased with 1 mL of buffer and one-drop (~21 µL/drop) fractions were collected starting near the void volume. The protein standards were separated by adding 4 µL of 6x loading dye to each fraction, boiling, and running 10 µL of each on 10% SDS-PAGE gels at 200 V. The bands were quantitated by staining with Sypro orange and scanning the gel with a FLA-5100 laser imager (Fujifilm).

When running Mcm samples, the column was first flushed out with 1-2 bed volumes of S/0.15. Next, 20-25 µL purified Mcm hexamer (or the equivalent amount of subcomplex) was loaded and allowed to enter the column. One bed volume of buffer was added, and 20 one-drop fractions were collected beginning near the void. The proteins were separated, stained, and quantified as above. Mcm2-7 and Mcm467 hexamers run slightly larger than thyroglobulin.

After filtration of samples, the column should be cleaned and stored properly. When in frequent use, it was convenient to run 1-2 bed volumes of 20% ethanol (+/- azide) through the column and store it saturated in the same. After heavy use, it was best to clean the column with two bed volumes of 6 M guanidine HCl followed by rinses with two bed volumes each of 20%

ethanol and buffer S/0.15. With proper care, many samples can be run on these columns, but they do have a finite lifespan (*i.e.*, protein stops eluting).

2.4.3 Two-dimensional gel electrophoresis

Briefly, tube gels (6 cm length, 1.3 mm width) were cast in capillary tubes using first-dimension gel solution (8.0 M urea, 4% acrylamide (30% acrylamide:5.4% bis-acrylamide), 2% Triton X-100, 2% high resolution 3/10 ampholyte (Fluka), 0.01% ammonium persulfate, and 0.1% TEMED) and were pre-run for 10 min at 12.5 V/cm, 15 min at 19 V/cm, and 15 min at 25 V/cm. The upper chamber buffer is 200 mM NaOH and the lower chamber buffer is 10 mM H_3PO_4, both thoroughly degassed. Mcm protein samples were mixed with equal volumes of first-dimension sample buffer (8.0 M urea, 2% Triton X-100, 5% β-mercaptoethanol, and 2% 3/10 ampholyte) for ≥10 min at room temperature prior to electrophoresis. For isoelectric focusing, samples were loaded directly onto tube gels, overlaid with two volumes of overlay buffer (4.0 M urea, 1% 3/10 ampholyte, 0.01% bromphenol blue), and separated in the first-dimension by electrophoresis for 10 min at 31 V/cm and 3.5 hr at 47 V/cm. Gels were then extruded from the tubes, equilibrated in SDS-PAGE sample buffer, and proteins separated in the second-dimension on 7% SDS-PAGE gels. Following separation, proteins were either visualized by Sypro orange staining, or transferred to nitrocellulose for Western blot analysis. A more detailed protocol follows below.

This method essentially follows the protocol as laid out in the 2-D Electrophoresis for Proteomics methods and product manual (Bio Rad). In addition to the buffers listed in **section 2.2**, the following stock solutions were made for the sake of convenience:

<u>Acrylamide stock</u>

37.5 mL 40% acrylamide
0.81 g bis-acrylamide
H_2O to 50 mL
Filter with 0.45 μm filter and store at 4°C in the dark.

Gel solution (make fresh!)
2.75 g Urea
665 μL Acrylamide stock
1 mL 10% Triton X-100
250 μL Ampholytes
985 μL H_2O
Warm in a 30°C water bath to dissolve urea and degas in a small sidearm flask for 15 min. Add 5 μL each 10 % ammonium persulfate and TEMED to polymerize.

Tube gels were poured by sealing the needle-end of a 5 mL syringe with parafilm and placing it upright in an eppendorf rack. The syringe was then filled by placing 8 or 9 capillary gel tubes inside, and the gel solution was poured in (the capillary tubes fill up from the bottom). The polyacrylamide was allowed to polymerize for ~1 hr, the capillary gel tubes were separated, and the excess gel and urea was wiped off. The tube gels can be stored for several days at room temperature in moistened Kim-Wipes wrapped in plastic. Before the samples were loaded, the tube gels were pre-electrophoresed for 10 min at 200 V, 15 min at 300 V, and 15 min at 400 V in the 2-D gel apparatus using UC and LC buffers. The buffer was then removed, and the tops of the tubes were flushed out.

To prepare the protein samples for electrophoresis in the first dimension, an equal volume of 1D sample buffer was added to the sample. This was incubated at room temperature for 10-15 min, loaded onto the tube gel with a needle, and then overlaid with SO buffer. Samples were electrophoresed for 10 min at 500 V and 3.5 hr at 750 V.

Specially poured slab gels were needed to run the samples in the second dimension. 7% SDS-PAGE gels were poured using standard methods, but no comb was added to the stacker. Instead, the stacker was poured nearly to the top of the gel plates and overlaid with water-

saturated butanol. The tube gels were ejected from their capillary casting tubes onto parafilm using a syringe loaded with SDS-PAGE running buffer, any curls or loops were straighten, and then the tube gels were slipped onto the stacker of the slab gel using a spatula. Tube gels were equilibrated by covering them with SDS-PAGE sample buffer for 10 min, and the slab gel was run and stained (typically with Sypro orange) as usual.

2.4.4 Quantitative western blots

Known amounts of Mcm hexamer and single subunit preparations were separated by SDS-PAGE, transferred to a nitrocellulose membrane, and analyzed by western blotting using subunit-specific antibodies. The corresponding chemiluminescent signal was quantified prior to signal saturation using an LAS-3000 Intelligent Dark Box (Fujifilm) and Image Gauge software. The amount of subunit in the hexamer was calculated using the single subunit titrations as standard curves. It was often useful to run samples in duplicate on different halves of the gel. The proteins can be transferred to nitrocellulose and blocked as usual, but then the membrane can be cut in half and probed with two different antibodies. This saved time, required less stripping/re-probing, and provided a backup if one membrane was damaged.

2.4.5 Native gradient gel analysis

Various proteins were separated by native gradient gel electrophoresis, and a variety of gradients were tested (both gel percentage and pore size). Results varied based on the protein sample, but the most successful set of conditions for analysis of the GINS complex is presented here. Prior to pouring the gradient, the following gel solutions were made:

	3.5% gel sol'n	12% gel sol'n	Stacker gel sol'n
37.5:1 acrylamide:bis	276 μL	942 μL	138 μL
10x TG buffer	250 μL	250 μL	125 μL (pH 6.8)
MilliQ H_2O	1.946 mL	604 μL	960 μL
40% glycerol	N/A	676 μL	N/A
10% ammonium persulfate	25 μL	25 μL	25 μL
TEMED	2.5 μL	2.5 μL	2.5 μL

The gels were poured in three steps: 1) a 500 μL 12% gel "bumper" was poured into the bottom gel caster, and 2) the gradient was then immediately poured. To form the gradient in a disposable pipet, 1.65 mL of the 3.5% gel solution was sucked up, gently followed by 1.65 mL of 12% solution, without mixing. The solutions were then mixed by pipetting in 2 or 3 air bubbles and letting them rise through the gel solutions, thus establishing the gradient. It was often useful to add a bit of bromphenol blue dye to the 12% gel solution. A gradient of blue color indicated a gradient of gel concentrations. The gradient was carefully added on top of the bumper and polymerized under a thin layer of water-saturated butanol for ≥30 min. 3) After the butanol was decanted, the gel caster was rinsed well with water, and the stacking gel and comb were added.

Proteins were loaded (~ 2 μg) without loading dye (loading dye may disrupt complex stability) and run at 200 V for 2 hr. The gels were silver stained as usual. For Sypro orange staining, the gel was incubated in 0.05% SDS for 20 min at room temperature. It was then briefly rinsed with MilliQ H_2O and Sypro stained as usual for ≥1 hr at room temperature. Silver staining could follow Sypro staining. Western blotting proceeded as usual after a longer (2 hr at 500 mA) transfer to the nitrocellulose membrane. The protein samples usually demonstrated some smearing, but defined bands were present.

2.4.6 Limited proteolysis

In theory, limited proteolysis of Mcm2-7 can be done with a variety of proteases (subtilisin, proteinase K, V8 protease, *etc*), but in practice I have only extensively used trypsin and chymotrypsin. Solutions of chymotrypsin were made in B2 buffer and diluted to a stock concentration of 50 μg/mL in the same. Single-use aliquots were made, snap frozen in liquid N_2, and stored at -70°C. Typical digest reactions contained 4 pmol Mcm hexamer (+/- preincubation with 5 mM ATP, 5 nM DNA, and/or 200 mM potassium glutamate), 2.5 ng chymotrypsin, and B2 in a final volume of 10 μL. Reactions were incubated for 10 min at room temperature and stopped with 5 μL of a kill cocktail (3 μL 6x SDS-PAGE sample buffer, 0.2 μL 100 mM PMSF, 0.4 μL inhibitor solution, and 1.4 μL B2 buffer). The potent inhibitor solution was made by dissolving 1 mg each of N-p-Tosyl-L-phenylalanine chloromethyl ketone (TPCK) and Nα-p-Tosyl-L-lysine chloromethyl ketone hydrochloride (TLCK), specific inhibitors of trypsin and chymotrypsin, respectively, into 1 mL of 100% EtOH and stored at -20°C. The samples were then boiled, spun down, and run on one or two 12% SDS-PAGE gels at 200 V. If the entire sample was loaded onto one gel, it was best visualized by Sypro orange staining. If the sample was split between 2 gels, it was best visualized by western blotting using a different antibody to probe each gel.

2.4.7 Mcm dimer pull downs

Chelating Sepharose Fast Flow resin (Amersham Biosciences) was prepared per the manufacture's instructions. Briefly, small aliquots of slurry were washed with excess MilliQ

H_2O and then treated with one volume of either 0.1 M $NiSO_4$ (charged) or MilliQ H_2O (uncharged). The resin was then washed in MilliQ H_2O followed by 3 washes and resuspended to 50% in binding buffer (1x PBS (pH 7.5), 10% glycerol). For the pull-downs, ~0.35 μg of Mcm dimer were incubated with 20 μL sepharose slurry at room temperature with rotation for 20 minutes. The reactions were spun down and washed with excess binding buffer. Bound proteins were eluted by resuspending the resin in 6x SDS-PAGE loading buffer, separated by electrophoresis, and visualized by Sypro orange staining. The subunits in the Mcm7/4 dimer co-migrate by SDS-PAGE and were separately detected by immunoblotting.

2.5 TRANSMISSION ELECTRON MICROSCOPY

Briefly, proteins were diluted to 50 μg/ml in buffer B3 supplemented with 5 mM ATPγS. They were then absorbed to glow-discharged, formvar/carbon-coated 400 mesh copper grids (Ted Pella, Redding, CA) and negatively stained with 2% uranyl acetate. Grids were visualized with an FEI Morgagni 286 transmission electron microscope at 80 kV and 56,000X (wide field) or 140,000X (individual particle) magnification. Micrographs were taken with an AMT digital camera (Peltier-cooled Hamamatsu ORCA-HR CCD camera) at a resolution of 2624x2624 pixels. Quantification and classification of Mcm complexes were done semi-automatically by selecting single particles from micrographs with BOXER (http://ncmi.bcm.tmc.edu/~stevel/EMAN/doc/) using reference particles of each class (random orientation, toroidal, split-ring). Particles were then manually categorized. Image averaging was performed as described [164]. In brief, representative images were chosen from the dataset of selected particles, and an image with good contrast was used as the initial reference in each case.

The image was low-pass filtered to remove very high-frequency noise, and all selected particles were correlation-aligned by an exhaustive search in 6° steps over the in-plane rotation angle, and within a radius of 10 pixels for the origin. The best-scoring 50% of the particles were combined to make a new reference model, and a subsequent refinement of orientation parameters was carried out in finer steps over a limited rotation range and translational offset. A more detailed protocol is described below.

Protein samples were diluted to 10-50 μg/mL (hexamers tend to fall apart at lower concentrations) in B2 buffer +/- nucleotide, DNA, salts, *etc*. and allowed to reach equilibrium at 30°C (~30 min). During that time, grids were glow discharged for 45 sec in a partially evacuated bell jar using a Tesla coil. Small aliquots of B2 and stain were also centrifuged at max speed to pellet any larger particulate matter. After protein equilibration, grids were prepared by the "flicker" technique. Generally, 5 μL of sample was spotted onto the grids and allowed to absorb for 60 sec. The drop was then flicked off onto a KimWipe, and the grid was washed with 7.5 μL of B2 for 30 sec. This drop was flicked off, and the grids were stained with three ~5 μL drops of negative stain; the first two drops were flicked off immediately, and the last drop was left to stain for 60 sec. The drop of stain was flicked off, excess stain was wicked away from the surface of the grid with the corner of a KimWipe, and the grids were air-dried. In most cases, the grids were immediately examined by TEM, but the quality did not noticeably diminish even after a week of storage in grid boxes in the absence of desiccation.

2.5.1 Negative stains

Various aqueous solutions of heavy metal salts (ammonium molybdate, phosphotungstate, uranyl acetate, and uranyl formate) were tested as negative stains for visualization of the Mcms. A range of concentrations were examined, but the best contrast was obtained with solutions of 2% (w/v). When 0.1% (w/v) trehalose was included in the stain, higher salt concentrations of 5-6% were preferred as trehalose decreases the overall density of the solution. Uranyl formate was generally made as a saturated solution and used immediately. All stains were filtered through a 0.22 μm pore membrane and stored in the dark.

2.5.2 Other EM resources

A simple rule of thumb for EM is that no two protein samples will behave the same. Often, trial and error (based on what was known about the biochemistry of the protein) was the simplest and quickest way to produce results. A healthy survey of the EM literature was also beneficial. Excellent reviews on negative staining [165, 166] provided a wealth of information. The work of Werner Baschong [167-170] and others [171, 172] on protein fixation and immunogold EM were also helpful.

2.6 DNA BINDING

2.6.1 Double filter binding assay

The double filter binding assay was based on [173]. The nitrocellulose filters were prepared by separating the membranes (BA85, Schleicher & Schuell) from their blue paper protectors and placing them in a plastic dish (P2 pipet tip box) filled with a small volume of MilliQ H_2O. The H_2O was decanted, a large volume of 0.5 M KOH was added, and the filters were incubated on a rocking platform for 25 min at room temp (this reduces non-specific binding of ssDNA to the filters, and because the timing is crucial it was never varied by more than +/- 1 min). The KOH was decanted and the filters were washed (at least 15 good rinses) in MilliQ H_2O. They were then rinsed twice with 1x TBS, pH 7.4 and stored at 4°C in TBS buffer.

The DEAE filters (DE81, Whatman) were separated from one another and placed in a plastic dish filled with a small volume of MilliQ H_2O. The H_2O was decanted, a large volume of 0.1 M Na_2EDTA, pH 8.8 was added, and the membranes were incubated on a rocking platform for 10 min at room temperature. The Na_2EDTA was decanted, and the filters were washed with a large volume of 1 M NaCl on the rocking platform for 10 min. The wash step was repeated twice more for 10 min each with fresh NaCl. The NaCl was removed, and the filters were quickly ($\leq$ 30 sec) washed in a small volume of 0.5 M NaOH. As for the nitrocellulose filters (above), the DEAE membranes were washed extensively in MilliQ H_2O, rinsed twice with 1x TBS, pH 7.4, and stored at 4°C in TBS.

Standard filter binding reactions contained 120-150 nM Mcm complex, 4 nM radiolabeled ssDNA probe, 5 mM ATP or ATPγS, 5 mM beta-glycerophosphate, and B2 buffer to a final volume of 12.5 μL. The reaction size could be successfully decreased to as little as

6.25 μL to save protein; smaller volumes increased the background signal (*i.e.*, "bounce" in the data). The reactions were incubated 30 min at 30°C. While this occurred, a water aspirator was used to draw a vacuum in a FH 225V Filter Manifold (GE Healthcare), and the "filter stacks" were set up. The stacks were made by placing a DEAE filter on the manifold first and covering with a nitrocellulose filter, all of which was topped with one of the stainless steel chimneys ("paper weights"). The stack was washed with 1 mL MilliQ water and equilibrated with 500 μL ice cold B2 buffer. After incubation, the reactions were spotted onto the filter stacks and quickly washed with an additional 500 μL of B2. The nitrocellulose and DEAE membranes were then separated, added to ≥ 3 mL of scintillation fluid, and quantified by scintillation counting. The amount of DNA bound was calculated using Equation 1,

$$DNA_{bound} = \frac{C_{NC}}{C_{NC} + C_{DEAE}}$$

where C_{NC} and C_{DEAE} are the radioactive counts retained on the nitrocellulose and DEAE membranes, respectively. The data points represent the averages of ≥ 3 repeats of the same experiment, and the error bars correspond to the standard deviations.

2.6.1.1 Measurement of association kinetics

Standard binding reactions (**Section 2.6.1**) were scaled up 3-fold. For preincubation experiments, Mcm complexes were either incubated with ATPγS or 100 mM potassium glutamate (as noted) for 30 minutes at 30°C prior to addition of radiolabeled oligo (#510 for reactions containing chloride or #826 for reactions containing glutamate) and the remaining reaction components at t = 0. At the indicated times, 5 μL samples were withdrawn and analyzed by filter binding. Final reactions contained 5 mM ATPγS, 4 nM radiolabeled oligo,

and 120 nM Mcm protein. In some cases, the association kinetics data was plotted as described [174, 175] using Equation 2,

$$\left[\frac{1}{(R)-(O)}\right]\ln\left[\frac{(O)[(R)-(RO)]}{(R)[(O)-(RO)]}\right]=k_a t$$

where (R) and (O) are the total concentrations of MCM and ssDNA, respectively, and (RO) is the concentration of MCM/ssDNA complex formed at time *t*.

2.6.1.2 Measurement of dissociation kinetics

Standard binding reactions (**Section 2.6.1**) were scaled up 3-fold. After incubation at 30°C, an excess of non-radiolabeled substrate was added as a competitor. At the indicated times, 5 μL samples were withdrawn and analyzed by filter binding. The dissociation kinetics data was plotted as previously described [174] using Equation 3,

$$\ln\frac{(RO)}{(RO)_0}=k_d t$$

where (RO) represents the concentration of MCM/ssDNA complex at time *t* and $(RO)_0$ is the initial concentration of MCM/ssDNA complex at t = 0.

2.6.1.3 Circular vs. linear ssDNA competition

Reactions contained 120 nM Mcm complex, 5 mM ATP, 5 mM β-glycerophosphate, and 4 nM radiolabeled oligo #826 (Table 1) with the indicated amount of either circular or linearized M13mp18 ssDNA in buffer B2 with a final volume of 12.5 μL. The reactions were incubated for 30 minutes at 30^{o}C and the results were quantified using the standard double filter binding assay.

2.6.1.4 Circularization assay

All reactions contained the same reagents (120 nM Mcm complex, 5 mM nucleotide, 5 mM β-glycerophosphate, 5 mM sodium fluoride, 5 nM radiolabeled oligo (#455 for experiments in chloride-containing buffer, #826 in glutamate-containing buffer), and 10 μg/μL circular, linear M13mp18 ssDNA, or 1x TE (no competitor control) in buffer B2 with a final volume of 40 μL) but varied in the order of addition. Reactions labeled "no comp" contained all of the reagents (except M13 competitor ssDNA) added simultaneously and incubated at 30°C. In the reactions labeled "cir 1st" and "lin 1st," all reagents except ATPγS were present at t = 0 and incubated at 30°C; nucleotide was added at t = 60 min and incubation continued at 30°C. In the reactions labeled "cir 2nd" and "lin 2nd," all reagents other than β-glycerophosphate, sodium fluoride, labeled oligo, and M13 ssDNA were present at t = 0 and incubated at 30°C; the remaining reagents were added at t = 60 min and incubation continued at 30°C. When indicated, 5 μL aliquots were removed from each reaction and Mcm/radiolabeled probe complexes were measured using the double filter binding assay. Note that there is a relatively high degree of ssDNA binding prior to ATP addition using oligo #455. The Mcm circularization assays were also repeated using a variety of different oligonucleotide probes. While most of them demonstrate less ATP-independent binding, they also provide less discrimination between circular ssDNA binding and linear ssDNA binding in this assay.

2.6.2 Magnetic bead binding assay

Streptavidin-coated Dynabeads (M280, Dynal Biotech ASA, Oslo, Norway) were prepared per the manufacturer's instructions. Biotinylated oligonucleotide #455 was immobilized on the beads

in buffer B1 for ≥30 min at 22 °C, and the oligo-bound beads were separated by a magnet and washed to remove unbound oligonucleotide. Experiments using a radiolabeled oligonucleotide indicate that about 90 pmol of oligonucleotide were bound per 1 mg of beads. For each binding experiment, 20 μL of beads were used. Following equilibration in buffer B3, the beads were resuspended in 25 μL reactions containing B3, protein, and nucleotide as indicated and incubated for ≥30 min at room temperature. The beads were separated from unbound reaction components with a magnet, washed once with 50 μL of either B3 or B3 supplemented with additional sodium chloride as indicated, resuspended in 10 μL B3, and analyzed by SDS-PAGE and Sypro orange staining.

2.6.3 Electrophoretic mobility shift assay

Standard MCM/ssDNA binding reactions were set up as for the double filter binding assay (**Section 2.6.1**) containing 4 nM of radiolabeled oligo #3 and 5 mM ATPγS. Following a 30 minute incubation at 30°C, the reactions were separated by electrophoresis at 4°C through a pre-chilled 3.5% native polyacrylamide gel (30:1 acrylamide:bis) containing 5% glycerol, 67 μg/ml acetylated BSA (Sigma), and 10 mM magnesium acetate for 1 hour at 15 volts/cm (150 V) in 0.5x TBE supplemented with 80 μg/ml BSA and 10 mM magnesium acetate. Protein/ssDNA complexes were imaged and quantified using a Fuji FLA-5100 phosphoimager and Image Gauge software.

2.7 HELICASE ASSAY

The helicase assay was performed essentially as described [63]. Briefly, synthetic replication forks were prepared by annealing an equimolar mixture of oligonucleotides #233 and 235 and then filling in the resulting 5' overhang with [^{32}P]dATP in the presence of the other dNTPs using reverse transcriptase. The resulting forks were then gel-purified from an 8% native acrylamide gel following electroelution into a dialysis membrane, ethanol-precipitated, and resuspended to a concentration of ~1 μM in 1x TE. The reactions were incubated for 1 h at 37 °C, stopped by the addition of unlabeled oligonucleotide #235 to 20 nM, proteinase K to 4 mg/ml, SDS to 0.4%, and a one-tenth volume of 10 x stop-load (25% w/v Ficoll (type 400), 100 mM EDTA, 0.1% SDS, 0.25% bromphenol blue, and 0.25% xylene cyanol) and heated at 50 °C for 20 min. The samples were then separated on an 8% polyacrylamide gel at room temperature. The gel was subsequently dried, and the results were imaged and quantified using Fuji FLA-5100 phosphoimaging and Image Gauge software.

2.7.1 Preparing radiolabeled forks

DNA forks were radiolabeled by 5'-end labeling with T4 polynucleotide kinase and [γ^{32}P]ATP (any oligo), filling in sticky ends with either Klenow Fragment (3'–> 5' exo$^-$) or M-MuLV reverse transcriptase and [α^{32}P]dATP ("Hurwitz" oligos, *e.g.* #233 & 235), or adding [α^{32}P]dATP to the 3' end using terminal transferase (any oligo). The best results came from forks that had been filled in as Mcm preparations occasionally contain a contaminating phosphatase activity. Labeling the forks with biotinylated dNTPs, *etc* could be done as above.

To form the forks, the oligos were mixed at equimolar concentrations in 1x NEB buffer #2 and annealed overnight in a PCR thermocycler using the following program:

95°C for 10 min
Gradient cooling @ 0.5°C/min
65 °C for 5 hr
Gradient cooling @ 0.5°C/min
25°C for 3 hr
4°C hold

While this was a convenient overnight step, it could be successfully shortened by incubating the oligo mixture in a 95°C heat block for 5 min and transferring it to a 75°C heat block for 15 min. The power to the heat block was then shut off, and the block cooled slowly to room temperature (~1 hr).

The forks were gel purified to separate them from unannealed oligos and free ^{32}P-ATP. This required a large 8% (29:1 acrylamide:bis) native gel (see below) run in 1xTBE.

5x TBE	9 mL
29:1 acrylamide:bis	9 mL
H_2O	27 mL
10% ammonium persulfate	400 µL
TEMED	100 µL

5 µL of 10x SL buffer was added to the forks, and the entire reaction was loaded in one lane on the gel. The gel was run at 200 V for 1-2 hr until the bromphenol blue dye was 1/3-1/2 of the way down the gel. Free ATP runs faster than the dye front but stays on the gel if the run is sufficiently short. After electrophoresis, the gel plates were dried with paper towels, one of the plates was removed, and the remaining plate/gel combination was wrapped in plastic wrap. The gel was either exposed to film for ~1 min or to a phosophoimaging plate (the Departmental plate marked “Do Not Use” works perfectly) for ~10 min. The gel was then aligned with either the film or printout of the phosphoimaging, and the fork band was excised with a razor blade.

To electroelute the forks, the gel slice was placed into a piece of clean dialysis tubing (Spectra/Por membrane, MWCO: 1,000) with 150 μL 0.5x TBE, one end was clamped off, bubbles were removed, and the other end was then clamped shut. This dialysis setup was placed into a small agarose gel electrophoresis chamber (filled with 1x TBE) such that the current would run perpendicular to the long edge of the gel slice. The forks were electroeluted at 100 V for 45 min, the current was reversed for 30 sec to free any fork interacting with the dialysis membrane itself, and the buffer inside the membrane was collected. This was repeated at least once more to recover the majority of the radioactive counts from the gel slice. The best results came from placing the dialysis setup back into the electrophoresis chamber in the same orientation as the first run. Additional repeats freed more forks from the gel, but as the TBE buffer heated up, forks fell apart. The forks were phenol/chloroform extracted, EtOH/NH_4OAc precipitated, and resuspended in TE.

The amount of contaminating free oligo (*i.e.,* background) was always determined. A small volume of the fork (~0.2 μL) was mixed with 1x SL buffer, either placed on ice or boiled and then placed on ice, and loaded onto a small 8% native TBE gel:

1.5 mL 5x TBE
2 mL 29:1 acryl to bis
4.45 mL H_2O
80 μL 10% APS
20 μL TEMED

The gel was run at 200 V for 30 min, dried, and exposed to an IP plate. The background (ratio of ssDNA counts to fork counts) was calculated with MultiGauge software.

2.7.2 Antibodies and blocking peptides

Antibodies were purchased from Santa Cruz Biotechnology (anti-Mcm2 (sc-6680) and SC-7 (sc-6688)) or are mouse monoclonals (anti-Mcm4 (AS6.1) and two different antibodies that recognize the Walker B box on all 6 subunits, (AS1.1 and AS4.1; ([126]; A. Schwacha and S. Bell, unpublished). Blocking peptide (NP-2) for SC-7 (sc-6688P) was from Santa Cruz Biotechnology, and blocking peptides to AS4.1 and AS1.1 (Walker B sequence, IDEFDKMAD, neutralizing peptide 1, NP-1) and a randomized Walker B sequence (IEKFMDDAD, randomized peptide, RP) were prepared by the Peptide Synthesis Facility at the University of Pittsburgh. For antibody neutralization of the Mcm467 helicase, a 1:6 dilution of the mouse monoclonal or a 1:30 dilution of the Santa Cruz antibodies were added to Mcm proteins and incubated for 30 minutes at 30°C prior to addition of DNA and ATP. Blocking peptides were added to a final concentration of ≤0.8 ng/μL and incubated with the antibodies for 30 minutes at 30°C prior to Mcm addition.

2.7.3 Chemical modifiers and inhibitors

Stock solutions (~13 mM) of the pyrimidinone-peptoid hybrid molecules MAL2-11B, MAL3-51, and MAL3-101 (a gift from Jeffrey Brodsky; [176]) were made in 100% DMSO. One hundred mM stock solutions of chemical modifiers (2-ethoxy-1-ethoxycarbonyl-1,2-dihydroquinoline (EEDQ; Aldrich), N,N'-dicycolhexylcarbodiimide (DCCD; Sigma), phenylglyoxal monohydrate (Aldrich), pyridoxal phosphate (Fluka), and 4-chloro-7-nitrobenzofurazan (Nbf; Fluka)) and quinolone antibiotics (nalidixic acid (Sigma), ofloxacin (Sigma), levofloxacin (Fluka), and ciprofloxacin (Fluka)) were made in 10% DMSO. In some cases, the compounds were not

completely soluble at 100 mM, but dilutions to 10 mM for stocks and 1 mM in reactions generally solublized everything.

2.8 COUPLING APYRASE TO BEADS

Apyrase (Sigma, Grade I) was dissolved to 1 mg/mL in C buffer and dialyzed extensively overnight in the same buffer at 4°C. The enzyme was then conjugated to cyanogen bromide-activated Sepharose 4B resin (Sigma) per the manufacturer's instructions. Briefly, beads were washed and swollen in 1 mM HCl, incubated with apyrase in C buffer for 2 hr at room temperature, and blocked for 2 hr at room temperature in B buffer. The beads were then washed alternately in C buffer and A buffer four times. After a final wash in C buffer, a small aliquot of beads was used to determine the ATPase activity of the preparation, and the rest of the resin was stored in sterile coupling buffer at 4°C.

2.9 DNA METHODS

2.9.1 Mutagenesis and cloning

Standard molecular biology techniques and derivations thereof (see below) were used to clone and mutagenize the Mcms and related proteins.

2.9.1.1 Mcm ATPase alleles

The *MCM* Walker A, Walker B, and arginine finger alleles (Table 4) were generated by megaprimer mutagenesis [177] and the resulting mutations verified by complete sequencing of the respective *mcm* gene. As was done previously [104], these alleles were cloned into three different vectors: 1) pUP169, a *TRP1 ARS/CEN* vector for genetic complementation testing that expresses a HA/His_{10} C-terminal epitope tagged version of each allele under the control of the *MCM5* promoter; 2) a *LEU2* integration vector for dominance testing that expresses each allele under the inducible *GAL1-10* promoter and adds a C-terminal 3xHA (pUP221), 3xMyc (pUP782), or FLAG (pUP184) epitope tag as indicated; and 3) into bacmid vectors to generate recombinant baculovirus for protein expression (Gibco Bac-to-Bac system). These C-terminal epitope tags have been previously shown to neither interfere with Mcm complex formation during recombinant protein production nor viability during genetic complementation [104]. Yeast strains used in this study are *bar1 lys2* derivatives of *S. cerevisiae* W303 [178].

2.9.1.2 *MCM4* beta-hairpin finger alleles

Bioinformatic analysis suggested that *S. cerevisiae* Mcm4 had a conserved beta-hairpin "finger" containing residues important for DNA binding [58]. Various mutageneses were carried out in order to test the importance of this region of the protein. Positive charge was eliminated by making alanine substitution mutations in Mcm4 at R445 & N447 or H465 & K467 via megaprimer PCR [177] using oligos #372 & 373 or 374 & 375 (respectively) as primers and pUP745 as a template. The reactions were treated with *Dpn*I for 1 hr at 37°C to degrade the parental plasmid DNA, the newly synthesized doubly nicked plasmids were transformed into XL10-Blue *E. coli*, and the mutations were verified by sequencing. The quadruply neutralized mutant was made by subjecting the R445A,N447A plasmid to second round of megaprimer PCR

using oligos #374 & 375. These constructs were transformed into the *S. cerevisiae MCM4* swapper stain (UPY115) and tested for viability.

An "amputation" allele of *MCM4* was made by deleting the putative beta-hairpin finger. Briefly, oligos #392 and 96 were used to amplify a portion of *MCM4* with the finger replaced by a glycine and proline (*Apa*I site) flanked on either side by two alanines. The PCR product was digested to make sticky ends and subcloned into *MCM4* in pUP229. Similarly, "constipation" alleles that made the beta-hairpin finger longer were created via PCR and subcloning as above but using oligos #389 (marked with *Eag*I), 390 (marked with *Bss*HII), or 391 (marked with *Apa*I). All mutations were verified by sequencing, and the constructs were transformed into *S. cerevisiae* strain pUP229 to test for dominant lethality.

2.9.1.3 Random PCR mutagenesis

Randomly mutagenized *mcm*s were created with the GeneMorph II EZClone Domain Mutagenesis Kit (Stratagene) following the manufacturer's instructions. Briefly, *MCM* genes were PCR-amplified from ~0.5 μg plasmid DNA (Table 2) using an error prone polymerase and oligos #354 and 285 as primers. The resultant PCR products were electrophoresed through a 0.7% agarose gel, stained with ethidium bromide, and quantified using an LAS-3000 Intelligent Dark Box (Fujifilm) and Image Gauge software. 500 ng of each PCR product was then used as a megaprimer to prime synthesis of the original plasmids by a high fidelity polymerase using an 18 min extension time. The reactions were then treated with 10 U *Dpn*I to digest the parental plasmid DNA, and XL10-Gold ultracompetent *E. coli* were transformed with 4 μL of the DNA.

The efficiency of the above protocol was often poor. To generate a larger library of usable plasmids, the megaprimers above were digested with *Xho*I/*Sac*I (*MCM2, 3,* and *4*),

*Xho*I/*Bss*HII (*MCM5* and *6*), or *Xho*I/*Bam*HI (*MCM7*) and ligated into pUP169 cut with the same restriction enzymes using T4 ligase. Ligation reactions (10 μL) proceeded overnight at room temperature, and XL10-Gold *E. coli* cells were transformed with the entire reaction. More than 4,000 clones were recovered for each transformation, and the individual transformants were pooled to create six randomly mutagenized *mcm* plasmid libraries (Table 2) for genetic screening.

Table 2. Plasmids and genes involved in random mutagenesis.

Amplified Gene	Parental Plasmid	Mutant plasmid library created
MCM2	pUP197	pMCM2*
MCM3	pUP201	pMCM3*
MCM4	pUP745	pMCM4*
MCM5	pUP208	pMCM5*
MCM6	pUP213	pMCM6*
MCM7	pUP217	pMCM7*

2.9.2 Baculovirus recovery and sequencing

The Mcm5DENQ baculovirus DNA was recovered by TCA-precipitating 1 mL of the SF9 cell spinner culture supernatant stock. The pellet was washed with 2 mL acetone, pipetting up and down to break up the pellet. The solution was then spun at max speed for 10 min at 4°C, the acetone removed completely, and the pellet allowed to dry. It was then treated/solublized with 200 μL SDS-Proteinase K for 1 hr at 37°C. The solution was phenol/chloroform extracted twice, and the baculovirus DNA was ethanol precipitated and resuspended in 20 μL TE. The *mcm5DENQ* gene was then PCR-amplified by standard methods using oligos #283 and 105 as primers. The same primers were then used for forward and reverse sequencing reactions by GENEWIZ, Inc.

2.9.3 Rescue of integrated plasmids

Genomic DNA was isolated from saturated overnight cultures (10 mL) by glass bead lysis. Briefly, cultures were pelletted in a tabletop centrifuge for 5 min at 1500 rpm, resuspended in 1 mL H_2O, and transferred to screw cap eppendorf tubes. The cells were pelletted at max speed in a microcentrifuge, washed with 1 mL H_2O, and pelletted as before. After removal of the water, the cells were resuspended in 200 µL Extraction Buffer (0.5 M NaCl, 0.2 M Tris-HCl (pH 7.6), 0.01 M EDTA, ±1% SDS) and freeze/thawed to help lysis. Glass beads were added to the 0.4-0.5 mL mark followed by 200 µL phenol/chloroform. The tubes were vortexed for 2.5 min, 300 µL each of extraction buffer (minus SDS) and phenol/chloroform were added, the tubes vortexed for an additional 1 min, and then spun down in a microfuge for 4 min. Genomic DNA was ethanol precipitated from the aqueous phase and resuspended in 50 µL TE. To recover the integrated plasmid DNA, 5 µL of genomic DNA was digested with *Bst*XI for 2 hr at 55°C, phenol/chloroform extracted, ethanol precipitated, resuspended in 20 µL TE, and ligated with T4 ligase. Half of the ligation reactions were then used to transform super-competent XL10-Gold *E. coli* cells. Plasmid DNA was mini-prepped from the transformants and sequenced to verify the presence of *mcm4* allele (oligo #306).

2.9.4 High efficiency yeast plasmid rescue

This method is based on the plasmid rescue protocol used by the Keeney Lab at Juniata College, Huntingdon, PA. Yeast strains were grown to high density overnight in 2 mL cultures, and each culture was harvested in a single 1.5 mL tube. The media was decanted, and 250 µL each of

Qiagen buffer P1 and glass beads were added. The culture was then vortexed for 3-5 min followed by addition of 250 μL Qiagen buffer P2 to aid in cell lysis. After gentle mixing, the solution was neutralized by 350 μL Qiagen buffer N3 and immediate but gentle mixing. Cellular debris was pelletted for 10 min at max speed in a microcentrifuge, and the supernatants were applied to QIAprep spin columns. The remainder of the procedure follows the Qiagen protocol. Briefly, the column was centrifuged for 45 sec and the flow-through discarded. The column was then washed with 750 μL Qiagen buffer PE and spun as above twice, discarding the flow-through each time. The column was placed into a clean tube, 50 μL Qiagen buffer EB was added and incubated for 1 min at room temp, and the column was then centrifuged for 1 min at max speed to elute plasmid DNA. Transforming chemically competent *E. coli* MH1 cells with 2-5 μL of the eluate was sufficient to recover hundreds of transformants.

2.10 ATPase ASSAY

ATPase assays were carried out essentially as described in [104]. Standard reaction conditions measured either "high affinity" (25 μL reaction containing 0.5 μg of Mcm protein, 250 μM Mg^{+2}ATP (unlabeled ATP spiked with a small amount of α^{32}P ATP at 800 Ci/mmol), and 100 μM potassium glutamate all in 1x H buffer) or "low affinity" (same as above but 2 μg Mcm and 5 mM Mg^{+2}ATP) ATPase activity. These were incubated at room temperature in duplicate for 0, 5, 10, and 30 min. The reactions were stopped by the addition of 0.5 μL 2% SDS and kept on ice until the time course was completed. Samples (1 μL) from each reaction were spotted in duplicate (1 cm apart from each other) on Cellulose PEI TLC plates (Baker), and thin layer

chromatography proceeded in 1 M formic acid/0.4 M LiCl in an enclosed glass chamber until the solvent front reached the top of the plate. Plates were dried in a fume hood, wrapped in plastic wrap, and exposed to a phosphoimager plate for ~12 hr. The plates were scanned with a FLA-5100 imager (Fujifilm), and the conversion of α^{32}P-labeled ATP to ADP was quantified using Image Gauge software. The resulting reaction rate was plotted as a function of time. ATP hydrolysis under these conditions is linear with respect to time and protein concentration [104]. Results are reported as the number of molecules of ATP hydrolyzed/Mcm complex/minute (turnover).

2.11 ARRAY SOUTHWESTERNS

Mcm INTAVIS (ABIMED) peptide arrays were made by the M.I.T. Biopolymers Laboratory (Cambridge, MA) by spotting 12mer peptides (that cover the entire sequence of all six *S. cerevisiae* Mcm proteins with a 3 amino acid overlap between each peptide) onto 384-place membranes. Each array contains an HA sequence at the first and last positions as a control. The membranes were blocked overnight at 4°C with 5% milk in TBST and washed extensively in 1x TBS. Protein (2 μg/mL in TBS) was then added and incubated for 1 hr at room temp. Primary and secondary antibody additions and imaging follow standard western blot procedures. The membranes can be stripped by the usual method for re-probing western blots or in 8 M urea/1% SDS for 1 hr at 50°C in a roller bottle. Antibody controls were carried out essentially by treating the arrays (without bound protein) as normal western blots. This background signal was subtracted from the protein signal for final quantification.

2.12 PHOSPHORYLATING AND DEPHOSPHORYLATING MCMS

Phosphorylation reactions contained 1x B2 buffer, 1 μg Mcm complex, 500 μM ATP (a mixture of [γ-^{32}P]ATP and unlabeled ATP), and limiting amounts of purified S-phase specific CDK (Cdc28p/Clb5p; a gift from the Bell lab, M.I.T.) and were incubated for up to 2 hr at 37°C. The reactions were stopped by the addition of 2x SDS-PAGE sample buffer, run on 10% denaturing gels at 200V, and visualized by phosphoimaging. CDK phosphorylation could be inhibited by the addition of modest concentrations of Sic1p (a gift from the Bell lab, M.I.T.). In addition to the reagents above, dephosphorylation reactions contained 400 units lambda protein phosphatase (λ-PPase, NEB), 1x λ-PPase buffer, and 2 mM $MnCl_2$. The reactions were incubated for 1 hr at 37°C and visualized as above.

3.0 DIFFERENCES IN THE SINGLE-STRANDED DNA BINDING ACTIVITIES OF MCM2-7 AND MCM467: *MCM2 AND MCM5 DEFINE A SLOW ATP-DEPENDENT STEP*

The contents of this chapter, with some additions and alterations, come from [126] and are reprinted following the guidelines of the American Society for Biochemistry and Molecular Biology Journals' Copyright Permission Policy.

3.1 SUMMARY

The Mcm2-7 complex, a hexamer containing six distinct and essential subunits, is postulated to be the eukaryotic replicative DNA helicase. Although all six subunits function at the replication fork, only a specific subcomplex consisting of the Mcm4, 6, and 7 subunits (Mcm467) and not the Mcm2-7 complex exhibits DNA helicase activity *in vitro*. To understand why Mcm2-7 lacks helicase activity, and to address the possible function of the Mcm2, 3, and 5 subunits, we have compared the biochemical properties of the *Saccharomyces cerevisiae* Mcm2-7 and Mcm467 complexes. We demonstrate that both complexes are toroidal and possess a similar ATP-dependent single-stranded DNA (ssDNA) binding activity, indicating that the lack of helicase activity by Mcm2-7 is not due to ineffective ssDNA binding. We identify two important differences between them. Mcm467 binds dsDNA better than Mcm2-7. In addition, we find that

the rate of Mcm2-7/ssDNA association is slow compared to Mcm467; the association rate can be dramatically increased either by pre-incubation with ATP or by inclusion of mutations that ablate the Mcm2/5 active site. We propose that the DNA binding differences between Mcm2-7 and Mcm467 correspond to a conformational change at the Mcm2/5 active site with putative regulatory significance.

3.2 INTRODUCTION

Cellular DNA is double-stranded, yet during DNA replication it must be separated into component single strands. Although DNA polymerases require a ssDNA template for activity, they have little or no intrinsic ability to unwind dsDNA (reviewed in [6]). DNA unwinding requires an ATP-dependent molecular motor termed the replicative helicase (reviewed in [35]). In both prokaryotes and eukaryotes, the loading and activation of this helicase is a central and limiting event during DNA replication. Initiation culminates in replicative helicase loading, whereas the start of elongation requires extensive separation of duplex DNA by the helicase (reviewed in [84, 179]). Despite the critical importance of the replicative helicase, both its exact identity and mechanism remain controversial in eukaryotes.

Numerous studies implicate the Mcm proteins as the replicative helicase. The Mcms are evolutionarily conserved from archaea to eukaryotes, with the archaea usually having a single MCM gene [180] and eukaryotes having six distinct and essential Mcm genes (reviewed in [73]). Each Mcm protein (numbered 2-7) is an AAA^+ ATPase, whose members include DNA helicases such as SV40 TAg and the papilloma virus E1 protein [33]. Similar to prokaryotic replicative helicases [181], the six Mcm subunits are both physically present in initiation and elongation

complexes and functionally essential for both phases of DNA replication; evidence strongly suggesting that all six Mcm subunits unwind DNA at the replication fork (reviewed in [84]).

Despite *in vivo* similarities to other replicative helicases, biochemical examination of the Mcm complex has provided confounding results. Whereas the archaeal proteins have robust helicase activity [59, 98-100], a hexamer containing the six eukaryotic Mcm subunits (Mcm2-7) lacks this activity [101-104, 122]. In contrast, a hexameric subcomplex that specifically contains Mcm4, 6, and 7 (Mcm467) possesses a weak helicase activity [101, 122, 147].

Despite the apparent dispensability of the Mcm2, 3, and 5 subunits for *in vitro* helicase activity, their ATP active sites are essential *in vivo*. Mutational analysis of the Walker A ATP binding motif indicates that all six Mcm subunits require this motif for both viability and S-phase progression [104, 182]. *In vitro* analysis of the corresponding Mcm2-7 mutant complexes, however, indicates that the six Mcm subunits fall into two functionally distinct subgroups [104]. The Walker A motif in the Mcm4, 6, and 7 subunits is essential for ATPase activity; whereas the ATP binding motifs of the Mcm2, 3 and 5 subunits contribute little to steady-state ATPase hydrolysis [104]. The discrepancy between the *in vivo* involvement of all six subunits in DNA replication and the *in vitro* participation of only a specific subgroup of Mcm subunits in DNA unwinding remains unexplained. Recently, Mcm2-7 has been isolated *in vivo* as part of a larger macromolecular complex having ATP-dependent helicase activity; this complex additionally contains the essential GINS complex and Cdc45, suggesting that these factors are activators of Mcm helicase activity [183].

Although Mcm467 has been extensively characterized biochemically, little work has been done with the Mcm2-7 heterohexamer. To determine why the Mcm2-7 complex lacks helicase activity, as well as to elucidate the function of the Mcm2, 3, and 5 subunits, we have

undertaken a comparative analysis of the ssDNA binding activity of the *S. cerevisiae* Mcm2-7 and Mcm467 complexes. Our studies with Mcm2-7 indicate that its lack of DNA helicase activity is not due to an inability to bind ssDNA, since both complexes have similar ssDNA binding affinities. However, we find an important difference between these complexes in ssDNA association rates. Since these two complexes differ in subunit composition (*i.e.,* Mcm2, 3, and 5), the functional difference between them suggests that the additional subunits regulate the manner in which the Mcm2-7 complex interacts with DNA.

3.3 RESULTS

3.3.1 Mcm2-7 and Mcm467 form toroidal complexes of differing helicase activity

Hexameric preparations of *S. cerevisiae* Mcm2-7 and Mcm467 were expressed in baculovirus infected insect cells and purified to homogeneity (Figure 7). Gel filtration and co-immunoprecipitation of the final preparations demonstrated that the complexes retained their hexameric size as was observed previously [104], and these preparations contained approximately equal stoichiometry of the specified Mcm subunits as determined two-dimensional gel electrophoresis and quantitative Western blotting (Figure 7B, C, D, and F). As described below, these preparations demonstrated an ATP-dependent ssDNA binding activity, the average specific activity of our preparations for this activity is ≥50% of total protein (Figure 7E and legend).

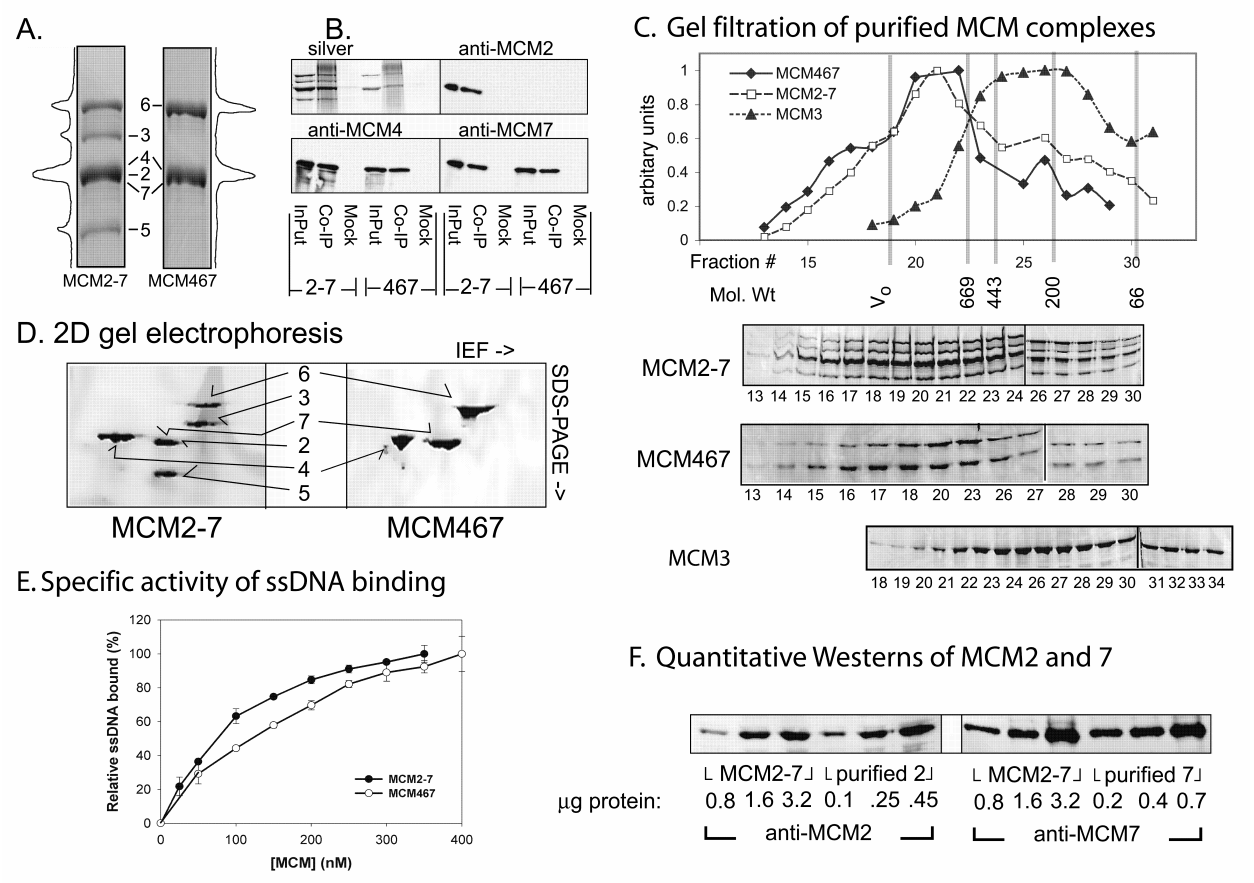

Figure 7. Characterization of purified Mcm2-7 and Mcm467 complexes.

A) SDS-PAGE and profile tracing of 3 pmol of representative Mcm2-7 and Mcm467 preparations. The identity of the Mcm subunits is as noted. The Mcm2, 4, and 7 subunits are of similar size and do not resolve. B) Co-immunoprecipitation of Mcm subunits from the final preparations. Western blots were used to verify that the co-migrating subunits in either the Mcm2-7 (Mcm2, 4, and 7) or Mcm467 (Mcm4 and 7) preparations. The same blot was stripped and re-probed for each Western. C) Gel filtration of final Mcm preparations. Preparations of Mcm2-7, Mcm467, and a single subunit preparation of Mcm3 as separated by gel filtration and the indicated fractions analyzed by SDS-PAGE. The calculated size of both the Mcm2-7 and Mcm467 hexamer is ~600 kDa, while that of the Mcm3 monomer is ~107 kDa**.** These data are consistent with our previous observation that Mcm2-7 runs at about 800 kDa and Mcm3 runs at about 200 kDa by gel filtration [104]. D) Two-dimensional electrophoresis of final Mcm preparations. Sypro orange stained gels are shown for Mcm2-7 (left) and Mcm467 (right). Indicated position of individual Mcm subunits were established by Western blotting using Mcm subunit-specific antibodies. Note that Mcm2 and Mcm7 could not be resolved by this approach. For Mcm467, the ratio of Mcm4:6:7 was 1.9:1:1.2, with Mcm6 being the least abundant subunit. Among various Mcm467 preparations used in this study, our quantitation suggests that up to 50-78% of the complexes have a 1:1:1 subunit stoichiometry. E) Examining the specific activity of ssDNA binding by our Mcm2-7 and Mcm467 preparations. ssDNA binding conditions are similar to that listed in Materials and Methods, except 100 nM of radiolabeled oligo 510 was used and ATPγS was present to 5 mM. ssDNA binding by the indicated amounts of Mcm2-7 or Mcm467 preparations are shown. Note: for technical reasons and difficulty of obtaining sufficient quantities, we are unable to conduct this binding experiment at sufficiently high reactant concentrations to accurately assess specific activity. Under the current conditions, the ratio of protein:DNA at each point represents the lower limit of specific activity. From this graph, 50% ssDNA binding of Mcm2-7 or Mcm467 corresponds to approximately 60% and 40%, of the calculated hexamers in these preparations, which we take as the minimal specific ssDNA binding activity. F) Quantitative Westerns to measure the amount of Mcm2 and Mcm7 in Mcm2-7 preparations. Indicated amounts of the final Mcm2-7 preparations and purified Mcm2 (left) or purified Mcm7 (right) were separated by SDS-PAGE, and

quantified by Western Blotting using subunit-specific antibodies. These data, in combination with the two dimensional gels in D), indicate that Mcm2 is the limiting subunit in these preparations. In the preparation shown, we calculate that relative to the purified Mcm2 standard, that one μg of Mcm2-7 complex contains 0.08 μg Mcm2. This is consistent with 48% of the Mcm2-7 complexes containing all 6 Mcm subunits in a 1:1:1:1:1:1 stoichiometry. Conclusion. Among the various Mcm2-7 and Mcm467 preparations used in this study, our data suggests that approximately 50% of the Mcm complexes in these preparations contain an equal subunit stoichiometry and roughly the same fraction is ssDNA binding competent. We however cannot exclude the possibility that a small fraction of the ssDNA binding observed in this dissertation emanates from Mcm subcomplexes, possibly pentamers.

Using transmission electron microscopy, the Mcm2-7 and Mcm467 preparations appear largely homogeneous (Figure 8A), with many individual complexes having a diameter (top) and height (side) of approximately 145 Å and an apparent central cavity 25-30 Å wide. Examination of hundreds of complexes from both preparations demonstrates that 20-30% appear as ring-shaped structures, with about half containing six distinct lobes (Figure 8A small insets). Image reconstruction of the ring-shaped structures indicates that both complexes are of similar size and have pseudo six-fold symmetry (Figure 8A large insets). These results are consistent with the published size and toroidal subunit organization of both eukaryotic Mcm complexes [124, 125, 127], as well as the archaeal MCM complexes [98, 117, 119, 121].

Both the Mcm467 and Mcm2-7 preparations were tested for helicase activity. While the Mcm467 complex displays ATP-dependent helicase activity (Figure 8B, lanes 4-7) similar to that of the SV40 large T antigen helicase (lane 3), Mcm2-7 displays no appreciable DNA unwinding (lane 8), and has an activity comparable to Mcm467 in the presence of ATPγS (lane 7). The difference in helicase activity between these two complexes reconfirms previous results [101, 102, 104, 122, 147, 184].

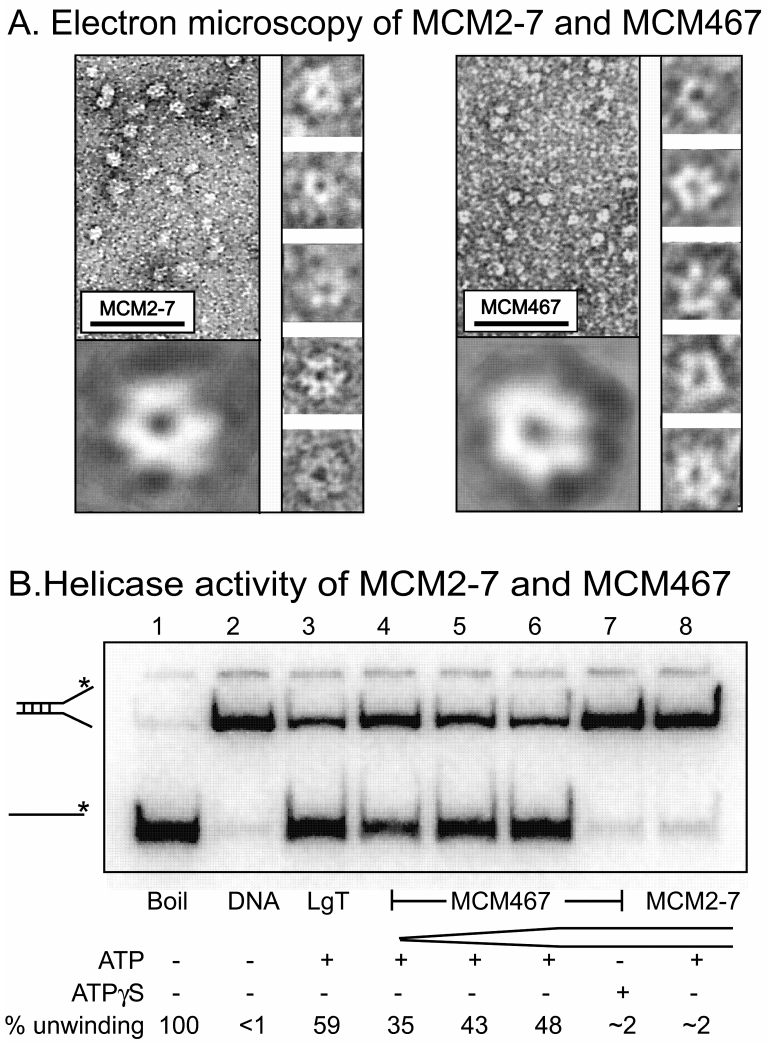

Figure 8. Comparison of Mcm2-7 and Mcm467.

A) Electron micrographs of both wide field and five individual hexamers of representative Mcm2-7 (*left panel*) and Mcm467 (*right panel*) preparations (supplemental materials). The *size bars* represent 100 nm (wide field) and 10 nm (individual hexamers), respectively. The large hexamer *inset* represents a composite of several dozen individual hexamers (supplemental materials). B) helicase assay. *Lane 1* shows dissociated ssDNA, and *lane 2* shows the position of the intact fork. *Lane 3* contains 1 pmol T-antigen monomer with ATP, and *lanes 4-6* contain 0.4, 0.8 and 1.6 pmol of Mcm467 with ATP. *Lane 7* contains 1.6 pmol of Mcm467 with ATPγS, and *lane 8* contains 1.6 pmol of Mcm2-7 with ATP. The percentage of DNA substrate unwound is indicated.

3.3.2 ATP-dependent ssDNA binding activity of the Mcm complexes

The ability of each Mcm preparation to bind a short mixed-sequence oligonucleotide (85 nt, #510, Table 1) using a filter binding assay was examined. Both complexes demonstrate ATP-dependent ssDNA binding as a function of either Mcm or ssDNA concentration (Figure 9A and B). Little ssDNA binding occurs in the absence of ATP (data not shown) or in the presence of GTP (Figure 9A). This interaction requires ATP binding but not hydrolysis; the poorly hydrolyzable ATP analog ATPγS [104] stimulates the extent of ssDNA binding for both complexes relative to ATP (Figure 9A). Further, this binding activity is Mcm-dependent, since it is abolished upon pre-incubation of either the Mcm2-7 or Mcm467 complex with a monoclonal antibody that specifically binds the Walker B site in each Mcm subunit (antibody AS1.1; data not shown; [185]; A. Schwacha and J. Bowers, unpublished). These data fit a hyperbolic function, consistent with a homogeneous population of molecules demonstrating non-cooperative binding. Repeats of this assay with shorter probes (oligos #3 (44 nt) and 775 (40 nt), Table 1) generate similar results (data not shown). Mcm phosphorylation appears to have little effect on ssDNA binding. Neither treating the complexes with lambda phosphatase to remove phosphorylation that may occur during insect cell expression, nor adding phosphates with a recombinant preparation of Cdc28/Clb5 (a gift from S. P. Bell, Mass. Institute of Technology) appreciably alters ssDNA binding levels (data not shown).

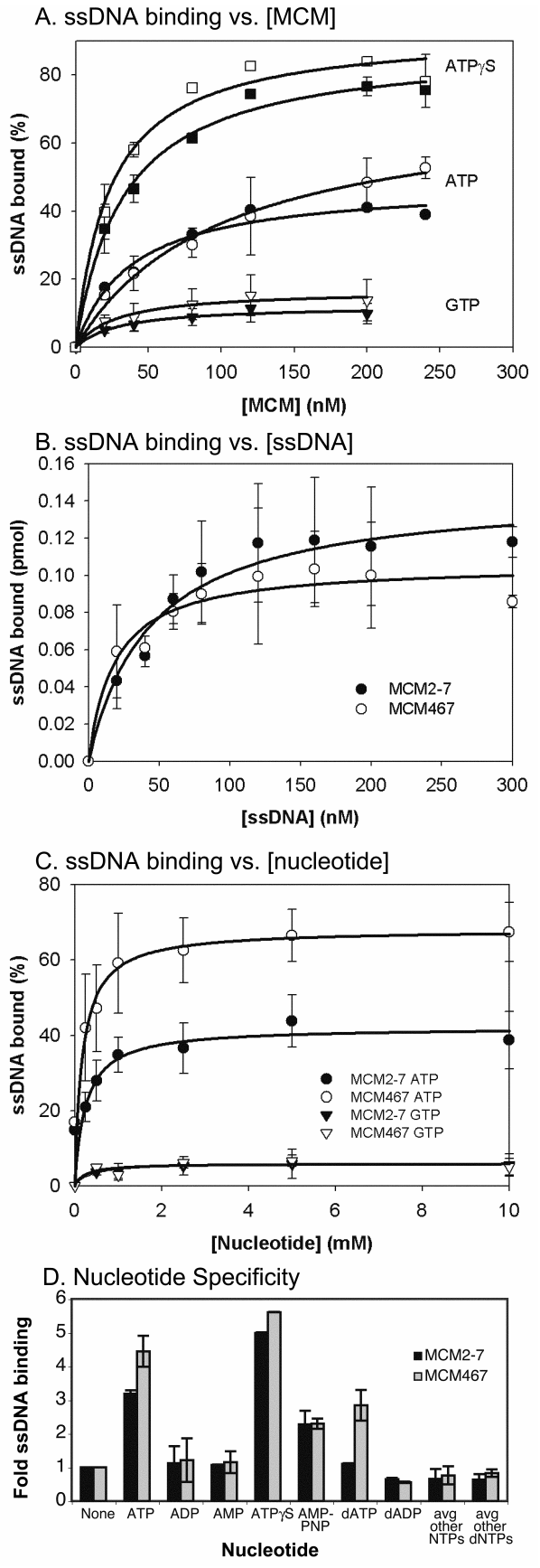

Figure 9. ATP-dependent ssDNA binding by Mcm2-7 and Mcm467 preparations.

Except as indicated, this filter binding assay uses 4 nM radiolabeled oligonucleotide #510 (Table 1) in a 12.5-µL reaction volume with 5 mM ATP and 120 nM of either Mcm2-7 or Mcm467. A) Mcm protein titrations. *Closed symbols*, Mcm2-7; *open symbols*, Mcm467. B) titration of ssDNA. Conditions were identical to those in *A* and used 5 mM ATP. C) ssDNA binding as a function of either [ATP] or [GTP]. D) Mcm ssDNA binding requires adenosine triphosphates. The *bar graph* represents standard filter binding reactions that contain 5 mM of the indicated nucleoside. The values indicated are relative to the level of ssDNA binding in the absence of added nucleotide (*None*).

From these graphs, an apparent K_d for ssDNA binding can be determined; using either ATP or ATPγS, both Mcm complexes have a K_d of ~35 ± 15 nM. The independent K_d values calculated from either the binding as a function of [Mcm] (Figure 9A) or [ssDNA] (Figure 9B) are in good agreement (Table 3). These values are in the range of those previously observed for Mcm467 (apparent K_d of ~2 nM using a 37mer oligonucleotide [124]) and the archaeal Mcm complex (apparent K_d of ~150-200 nM using a fork substrate [143]), and are typical of hexameric helicases (60 pM to 200 nM; [35]).

ATP-dependent ssDNA binding was further examined as a function of nucleotide concentration (Figure 9C). Both Mcm complexes have similar ATP dependencies (the $k_{1/2(ATP)}$ for Mcm2-7 and Mcm467 being 248±152 and 177±82 μM, respectively) with maximal ssDNA binding coinciding with physiological ATP concentrations (~3 mM; [186]). The nucleotide specificity of ssDNA binding by both Mcm complexes was also tested (Figure 9D). The triphosphate form of adenosine is needed to promote ssDNA binding, since neither ADP, AMP, dADP, nor any non-adenosine nucleotide support this activity (Figure 9D).

Table 3. Mcm physical constants determined in this study. [d]

Physical constant	Mcm2-7	Mcm467
ssDNA interactions		
K_d as a function of [Mcm], ATP	38.0±8.5 nM	50.0±18.2 nM
K_d as a function of [Mcm], ATPγS	32.8±4.3 nM	23.5±4.7 nM
K_d as a function of [ssDNA], ATP	43.6±9.7 nM	18.4±5.9 nM
K_d from EMSA, ATPγS	N.A.	~40 nM
$k_{a\ (apparent)}$, ATPγS (no pre-inc)	$4.22x10^5$ $M^{-1}min^{-1}$	$1.82x10^6$ $M^{-1}min^{-1}$
$k_{a\ (apparent)}$, ATPγS (pre-inc)	$2.28x10^6$ $M^{-1}min^{-1}$	$1.69x10^6$ $M^{-1}min^{-1}$
$k_{d,slow}$, ATPγS	0.0068 min^{-1}	0.002 min^{-1}
$k_{d,fast}$, ATPγS	0.0407 min^{-1}	0.0241 min^{-1}
K_d calculated from rate constants	17.8 nM	14.3 nM
dsDNA interactions		
Kd as a function of [dsDNA], ATPγS	2.1±0.2 μM	5.60±0.6 μM

[d] These physical constants are not corrected for the ssDNA binding specific activity of our preparations, which average about 50% (see Figure 7).

3.3.3 The identity of Mcm subunits within the Mcm·ssDNA complexes

The protein requirements for ssDNA binding were examined next. Filter binding experiments using various Mcm subcomplexes demonstrated little or no ssDNA binding, however when these subcomplexes were combined to generate either a Mcm467 (Mcm4/6 dimer + Mcm7 monomer) or Mcm2-7 (Mcm2/4/6 trimer + Mcm3/5/7 trimer) complex, high levels of ssDNA binding were recovered (data not shown, Figure 10A). These results indicate that ssDNA binding is not an intrinsic property of any individual subunit, but requires considerable oligomerization of Mcm subunits. The only subcomplex that demonstrated substantial ssDNA binding was a Mcm pentamer lacking Mcm6 (Figure 10A). This subcomplex is largely present as a variety of split-ring structures rather than a closed toroid as visualized by EM (data not shown) and illustrates that while higher order Mcm oligomerization is required for ssDNA binding, closure of the ring structure is not.

To identify the Mcm subunits that stably associate with ssDNA, binding experiments were performed using magnetic streptavidin beads coupled to biotinylated ssDNA (Figure 10B). Following addition of either the Mcm2-7 or Mcm467 complexes, the beads were washed in buffers of increasing salt concentration, and the proteins retained on the beads were analyzed by SDS-PAGE followed by either silver staining (Figure 10B) or Western blotting to identify co-migrating Mcm subunits (data not shown). In both cases, all input Mcm subunits were retained on the beads in a ssDNA-dependent manner, strongly consistent with the notion that intact Mcm hexamers bind ssDNA. Furthermore, these interactions are stable in moderate concentrations of salt as observed for Mcm complexes on chromatin isolated during S-phase (stable to >250 mM; [187]), in contrast to the salt-sensitive chromatin binding observed during G1 [187, 188].

To examine the oligomeric state of the Mcm/ssDNA complexes, an electrophoretic mobility shift assay (EMSA) was used (Figure 10C). The ability of Mcm complexes to bind ssDNA in this assay varies widely*:* several studies only observe a shift of Mcm467 in the presence of a cross-linking agent [122, 124], or that the shift is inhibited in the archaeal Mcms by ATPγS [98]. However, other studies with Mcm467 have observed ATPγS-dependent mobility shifts [103, 147]. Using the Mcm467 complex and radiolabeled oligo #3 (44 nt), we observe nucleotide-dependent binding (using ATPγS); titrations with increasing amounts of Mcm467 suggests a K_d of a magnitude similar to the K_d observed by filter binding (Table 3, ~40 nM). However, unlike the filter binding experiments, this activity is only supported by ATPγS but not ATP (Figure 10C lane 5). Only one shifted band was present throughout the range of the protein titration, suggesting that the Mcm467/ssDNA complex represents a single, defined species, although we cannot rule out the possibility of different co-migrating Mcm/ssDNA complexes. This conjecture is further supported by experiments using the longer oligo 510 (85 nt) as a probe; again only a single shifted species was observed over the range of Mcm concentrations (data not shown).

In contrast, under identical assay conditions, the Mcm2-7 complex demonstrates little or no electromobility shift (Figure 10C lanes 6-8, maximum shift = ~5%). These results suggest that even though the K_d values for these two complexes are similar as determined by filter binding, the Mcm2-7 complex is more susceptible to dissociation from ssDNA under these conditions than the Mcm467 complex.

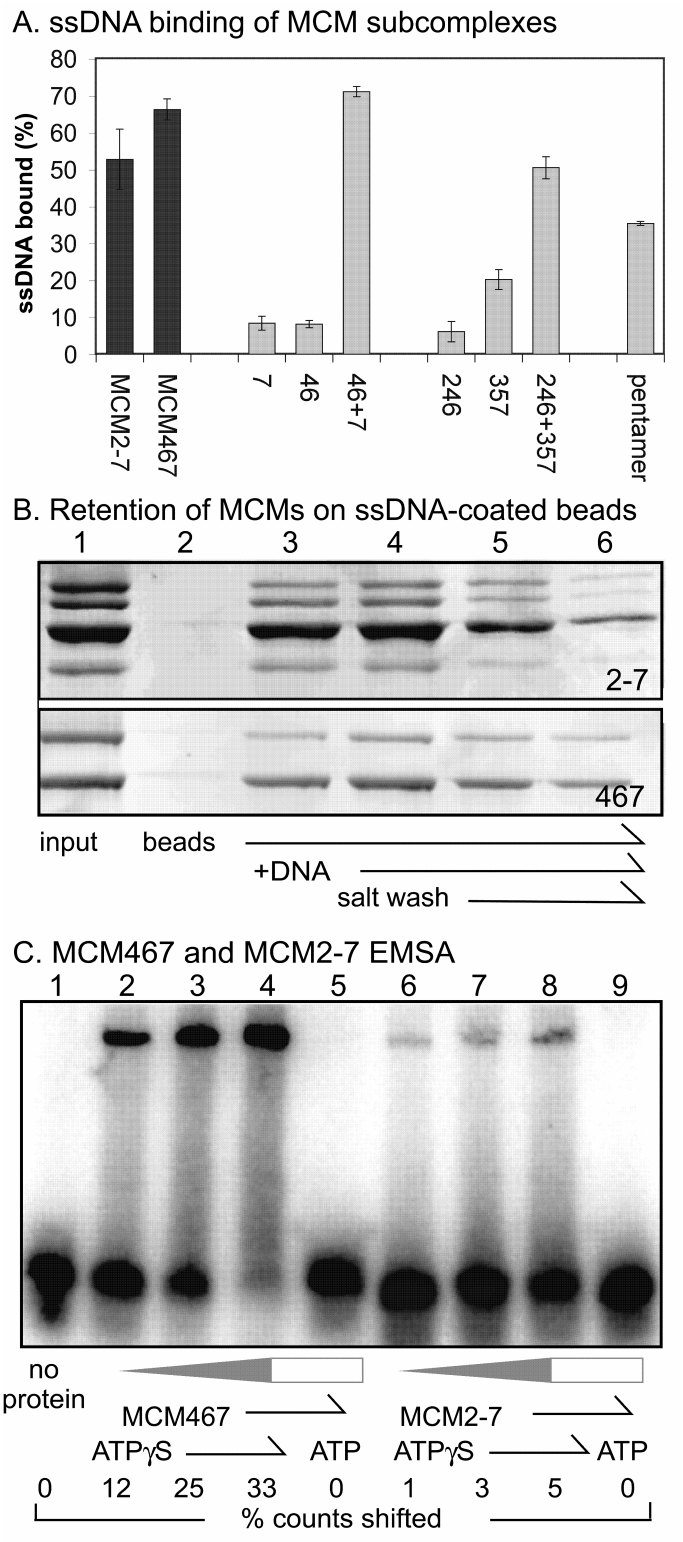

Figure 10. Mcm subunit involvement in ssDNA binding.

A) Filter binding of 120 nM of the indicated Mcm subcomplexes with ssDNA, 5 mM ATPγS, and 4 nM oligonucleotide #510 (Table 1). B) A magnetic bead binding assay containing biotinylated ssDNA. *Lane 1*, input protein (2.5 pmol) alone; *lane 2*, naked beads incubated with protein; *lane 3*, ssDNA-coated beads incubated with protein; *lanes 4-6*, ssDNA-coated beads incubated with protein and 5 mM ATP. The reactions in *lanes 1-4* were washed with buffer containing 50 mM NaCl; the sample in *lane 5* was washed with buffer containing 250 mM NaCl, and the sample in *lane 6* was washed with buffer containing 500 mM NaCl. Although the assay is ssDNA-dependent, it is not ATP-dependent. We speculate that the effective ssDNA concentration on the surface of the beads is sufficiently high to drive Mcm binding even in the absence of ATP. C) Electrophoretic mobility shift assay of Mcm/ssDNA binding. The reactions contained radiolabeled oligonucleotide 3 (Table 1) and 5 mM ATP or ATPγS with increasing amounts of Mcm protein (see "Materials and Methods" for details). *Lane 1*, no protein; *lanes 2-4*, 37.5, 75, 150 nM Mcm467 with 5 mM ATPγS; *lane 5*, 150 nM Mcm467 with 5 mM ATP; *lanes 6-8*, 37.5, 75, 150 nM Mcm2-7 with 5 mM ATPγS; *lane 9*, 150 nM Mcm2-7 with 5 mM ATP. The percentage of total counts shifted is noted.

3.3.4 Polynucleotide substrate requirements for Mcm·ssDNA binding

The sequence specificity of Mcm/ssDNA binding was assayed using the ability of unlabeled polynucleotides to compete with radiolabeled ssDNA for binding. Prior to addition of Mcm complexes, labeled oligonucleotide was mixed together with a 1-fold (not shown), 10-fold (not shown) or 100-fold (Figure 11A) weight excess of the indicated DNA or RNA homopolymers; the observed competition was dosage-dependent and increased with higher competitor levels. In general, the Mcm2-7 complex demonstrates a higher degree of sequence specificity than Mcm467. As previously reported [101, 147], poly(dT) is the best competitor for Mcm467; however, Mcm2-7 demonstrates an even higher preference (about 2.5 times better competition) for poly(dT) than Mcm467. Similarly, poly(dC) competes for ssDNA binding with both Mcm2-7 and Mcm467, although not to as high a degree as poly(dT). In addition, polyribonucleotides are also capable of competing for binding, with poly(G) and poly(U) being the most effective. RNA binding by Mcm467 has previously been shown [142].

The DNA length-dependence of the Mcm/ssDNA interaction was next tested (Figure 11B). Competition experiments using unlabeled poly(dT) oligonucleotides of various defined lengths indicate that ssDNA of 15 nt is capable of competing, although maximum competition requires a length of ≥40 nt. The results were the same for both complexes, and are similar to previous studies of ssDNA binding by Mcm467 (between 37 and 50 nt; [103, 122, 124, 147]). These experiments do not indicate the location of the ssDNA binding site within either Mcm complex. However, assuming an axial rise of approximately 3.5 Å/base for single-stranded poly(dT) [189], a 40 nt oligo corresponds to a length of 122.5-140 Å. This is similar to the

observed length of the central channel (~145 Å, Figure 7C), consistent with the likelihood that ssDNA binding occurs in this region.

The ability of the Mcm2-7 and Mcm467 complexes to bind blunt-ended dsDNA was also examined. Using a double-stranded form of our standard probe (85 bp, Materials and Methods), filter binding was performed as a function of Mcm concentration (data not shown). The binding affinity of either complex for dsDNA was considerably less than for ssDNA, precluding a determining of a K_d by this approach Like the ssDNA binding activity, dsDNA binding is ATP-dependent and is blocked by pre-incubation with antibody AS1.1 (data not shown). To obtain an estimate of K_d, a competition experiment was conducted to quantify the ability of dsDNA to compete for Mcm ssDNA binding, yielding a K_d of approximately 5.60 μM for Mcm2-7 and 2.12 μM for Mcm467 (Figure 11C, Table 3). Mcm467/dsDNA binding has been previously observed for probes with 3' ssDNA tails [52, 63], but we find that probes containing either a 10 nt 3' or 5' extension are bound similarly to the blunt ended probe (data not shown).

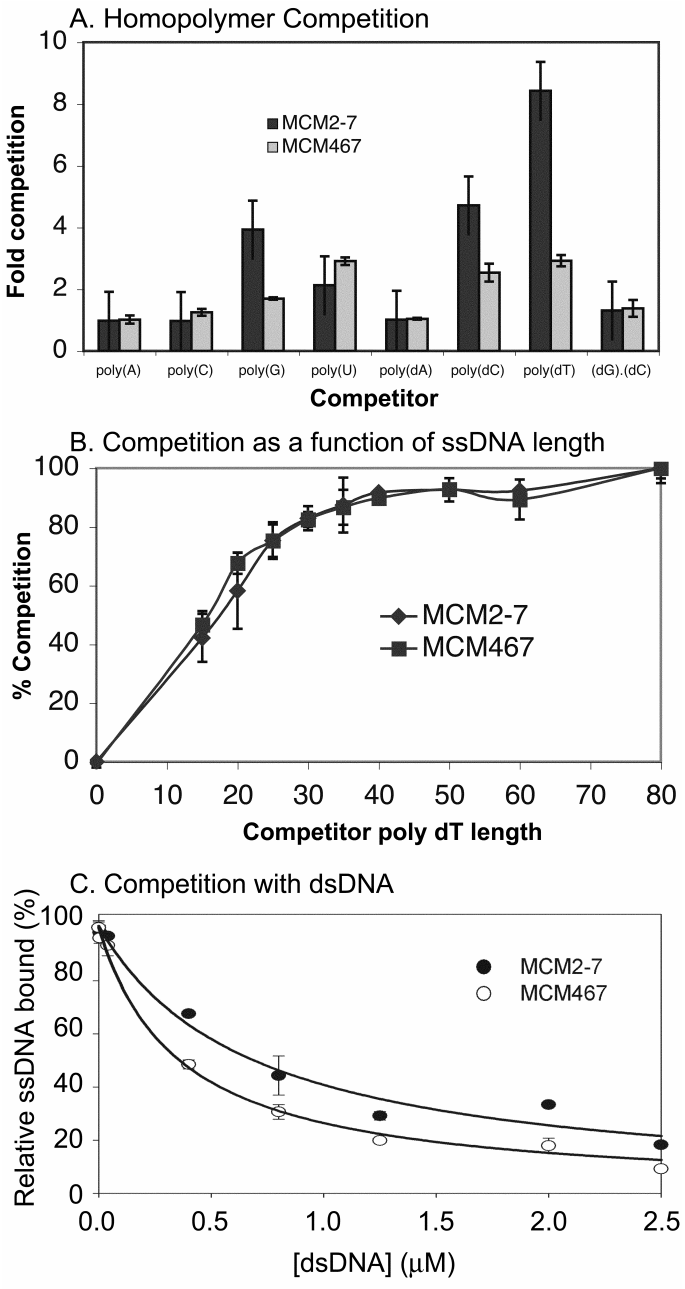

Figure 11. Substrate requirements for Mcm binding.

The reactions in A) and B) contained unlabeled competitor RNA or DNA with 120 nM Mcm2-7 or Mcm467, 5 mM ATPγS, and either 4 nM radiolabeled oligonucleotide 510 (A) or oligonucleotide 778 ((B); Table 1). Competitor and radiolabeled ssDNA substrates were mixed prior to protein addition. A) competition of 100-fold weight excess of unlabeled ssRNA, ssDNA, and dsDNA homopolymers for either Mcm2-7 or Mcm467 binding to labeled oligonucleotide. The results were plotted as fold competition, where a 10-fold competition corresponds to a 90% reduction in Mcm binding to the labeled oligonucleotide. B) the addition of 100-fold molar excess of unlabeled poly(dT) competitor ssDNA oligonucleotides of length 15, 20, 25, 30, 35, 40, 50, 60, or 80 nt to standard binding reactions containing radiolabeled poly(dT) 80mer. C) the indicated amount of unlabeled dsDNA substrate was added to standard ssDNA binding reactions (4 nM ^{32}P-labeled oligonucleotide 510, 120 nM Mcm hexamer, 5 mM ATPγS, final volume of 12.5 μL). The reactions were incubated and filtered as described under "Double Filter Binding Assay." The data were normalized to the "no competitor" reaction and plotted as hyperbolic decay using nonlinear regression. The IC_{50} = 683 ± 78.6 nM and 360 ± 26.5 nM for Mcm2-7 and Mcm467, respectively.

3.3.5 Mcm2-7 and Mcm467 associate differently with ssDNA; Mcm2-7 has an additional ATP-dependent step

To further examine ssDNA binding by both complexes, the dissociation and association rates (k_d and $k_{a\ (apparent)}$, respectively) were measured. The observed dissociation for the two complexes was quite similar and slow (Figure 12), with the Mcm467 complex having a slightly slower k_d than the Mcm2-7 complex. Interestingly, their apparent association rates were quite different (Figure 13A). Using ATPγS, the Mcm467 complex binds ssDNA quickly, with ~50 % of total binding occurring in ~2.5 minutes; the Mcm2-7 complex binds ssDNA very slowly, with 50% ssDNA binding occurring in approximately 12 minutes. Substituting ATP for ATPγS gave similar results (not shown).

The difference in the association rates between these two complexes was further investigated. We reasoned that the relatively slow association of the Mcm2-7 complex with ssDNA could reflect one or more additional ATP-dependent steps by Mcm2-7 prior to productive ssDNA binding. To test this hypothesis, both complexes were separately pre-incubated with ATPγS for 30 minutes, and then ssDNA was added. While pre-incubation with nucleotide has little effect on the kinetics of Mcm467 binding, nucleotide pre-incubation with Mcm2-7 greatly accelerates its association rate to resemble that of Mcm467 (Figure 13B). Similar results were obtained using ATP (data not shown). These data demonstrate that the slow association of Mcm2-7 in the absence of ATP pre-incubation reflects an interaction between the Mcm2-7 complex and ATP rather than slow ssDNA binding. To obtain association constants (Table 3), the results were re-plotted in the manner of von Hippel and coworkers (Figure 13C; [175]).

It should be noted that even at the faster association rate, the ssDNA binding activity of the Mcms is considerably slower than would be anticipated for simple diffusion-limited bimolecular rates (10^7-10^8 $M^{-1}s^{-1}$), and is somewhat slower than what is commonly observed other hexameric helicases [35, 190]. Since ssDNA binding likely occurs within the central channel of the complex, the relatively slow binding that is observed may correspond to specific ssDNA loading into the channel rather than simple binding *per se*.

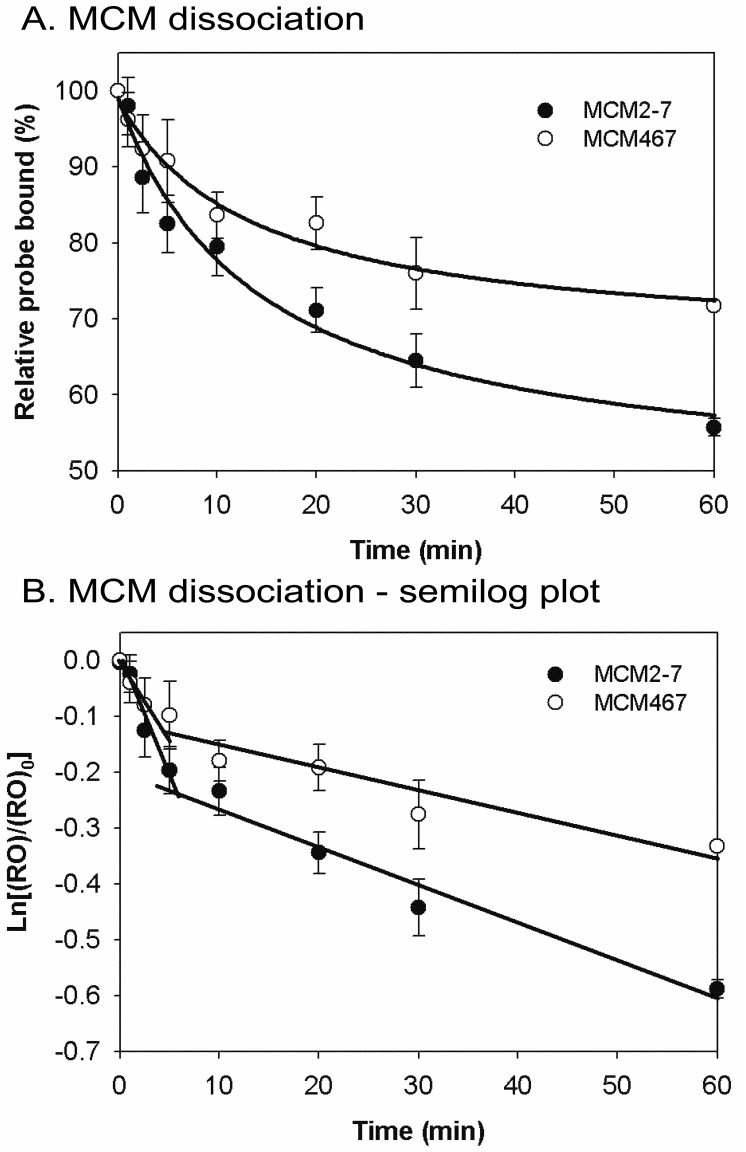

Figure 12. Kinetics of Mcm/ssDNA dissociation.

The data for each set was normalized to a maximal ssDNA binding of 100%. A) Dissociation rates of Mcm2-7 and Mcm467 from ssDNA. Binding conditions used 5 mM ATPγS and radiolabeled oligo 510 (Table 1). B) The data in A as a semi-log plot; slope = k_d. Plotting these data on a semi-log scale reveals that both complexes dissociate in a similar biphasic manner, with a relatively fast initial off-rate, followed by a much slower dissociation (Mcm467 $k_{d,fast}$ = 0.0241 min^{-1}, Mcm467 $k_{d,slow}$ = 0.002 min^{-1}, Mcm2-7 $k_{d,fast}$ = 0.0407 min^{-1}, Mcm2-7 $k_{d,slow}$ = 0.0068 min^{-1}). The biphasic nature of the plot suggests binding heterogeneity. Although in principle our ssDNA probes are long enough to facilitate cooperative binding of two Mcm complexes, repeats of these experiments using a shorter probe that should only allow binding of a single Mcm complex (oligo 3, Table 1) produced a similar biphasic dissociation (data not shown). In addition, treating our complexes with lambda phosphatase to generate a uniform population of unphosphorylated Mcm complexes also did not affect these results (data not shown).

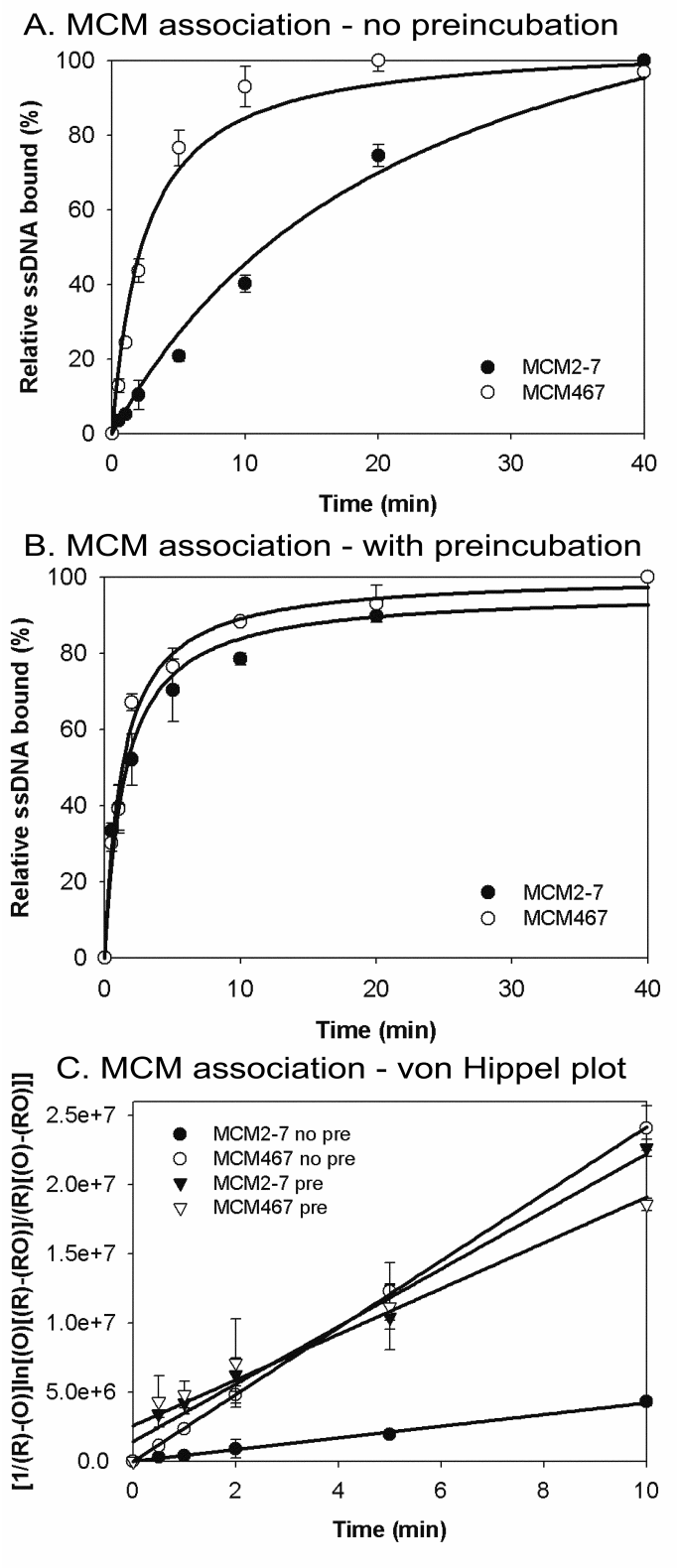

Figure 13. Kinetics of Mcm/ssDNA association.

A) association rates of Mcm2-7 and Mcm467. Standard binding reactions were scaled up 10-fold, Mcms were added at $t = 0$, and 5-µl samples were withdrawn at the indicated times and analyzed by filter binding. The reactions contain 5 mM ATPγS, 4 nM radiolabeled oligonucleotide 510 (Table 1), and 120 nM Mcm protein. B) effect of nucleotide preincubation on Mcm·ssDNA association rates. Preparations of Mcm2-7 or Mcm467 were preincubated with ATPγS for 30 min at 30 °C prior to the addition of labeled oligonucleotide 510 at t = 0. C) the data in A.) (*no pre*) and B.) (*pre*) were replotted in the manner of von Hippel [175]; slope = k_a.

3.3.6 The involvement of Mcm ATP active sites in ssDNA binding

To determine which Mcm ATP active sites contribute to ssDNA binding, we tested mutant Mcm2-7 complexes containing alanine substitution mutations of the universally conserved lysine within the Walker A ATP binding motif (the Mcm KA mutants; Figure 14A). These mutant complexes were expressed and purified as stable heterohexamers in a manner identical to the wild type complexes. We previously characterized such mutant complexes for their effects on steady-state ATP hydrolysis; inclusion of any one such mutant subunit in the context of the remaining five wild type subunits largely abolishes ATP hydrolysis of the entire heterohexamer [104].

Seven mutant Mcm2-7 complexes were tested for ATP-dependent ssDNA binding. Six complexes contain a single indicated KA mutant subunit in the presence of five other wild type subunits, the seventh complex contains the KA mutation in all six Mcm subunits (6XKA). Figure 14B shows that the 6XKA complex is completely unable to bind ssDNA, indicating that either the Mcm Walker A mutations block nucleotide binding rather than hydrolysis, or alternatively, prevent the effects of ATP binding from being transmitted to the DNA binding domain(s). In contrast, the other Mcm complexes demonstrate a range of ssDNA binding activities. The complex containing the Mcm4KA mutation is completely devoid of ATP-stimulated ssDNA binding; complexes containing the mutation in Mcm2 or Mcm6 bind ssDNA at essentially wild type levels; and complexes with mutations in Mcm3, Mcm5, or Mcm7 demonstrate intermediate levels of binding.

The ssDNA binding activity of these complexes was further explored by measuring their nucleotide dependency (Figure 14C). In most cases, ssDNA binding is stimulated by both ATP

and ATPγS in a manner similar to the wild type Mcm2-7 complex. However, we have repeatedly noticed that the Mcm2-7 preparations containing the Mcm7KA mutation demonstrate elevated levels of ATP-independent ssDNA binding; this binding is only stimulated slightly by ATPγS but not by ATP. The significance of this observation is currently unknown. Nevertheless, these results indicate that unlike steady-state ATP hydrolysis [104], participation of the six Mcm ATPase active sites in ssDNA binding is very different, with only the Mcm4 subunit, and to a smaller extent the Mcm7 subunit, being key to this activity.

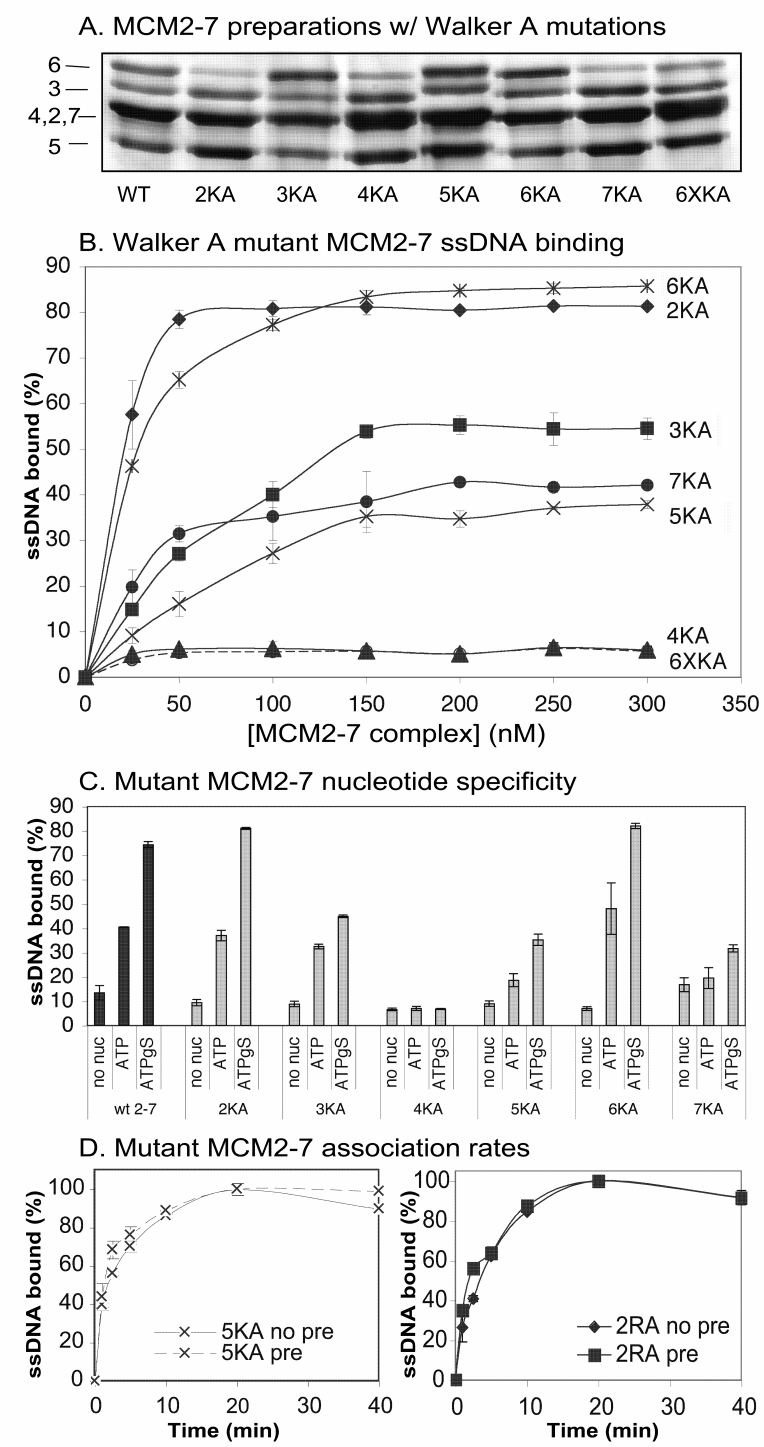

Figure 14. Effect of Walker A substitution mutations on Mcm2-7/ssDNA binding.

A) SDS-PAGE gel of 2 pmol each of the indicated Mcm2-7 preparations following silver staining. B) titrations of mutant Mcm2-7 complexes for ssDNA filter binding experiments. These experiments are identical to those in Fig. 2A, except that each Mcm2-7 preparation contained a KA mutation in the indicated subunit, whereas the remaining five subunits are wild type. The 6XKA preparation contains the Walker A mutation in all six subunits. The reactions used 4 nM radiolabeled oligonucleotide 510 (Table 1) in the presence of 5 mM ATPγS. C) nucleotide stimulation of ssDNA binding by the KA mutant Mcm2-7 preparations. The indicated binding reactions either contained no nucleotide (no nuc), 5 mM ATP, or 5 mM ATPγS (ATPgS) with 4 nM oligonucleotide 510 and 120 nm of mutant complex. D) mutant Mcm/ssDNA association kinetics. The association plots for Mcm5KA (left) and Mcm2RA (right) hexamers are shown. These experiments were conducted the same as in Fig. 13A (no pre) and Fig. 13B (pre).

3.3.7 The difference in ssDNA association rates between Mcm2-7 and Mcm467 depends upon the Mcm2/5 active site

Mcm2-7 contains three Mcm subunits that Mcm467 lacks: Mcm2, 3, and 5. Since the Mcm2-7 and Mcm467 complexes differ in their association rate with ssDNA, the Mcm2, 3, or 5 subunits are likely to be involved in this effect. Knowing that pre-incubation with ATP relieves the difference in ssDNA association rates between Mcm2-7 and Mcm467, we reasoned that a mutation in the ATPase active site of Mcm2, 3, or 5 may alter the ssDNA association rate of Mcm2-7. Of the KA mutant Mcm complexes that still demonstrate ATP-dependent ssDNA binding, association kinetics were measured with and without ATP pre-incubation. Complexes that contain KA mutations in Mcm2, 3, or 6 give results similar to the wild type Mcm2-7 complex; in these cases, pre-incubation of the complex with ATP increases the association rate to Mcm467 levels (Figure 15). In sharp contrast, a Mcm2-7 complex containing the Mcm5 Walker A mutation binds ssDNA at a similar fast rate in both the presence and absence of ATP pre-incubation (Figure 14D left). This indicates that the Mcm5 ATP active site is uniquely involved in the slow ATP-dependent step in Mcm2-7 ssDNA association.

The Mcms, as most AAA^+ ATPases, form ATP active sites at subunit interfaces; one subunit contributes a Walker A motif, while the adjacent subunit contributes an essential arginine [102]**.** The Mcm5 Walker A motif is predicted to form an active site with the essential arginine of Mcm2 [102]. To test the involvement of Mcm2 in the Mcm2-7 association rate, we generated Mcm2-7 complexes with appropriate arginine to alanine substitutions (R->A; **Chapter 4**) and assayed their association rates. Strikingly, only the Mcm2-7 complex containing the Mcm2RA mutation demonstrated an accelerated ssDNA association rate (data not shown, Figure 14D

right). This result further substantiates the involvement of the Mcm2/5 active site in Mcm2-7 ssDNA association.

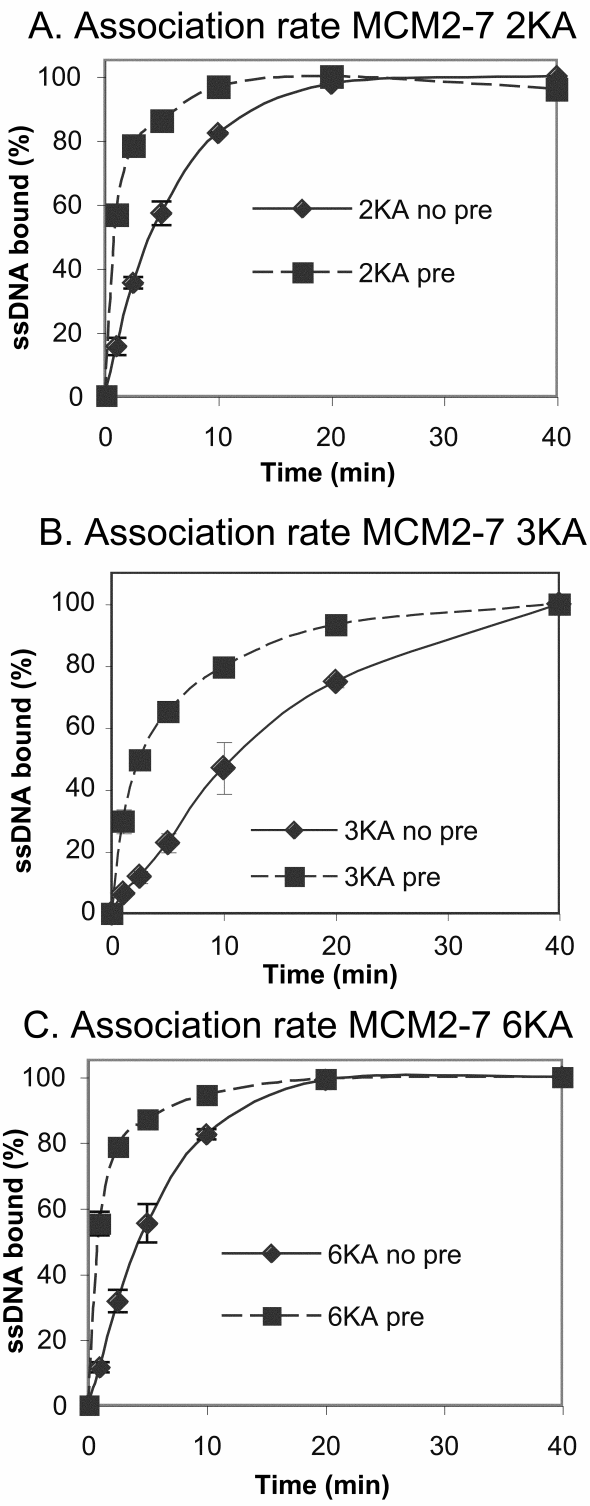

Figure 15. Association of Mcm2-7 complexes containing either the A) Mcm2K, B) Mcm3KA, or C) Mcm6KA mutant subunit.

Assays were performed as in Figure 13A.

3.4 DISCUSSION

Our comparative analysis of the ssDNA binding properties of the Mcm2-7 and Mcm467 complexes reveals similarities and key functional differences both between these complexes and in relation to other helicases. In common with typical hexameric helicases, both Mcm complexes demonstrate (pseudo)six-fold symmetry and ATP-dependent ssDNA binding. However, unlike typical homohexameric helicases that contain functionally equal subunits and bind ssDNA in a sequence-independent manner, our data indicate that the Mcm2-7 subunits have differential involvement in ssDNA binding, and a marked binding preference for poly(dT). Although both complexes have similar ssDNA binding affinities, they differ in their ssDNA association kinetics, evidence suggesting that the Mcm2, 3, and 5 subunits regulate the loading or activation of the Mcm2-7 complex *in vivo*. Further, our data demonstrate that the lack of helicase activity by the Mcm2-7 complex is not due to an inability to bind ssDNA, as previously suggested [102].

3.4.1 The Mcm complex has unusual properties for a hexameric helicase

Although helicases usually bind ssDNA in a sequence-independent manner [35], the Mcms prefer to bind to polypyrimidine tracts. While this property was previously observed for Mcm467 [103, 147], we show that this preference is even stronger with Mcm2-7 (Figure 11A). Since eukaryotic replication origins are usually A/T-rich [152-155] and often contain poly(dT) tracts [191, 192], an increased affinity to poly(dT) sequences could facilitate loading of the

Mcms onto replication origins as previously proposed [147]. However, this enhanced affinity for poly(dT) is also potentially disruptive during elongation *in vivo*: helicases need to freely translocate along DNA, and a high affinity toward poly(dT) might impede translocation and cause the replication fork to pause. Such events are deleterious; pausing leads to fork collapse and the production of potentially lethal DNA double strand breaks [193]. Possible fork pausing by the Mcm complex during normal replication may have broader implications for human health, since DNA replication in eukaryotes sometimes pathologically results in chromosome breaks at A/T-rich sequences referred to as fragile sites (reviewed in [194]).

In contrast to homohexameric helicases, the individual Mcm subunits contribute differentially to ssDNA binding. Analysis of Mcm2-7 complexes containing Walker A mutant subunits reveals that, unexpectedly, only the active site on Mcm4 is absolutely required for this activity, while the Mcm7 active site is required to make the interaction ATP-dependent. Previous analysis supports these observations. In *S. pombe,* Mcm complexes containing the Mcm4KA mutation lose association with chromatin [182]. In contrast, Mcm6KA mutant complexes can still bind chromatin in a semi-purified *Xenopus in vitro* DNA replication system [122, 129]. One puzzling feature of the Mcm2-7 complex is why it contains six distinct subunits. Our data suggests this arrangement has allowed individual subunits to evolve specialized functions, with some subunits specializing in ssDNA binding (Mcm4 and 7), while other subunits may specialize in regulating this association (Mcm2 and 5, below).

3.4.2 Key differences between the two Mcm complexes

Both the archaeal Mcm complex [58, 59, 139, 141, 163] and the eukaryotic Mcm467 complex [52, 163] bind dsDNA. This characteristic has fueled speculation that Mcm2-7 might function as

a dsDNA pump [195]. Although we demonstrate that both complexes have an ATP-dependent dsDNA binding activity, their affinity for dsDNA is approximately 100-fold lower than for ssDNA. Since Mcm467 binds dsDNA better than Mcm2-7, it suggests that the Mcm2, 3, or 5 may subunits negatively affect dsDNA binding, raising the possibility that regulation of these subunits may facilitate dsDNA interaction under certain conditions. The poor affinity of Mcm2-7 for dsDNA does not definitively rule out its involvement as a pump, however. Further mutational analysis of the Mcm complex using mutants that specifically affect dsDNA binding (as have been developed in the archaeal MCM complex; [59]) will be required to determine the *in vivo* significance of dsDNA binding.

Unexpectedly, Mcm2-7 and Mcm467 bind ssDNA with different kinetics. Although the Mcm467 complex binds ssDNA relatively quickly, Mcm2-7 binds approximately five times more slowly. The slow ssDNA association by Mcm2-7 is due to an interaction involving ATP, since pre-incubation of the Mcm2-7 complex with ATP removes this kinetic barrier. The effects of pre-incubation occur very slowly, requiring about 20-25 minutes of Mcm/ATP pre-incubation to stimulate maximal ssDNA binding (data not shown). This slow rate does not reflect slow ATP binding to the complex, as no noticeable time lag was observed in steady-state ATPase hydrolysis studies of the Mcm2-7 complex (A. Schwacha, unpublished). We hypothesize that the slow step corresponds to an ATP-dependent conformational change by the Mcm2-7 complex. Since the obvious differences between these two complexes are the Mcm2, 3, and 5 subunits, it is reasonable to expect that these subunits are responsible for the difference in ssDNA association. This expectation is confirmed by our finding that the Mcm5KA and Mcm2RA mutant complexes bind ssDNA quickly without ATP pre-incubation, implying the involvement of these subunits in this slow ssDNA association step.

3.4.3 The possible nature of the Mcm2-7 ATP-dependent conformational change

As previously demonstrated [102], the ATP active sites within the Mcm complex lay at dimer interfaces, with one subunit contributing a Walker A motif, while the other subunit contributes a catalytically essential arginine "finger". This arrangement is typical for AAA^+ ATPases (reviewed in [77]). To fit these subunit associations onto the observed toroidal structure, Mcm2 and Mcm5 need to be juxtaposed to form an active site, with Mcm5 contributing the Walker A motif, and Mcm2 contributing the essential catalytic arginine [102].

The effect of the either the Mcm5KA or Mcm2RA mutation on the association of Mcm2-7 with ssDNA is puzzling. Both motifs likely ablate important contacts with ATP, suggesting that normally the slow association reflects an inhibitory nucleotide, or other possible inhibitor, bound at this site. In contrast, pre-incubation of Mcm2-7 with ATP increases ssDNA association, suggesting that ATP binding is responsible for this effect. We suggest that both situations may serve to displace some inhibitory interaction at the Mcm2/5 active site – either of a protein-protein or protein-ligand nature – resulting in a conformational change that increases the ssDNA association rate. One possible inhibitor could be ADP that has remained tightly bound to this site during protein purification, a common property of ATPases [196, 197].

Is this proposed conformational change at the Mcm2/5 interface physiologically relevant? In common with the other Mcm genes, *MCM2* and *MCM5* are essential, indicating that the Mcm467 helicase activity is insufficient to carry out *in vivo* DNA replication. Yet our analysis indicates that neither Mcm2 nor Mcm5 have critical involvement in ssDNA binding or steady state ATP hydrolysis [104] suggesting that their essential *in vivo* function depends upon some yet undiscovered activity.

Available evidence supports a regulatory role for these two subunits in DNA association. Unlike the other five Mcm subunits, Mcm2 specifically binds chromatin [198]. Further, both Mcm2 and the Mcm5 are linked to the Cdc7/Dbf4 regulatory kinase which aids in cell cycle-dependent assembly of the elongation complex and functions immediately downstream of Mcm2-7 loading at replication origins [84]. While the mechanistic role of Cdc7/Dbf4 phosphorylation is poorly understood, the Mcm complex is likely to be the focus of its activity. A specific mutant in Mcm5 [199] exists that bypasses the normally essential function of Cdc7 in DNA replication, and the Mcm2 subunit is a major substrate for this kinase [200, 201]. These results suggest that both Mcm2 and Mcm5 serve a regulatory function, possibly to activate Mcm2-7 helicase activity. Perhaps Mcm phosphorylation by the Cdc7/Dbf4 kinase causes a favorable conformational change at the Mcm2/5 site that activates the Mcm2-7 complex's DNA unwinding activity *in vivo*.

4.0 SUBUNIT ORGANIZATION OF MCM2-7 AND THE UNEQUAL ROLE OF ACTIVE SITES IN ATP HYDROLYSIS AND VIABILITY

The contents of this chapter, with some additions and alterations, come from [202] and are reprinted in accordance with the guidelines of the American Society for Microbiology.

4.1 SUMMARY

The Mcm2-7 complex is a toroidal AAA^+ ATPase and the putative eukaryotic replicative helicase. Unlike a typical homohexameric helicase, Mcm2-7 contains six distinct, essential, and evolutionarily conserved subunits. Precedent from other AAA^+ proteins suggests that Mcm ATPase active sites are formed combinatorially, with Walker A and B motifs contributed by one subunit and a catalytically essential arginine (arginine finger) contributed by the adjacent subunit. To test this prediction, we used co-purification experiments to identify five distinct and stable Mcm dimer combinations as potential active sites; these subunit associations predict the architecture of the Mcm2-7 complex. Through the use of mutant subunits, we establish that at least three sites are active for ATP hydrolysis and have a canonical AAA^+ configuration. In isolation, these five active site dimers have a wide range of ATPase activities. Using Walker B and arginine finger mutations in defined Mcm subunits, we demonstrate that these sites similarly make differential contributions toward viability and ATP hydrolysis within the intact hexamer.

Our conclusions predict a structural discontinuity between Mcm2 and Mcm5, and demonstrate that in contrast to other hexameric helicases the six Mcm2-7 active sites are functionally distinct.

4.2 INTRODUCTION

Replicative helicases are essential motor proteins that use nucleoside triphosphate-fueled conformational changes to unwind duplex DNA (reviewed in [35]). In eukaryotes, a ring shaped heterohexameric ATPase called the minichromosome maintenance (Mcm2-7) complex is believed to fulfill this role (reviewed in [73]). In combination with several other DNA replication factors (Cdc45 [97] and the GINS complex [94]), Mcm2-7 is physically present and functionally required for both the initiation and elongation phases of DNA replication (reviewed in [84]). These properties are reminiscent of the *E. coli* DNA replicative helicase DnaB [179], and strongly implicate Mcm2-7, possibly in combination with Cdc45 or the GINS complex, as the eukaryotic replicative helicase (reviewed in [183]).

In contrast to homohexameric helicases, Mcm2-7 is formed from six different and individually essential subunits (numbered 2–>7) that are all members of the AAA^+ ATPase family [77]. This unique situation makes Mcm2-7 an attractive system for studying the coordination between ATP hydrolysis and motor function, since mutant complexes can be engineered with defined alterations at precise locations within the complex for study (*e.g.*, [104]). The differences between the six subunits are likely of functional significance, since each Mcm subunit forms a conserved and essential gene family dating back to the earliest evolutionary split between eukaryotes and the archaea [77].

Although Mcm2-7 awaits structural analysis, precedent from AAA^+ members suggests that Mcm ATPase active sites are formed *in trans* from a conserved Walker A and B motif from one subunit and a catalytically essential "arginine finger" from the other [77, 78]. Five unique dimeric combinations likely corresponding to ATPase active sites have been identified [102]. For one dimer composed of Mcm3 and Mcm7 (Mcm3/7), mutational analysis demonstrated that this dimer is a true active site with a typical AAA^+ composition [102, 104]. However, it is unknown if the remaining dimers have a similar active site arrangement.

Unlike a typical homohexameric helicase in which the six active sites participate equally (*e.g.*, [54, 55]) the ATPase active sites in Mcm2-7 may be functionally non-equivalent. Although historically Mcm2-7 lacks *in vitro* helicase activity, a Mcm subcomplex specifically containing only Mcm4, 6, and 7 (Mcm467 complex) has a weak helicase activity [63, 101, 103]. This observation differentiates between Mcm subunits involved in helicase activity (Mcm4, 6, and 7) and those that lack helicase activity (Mcm2, 3, and 5). In addition, the five putative Mcm active site dimers have a wide range of ATPase activities [102]. However, both observations involve Mcm subcomplexes, and the relevance of these data to the intact Mcm2-7 hexamer is unknown.

To compare the activity of the isolated dimers to their corresponding activity within the Mcm2-7 hexamer, we generated and studied mutants within the six Walker B and arginine finger motifs. In addition to Mcm3/7, at least two additional active sites, Mcm7/4 and Mcm6/2, function in a combinatorial nature similar to other AAA^+ proteins. Our data supports a specific subunit architecture for Mcm2-7 that contains a physical discontinuity between Mcm2 and Mcm5. We also find a good correlation between the varied ATPase activity of isolated dimers and their contribution toward ATPase activity and viability within the Mcm2-7 hexamer. These

data demonstrate that unlike other hexameric helicases, active sites within Mcm2-7 contribute unequally toward activity.

4.3 RESULTS

4.3.1 Isolation of Mcm dimers

Mcm2-7 forms a toroidal hexamer; if active sites form at dimer interfaces, the complex should contain six specific dimeric active sites. Although a previous study assembled five distinct Mcm dimers from purified subunits [102], we have observed that *S. cerevisiae* Mcm4 and Mcm5 are poorly soluble in isolation (below), raising the possibility that some potential dimer combinations might have been missed. As an alternative approach, we assayed stable dimer formation following co-expression of all possible subunit combinations within a common cytoplasm. Each of the fifteen pairwise combinations of Mcm-encoding baculovirus were individually used to co-infect insect cells. In each case, only one of the two subunits contained a C-terminal polyhistidine (10x) affinity tag, a modification that does not compromise cell growth or viability [104].

To assay Mcm subunit association, the co-expressed Mcms were subjected to metal affinity chromatography, and the retention of both subunits was examined (Figure 16A). Since Mcm2, 4, and 7 resolve poorly by SDS-PAGE, western blot analysis was used to assess the subunit composition of these combinations (Figure 16B). Although Mcm2/4 demonstrated a low level of association upon the initial purification (Figure 16B left), this apparent interaction was lost upon additional purification (data not shown) and was excluded from further analysis. In

total from among the fifteen possible subunit combinations, five dimeric associations were recovered for further study: Mcm3/7, 6/2, 7/4, 4/6, and 5/3. Since this experimental procedure enriches for his-tagged subunits irrespectively of their physical association to the untagged subunits, these preparations were further purified to homogeneity. Quantification of band intensities from these purified dimeric preparations (Figure 16C) or by quantitative Westerns of the Mcm7/4 preparation (Figure 16D) indicates that the two subunits within each final preparation have nearly equal stoichiometry, with an excess of one subunit over the other of ≤30%.

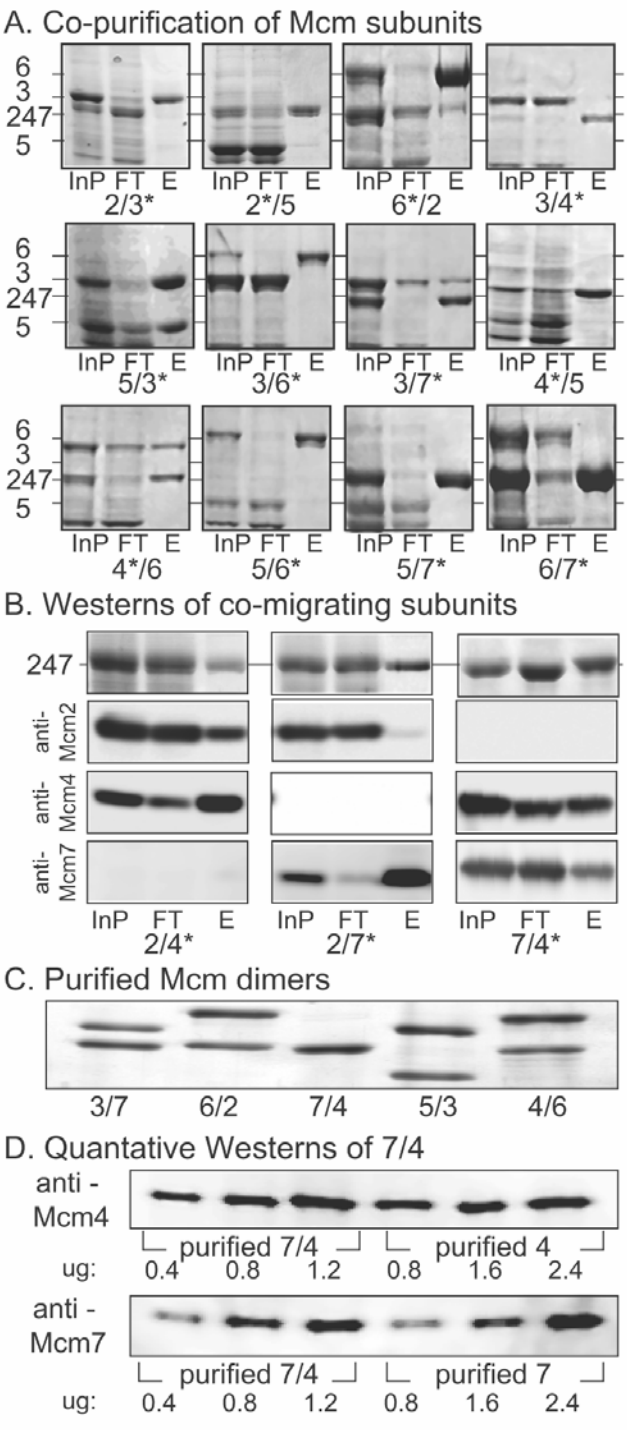

Figure 16. Identification and ATPase activity of stable Mcm dimeric assemblies.

A) SDS-PAGE gel of column fractions following metal chelate chromatography of co-expressed Mcm subunits. The subunit labeled with (*) contains the C-terminal polyhistidine tag. InP = input extract; FT = column flow through; and E = purified eluate fraction. B) Association of subunits that co-migrate on SDS-PAGE. The analysis is the same as in 1A, except that Western blotting using subunit-specific antibodies was performed. Top row, indicated fractions stained with Coomassie blue, bottom 3 rows, Western blots with indicated Mcm antibody. C) Silver-stained SDS-PAGE of purified stable dimeric Mcm subunits. D) Quantitative Western blots to measure subunit stoichiometry within the purified Mcm7/4 dimer.

4.3.2 Physical characterization of dimeric Mcm preparations

Gel filtration was used to confirm the physical association between Mcm subunits and determine their oligomerization state. Isolated Mcm subunits were first examined to provide a point of reference. The six His-tagged Mcm subunits were individually expressed in our baculovirus system. Preparations of Mcm2, 3, 6, and 7 yielded soluble proteins that were subsequently purified to homogeneity, while Mcm4 and Mcm5 are largely insoluble, and their analysis was not further pursued (data not shown). Based upon their estimated molecular weights (which range from 86 kDa (Mcm5) to 113 kDa (Mcm6)), the resulting elution volumes of these single subunit preparations are consistent with a molecular weight in the monomer/dimer range for Mcm3 and 7, in the dimer/trimer range for Mcm6, while the elution volume of Mcm2 is consistent with a hexameric oligomerization (Figure 17A). These results are consistent with the previous observation that isolated Mcm subunits have a variable propensity to oligomerize [102].

Aliquots of the final dimeric preparations were next analyzed. To claim stable dimerization, both participating subunits must co-elute, and additionally, one or both subunits must demonstrate a different elution profile than the corresponding single subunit preparation. By this criterion, physical interaction between Mcm subunits was demonstrated for four of the five dimeric preparations. Mcm3/7, 5/3, and 6/2 eluted as apparent dimers, whereas Mcm7/4 eluted as a hexamer (Figure 17B). Physical association between subunits in the Mcm4/6 preparation could not be confirmed, since the elution of Mcm4 was not examined, and the resulting Mcm4/6 preparation elutes at the same position as Mcm6 alone. The size of our Mcm3/7, 5/3, and 6/2 complexes is smaller than previously observed, possibly reflecting a structural difference between dimers formed by *in vivo* co-expression (this study) as opposed to

in vitro reconstitution [102, 104]. In contrast, the hexameric size of Mcm7/4 is significantly larger than previously reported [102], although it should be noted that a significant amount of Mcm7/4 eluted at a hexameric size in this prior study.

To confirm the stability of these subunit associations, pull down experiments that target the poly-histidine epitope tags on an individual subunit were conducted (Figure 17C). Quantitation of the two subunits within each preparation by either Sypro staining of SDS-PAGE gels, or by quantitative Western blots (e.g., Mcm7/4), indicate for all of the preparations except Mcm4/6, approximately the same subunit stoichiometry in the pull down fraction as in the input (≤30% excess of one subunit over another). Although these experiments confirm subunit association within the Mcm4/6 dimer, the pull down recovered approximately twice as much Mcm6 as Mcm4, suggesting that this dimer may be relatively unstable. These experiments are in good agreement with our gel filtration results, and with the possible except of Mcm4/6 indicate a good physical association between subunits in these preparations.

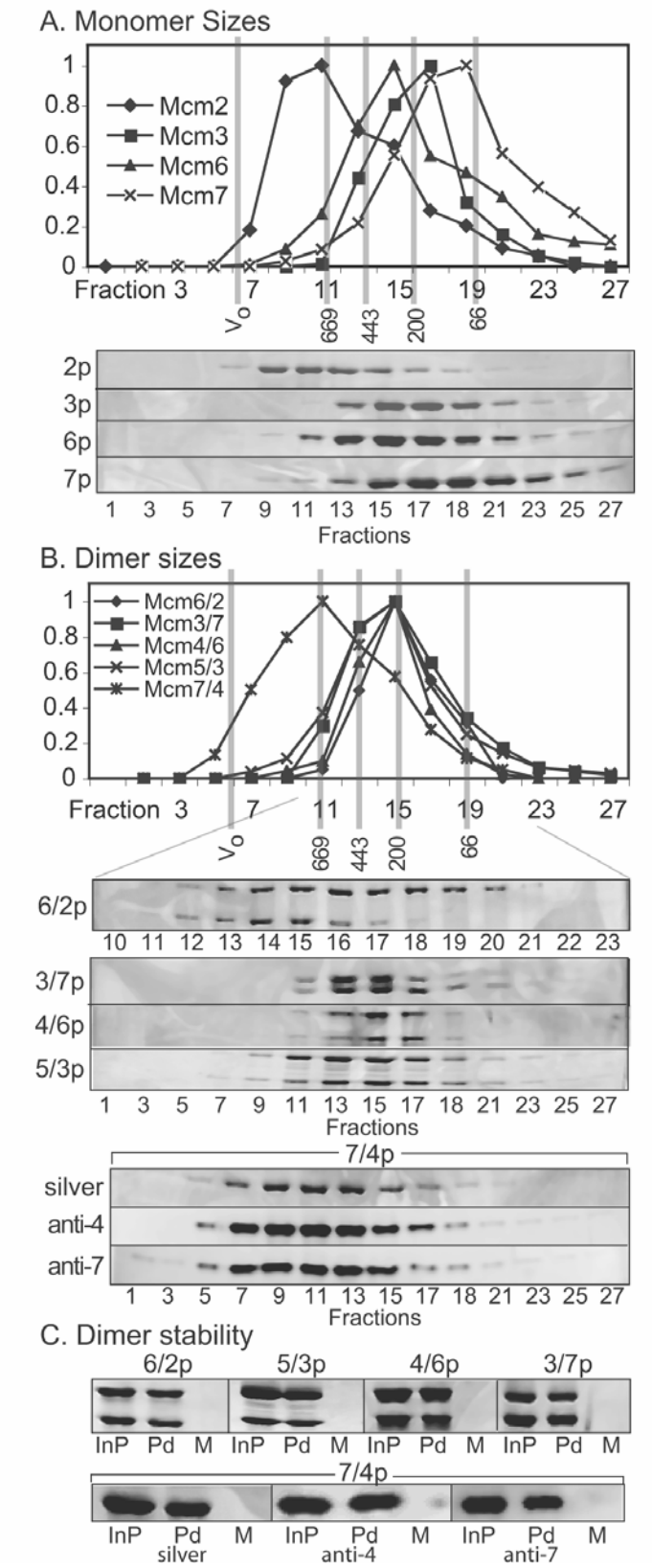

Figure 17. Oligomerization and stability of Mcm dimers.

A) Gel filtration of the indicated Mcm single-subunit preparations. B) Gel filtration of final purified dimeric preparations. In both A) and B) the elution volumes of the indicated molecular weight markers are shown; Sypro orange staining or Western blot analysis of the indicated fractions are shown. C) Pull downs of indicated Mcm dimers by metal affinity chromatography. InP = input protein, Pd = pull down of protein retained on the beads, M = mock, represents analogous pull down experiment conducted without charging the affinity resin with nickel.

4.3.3 The involvement of the Walker B motif in the Mcm3/7 active site

The resulting five dimeric complexes were assayed for ATP hydrolysis (Figure 18A) and found to differ greatly in activity: Mcm3/7 demonstrated high ATPase activity similar in magnitude to the intact Mcm2-7 hexamer, Mcm6/2 and Mcm7/4 had moderate activity, and Mcm5/3 and 4/6 nearly lacked activity. As no stimulation of ATPase activity had been previously observed upon addition of ssDNA to either the intact Mcm2-7 complex [104] or isolated dimers [102], ssDNA was omitted from these reactions. These levels of ATP hydrolysis in our dimer preparations are similar to the previous study [102], confirming the validity of our experimental approach.

To study the composition of ATPase motifs in individual active sites, appropriate *mcm* mutations were generated. (Materials and Methods (**2.9.1.1**); Table 4). Mutations in the Mcm Walker A (KA) and arginine finger (RA) motifs have been described [102, 104]. Since previous attempts to study Mcm Walker B motifs with alleles containing a single aspartate-to-alanine substitution (DEFD–>AEFD) proved unsuccessful [104], double mutations were constructed that changed the first two acidic residues into their uncharged amide counterparts (DE–>NQ, referred to subsequently as *DENQ* alleles). In contrast to the previous Walker B alleles [104], the *DENQ* alleles in five of the six subunits proved lethal (Table 4, below), consistent with the hypothesis that they functionally ablate the corresponding active site.

Dimeric complexes containing either the Mcm3DENQ or the Mcm7DENQ mutation were expressed, purified, assayed for ATPase activity (Figure 18B), and compared to analogous dimers that contain either the Walker A (KA) mutations [104] or arginine finger (RA) mutations [102]. As previously shown, Mcm7 contributes the catalytically essential Walker A motif, while Mcm3 contributes the essential arginine finger motif [102, 104]. Our results demonstrate that

Mcm7, but not Mcm3, also contributes the Walker B motif to the Mcm3/7 active site (Figure 18B). In addition, these data confirm that our Walker B and arginine finger mutants eliminate catalysis with little or no effect on subunit association, validating them as good candidates to test the role of individual ATPase active sites within the Mcm2-7 hexamer (below).

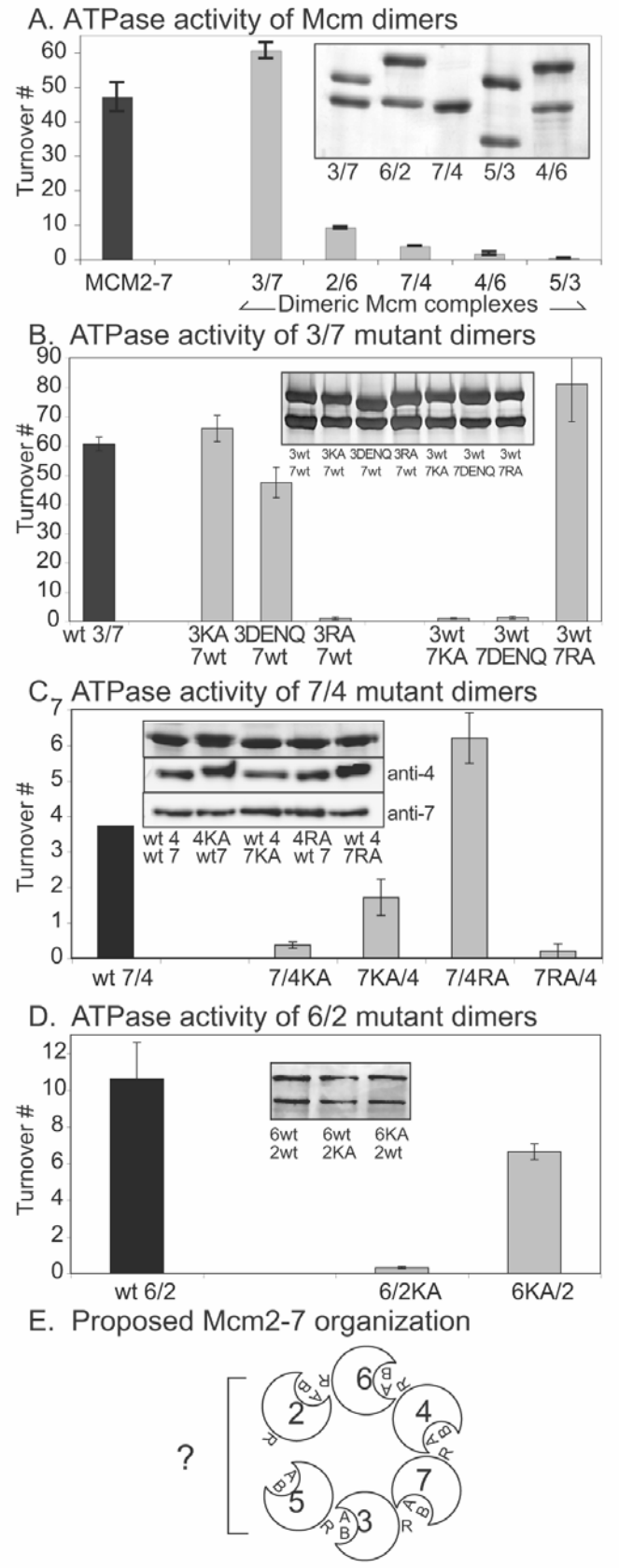

Figure 18. Contribution of ATPase motifs to active site function.

A) ATPase activity of stable dimeric preparations. wt = the activity of the wild type Mcm2-7 heterohexameric preparation. B-D) ATPase activity of Mcm dimers containing the indicated mutant or wild type Mcm subunits. Insets show silver stained SDS-PAGE gels or Western blot analysis of equivalent amounts of the final preparations. E) Proposed subunit organization of Mcm2-7.

Table 4. *MCM* alleles and mutant phenotypes.

Alleles	Walker B mutants	Alleles	Arg. finger mutants
mcm2DENQ	604-LI**DE**FDKMN	*mcm2R676A*	673-LS**R**FD
mcm3DENQ	470-CI**DE**FDKMT	*mcm3R542A*	539-LS**R**FD
mcm4DENQ	629-CI**DE**FDKMS	*mcm4R701A*	698-LS**R**FD
mcm5DENQ	477-CI**DE**FDKMR	*mcm5R549A*	546-LS**R**FD
mcm6DENQ	636-CI**DE**FDKMD	*mcm6R708A*	705-MS**R**FD
mcm7DENQ	521-CI**DE**FDKMD	*mcm7R593A*	590-LS**R**FD
MCM consensus	IDEFDKM		SRF

Phenotypes:

Genetic complementation[e]

		Mutants		
Gene	wild type	Walker A[f]	Walker B	Arg finger
MCM2	+	-	±	-
MCM3	+	-	-	-
MCM4	+	-	-	+
MCM5	+	-	-	-
MCM6	+	-	+	-
MCM7	+	-	-	-

Over-expression Lethality[g]

MCM2	-	+	-	+++
MCM3	-	-	±	+++
MCM4	-	+++	-	-
MCM5	-	+	±	+
MCM6	-	+++	-	-
MCM7	-	+++	+++	+++

[e] Complementation experiments express the indicated *MCM* genes under the control of the *MCM5* promoter on an ARS/CEN plasmid over a deletion of the corresponding gene. *MCM2* alleles were untagged, the other genes contained a C-terminal HA/His_{10} epitope tag.

[f] The phenotypes of the Walker A alleles are reprinted from [104] and are included for purposes of comparison.

[g] Over-expression lethality experiments were performed using integrated constructs under the control of the *GAL1-10* promoter. *MCM2* alleles were untagged, while the other alleles contained a C-terminal epitope tag: *MCM3* alleles contained a 3xHA tag, *MCM4* alleles contained either a 3xHA or 3xMyc tag, while the *MCM5*, *6*, and *7* alleles contained a single FLAG tag. Western blot analysis was preformed to verify galactose-induced expression of full-length protein.

4.3.4 Characterization of the Mcm7/4 and Mcm6/2 active sites and subunit architecture of Mcm2-7

In contrast to the Mcm5/3 and Mcm4/6 dimers, the Mcm7/4 and Mcm6/2 dimers retained sufficient ATPase activity to allow their functional analysis. To study these sites, a set of mutant Mcm7/4 and Mcm6/2 dimers were expressed and purified. Although neither the Mcm6RA nor Mcm2RA mutations affected the stability of the Mcm2-7 hexamer (Figure 19), we were unsuccessful in purifying stable dimers containing these alleles (data not shown). The remaining dimers were assayed for ATP hydrolysis (Figure 18C and D).

In contrast to Mcm3/7, analysis of the Mcm7/4 and Mcm6/2 dimers yielded more complex results (Figure 18C and D). The Mcm7RA mutation specifically blocked ATP hydrolysis in Mcm7/4 and thus indicated that Mcm7 contributes the catalytically essential arginine finger residue. However, both Walker A motifs contributed to ATPase activity: the Mcm4KA mutation nearly eliminated ATPase activity while the Mcm7KA mutation significantly reduced ATP hydrolysis. Mcm6/2 provided similar results; in this case Mcm2KA nearly eliminated ATP hydrolysis whereas the Mcm6KA noticeably reduced this activity. Assuming that the Walker A motif that has the greatest effect on ATPase activity is at the dimer interface, our results support the predicted participation of these motifs [102]. Although the low ATPase activity of the Mcm5/3 and Mcm4/6 dimers prevented a similar analysis, as a working hypothesis we will assume that they represent AAA^+ ATPase active sites as previously proposed [102]. Hereafter, we will name each active site such that the subunit contributing the arginine finger residue comes first, followed by the subunit contributing the Walker motifs.

To summarize our data, we propose a subunit organization for the Mcm2-7 complex (Figure 18E). Although these data predict a linear structure with Mcm2 or 5 at either end, hexamerization of Mcm2-7 into a toroid likely forces these two subunits into close juxtaposition to form an active site (see **Section 4.4.1**). This model is similar to that previously proposed [102].

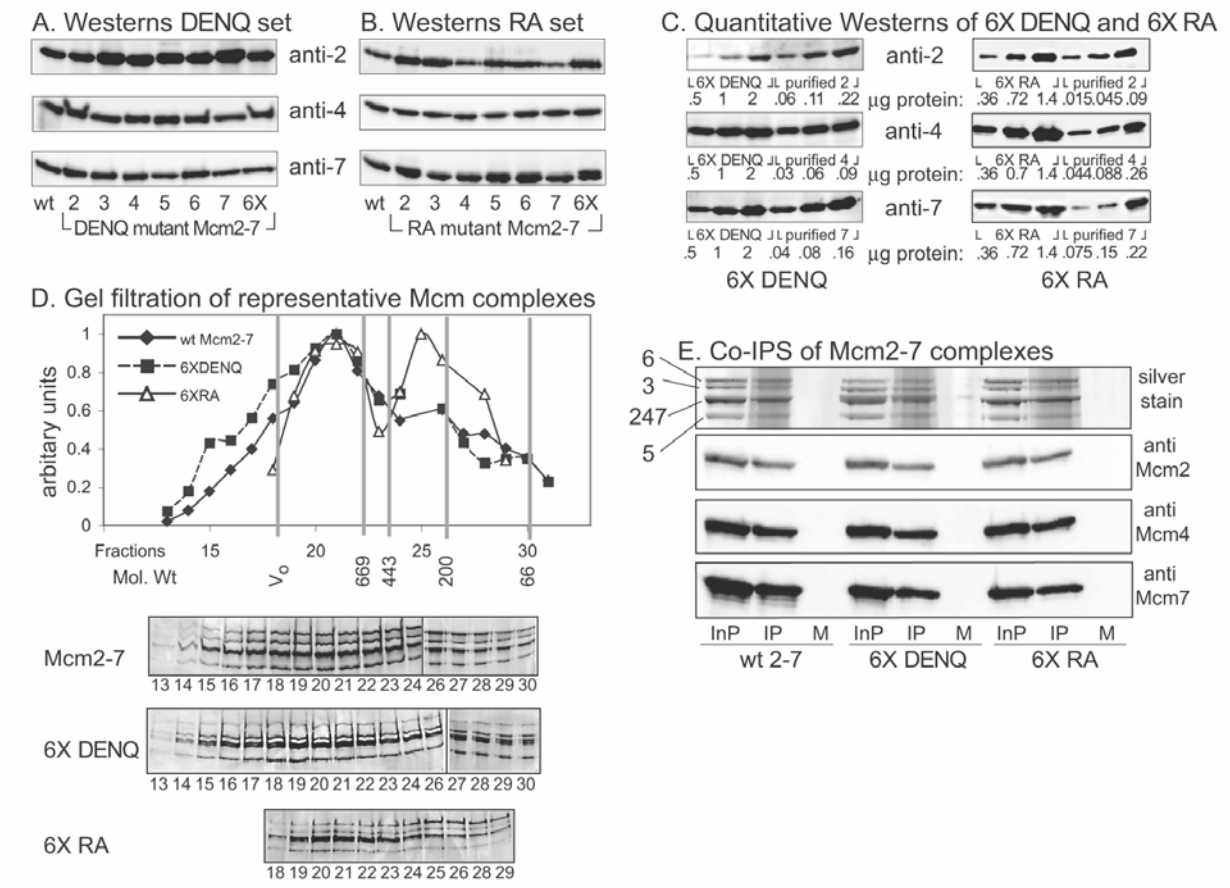

Figure 19. Abundance of the Mcm2, 4, or 7 subunits in Mcm2-7 A.) DENQ and B.) RA mutant hexamer preparations.

Equal amounts (0.25 µg) of each of the indicated Mcm2-7 preparations separated by SDS-PAGE, and subjected to Western blot analysis using antibodies to Mcm2, 4, or 7 as described in Methods and Materials. "wt" = wild type Mcm2-7 preparation, 6X refers to a Mcm2-7 hexamer with all six subunits containing either the A) DENQ mutation or the B.) RA mutation. Quantitation of the Western blots in A) and B) indicates that subunit amounts varied <2-fold among the various wild type and mutant Mcm2-7 preparations. C) Representative quantitative Westerns of the 6X DENQ (left) and 6X RA preparations. D) Gel filtration of final representative wild type, 6X RA and 6X DENQ Mcm2-7 preparations. Although the wild type Mcm2-7 and 6X DENQ preparations predominantly contain a high molecule weight species of predicted hexameric size as observed previously [104], the 6X RA preparation contains an extra peak corresponding to an excess of Mcm6 in this particular preparation. E) Mcm2-7 complex stability in the presence of either the Walker B or the arginine finger alleles. Purified Mcm2-7 (left), 6X DENQ (center), and 6X RA (right) were immunoprecipitated as described in Materials and Methods. Inp = input Mcm complex; IP = immunoprecipitated Mcm complex; M = mock immunoprecipitations (no antibody). A silver-stained gel is shown, as well as Westerns using subunit-specific antibodies to Mcm2, Mcm4 and Mcm7 as indicated.

4.3.5 Importance of the Walker B and arginine finger motifs to Mcm2-7 *in vivo* function

The Walker A box KA mutations of Mcm2-7 have been previously analyzed and cause two effects: not only do they block ATP hydrolysis at the corresponding active site, they also block ATP hydrolysis of the remaining wild type active sites [104]. To separate the catalytic vs. regulatory contributions of the Mcm active sites, alleles that uncouple these two activities are required. Studies of other ATPases have found that the Walker B and arginine finger motifs are often only needed for ATP hydrolysis but not binding (reviewed in [203]), suggesting that unlike the KA mutations, the latter mutations might be suitable for studying the contributions of individual active sites without blocking ATP hydrolysis of the entire complex.

To this end, we tested the Walker B (*DENQ*) and arginine finger (*RA*) alleles of all six Mcm genes for genetic complementation in *S. cerevisiae* (Table 4). As an example, the phenotypes of the *mcm6* and *mcm7* alleles are shown (Figure 20). Although all *mcm* constructs are viable in the presence of an additional plasmid-borne copy of the wild type gene (Figure 20A, Glu), most *mcm* alleles demonstrate little or no growth when the Walker B or arginine finger allele provides the sole copy of that *MCM* gene (Figure 20A, FOA; Table 4 shows the results of all twelve mutations). The lack of viability is not due to the defective expression of these alleles, since they express protein at levels comparable to the corresponding wild type gene (data not shown). Interestingly, several alleles retained viability; *mcm2DENQ* has a slow growth phenotype, whereas mutations in the Mcm4/6 active site (*mcm4RA* and *6DENQ*) have apparently normal growth (Table 4). Fluorescence activated cell sorter analysis of the *mcm2DENQ* mutant indicates that it accumulates cells in S-phase relative to its congenic wild type strain (E. Tsai, C. Poth, and A. Schwacha, unpublished), suggesting a DNA replication defect. No other defects are evident for these three viable *mcm* alleles; in an otherwise wild type strain background, they

have normal viability and resistance to the DNA replication inhibitors hydroxyurea and methyl methanesulfonate (R. Elbakri and A. Schwacha, observation). These results suggest that ATP hydrolysis by the Mcm4/6 active site is dispensable for *in vivo* Mcm2-7 function.

We also tested the *DENQ* and *RA* alleles for dominant lethality upon overexpression, a phenotype previously associated with other Mcm alleles (Table 4, [104, 182]). Toward this end, the *mcm* Walker B and arginine finger alleles were integrated into an otherwise wild type strain and expressed by the strongly inducible *GAL* promoter. As an example, analysis of the *mcm6* and *7* alleles are shown (Figure 20B). All *mcm7* alleles (*7KA*, *7DENQ*, and *7RA*) demonstrate a strong dominant lethal phenotype upon exposure to galactose, whereas among alleles of *mcm6*, only the *mcm6KA* allele demonstrates dominant lethality (Figure 20). Table 4 shows the results with the other alleles. Dominant negative effects were generally weak with the *DENQ* alleles. Only *mcm2DENQ* and *mcm3DENQ* demonstrate a slight growth defect. The *RA* alleles in general demonstrated a stronger dominant effect; *mcm2RA* and *3RA* caused lethality, whereas *mcm5RA* resulted in slow growth. Note that *MCM7* is unique, since it is the only subunit that demonstrates a strong dominant lethal phenotype for all three mutations (*KA*, *DENQ*, and *RA*), suggesting a special role for Mcm7 within the complex (see below). With the exception of *MCM7*, however, our findings suggest that dominant effects are associated with particular classes of mutants rather than particular active sites.

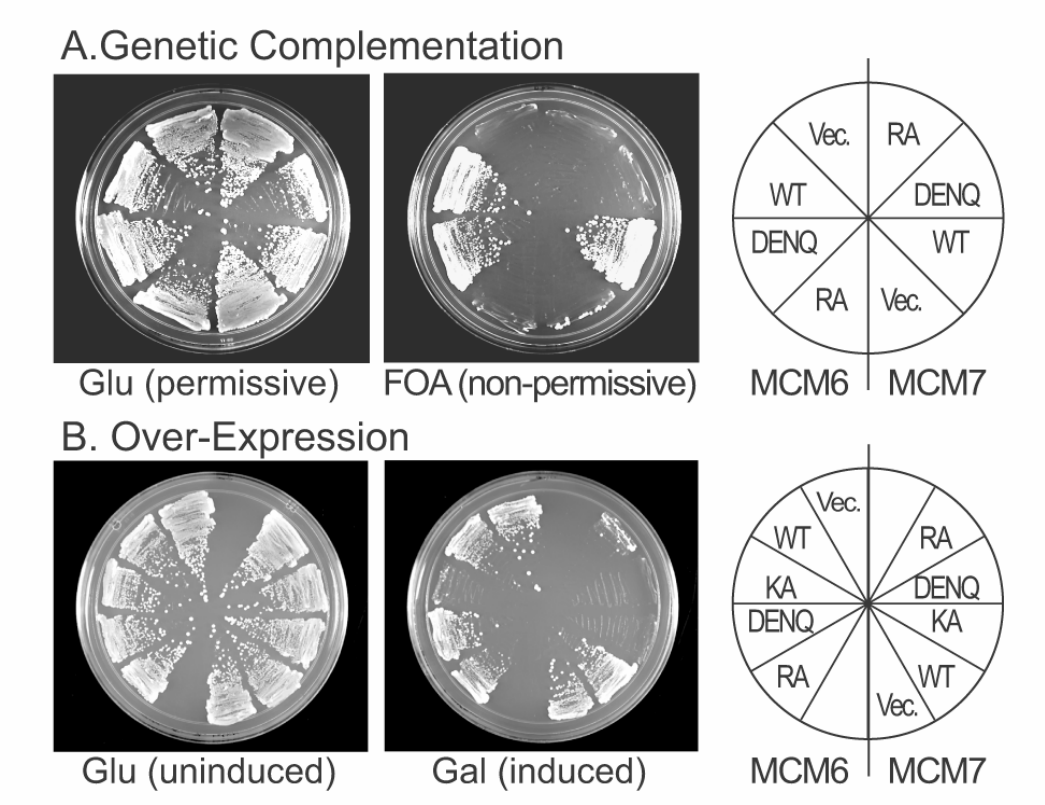

Figure 20. Analysis of the Walker B and arginine finger alleles of *mcm6* and *mcm7*.

A) Genetic complementation. Yeast tester strains contained chromosomal deletions of either *MCM6* or *MCM7* as indicated, and their viability is maintained by a *URA3* plasmid expressing a wild type copy of the corresponding *MCM* gene. *TRP1* plasmids containing either an expressed copy of the indicated allele (wild type, *DENQ*, *RA*) or an empty *TRP1* vector (vector) were transformed into these strains. Glu = permissive conditions, FOA = non-permissive conditions in which viability depends upon the indicated *mcm* allele. B) Dominant overexpression of *mcm* alleles. The indicated *mcm* alleles were expressed under the inducible *GAL1-10* promoter and integrated into the chromosomal *LEU2* gene. Glu = uninduced conditions, Gal = induced conditions.

4.3.6 The Mcm active sites contribute differentially to ATP hydrolysis

If Mcm active sites contribute equally to ATP hydrolysis, Mcm2-7 complexes containing any of the Walker B or arginine finger mutants should have similar defects in ATP hydrolysis. To directly test this hypothesis, we expressed and purified Mcm2-7 complexes that contained the specified mutant subunit in the company of five other wild type subunits (Materials and Methods). The resulting mutant Mcm2-7 preparations form complexes of hexameric size that contain all six Mcm subunits (Figure 21A, Figure 19).

We assayed the mutant Mcm2-7 complexes for ATPase activity. To verify that the *DENQ* and *RA* alleles in fact eliminate ATP hydrolysis, we generated and assayed complexes simultaneously containing either the DENQ or RA mutations in all six subunits (6X); these complexes are completely devoid of ATP hydrolysis (Figure 21A and B). The single mutant Mcm2-7 preparations were next assayed. Although most of these alleles are lethal, many of the corresponding mutant Mcm2-7 complexes demonstrate only relatively minor defects in ATP hydrolysis (Figure 21A and B), suggesting that unlike the Walker A mutants [104], the Walker B and arginine finger mutations appear to only block ATP hydrolysis at the affected active site, rather than blocking ATP hydrolysis of the entire Mcm2-7 complex.

Five Mcm2-7 mutant preparations showed significant loss of ATP hydrolysis. The Mcm4DENQ, Mcm7DENQ, and the Mcm3RA mutant complexes were the most severely affected, whereas preparations containing either the Mcm5DENQ or Mcm7RA mutations decreased ATP hydrolysis to the same levels observed for an Mcm2-7 complex with a single Walker A mutant subunit [104]. Four of these five mutations target the Mcm3/7 and 7/4 active sites, demonstrating that the bulk of *in vitro* ATP hydrolysis of Mcm2-7 comes from these two

sites. The exception to this is the Mcm5DENQ mutation. However, unlike the other four mutant complexes, the ATPase activity of a complex containing the corresponding arginine finger allele (Mcm2RA) demonstrated only a small defect in ATP hydrolysis. This may suggest that the Mcm5DENQ mutation causes an allele-specific loss of ATP binding to this site, thus mimicking the effect of the Mcm5KA allele in blocking ATP hydrolysis from the entire Mcm2-7 complex. These results directly demonstrate that the active sites within Mcm2-7 contribute unequally to Mcm function, with the relative contribution of each active site in the hexamer toward ATP hydrolysis and *in vivo* function roughly corresponding to relative ATPase activity of the isolated active site dimers (*i.e.*, Mcm3/7 > Mcm4/7 and Mcm6/2 > Mcm5/3 and Mcm4/6).

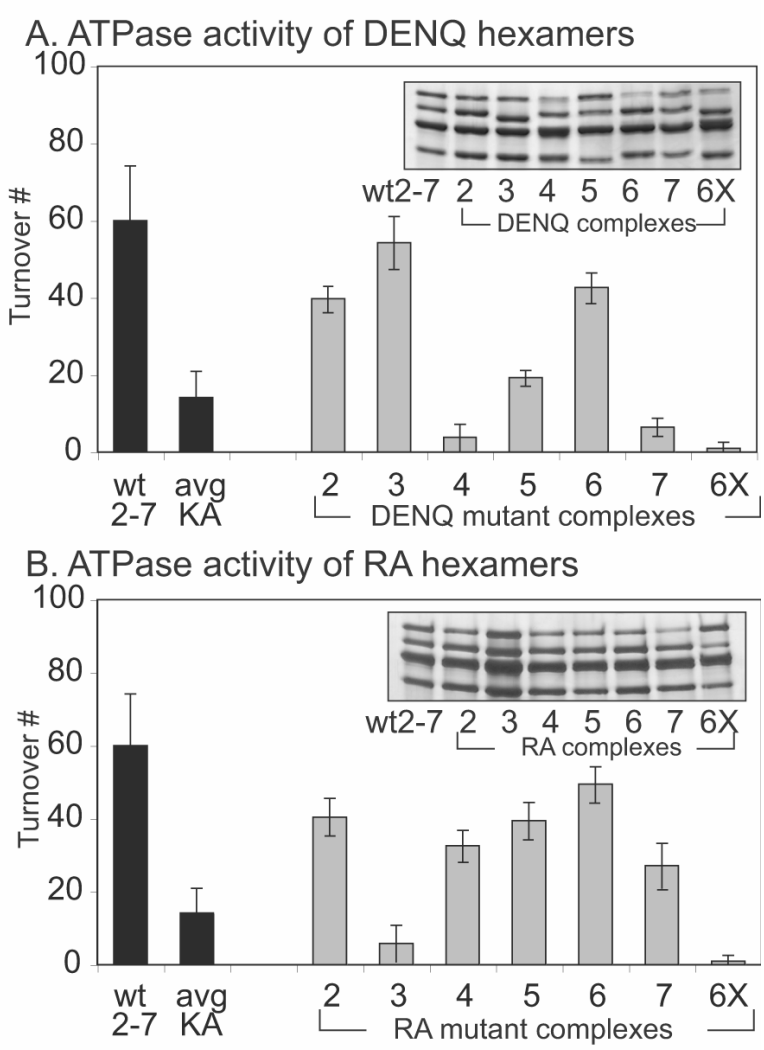

Figure 21. ATPase activity of Mcm2-7 heterohexamers containing subunits with either Walker B or arginine finger mutations.

A) & B) show the ATPase activity of Mcm2-7 complexes containing the indicated mutant A) Walker B or B) arginine finger allele subunit in the presence of the five other wild type subunits. Insets show a silver-stained gel of equivalent amounts of the indicated Mcm complexes. Avg KA equals the average ATPase activity of Mcm2-7 containing the Walker A mutations in any of the six individual subunits [104].

4.4 DISCUSSION

Our analysis of the Mcm2-7 active sites, both as isolated dimers and within the context of the Mcm2-7 heterohexamer, strongly indicates that they contribute unequally toward ATP hydrolysis and viability. This suggests that, in contrast to various models of helicase function [54, 55], equal involvement of the six active sites is not mechanistically essential for Mcm2-7 function.

4.4.1 Mcm subunit architecture

Our dimer association experiments support a previously predicted subunit architecture and active site configuration for Mcm2-7 (Figure 18E) [102]. Although we only explicitly demonstrate canonical AAA^+ ATPase active site composition for Mcm3/7 and Mcm7/4, these associations severely constrain the possible composition of the remaining active sites. Importantly, these dimer pairs can be arranged in a linear order, with Mcm2 and Mcm5 at either end. However, since Mcm2-7 forms a toroidal structure [35, 98, 124, 126, 127], the association of Mcm2 and Mcm5 with the remaining Mcm subunits likely drives circularization and formation of the Mcm2/5 active site. Although neither this study nor a previous study [102] provide direct evidence for the Mcm2/5 site, denaturing immunoprecipitation of Mcm subunits from *Drosophila* [204] and humans [130] both identify a specific cross-linking-dependent physical interaction between Mcm2 and Mcm5 that is highly labile in the absence of cross-linking [132].

4.4.2 Possible coordination among Mcm ATPase active sites

Within the Mcm7/4 and Mcm6/2 dimers, the Walker A motifs in both subunits appear to contribute to ATP hydrolysis. Since the Walker A motif typically serves to bind nucleotide (reviewed in [203]), this result suggests that ATP binding to the non-catalytic site of these dimers positively regulates activity at the adjoining catalytically-competent site. Such a feature could be used to coordinate ATP hydrolysis among the Mcm active sites; binding and hydrolysis of ATP at one site would stimulate activity of the adjacent site. Owing to the circular nature of the Mcm complex, this would lead to a defined hydrolysis order around Mcm2-7 (discussed more below). Alternatively, in the case of Mcm7/4 which oligomerizes into a hexamer (Figure 17B), a possible non-canonical active site might be formed between the Mcm7 Walker A motif and the Mcm4 arginine finger motif; inclusion of the Mcm7KA allele into this complex might simply block ATP hydrolysis from this putative site. Note that ATP hydrolysis at Mcm3/7 is independent of the non-catalytic Walker A motif, a fact that may be relevant to the unique functional importance of this site (below).

4.4.3 The unequal involvement of Mcm active sites

We identified a correlation between the ATPase activity of isolated Mcm dimers and their functional importance within the intact Mcm2-7 complex. The Mcm3/7 and Mcm7/4 active sites demonstrate good to moderate ATP hydrolysis as isolated dimers, and analysis of the ATPase activity of Mcm2-7 complexes containing mutants that affect ATP hydrolysis at these active sites indicated that they are especially critical to hydrolysis within the complete Mcm2-7 hexamer. In contrast, Mcm4/6 lacks ATPase activity in isolation, and mutations within this site cause

negligible ATPase defects within isolated Mcm2-7 complexes. This correlation between the activity of isolated dimers and Mcm2-7 mutations is not absolute, since Mcm6/2 demonstrates ATP hydrolysis as an isolated dimer but appears to contribute little to ATP hydrolysis within the Mcm2-7 hexamer. This observation suggests that the activity of individual active sites is likely constrained within the context of the hexamer. It is interesting to note that for several active sites the corresponding Walker B and arginine finger mutations have similar phenotypes: *e.g.*, both 3RA and 7DENQ mutant hexamers are almost completely defective for ATP hydrolysis, whereas both the 4RA and 6DENQ mutants demonstrate normal viability. This strong correlation between mutations proposed to target the same active site for both *in vivo* and *in vitro* activities provides additional support for the proposed active site composition. Correlating our results with additional data suggests particular functions for specific Mcm active sites:

4.4.3.1 Mcm3/7 and Mcm7/4 – regulated core of the Mcm motor

Mutations within these two active sites uniquely inhibit steady-state ATP hydrolysis of Mcm2-7. Furthermore, Walker A mutations in either Mcm7 or Mcm4 uniquely inhibit the ability of Mcm2-7 to bind ssDNA in an ATP-dependent manner [126]. Since both ATP hydrolysis and ssDNA interactions are directly required for DNA unwinding, our results strongly implicate these active sites in coupling ATP hydrolysis to helicase activity. Mcm7 appears to be particularly important: it is a common subunit in both active sites, and unlike any other Mcm subunit, overexpression of any of the three *mcm7* ATPase mutants (*mcm7KA*, *DENQ*, or *RA*) causes lethality. The functional prominence of Mcm7 would make it a good regulatory target for modulating the ATPase activity of the entire Mcm2-7 complex. It is interesting to note that various putative negative regulators of Mcm2-7 (DNA-damage checkpoint proteins Rad17 [205], ATRIP [206] and the retinoblastoma protein [207]) specifically bind to the C-terminus of Mcm7.

4.4.3.2 Mcm4/6 – a structural element?

Among our ATPase alleles, only the *Mcm6DENQ* and the *Mcm4RA* alleles demonstrate completely normal viability and growth rate (Table 4). In *S. pombe,* the *mcm6* Walker B mutations are also viable [182]. This is in sharp contrast to the *mcm6KA* allele, which is lethal and blocks ATPase activity of Mcm2-7 [104]. Curiously however, the Mcm6DENQ mutant blocks helicase activity from both the murine Mcm467 complex [122], as well as the *S. cerevisiae* complex (Figure 22). These data suggest that the Mcm6DENQ mutation (and probably the Mcm4RA mutation) does indeed block ATP hydrolysis at the Mcm4/6 site. Since the Walker B and arginine finger motifs are often involved with ATP hydrolysis, while the Walker A motif often makes larger contributions to nucleotide binding (reviewed in [203]), these results suggest that the Mcm4/6 site may need to only bind but not hydrolyze ATP for *in vivo* function. There is considerable precedence for ATP binding sites serving structural rather than catalytic roles: three of the six ATPase sites in the F1-ATPase need to bind but not hydrolyze ATP [208], and the "stator" subunit of the DNA replication processivity clamp loader retains a non-functional ATP active site [209, 210].

4.4.3.3 Mcm2/5 – an ATP-dependent gate?

Additional data from our lab supports a unique involvement of the Mcm2/5 active site in both the association rate of Mcm2-7 with ssDNA [126] and its ability to bind circular ssDNA [211]. In combination with the putative labile nature of the Mcm2/5 active site, these results are consistent with an ATP-dependent topological closure of the Mcm2-7 ring at the Mcm2/5 active site ("gate"). The functional significance of this putative gate is under investigation.

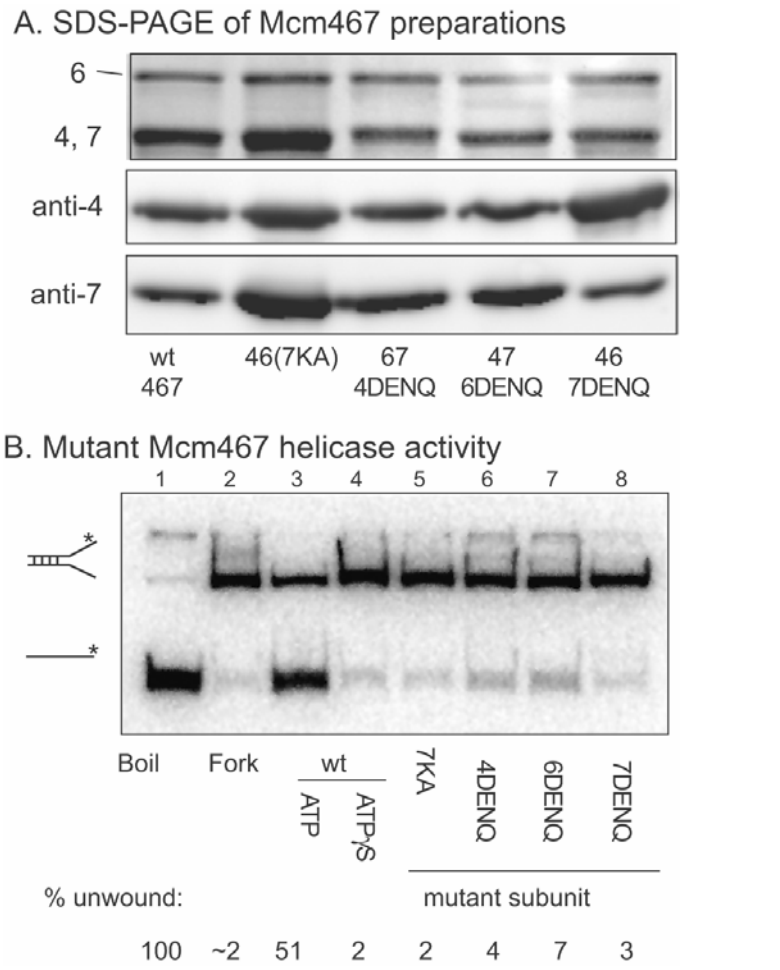

Figure 22. Contribution of Walker B motifs to Mcm467 helicase activity.

A) Silver-stained gel of equimolar amounts of the indicated wild type or mutant Mcm467 preparations. B) Ability of Mcm467 complexes to unwind a short forked DNA substrate. This assay was conducted as described in [126]. Lanes 3 and 4 contain the wild type Mcm467 complex, lane 5 contains a Mcm467 complex with Mcm7KA, likewise, lanes 6, 7, and 8 contain Mcm467 preparations with the Mcm4DENQ, Mcm6DENQ, or Mcm7DENQ mutation respectively. The amount of unwinding was quantified and is as shown. Lane 4 contained the non-hydrolyzable ATP analog ATPγS [104]; all other lanes contain ATP.

4.4.3.4 Function of the other Mcm active sites

Molecular motors couple ATP binding and hydrolysis to produce work that likely necessitates a fixed ATP hydrolysis cycle in which the participating active sites fire once in a defined order during each cycle. Our analysis indicates that Mcm6/2 and Mcm5/3 sites contribute little to *in vitro* ATP hydrolysis within Mcm2-7, suggesting that they are not part of a fixed ATP hydrolysis cycle that unwinds DNA. However, they are needed for *in vivo* function, suggesting that perhaps they have a function that is not directly related to DNA unwinding, e.g., to load the Mcms onto DNA during initiation, or alternately, assist unloading of the complex during termination.

4.4.4 Relationship between Mcm ATPase active sites and helicase activity

Although our analysis of the Mcm Walker B and arginine finger mutants indicates the unequal involvement of these sites in Mcm2-7 function, definitive verification will require being able to study the DNA binding and helicase activity of these mutant complexes. Despite the historic inability to demonstrate helicase activity from purified Mcm2-7 [63, 101, 123, 126], a recent report demonstrating *in vitro* helicase activity from this complex in the absence of either the GINS or Cdc45 [211] offers the promise of being able to finally study the mechanistic contribution of the Mcm ATP active sites toward DNA unwinding.

5.0 THE MCM2-7 COMPLEX HAS *IN VITRO* HELICASE ACTIVITY

The contents of this chapter, with some additions and alterations, come from [211] and are reprinted following the guidelines of Cell Press's Authors' Rights statement.

5.1 SUMMARY

Helicases unwind duplex DNA ahead of the polymerases at the replication fork. However, the identity of the eukaryotic replicative helicase has been controversial: *in vivo* studies implicate the ring-shaped heterohexameric Mcm2-7 complex, although only a specific subset of Mcm subunits (Mcm467) unwind DNA *in vitro*. To address this discrepancy, we have compared both Mcm assemblies and find that they differ in their linear single-stranded DNA association rate and their ability to bind circular single-stranded DNA. These differences depend upon the Mcm2/5 interface, which we hypothesize serves as an ATP-dependent "gate" within Mcm2-7. Importantly, we find that reaction conditions that putatively close the Mcm2-7 "gate" reconstitute Mcm2-7 helicase activity. Unlike Mcm467, Mcm2-7 helicase activity is strongly anion-dependent. Our results show that purified Mcm2-7 acts as a helicase, provide functional evidence of a Mcm2/5 gate, and lay the foundation for future mechanistic studies of this critical factor.

5.2 INTRODUCTION

Replicative helicases are motor proteins that use ATP binding and hydrolysis to unwind duplex DNA into single-stranded substrates for DNA polymerase. In eukaryotes, *in vivo* observations implicate the Mcm2-7 complex as the replicative helicase (reviewed in [84]). Mcm2-7 is a heterohexamer of six essential but non-identical subunits (numbered 2 through 7) that are each AAA^+ ATPases [73]. Although little structural information exists for this complex, it is known to be toroidal [124, 126, 127], and similar to other AAA+ proteins it has ATPase active sites at dimer interfaces with one subunit contributing the Walker A motif and the adjoining subunit contributing an essential arginine [102, 146].

Despite these *in vivo* observations, Mcm2-7 has been reported to lack *in vitro* helicase activity [102, 104, 126]. Interestingly, both an archaeal MCM complex (reviewed in [108]) and an alternative hexameric Mcm complex containing only three of the six eukaryotic Mcm subunits (Mcm4, 6, and 7; the Mcm467 complex) have DNA unwinding activity [63, 101, 103]. Recently, a larger complex containing Cdc45, Mcm2-7, and *G*INS has been isolated and shown to have *in vitro* helicase activity (CMG complex [105]).

Here, we report the reconstitution of Mcm2-7 helicase activity. Through a detailed biochemical comparison of the Mcm2-7 and Mcm467 complexes, we learn that these Mcm assemblies differ in their ability to bind circular ssDNA. The source of this difference is an ATPase active site composed of Mcm2 and Mcm5 (the Mcm2/5 active site). We hypothesize that the Mcm2/5 active site functions as an ATP-dependent gap or "gate" in the toroid and find that the biochemical activities of Mcm2-7 but not Mcm467 are anion-dependent. Moreover, we discovered that reaction conditions that preferentially reduce the ability of the complex to bind circular ssDNA (close the "gate") reconstitute Mcm2-7 helicase activity. These findings provide

direct biochemical evidence that the Mcm2-7 complex is a DNA helicase, predict an *in vivo* role for the Mcm2/5 active site in Mcm2-7 loading or activation, and remove a major biochemical obstacle toward mechanistic studies of the Mcm2-7 complex.

5.3 RESULTS

5.3.1 Mcm2-7 binds circular ssDNA with higher affinity than Mcm467

Both Mcm467 and Mcm2-7 form toroidal hexamers and likely bind ssDNA within their central channel [126]. To test the topological consequences of the toroidal structure, competition experiments were conducted to compare their ability to bind linear or circular M13 ssDNA (Figure 23A). Using an established filter binding assay utilizing a radiolabeled linear oligonucleotide probe [126], we find that although unlabelled linear ssDNA effectively competes for binding by either Mcm complex, circular ssDNA competes well with Mcm2-7 but poorly with Mcm467 (Figure 24A). Similar results were obtained using circular and linear phage ϕX174 ssDNA as a competitor and several different radiolabeled oligonucleotides (data not shown). This result suggests that Mcm467 topologically excludes circular ssDNA from its central channel, whereas Mcm2-7 either transiently opens its ring structure or binds circular ssDNA on an external surface.

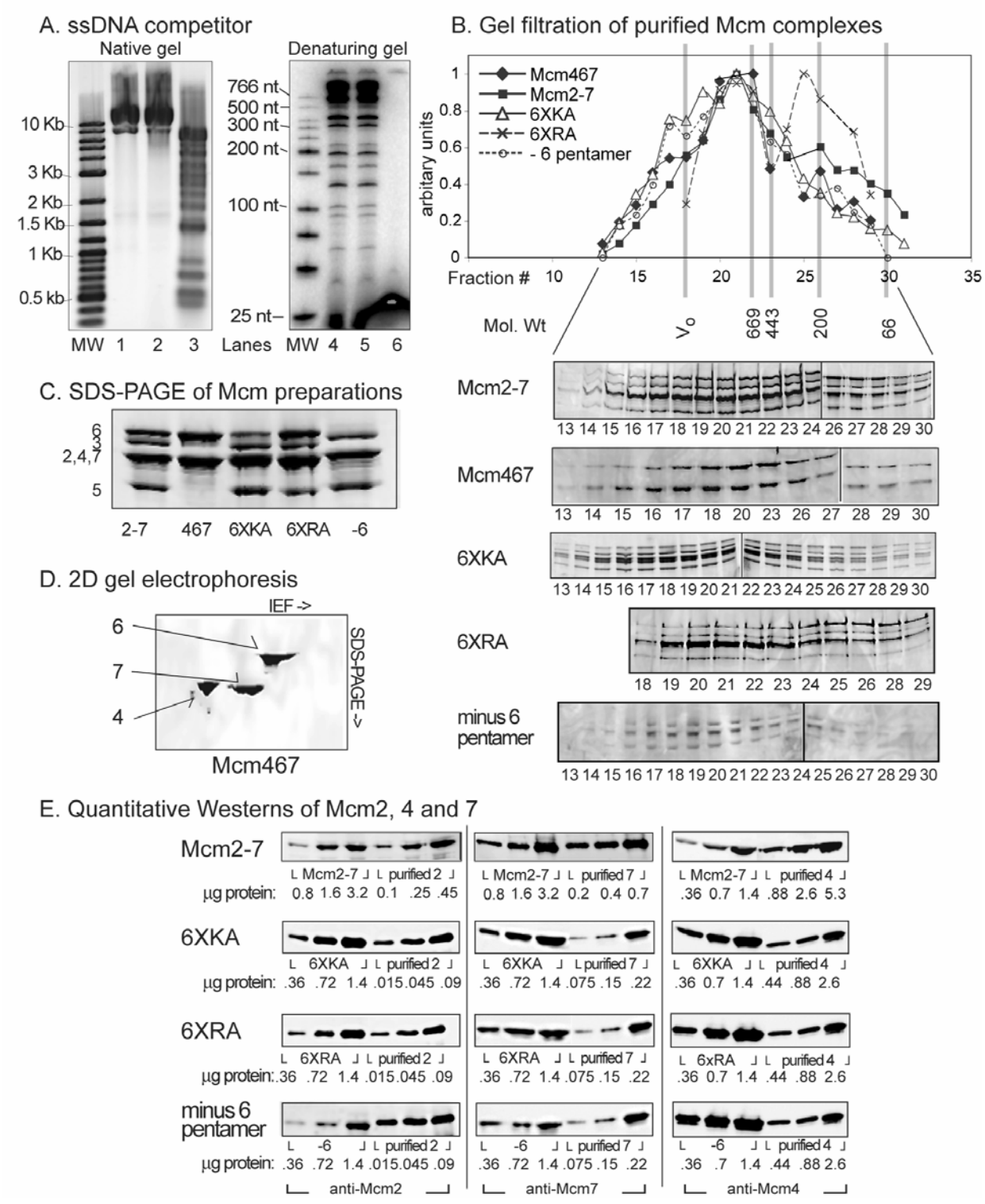

Figure 23. Characterization of single-stranded M13 substrates and representative purified Mcm preparations.

A) *HhaI* cleaves both single-stranded and double-stranded M13. Left) Native gel analysis. 0.7% agarose gel, stained with Sybr Gold (Molecular Probes), and visualized on a Fuji FLA-5100 Fluorescence imager. MW = dsDNA molecular weight markers of the indicated length. Lane 1, 1 µg of circular M13 ssDNA; lane 2, 1 µg of circular

M13 ssDNA treated with T4 DNA polymerase; lane 3, 1 μg circular M13 ssDNA treated with the restriction endonuclease *Hha*I. Note that the molecular weight markers used are for reference, and since this is a native gel, the position of single stranded DNA fragments do not correspond to their true molecular weight. This result confirms that *Hha*I cleaves single stranded DNA and that treatment with T4 DNA polymerase does not substantially degrade circular ssDNA. Right) 6% denaturing polyacrylamide gel analysis. All DNA fragments were 5' end-labeled with γ^{32}P-ATP and polynucleotide kinase and visualized on a Fuji phosphoimager. MW = ssDNA molecular weight markers of the indicated length. Lane 4, M13 dsDNA following cleavage with *Hha*I; lane 5, M13 ssDNA following cleavage with *Hha*I. Note that the banding pattern in lanes 4 and 5 are identical, indicating that *Hha*I cleaves at the same sites in both single-stranded and double-stranded DNA. Many of the expected M13 fragments are of similar size and do not completely resolve on this gel. In lane 6, the same amount of M13 ssDNA cleaved with *Hha*I and further treated with T4 DNA polymerase. Comparison of lanes 2 and lane 6 demonstrate that T4 polymerase effectively degrades linear but not circular ssDNA. B.) Analytical gel filtration of representative Mcm preparations. Indicated preparations were separated by gel filtration and the fractions analyzed by SDS-PAGE. The calculated size of both the Mcm467 and Mcm2-7 hexamer is ~ 600 kDa. The "6XKA" and "6XRA" preparations contain either the Walker A box K–>A mutation or the arginine finger R–>A mutation in each of the six MCM subunits and thus represent the most extreme mutant Mcm2-7 complexes. Our preparation of 6XRA contains excess Mcm6, which generates an additional low molecular weight peak. C) SDS-PAGE of 3 pmol of representative wild type and mutant Mcm preparations. The identity of the Mcm subunits is as shown. Note that Mcm2, 4, and 7 are of similar molecular weight do not resolve from one another by 1-dimensional SDS-PAGE. D) Two-dimensional gel electrophoresis of Mcm467 preparation. Following quantitation, the ratio of Mcm4:6:7 was 1.9:1:1.2, with Mcm6 being the least abundant subunit. Among various Mcm467 preparations used in this study, our quantitation suggests that up to 50-78% of the complexes have a 1:1:1 subunit stoichiometry. Similar 2D analysis was not conducted with Mcm2-7, since 2 Mcm subunits do not resolve well under these conditions. E) Quantitative Westerns of Mcm preparations. To measure the amounts of the individual co-migrating Mcm4, 2, and 7 subunits, quantitative Westerns were performed, using known amount of appropriate Mcm single subunit preparations as standards. **Summary.** In combination with the quantitation of Sypro Orange stained bands belonging to Mcm6, Mcm3 and Mcm5, the results from quantitative Westerns allow us to calculate the fractions of Mcm subunits that are potentially present as heterohexameric complexes. For the wild type Mcm2-7 complex, these results are consistent with ≥50% of the subunits being in a heterohexameric form. For 6XRA, 6XKA, and minus 6 pentamer, the values are 42%, 30%, and 15%, respectively. From previous work [126], we know that the specific activity of the wild type complexes for ssDNA binding are approximately 50%, and that among the mutant complexes used in this study, the specific activity is within approximately two-fold of the wild type complexes.

ATP binding stimulates the oligomerization of some helicases (*e.g.*, [212]). To examine a potential role for ATP in closure of the Mcm2-7 toroid, we modified our competition assay into an order of addition assay to test if ATP preincubation of Mcm2-7 decreases its ability to bind circular ssDNA (Figure 24B). To simplify experimental interpretation, the non-hydrolyzable nucleotide analog ATPγS was used. This assay was conducted in two steps (Mcm circularization assay, Figure 24C): the Mcms are first incubated for an hour with either ATPγS in the absence of DNA, or with a mixture of radiolabeled linear ssDNA probe and unlabeled competitor ssDNA (either linear or circular single-stranded M13) in the absence of ATPγS. In the second step, the complete reaction is reconstituted (*i.e.*, the ssDNA mixture is added to the ATPγS preincubation, or ATPγS is added to the ssDNA preincubation), and Mcm association with the radiolabeled oligonucleotide is quantified over time by filter binding. Since probe binding and competition are inversely related, quantitation of probe binding provides an assessment of competition. For Mcm2-7, ATPγS preincubation reduces the efficiency of circular ssDNA as a competitor (Figure 24B, cir 1st vs. cir 2nd), with negligible effects on the ability of linear ssDNA to compete (Figure 24B, lin 1st vs. lin 2nd). The ability of ATPγS preincubation to block circular ssDNA competition/binding is remarkably stable (≥7 hours, Figure 24B) and qualitatively similar results were obtained when ATP was substituted for ATPγS (data not shown). This result indicates that ATP occupancy of one or more active sites inhibits binding to circular ssDNA and is consistent with a model in which ATP stimulates closure of the Mcm2-7 ring. To simplify our presentation, we will subsequently refer to circular ssDNA competition as circular ssDNA binding.

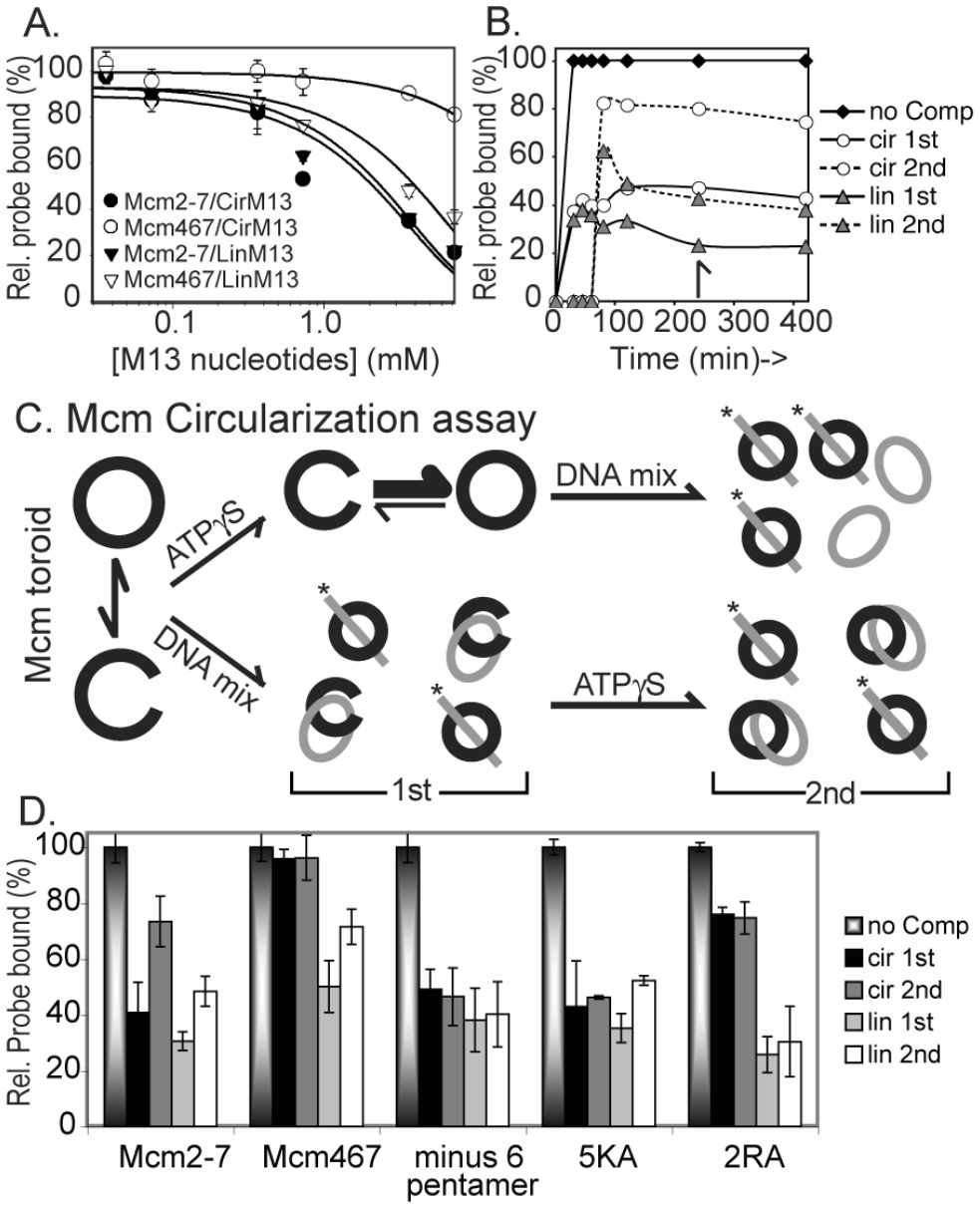

Figure 24. Effects of ssDNA topology on Mcm binding.

A) Radiolabeled oligo #826 binding in the absence of competitor ssDNA = 100%; other values represent binding competition in the presence of the indicated amounts of unlabeled M13 ssDNA (cir = circular, lin = linear, mM nucleotides). The IC_{50} values: Mcm2-7 with circular ssDNA, 1.6±4 mM; Mcm2-7 with linear ssDNA, 1.8±3 mM; and Mcm467 with linear ssDNA 3.8± 0.6 mM. Mcm467 with circular ssDNA has an affinity too low to accurately measure. From extrapolation of the available data points, we estimate its IC_{50} at > 32 ±8 mM. B) Time course of Mcm2-7 circularization. 100% represents probe binding in the absence of ssDNA competitor. The 240 minute values were used in 1D. C) Circularization assay. Intact or split circles = Mcm hexamers. DNA mix = radiolabeled oligo #455 (grey line with *) and either linear (not shown) or circular (grey oval) unlabeled M13 competitor; 1st and 2nd refer to the addition order of the DNA mix relative to the ATPγS. D) Comparison of circularization assays at t = 240 min for the indicated wild type and mutant Mcm preparations. Conditions were identical to 1B.

Similar circularization experiments were conducted with Mcm467 (Figure 25A). To facilitate comparison, results from the 240-minute time point are shown (Figure 24D). In sharp contrast to Mcm2-7, circular ssDNA binds poorly regardless of ATP addition order. To determine if a complete Mcm complex is required for this effect, we examined a pentameric Mcm complex lacking Mcm6 (minus 6 pentamer) that has a predominately open-ring structure (Figure 25C). Results from the circularization assay (Figure 25B) indicate that this complex binds both circular and linear ssDNA equally and independently of ATPγS addition order (Figure 24D), consistent with this assay providing a read-out for Mcm complex topology.

Taken together, a parsimonious interpretation of these results would be that circular ssDNA binds within the central channel of Mcm complexes, and that the Mcm2-7 toroid contains a gap ("gate") that Mcm467 lacks. Since the main differences between these two complexes are the Mcm2, 3, and 5 subunits, the simplest hypothesis is that the gate involves one or more of these subunits. Although other interpretations are possible, this hypothesis provides the motivation for many of the following experiments.

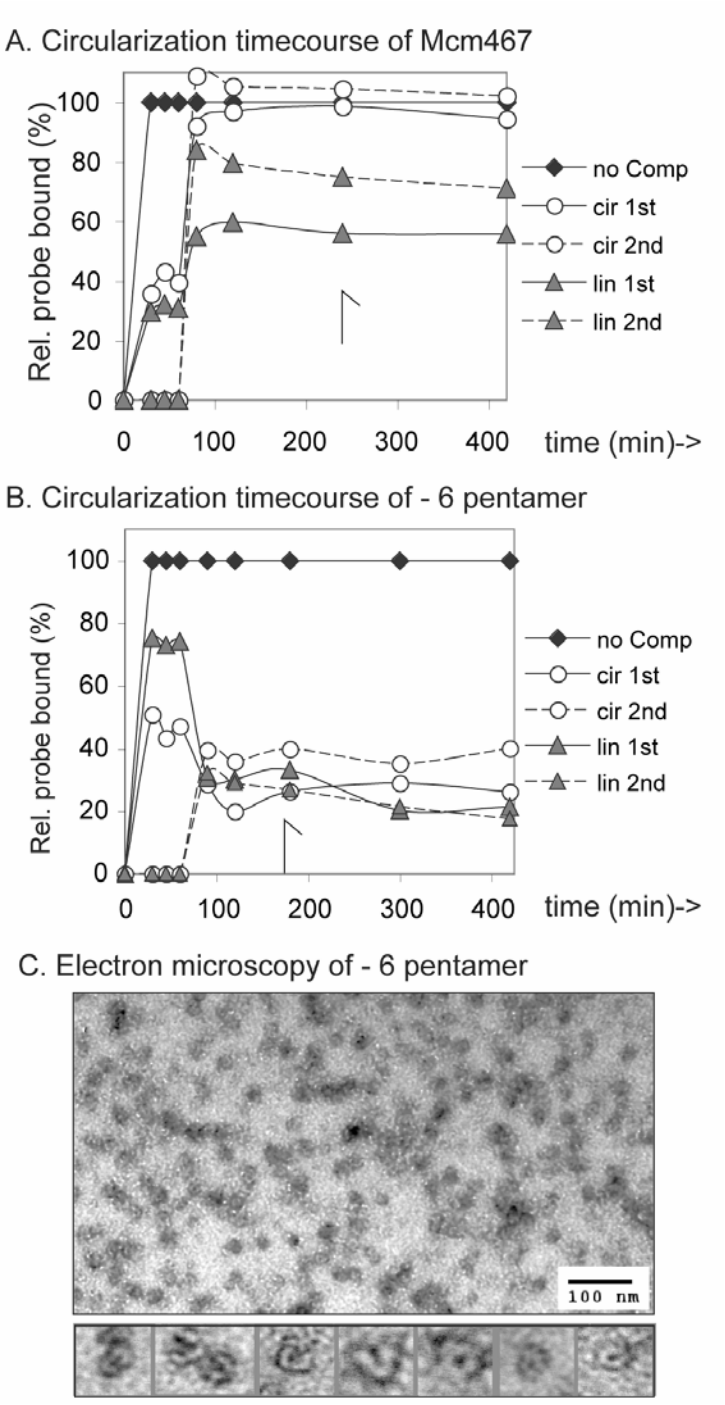

Figure 25. Circularization assays.

A) Circularization time course of the Mcm467 complex, and B) Circularization time course for the Minus 6 pentamer. Experimental conditions were identical to Figure 1B; arrows indicate data used in Figure 24D. C) Electron microscopy of minus 6 pentamer in the presence of ATPγS. 60 Individual complexes (inset) were manually counted and classified as either open rings (57%), closed rings (24%), or intermediate/indeterminate (19%); this ratio was unaffected by the presence of absence nucleotide. This preparation demonstrated approximately 2-fold (Mcm2-7) to 3-fold (Mcm467) more open rings than the analogous hexameric preparations (Data not shown, [126]).

5.3.2 The Mcm2/5 ATPase active site mediates circular ssDNA interactions in Mcm2-7

Since Mcm ATPase active sites are formed at dimer interfaces [102], the relationship between ATP addition order and circular ssDNA binding would be explained if a specific ATPase active site corresponds to the Mcm2-7 gate. To test this possibility, we examined mutant Mcm2-7 complexes containing a single subunit with a lysine to alanine substitution (KA alleles) in the Walker A box [104] in the company of five wild type subunits. Since the KA mutations in Mcm4 and Mcm7 interfere with ATP-dependent ssDNA binding [126], their analysis was not pursued. Circularization assays using the Mcm2KA, 3KA, or 6KA complexes yielded results similar to wild type Mcm2-7, with ATPγS preincubation causing a reduction in circular ssDNA binding (Figure 26A). However, similar to the minus 6 Mcm pentamer, the Mcm5KA complex displays good binding to circular ssDNA independent of ATP addition (Figure 24D).

To further characterize the role of Mcm5 in circular DNA binding, additional Mcm mutations were examined. Subunit association studies suggest that Mcm2 and Mcm5 form an ATPase active site, with Mcm5 contributing the Walker A motif and Mcm2 contributing the essential arginine [102]. Alanine substitutions were made in the putative arginine finger of each subunit (RA alleles), and a set of six Mcm2-7 complexes analogous to the KA set were expressed and purified. The characterization of these alleles is presented elsewhere (**Chapter 4**; **Appendix A**); however, none of these changes substantially interferes with the *in vitro* oligomerization or stability of the Mcm2-7 complex (Figure 23B and E), and only the Mcm3RA mutation blocks *in vitro* ssDNA binding (data not shown). Although the Mcm4RA, 5RA, 6RA, and 7RA complexes exhibit qualitatively wild type Mcm2-7 activity in the circularization assay (Figure 26B), the Mcm2RA complex binds circular ssDNA equally and independently of ATP addition order (Figure 24D). However, in contrast to the Mcm5KA complex but similar to the

Mcm467 complex, the 2RA complex binds circular ssDNA poorly under both conditions suggesting that this mutant complex forms a closed toroid even in the absence of ATPγS. Taken together, these results implicate ATP binding by the Mcm2/5 dimer interface as particularly important for the circular ssDNA binding.

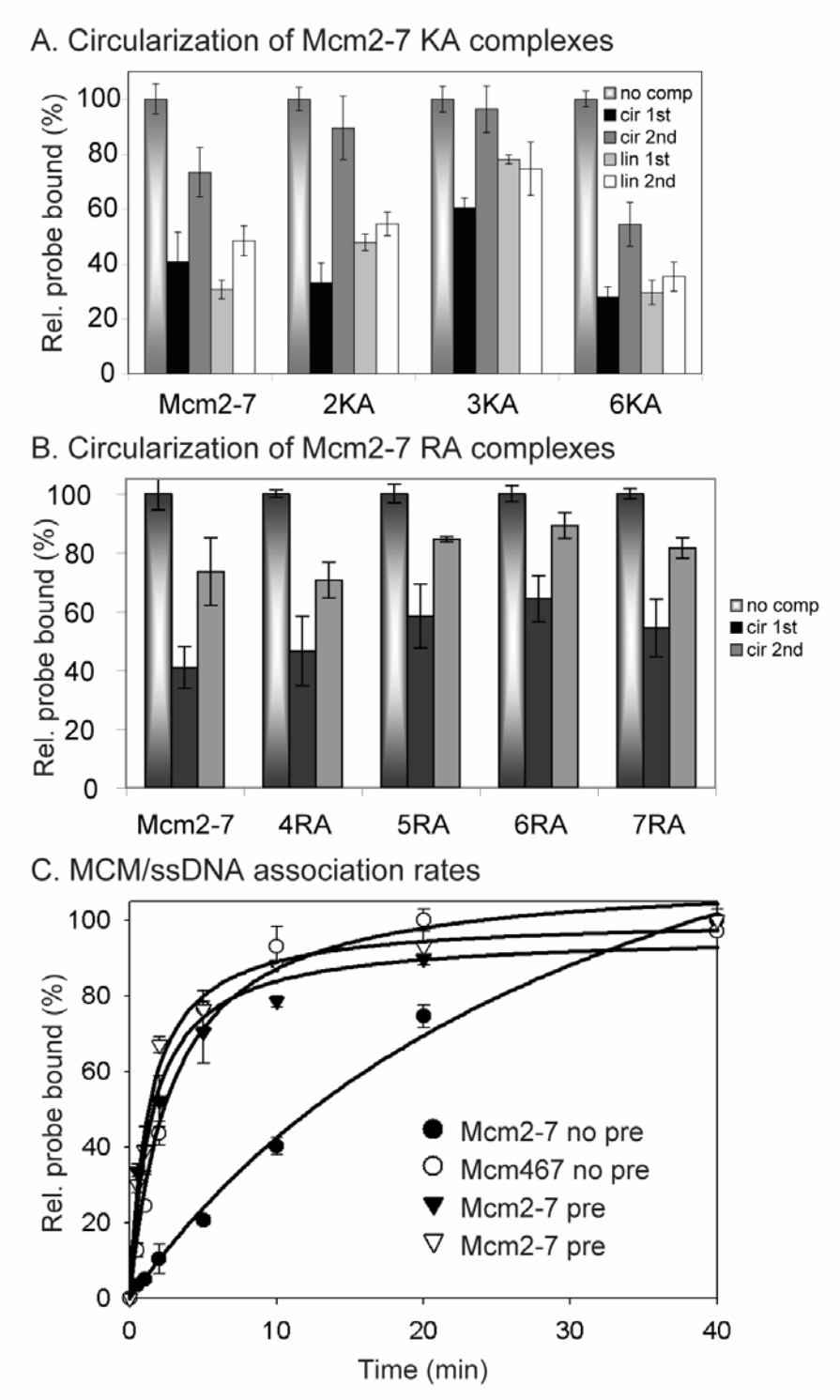

Figure 26. Additional Mcm circularization and association experiments.

A) & B) Comparison of circularization assay at t = 120 min for the indicated wild type and mutant Mcm2-7 preparations. Experiments were conducted as in Figure 1B. C) Wild type Mcm2-7 and Mcm467 ssDNA association rate experiments conducted in either the presence (pre) or absence (no pre) of a 30 minute ATPγS preincubation.

5.3.3 Relationship between Mcm2-7 circularization and ssDNA association rate

We have previously reported another Mcm2-7 activity that varies with ATP preincubation [126]. Mcm467 binds ssDNA >5-fold more quickly than Mcm2-7. However, preincubation of Mcm2-7 with ATP increases its association rate to Mcm467 levels, ([126], summarized in Figure 26C). Moreover, this association rate enhancement is also mediated by the Mcm2/5 active site, since Mcm2-7 complexes with either the Mcm2RA or 5KA mutation bind ssDNA at the same rate as Mcm467 even without ATP preincubation [126].

The dependence of ssDNA association rate and circular ssDNA binding upon ATP addition order suggests a common mechanism. In support of this conjecture, we find that both activities (*i.e.*, ssDNA association rate enhancement and inability to bind circular ssDNA, Figure 27A) depend upon extensive ATP preincubation (25-30 minutes) to achieve their maximal effect, consistent with a slow ATP-dependent conformational change within Mcm2-7. Nevertheless, these two activities can be experimentally uncoupled. Whereas the minus 6 pentamer binds circular ssDNA independent of ATP addition order (Figure 24D), its association rate is still enhanced following ATP preincubation (Figure 27B). These results indicate that although an artificial gap in the Mcm complex can substitute for the Mcm2/5 site to facilitate circular ssDNA binding, the association rate activity may be mechanistically distinct.

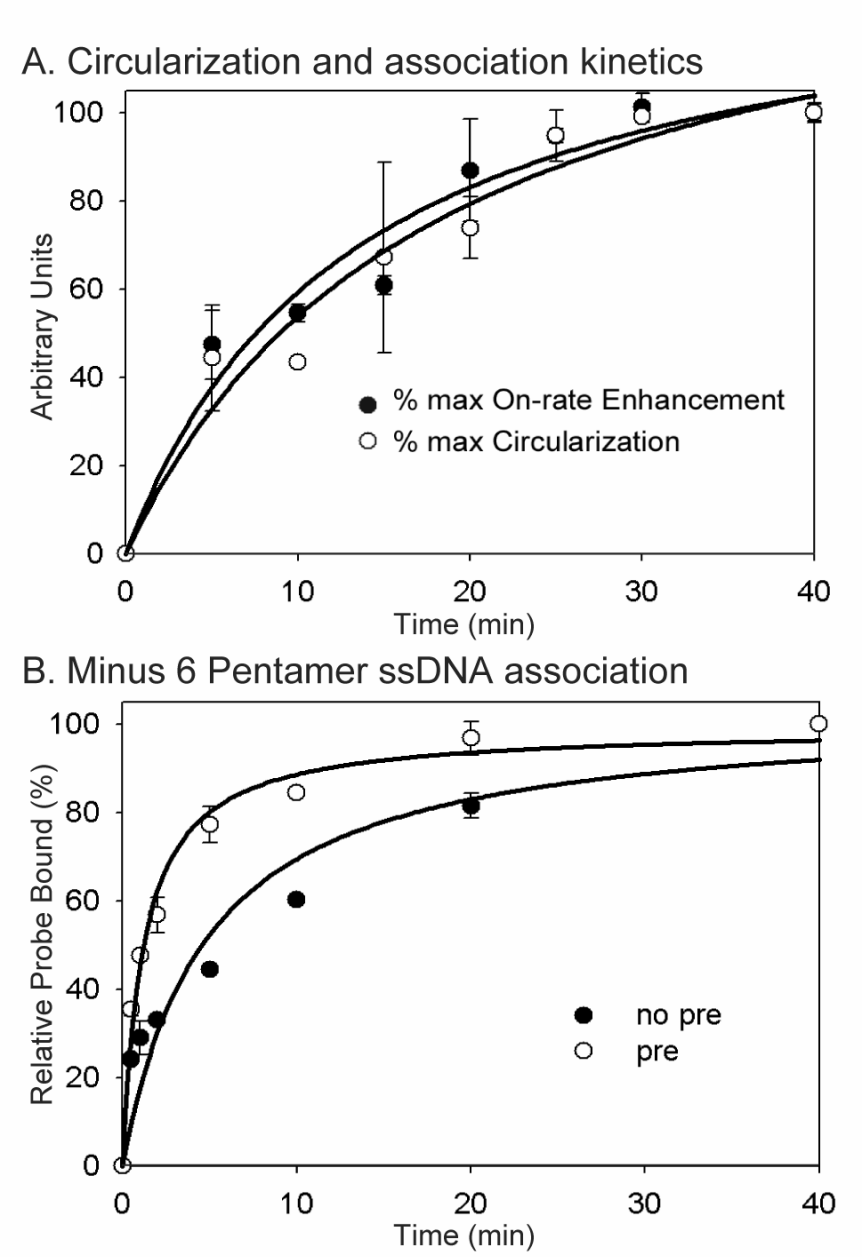

Figure 27. Relationship between Mcm/ssDNA association rate and circularization.

A) Mcm2-7 was preincubated with ATPγS for the indicated times and then added to circularization and association rate assays. 100% corresponds to either the maximum association rate activity observed, or the least effective competition with circular ssDNA. B) Association rate of the minus 6 pentamer to oligo #510 in the absence (no pre) or presence (pre) of ATPγS preincubation.

5.3.4 Activation of the Mcm2-7 helicase

We considered the possibility that the lack of Mcm2-7 helicase activity is related to the closure of the Mcm2/5 gate. Although preincubating Mcm2-7 with ATP failed to reconstitute helicase activity (data not shown), additional possibilities were considered. We note that the role of ATP in Mcm2-7 gate closure seems contradictory: both ATP preincubation (suggesting a positive role for ATP) and inactivation of the Mcm2/5 ATPase active site (suggesting a negative role for ATP) have similar effects on circular ssDNA binding and association rate. An explanation consistent with our findings would be that each treatment displaces an unknown inhibitor from the Mcm2/5 active site.

Investigations of such an inhibitor lead to the reconstitution of Mcm2-7 helicase activity. One specific possibility was that ADP that either co-purified with the complex or was formed under assay conditions inhibits Mcm2-7 helicase activity. Although our helicase assay contains an efficient ATP regenerating system, extremely low residual amounts of ADP might be sufficient to poison Mcm2-7 helicase activity. By increasing the concentration of ATP regeneration components (phosphocreatine and creatine kinase) several fold to further decrease ADP levels, Mcm2-7 helicase activity was uncovered (Figure 28A compare lanes 4 and 8). This new DNA unwinding activity was both Mcm- dependent (blocked by Mcm-specific antibody AS1.1, Figure 28A, lane 9-11) and ATP-dependent (Figure 28A, compare lanes 4 and 12) with a $k_{1/2}$ = 1.8 mM for ATP (data not shown).

Further investigation reveals that Mcm2-7 helicase activity is not inhibited by ADP but by specific ions in the standard assay. We found that the activation of the Mcm2-7 helicase only required the phosphocreatine component of the ATP regenerating system (Figure 28A, compare

lane 4 to lanes 5-7), indicating that ATP regeneration is unnecessary for helicase activity. Given the positive effect of phosphocreatine, we investigated if other salts/ions would stimulate this activity. We tested a variety of representative anions, cations, and volume excluders (Figure 28B). Only acetate and glutamate supported Mcm2-7 helicase activity, indicating that unlike many other enzymes, Mcm2-7 helicase activity is anion-specific and shows little dependence on the Hofmeister series [213, 214]. As potassium glutamate provided the largest stimulation, it was used in subsequent experiments.

To address if certain anions inhibit helicase activity rather than fail to support it, assays containing mixtures of glutamate and chloride were conducted (Figure 28C). Although 50 mM potassium glutamate supports helicase activity, addition of modest concentrations of potassium chloride inhibits the activity. Conversely, although 50 mM potassium chloride blocks helicase activity, addition of sufficient glutamate partially restores helicase activity. These results indicate that chloride and glutamate have opposite effects on Mcm2-7 helicase activity, consistent with the hypothesis that glutamate displaces inhibitory ions (*e.g.*, chloride) from Mcm2-7.

Since helicase activity has not been previously observed from Mcm2-7, its activity is presumably more sensitive to ionic conditions than Mcm467. To test this hypothesis, the ability of glutamate to stimulate helicase activity from both Mcm2-7 and Mcm467 was compared (Figure 28D). Although glutamate stimulates Mcm467 helicase activity <2-fold over a range of 0-200 mM, Mcm2-7 helicase activity is stimulated at least 50-fold over the same concentration range. This result accounts for the previous inability to detect Mcm2-7 helicase activity and suggests that the basis of this glutamate stimulation involves Mcm2, 3, and/or 5.

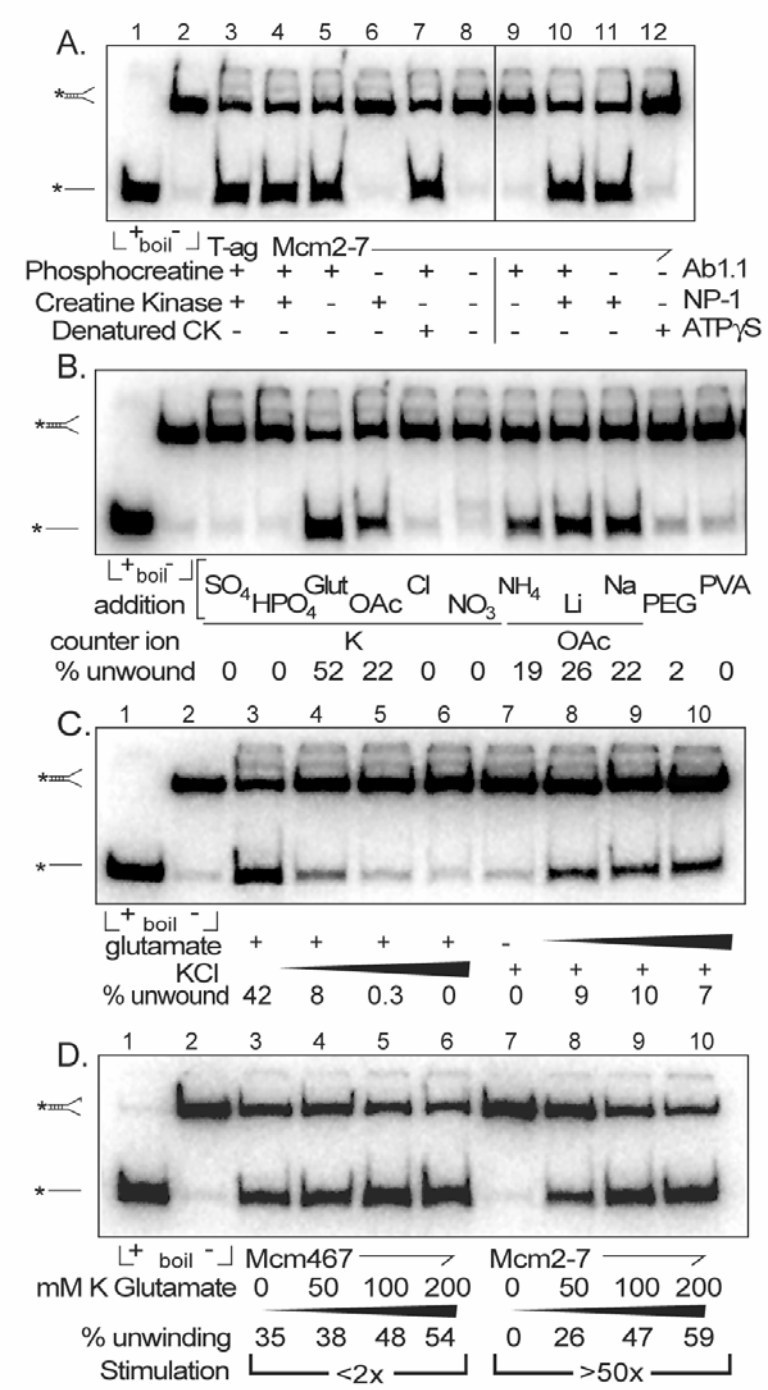

Figure 28. Mcm2-7 helicase activity.

A) Phosphocreatine activates Mcm2-7 helicase activity. Lane 1 shows denatured fork substrate (+ boil); lane 2 shows the intact fork (- boil). Lane 3 contains 1 pmol T antigen monomer. Lanes 4-12 contain 400 ng Mcm2-7. In lanes 9-12, and where indicated in lanes 3-8, reactions contain 100 mM phosphocreatine, 100 μg/mL creatine kinase, or both. In lane 7, the ATP regenerating system was boiled (Denatured CK) prior to use. The reactions in lanes 9-12 contain antibody AS1.1, neutralizing peptide (NP), or both as indicated. The reactions in lanes 4 and 12 are equivalent, but 5 mM ATPγS was substituted for ATP in lane 12. B) Mcm2-7 helicase activity is anion dependent. Standard helicase reactions containing 400 ng Mcm2-7 were supplemented with either the indicated salt (100 mM, Glut = glutamate, OAc = acetate) or volume excluder (1% (w/v); PEG = polyethylene glycol 8000, PVA = polyvinyl alcohol). C) Competition between glutamate and chloride for Mcm2-7 helicase activity. Reactions contained 50 mM of either potassium glutamate (lanes 3-6) or potassium chloride (lanes 7-10), and 0, 50, 100 or 200 mM of the corresponding salt as noted. D) Helicase activity of Mcm467 and Mcm2-7. Reactions contained standard helicase buffer with 5 mM phosphocreatine and 20 μg/ml creatine kinase, and contained either no Mcm (lanes 1 & 2), 400 ng Mcm467 (lanes 3-6), or 400 ng Mcm2-7 (lanes 7-10) and were supplemented with potassium glutamate as indicated.

5.3.5 Mcm2-7 helicase activity correlates with reduced ability to bind circular ssDNA

To understand why glutamate facilitates Mcm2-7 helicase activity, we examined its effects on ssDNA binding. The reconstitution of helicase activity does not correspond to an increased affinity for ssDNA, since glutamate does not alter the ssDNA binding constant of Mcm2-7 (Figure 29A). However, preincubation of Mcm2-7 with glutamate generates results similar to ATP preincubation: it decreases the ability of Mcm2-7 to bind circular but not linear ssDNA (Figure 29B) and enhances the apparent association rate between Mcm2-7 and linear ssDNA (Figure 29C). Similar to ATP preincubation, the maximal effect of glutamate preincubation on either activity requires about 25-30 minutes (data not shown). Moreover, both glutamate and ATP preincubation of any of the different Mcm2-7 KA or RA mutant complexes produces qualitatively similar results for both the ssDNA association rate and circularization (Figure 29B and D, Figure 30A). Complexes containing the Mcm5KA or 2RA subunits were immune to glutamate preincubation, whereas Mcm2-7 complexes containing the other mutant subunits demonstrated an increase in their apparent association rate and circularization similar to those observed following ATP preincubation (Figure 29B and D, Figure 30B). However even upon increasing the concentration of glutamate (data not shown), ATP preincubation is more effective than glutamate preincubation with wild type Mcm2-7, suggesting that these two ions may function through slightly different but overlapping mechanisms. These results suggest that like ATP preincubation, glutamate preincubation acts through the Mcm2/5 active site and functions to close the gate in the Mcm2-7 toroid.

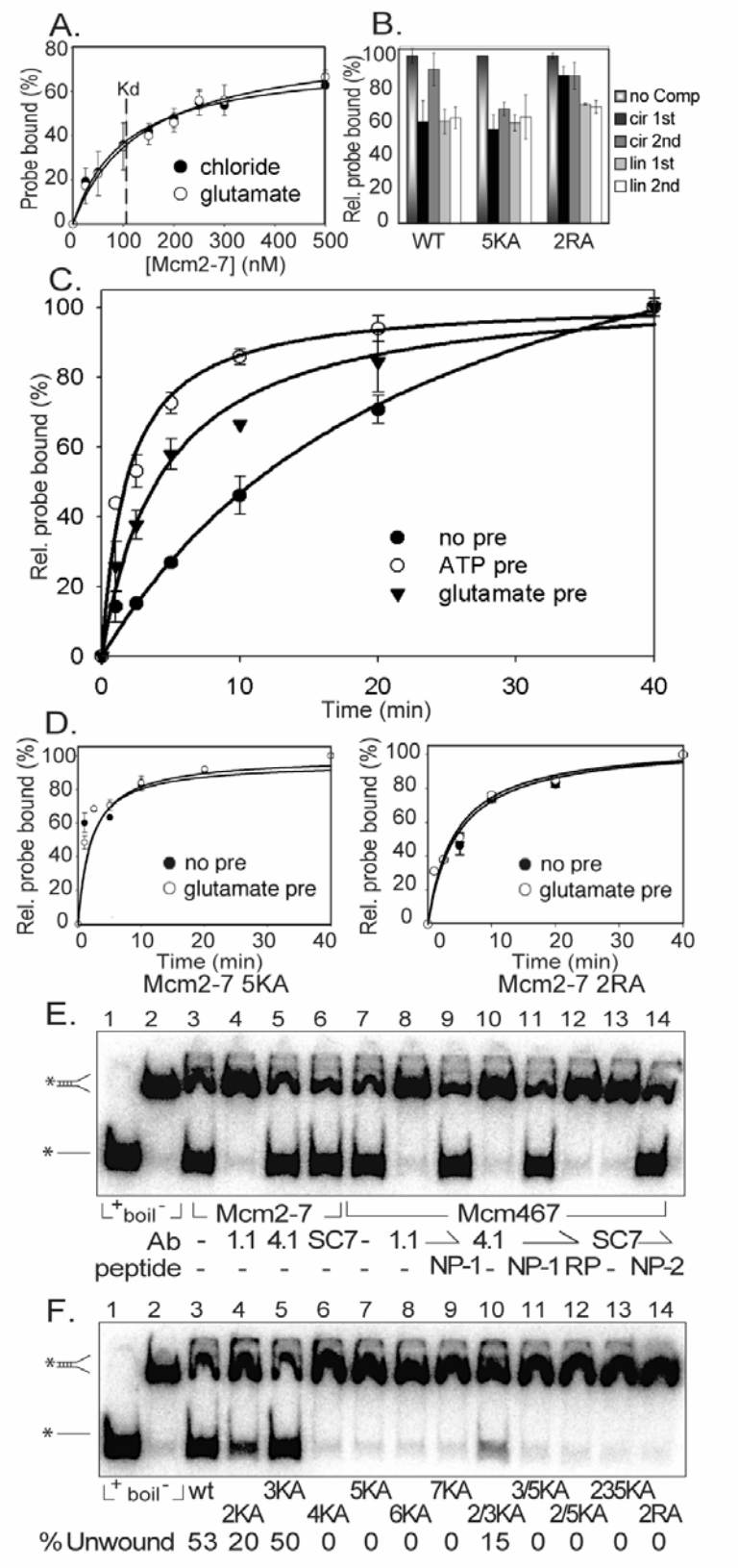

Figure 29. The effects of glutamate and Mcm mutations on Mcm2-7 helicase activity.

A) Glutamate does not affect the affinity of Mcm2-7 for ssDNA. Standard filter binding reactions were carried out in buffer B2 (modified to lack potassium chloride) supplemented with either 100 mM potassium chloride or 100 mM potassium glutamate using radiolabeled oligo #826. The K_d in the presence of chloride = 100 ± 14 nM while the K_d in the presence of glutamate = 130 ± 22 nM. B) Glutamate preincubation stimulates Mcm2-7 ring closure. Reactions were set up essentially as in Figure 24C, but the ATPγS preincubation was replaced by preincubation with 100 mM potassium glutamate; ATPγS was added to the reactions in all cases after 1 hour of either glutamate or ssDNA preincubation. The 120 time point is shown for each complex (1 hour preincubation plus 1 hour with all reaction components). C) Glutamate preincubation stimulates Mcm2-7 on-rate. Reactions were set up essentially as in Figure 27B, but the ATPγS preincubation was replaced by preincubation with 100 mM potassium glutamate. Radiolabeled oligo #826 was used. D) Association rates of Mcm2-7 complexes containing either Mcm5KA or 2RA in the absence (no pre) or presence (glutamate pre) of glutamate preincubation. E) Antibody inhibition of the Mcm467 helicase. NP-1 = neutralizing peptide for AS1.1 and AS4.1, NP-2 is the neutralizing peptide for SC-7, and RP is a sequence randomized version of NP-1. F) Mcm2-7 Walker A box mutations inhibit helicase activity. Reactions contain 400 ng of the indicated wild type or mutant Mcm2-7 preparation.

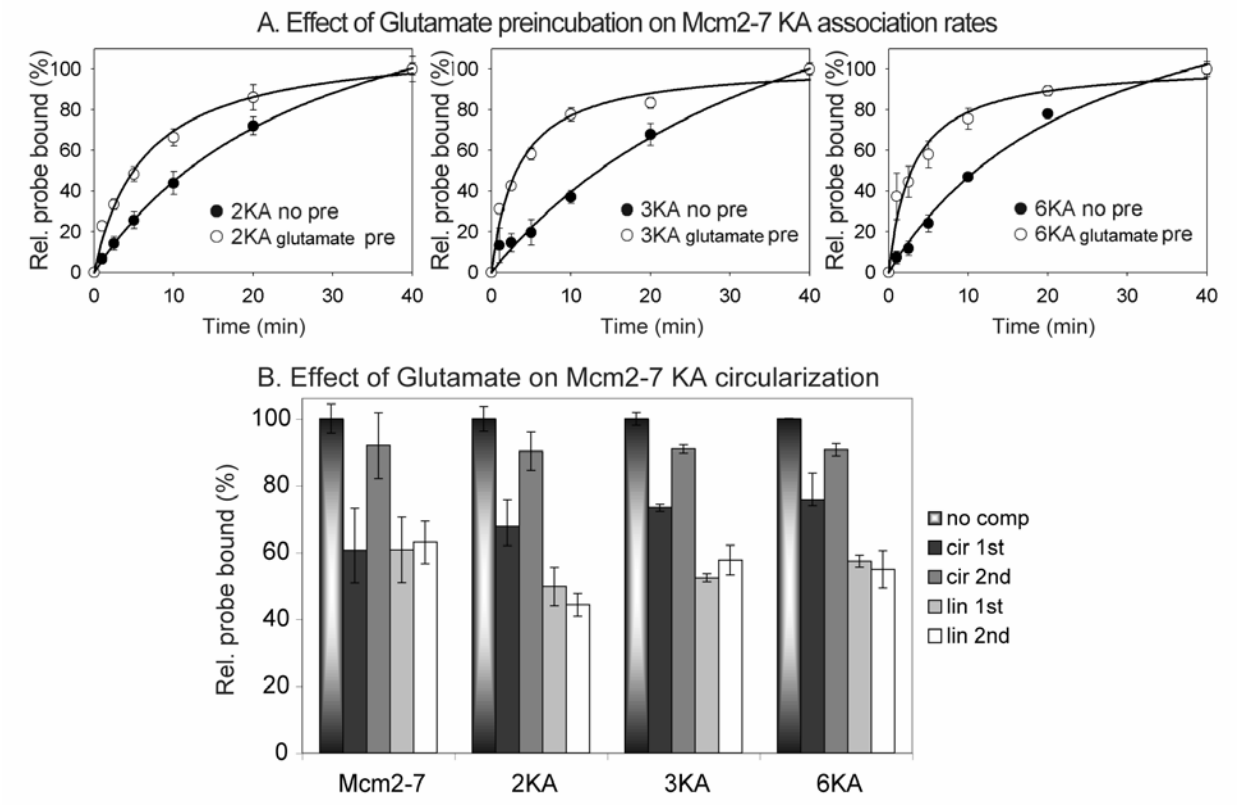

Figure 30. Glutamate and ATP preincubation have similar effects on Mcm2-7 mutant complexes.

A) Glutamate preincubation and the association rate of Walker A mutant Mcm2-7 complexes. Experiments were conducted identically to Figure 29C and compare the observed association rate of the complexes either without (no pre) or with (glutamate pre) preincubation with 100 mM potassium glutamate. B) Glutamate preincubation and the circularization of Walker A mutant complexes. Experimental conditions were identical to those used for Figure 29B.

5.3.6 Mcm2-7 helicase activity requires at least five of the six Mcm subunits

Although our results suggest that glutamate stimulates the Mcm2-7 helicase through closure of the Mcm2/5 gate, other trivial explanations are possible. One is that glutamate dissociates Mcm2-7 into functional Mcm467 complexes. Immunoprecipitation of Mcm2-7 with a Mcm4-specific antibody in the presence of either 200 mM potassium chloride or potassium glutamate was equally efficient and yielded identical results (Figure 31A), arguing against the bulk disruption of Mcm2-7 by glutamate. The possibility remains however that glutamate liberates a small but catalytically significant amount of Mcm467.

To test this possibility directly, we examined our collection of Mcm antibodies for any that would neutralize only one of the two complexes. Two antibodies were identified that specifically inhibit Mcm467 helicase activity with no effect upon Mcm2-7 activity: one targets the extreme N-terminus of Mcm7 (SC-7), while the other targets the Walker B motif common to all six subunits (AS4.1) (Figure 29E, compare lanes 5 and 6 with 10 and 13). The reversal of helicase inhibition by specific blocking peptides confirms the antibody specificity (compare lanes 10 to 11 and 13 to 14). Although neither antibody blocks the binding of Mcm467 to ssDNA (not shown), SC-7 is able to dissociate the Mcm467 hexamer but not Mcm2-7 (Figure 31B), suggesting a possible mechanism for Mcm467 inactivation. These data strongly indicate that the helicase activity of Mcm2-7 does not involve the fortuitous generation of Mcm467.

To verify the subunit composition of the active helicase, Mcm2-7 complexes containing Walker A mutations in individual subunits were assayed. Although Walker A mutations in Mcm4, Mcm6, and Mcm7 completely abolish helicase activity (Figure 29F lanes 6, 8 and 9), analogous mutations in Mcm2 and Mcm5 eliminate (Mcm5) or considerably reduce (Mcm2)

helicase activity (Figure 29F lanes 4 and 7). In addition, the complex containing the 2RA mutation is completely devoid of activity, confirming the involvement of Mcm2 in helicase activity (Figure 29F lane 14). In contrast, the Mcm3KA complex retains nearly wild type levels of helicase activity, suggesting that this ATP binding site may not be essential for helicase activity.

Although Walker A mutations in individual Mcm subunits block ATPase activity of Mcm2-7, double or triple mutant complexes that contain combinations of the Mcm2KA, 3KA, or 5 KA subunits restore ATPase activity [104]. To test if these combinations also restore helicase activity, we assayed Mcm2-7 complexes containing two (2/3KA, 3/5KA, or 2/5KA) or three (2/3/5KA) mutant subunits (Figure 29F lanes 10-13). The recovery of ATPase activity in these mutants does not result in a reactivation of helicase activity. In combination, our results confirm the involvement of at least five of the six subunits in Mcm2-7 helicase activity.

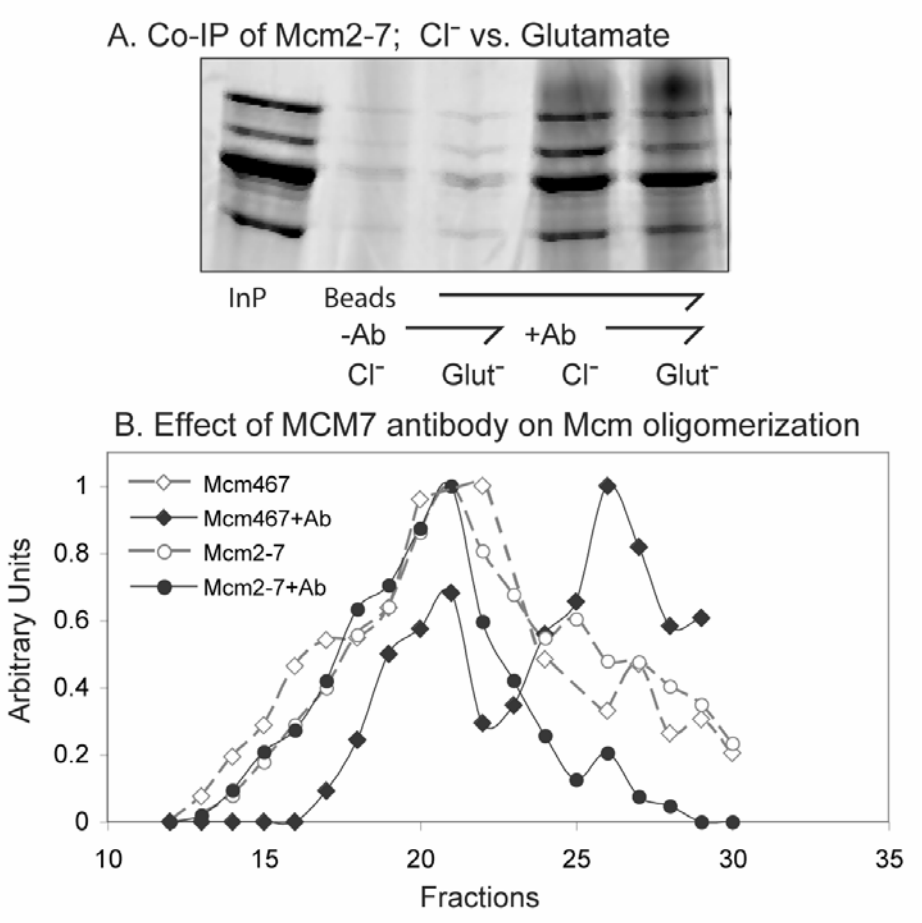

Figure 31. Mcm2-7 helicase activity is not due to free Mcm467.

A) Co-IP experiment using antibody AS6.1 (anti-Mcm4) with Mcm2-7 in the presence of either potassium chloride (Cl^-) or potassium glutamate ($Glut^-$). B) Effects of the anti-Mcm7 antibody (SC-7) on Mcm467 and Mcm2-7 oligomerization. This experiment was conducted identically to Figure 23B, except that antibody-containing experiments involved preincubation of either Mcm2-7 or Mcm467 preparations with 60 ng antibody per picomole of hexamer for 30 minutes at 30°C prior to gel filtration. Note: Although we do not know the structural basis for the antibody distinction between Mcm467 and Mcm2-7, considerations of the probable subunit organization of Mcm2-7 and Mcm467 suggests that the Mcm7 subunit contacts are likely to be different, with Mcm7 dimerizing with Mcm3 in the Mcm2-7 complex and putatively dimerizing to Mcm6 in the Mcm467 complex. Since direct physical interactions have not been observed in prior studies between Mcm6 and Mcm7 ([102]; Bochman, Schwacha and Bell, in preparation), we surmise that the hypothetical dimer interface between them in Mcm467 is likely to be relatively weak, thus allowing appropriate antibodies to split the complex apart at this interface.

5.4 DISCUSSION

The prior observation that Mcm2-7 lacks helicase activity can now be rationalized. The anions present in previously published helicase assays would have blocked Mcm2-7 unwinding activity [63, 101, 123]. The correlation between inability to bind circular ssDNA and helicase activity suggests that circularization of the complex is essential for DNA unwinding, an observation supported by studies of other hexameric helicases (*e.g.*, [57]).

Our findings appear to conflict with a recent study indicating that Cdc45 and the GINS complex are required for *in vitro* Mcm2-7 helicase activity (CMG complex, [105]). Although our data clearly demonstrate that Ccd45 and the GINS complex are not absolutely required for *in vitro* Mcm2-7 helicase activity, our results do not preclude the possibility that these factors may assist Mcm2-7 unwinding activity under more stringent *in vitro* or *in vivo* conditions. Indeed, our findings suggest that Ccd45 or the GINS complex may act on the Mcm2-7 complex to close the Mcm2-7 ring. As has been true for elucidating the mechanism of DNA replication in *E. coli*, the function of individual components is frequently obtained by studying both whole complexes and their parts. For example, it was the study of the gamma-complex not the DNA pol III holoenzyme that identified its clamp loading function (Reviewed in [215]). Our studies lay the foundations to examine the mechanistic contribution of the different Mcm subunits within the Mcm2-7 helicase in a manner that will complement studies of the larger CMG complex.

5.4.1 Role of glutamate and the Mcm2/5 "gate" in Mcm2-7 helicase activity

Given that chloride competes with glutamate in facilitating Mcm2-7 helicase activity (Figure 28C), glutamate likely serves to displace inhibitory anions. Since DNA is itself negatively

charged, helicase stimulation cannot involve the binding of glutamate to DNA. Moreover, since glutamate changes the ability of Mcm2-7 to bind different topological forms of ssDNA rather than changing its affinity for ssDNA (Figure 29A), glutamate likely facilitates a conformational change in the complex.

The finding that glutamate mimics many of the effects of ATP, a known Mcm2-7 substrate, further suggests the physiological relevance of the effects of glutamate. Although chloride is commonly present in many *in vitro* enzymatic reactions, it is not the major cellular anion in eukaryotes (see [216] and references therein). In fact, in *S. cerevisiae*, the intracellular chloride concentration is only ~0.15 mM (at extracellular pH 4.0 and media [Cl^-] of 5 mM) [217].

The inverse correlation between circular ssDNA binding and helicase activation lead us to hypothesize that this conformational change corresponds to topological closure of the Mcm2-7 toroid. Consistent with this notion, the minus 6 pentamer, which is presumably unable to fully circularize, lacks helicase activity (not shown). Analysis of the Mcm5KA and Mcm2RA mutant complexes suggests that the Mcm2-7 discontinuity corresponds to the Mcm2/5 ATPase active site. Interestingly, these two mutations have opposite effects on gate closure: Mcm5KA increases the ability of Mcm2-7 to bind circular ssDNA (*i.e.*, gate open), whereas the 2RA mutation decreases its ability to bind circular ssDNA (*i.e.*, gate closed). Studies of other AAA^+ proteins show that mutations in the Walker A motif commonly block both ATP binding and hydrolysis, whereas arginine finger mutants likely bind ATP but are unable to hydrolyze it [203]. If this precedent applies to Mcm2-7, it suggests that ATP (ATPγS) binding but not hydrolysis stimulates closure of the gate. Since the Mcm2RA complex lacks helicase activity (Figure 29F lane 14), we infer that at some stage during DNA unwinding, ATP hydrolysis at the Mcm2/5 site

is required. Although our data suggest that the Mcm2/5 ATPase active site is the gate, we cannot preclude the possibility that additional residues involved in the dimer interface (such as the N-terminus [58]) also contribute to gate formation. A previous study indicating that the Mcm2/5 active site is particularly labile [102] further supports our proposal. We note, however, that since ATP preincubation by itself is unable to stimulate Mcm2-7 helicase activity, glutamate must serve an additional role in helicase activation, perhaps to displace inhibitory ions from additional sites in Mcm2-7.

5.4.2 Possible role of the Mcm2/5 gate during DNA replication

An ATP-regulated gate in Mcm2-7 has obvious potential implications for the loading or activation of the complex during DNA replication (Figure 32). Since Mcm2-7 oligomerizes prior to nuclear transport (reviewed in [84]), it is likely that toroid opening is needed to allow DNA passage into the central channel. The relative weakness of the Mcm2/5 active site makes this an ideal entry point for DNA, suggesting that ATP hydrolysis at the Mcm2/5 site may facilitate Mcm2-7 loading onto replication origins. In addition, our results suggest that the *in vitro* helicase activity of Mcm2-7 requires closure of the Mcm2/5 gate. *In vivo*, the helicase activity of the Mcm2-7 complex appears to be blocked until the G1/S transition [218]. Origin unwinding depends on the activity of the Cdc7/Dbf4 kinase [218], and the Mcm2-7 complex is widely believed to be the main substrate for this kinase. Although *in vivo* the relatively high cellular levels of acetate or glutamate may favor transient Mcm gate closure, Cdc7/Dbf4 phosphorylation and the subsequent association of Cdc45 and GINS may serve to stabilize this closure to enable Mcm2-7 to processively unwind large regions of chromatin.

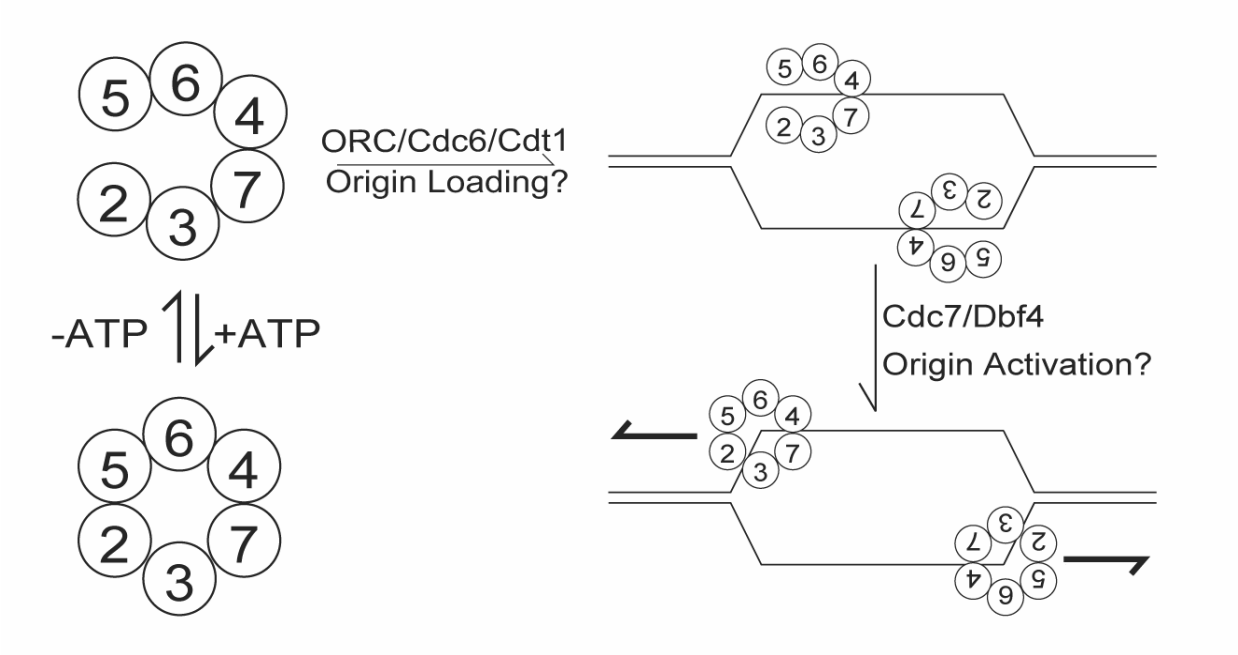

Figure 32. Hypothetical model of the Mcm2/5 "gate."

Prospective roles in either origin loading by Cdc6/Cdt1 or helicase activation by Cdc7/Dbf4 are shown.

6.0 DISCUSSION, CONCLUSIONS, AND FUTURE CONSIDERATIONS

6.1 UNEQUAL CONTRIBUTION OF ATPASE ACTIVE SITES TO MCM2-7 ACTIVITY

In sharp contrast to other helicases (archaeal MCMs included), Mcm2-7 ATPase active sites are formed by unique subunits, and current evidence strongly indicates that the individual active sites contribute differentially to function both *in vivo* and *in vitro*. This raises the possibility that individual Mcm active sites may have become specialized for different activities during evolution. The current evidence supporting this claim is discussed below.

6.1.1 Helicase activity – discovery of the Mcm467 subcomplex

Although *in vitro* helicase activity has historically not been observed for Mcm2-7 [101, 102, 104, 129], it was found that a hexameric Mcm subcomplex containing two copies each of the Mcm4, 6, and 7 subunits possessed an unprocessive, ATP-dependent, 3'–>5' DNA unwinding activity [63, 101, 128, 219]. Addition of either Mcm2 or the Mcm3/5 dimer [125] inhibits this activity. These facts immediately implied that ATPase active sites formed by Mcm4, 6, and 7 are inherently different than those formed by Mcm2, 3, and 5.

6.1.2 Characterization of Mcm2-7 ATPase active sites and subunit architecture of the complex

In common with other ATPases, Mcm ATPase active sites require participation of conserved structural motifs (Walker A box, Walker B box, and arginine finger; [33]). In addition, as AAA+ ATPases, Mcm active sites are expected to form *in trans* at dimer interfaces [77]. Work by the O'Donnell lab [102], that was later confirmed and expanded (**Chapter 4**), supports the basic validity of these ideas. Using different techniques, both studies identified five stable Mcm dimer pairs: Mcm5/3, 3/7, 7/4, 4/6, and 6/2 that have very different levels of ATP hydrolysis. The Mcm3/7 dimer has substantial activity [102, 104], Mcm7/4 and 6/2 have intermediate levels of ATPase activity, and Mcm3/5 & 4/6 demonstrate little or no ATP hydrolysis.

Given the unique combinatorial nature of these active sites, the identity of dimeric complexes predicts an apparent linear arrangement of subunits within the complex and the composition of structural motifs within each ATPase active site (Figure 6C). To rectify these findings with the toroidal subunit arrangement visible for the Mcm complex by electron microscopy [126], the Mcm2 and Mcm5 subunits need to be in close juxtaposition. This subunit organization predicts a structural weakness between Mcm2 and Mcm5, and is consistent with Mcm2-7 chemical cross-linking studies from diverse sources [130, 204].

6.1.3 Involvement of ATPase motifs in Mcm2-7 activity

The contribution of the Walker A, Walker B, and arginine finger motifs in each subunit to both the *in vitro* and *in vivo* activities of the *S. cerevisiae* Mcm2-7 complex has been studied (this dissertation; [102, 104, 126]). Many of these observations are also supported by less extensive

studies in *S. pombe* [182] and mice [122]. Although the details of these data are complex, the following general observations can be made:

6.1.3.1 The Mcm active sites contribute differentially to steady-state ATP-hydrolysis

Evidence obtained by the use of Walker A (K–>A) mutations indicates that ATP hydrolysis within Mcm2-7 is coordinated; inclusion of a single Mcm subunit containing such a mutation in the presence of five wild type subunits is capable of poisoning the activity of the entire complex to a nearly equal extent [104]. This result is unique to the Walker A alleles, since analogous mutations in the Walker B and arginine finger motifs differentially affect ATP hydrolysis (**Chapter 4**). Although the reasons for the difference between these mutations are not yet known, precedent from other ATPases suggests that the difference between them may involve the distinction between ATP binding and ATP hydrolysis [203]. The Walker A alleles likely block ATP binding (and thus hydrolysis as well), while the Walker B and arginine finger alleles are putatively defective in ATP hydrolysis but not binding. Thus, the Mcm2-7 complexes containing individual subunits with Walker A mutations provide little information concerning the importance of individual sites in bulk ATP hydrolysis. However, both the Walker B and arginine finger alleles support the notion that most of the ATP hydrolysis emanates from the Mcm3/7 and 7/4 active sites with little contribution from the other sites.

6.1.3.2 The Mcm active sites contribute differentially to ssDNA binding

The Mcm2-7 complex, in common with most helicases [35], demonstrates ATP-dependent ssDNA binding activity (**Chapter 3**). So far, only the KA mutants have been extensively examined for their effects on this activity. Among them, the Mcm4KA allele (part of the Mcm4/7 active site) completely abolished ssDNA binding, while the 7KA (part of the Mcm3/7

site) greatly reduces binding with residual binding being ATP-independent. These data again support the premise that the Mcm3/7 and 7/4 sites are also key to ssDNA binding. Initial work on complexes containing the DENQ and RA mutations confirms these results (**Appendix A**).

6.1.3.3 The Mcm active sites contribute differentially to helicase activity

As previously mentioned, historically only the Mcm467 subcomplex had helicase activity [102, 104, 126]. Under the reaction conditions used in those studies, the entire Mcm2-7 complex lacked DNA unwinding activity. More recently, new reaction conditions have allowed the demonstration of *in vitro* helicase activity for the Mcm2-7 complex for the first time (**Chapter 5**). Using the improved assay, the activity of Mcm2-7 complexes containing KA mutations in each of the six subunits was individually examined. Single mutant complexes containing either Walker A mutant Mcm4, 5, 6, or 7 subunits are completely devoid of DNA unwinding. Complexes containing a Mcm2KA mutant have only a slight unwinding defect, and the Mcm3KA complex demonstrates no observable defect in DNA unwinding under these experimental conditions.

While other models are likely possible, the above data are consistent with the proposition that the Mcm3/7, 7/4 (and possibly 4/6) active sites are the main sites of motor (*i.e.*, ATPase and helicase) activity. Further, the remaining active sites are essential *in vivo* but antagonize this function under at least some experimental conditions. Thus, to truly understand how Mcm2-7 functions, the role of the Mcm2, 3, and 5 subunits needs to be ascertained. Recent work suggests a plausible role for these subunits (below).

6.2 EVIDENCE THAT THE MCM2/5 DIMER INTERFACE FUNCTIONS AS AN ATP-DEPENDENT "GATE"

Through an extensive comparison of the ssDNA binding activities of the Mcm2-7 and Mcm467 complexes, several informative differences in their activities were uncovered that provide clues regarding Mcm2, 3, and 5 function (**Chapters 3 & 5**). The analysis of Mcm2-7 complexes containing defined mutations in the ATPase active sites of each subunit indicates that the differences between Mcm2-7 and Mcm467 could be traced to the Mcm2/5 dimer interface.

6.2.1 Mcm2-7 and Mcm467 differ in their ability to bind circular ssDNA

Although Mcm2-7 and Mcm467 have similar affinities toward linear ssDNA, the two complexes differ in their association rate with linear ssDNA, and their ability to bind circular ssDNA. Mcm467 has an apparent affinity ~20 times lower for circular rather than linear ssDNA of the same sequence, while under the same conditions, Mcm2-7 binds both linear and circular substrates with similar affinity (**Chapter 5**). However, this effect depends upon the temporal order in which ATP enters the reaction; if Mcm2-7 is preincubated with ATP prior to addition of DNA, it demonstrates a bias toward linear ssDNA rather than circular ssDNA (similar to Mcm467). In contrast, the ability of Mcm467 to bind linear and circular ssDNA is unaffected by ATP pre-incubation. With hexameric helicases, ssDNA binds within the central channel [35], so this difference between Mcm2-7 and Mcm467 appears to reflect their relative abilities to topologically close their toroidal structures. Thus, the simple hypothesis is that Mcm467 normally forms a tightly closed toroid that is poorly able to bind ssDNA lacking a free end, while

Mcm2-7 has the ability to transiently open its toroidal structure in an ATP-dependent manner to allow ssDNA access to the central channel.

6.2.2 Mcm467 and Mcm2-7 differ in their ssDNA association rate

The second observed difference in ssDNA binding between the two Mcm complexes is the difference in the association rate with linear ssDNA: Mcm467 binds relatively quickly, while under identical conditions Mcm2-7 binds > 5 times more slowly. Similar to the observation with circular ssDNA binding, preincubation of Mcm2-7 with ATP increases its ssDNA association rate to the level observed for Mcm467.

6.2.3 Involvement of the Mcm2/5 ATPase active site with Mcm2-7 ATP preincubation effects

Since ATP preincubation dramatically changes the ssDNA binding activity of Mcm2-7, one or more ATP active sites are likely involved in this effect. Moreover, since Mcm467 lacks these preincubation effects, the basis of the differences likely reside in one or more ATPase active sites found in Mcm2-7 but not Mcm467 (*i.e.*, involving Mcm2, 3, and/or 5). To directly determine the ATPase active site(s) responsible, ATPase mutant Mcm2-7 complexes were tested for ATP preincubation differences in both their ssDNA association rate (**Chapter 3**) and ability to bind circular ssDNA (**Chapter 5**). Among the mutations, only two altered the ability of Mcm2-7 to bind circular ssDNA: Mcm2RA and Mcm5KA.

As noted earlier, these two motifs are predicted from subunit association studies to be present in the same active site (Mcm2/5). Interestingly, the two mutations have opposite effects

on circular ssDNA binding (Mcm2RA = closed, Mcm5KA = open), and both mutations eliminate the ATP preincubation-dependent on-rate enhancement. Although the bases for the difference between the two mutants in circular ssDNA binding are unknown, these results are consistent with the common result that Walker A mutations (5KA) largely block both ATP binding and hydrolysis, whereas arginine finger mutations (2RA) should be able to bind ATP but not hydrolyze it. These results, in combination with the Mcm subunit association studies indicating a relatively poor connectivity between Mcm2 and 5, suggest the presence of a reversible ATP-dependent discontinuity in the Mcm2-7 toroid – closed when Mcm2/5 binds ATP, and open when the active site is empty.

6.2.4 Role of ATP at the Mcm2/5 active site

Oddly, ATP appears to both promote and inhibit the ssDNA association rate effect and the ability to bind circular ssDNA: ATP preincubation (suggesting a positive role) and mutations that ablate the Mcm2/5 active site (suggesting a negative role) have similar effects. These data imply that the role of ATP in this process may be indirect. A specific possibility may be that in either case, the real problem is the presence of an inhibitor in the Mcm2/5 active site that can be displaced by either competition with ATP or by ablation of the inhibitor binding site by mutation.

6.2.5 Does Mcm2/7 helicase activity require closure of the Mcm2/5 gate?

Among better studied hexameric helicases [35], it is believed that physical continuity between subunits is necessary to coordinate DNA unwinding, suggesting that a gap in the toroid, as predicted for an open Mcm2/5 gate, would block DNA unwinding. Although attempts to close

the Mcm2/5 gate by ATP preincubation did not reconstitute helicase activity, the alternative possibility that the standard helicase reaction conditions contained an inhibitor was pursued.

Consideration of both the extensive ATPase literature as well as unpublished experimental data led to the identification of several putative inhibitors. In the end, we observed that ssDNA binding was very sensitive to the nature of the salt present in the binding buffer; although sodium chloride supports ssDNA binding, the sodium salts of fluoride, bromide and iodide do not (M. Bochman, unpublished). This eventually led to the finding that small anions inhibit Mcm2-7 helicase reactions, while large anions like glutamate specifically activate that activity.

6.2.6 Glutamate may stimulate Mcm2-7 helicase activity by closing the Mcm2/5 gate

While the mechanism is often poorly understood, the biochemical activities of numerous proteins have been found to be chloride-sensitive and are stimulated by the presence of either glutamate or acetate. *S. cerevisiae* RNA polymerase II is one particularly important example; the solution to this chloride inhibition problem led to the establishment of an *in vitro* assay that proved essential for the elucidation of eukaryotic transcription [220]. In the case of Mcm2-7, glutamate does not alter the affinity of the protein for DNA since the ssDNA dissociation constant is the same with either 100 mM potassium glutamate or chloride. Moreover, because the effect is anion-specific, it is unlikely to be occurring through alterations of DNA (a polyanion), but rather must function by causing an alteration of the Mcm complex itself. Analysis of the effect of glutamate on the association rate and circular ssDNA binding of Mcm2-7 provides evidence that glutamate helps close the Mcm2/5 gate: glutamate preincubation of Mcm2-7 both increases the ssDNA association rate and specifically reduces the ability of the complex to bind circular

ssDNA (**Chapter 5**). Limited proteolysis of Mcm2-7 also implicates a conformational change in the presence of glutamate (M. Bochman, unpublished).

6.3 POSSIBLE *IN VIVO* ROLE OF THE MCM2-7 ATPASE ACTIVE SITES

As stated above, the *in vitro* data are consistent with the proposition that the Mcm3/7 & 7/4 active sites are the main sites of motor/DNA unwinding activity, while Mcm2/5 forms an ATP-dependent gate within the Mcm2-7 toroid. No *in vivo* evidence yet exists to indicate that the Mcm2/5 gate has significance, but little imagination is required to appreciate the potential uses for a regulated gate within the helicase for Mcm2-7 loading onto DNA during G1. Additionally, as an important part of the regulation of eukaryotic DNA replication, Mcm2-7 is apparently inactive for DNA unwinding during G1, but is activated during early S-phase, likely with the help of the essential Cdc7/Dbf4 kinase (DDK). In this regard, it is interesting to note that a specific mutation has been isolated in *mcm5* that obviates the need for DDK [199], and that among the Mcm subunits, Mcm2 is particularly heavily phosphorylated by DDK [200, 201], suggesting a connection between the putative activation of the Mcm2-7 helicase by DDK phosphorylation and the Mcm2/5 gate.

Based not only on the unique composition of each active site within the hexamer but also the putative specialized functions that they may serve, Mcm2-7 is an ATPase without an equal. This could explain why bioinformatically it does not even cluster with known replicative helicases but appears more similar to enzymes like magnesium chelatase [77]. This elaboration on a common AAA+ theme must be evolutionarily beneficial however as the six Mcms represent one of the most conserved gene families in eukaryotes (D. Botstein, personal communication).

6.4 ISSUES ON THE HORIZON OF MCM2-7 RESEARCH

6.4.1 Possible role of Mcm2-7 accessory factors

In addition to the Mcms, two other replication factors, the GINS complex and Cdc45, have been shown to be essential for fork progression [183]. Recently, Mcm2-7 has been purified from *Drosophila* extracts as part of a larger complex containing both additional replication factors (CMG complex) and possessing demonstrable helicase activity [105]. This adds to the notion that Cdc45 and GINS are essential *in vivo* for the DNA unwinding activity of Mcm2-7. Although the demonstration of helicase activity from the isolated *S. cerevisiae* Mcm2-7 complex indicates that these additional factors are not essential to unwind short helicase substrates *in vitro*, it does not indicate that Mcm2-7 in isolation is sufficient for the more difficult job of unwinding long expanses of chromatin *in vivo*.

The GINS complex and Cdc45 might contribute to Mcm2-7 *in vivo* function in at least two ways. First, to counteract the potential lability of the Mcm2/5 gate, these proteins may work to help maintain gate closure and essentially act as processivity factors to help prevent dissociation of the Mcm2-7 from DNA during elongation. Indeed, recent structural work with GINS indicates that this molecule is toroidal in nature [221, 222], suggesting that the complex might also function by encircling DNA. Simultaneous binding of GINS to Mcm2-7 would help prevent spontaneous dissociation of the replicative helicase during elongation. Alternatively, the nonequivalent and complicated functional involvement of individual ATPase active sites suggests that that individual Mcm sites may be regulated *in vivo*. Precedent from a multitude of other NTP hydrolases such as RAS, the activity of these proteins are regulated by factors that act to either regulate the nucleotide occupancy (exchange factors) of the active site, or its turnover

(GAPs) [223]. Either the GINS complex or Cdc45 might well serve in such capacities to increase the efficiency or regulation of the Mcm2-7 helicase.

6.4.2 What is the role of Mcm2-7 phosphorylation?

In vivo, it is known or suspected that several Mcm subunits are phosphorylated by CDKs (reviewed in [84]), DDK [200, 201], and the ATM/ATR [206] kinases. The relevance of these phosphorylation events is unknown, but many researchers are actively pursuing this question. For instance, recent work on mammalian Mcm3 has shown that CDK1 phosphorylation on Ser-112 (a residue conserved from yeast to humans) is crucial for incorporation of Mcm3 into the Mcm2-7 heterohexamer [224].

However, work in the Schwacha lab directly contradicts most of the theories of the importance of CDK and ATM/ATR phosphorylation. The known and putative CDK, ATM, and ATR phosphorylation sites on all six of the *S. cerevisiae* Mcms have been mutated (Ser/Thr –> Ala), and these mutations have absolutely no effect on viability (M. Patel, R. Elbakri, A. Schwacha, unpublished data). Additionally, treating purified Mcm2-7 with either lambda phosphatase (to completely dephosphorylate the Mcms) or Cdc28/Clb5 (the yeast CDK1 homologue) has no effect on the complex's *in vitro* activities described in this dissertation (M. Bochman, unpublished data).

Mcm phosphorylation by DDK is perhaps more relevant and forms the basis for the hypothetical model of Mcm2/5 gate closure *in vivo* (**Figure 32**). Many investigators (including Bob Sclafani (U. Colorado), Steve Bell (M.I.T.), and Dan Kaplan (Vanderbilt)) are currently investigating the interplay between Mcm2-7 and DDK (personal communications). In an effort to answer lingering biochemical questions, Nick Simon is also attempting to over express and

purify *S. cerevisiae* DDK in the Schwacha lab. Considering the renewed interest in DDK, it seems plausible that CDK will soon have to share some of the replication limelight with its forgotten cousin.

6.4.3 Replication in the context of chromatin

In eukaryotes, DNA exists in a condensed state as chromatin, an array of nucleosomes that each contain 147 bp of DNA coiled around a histone octomer. Until recently, the DNA replication field has largely ignored chromatin, ostensibly because it adds just one more layer of complexity to an already complex problem. However, ignoring chromatin obviously will not make it go away. It has become clear that impediments exist on DNA (tightly bound proteins, histones, *etc*.) that can affect replication fork progression.

With regard to the Mcm2-7 complex, it is unknown if it can generate sufficient force while translocating along DNA to dislodge a histone roadblock. The archaeal MCM complex can unwind templates bound by archaeal histones [161], but similar work on Mcm467 [163] suggests that it would likely be unable to function on such a substrate. Now that conditions have been found in which Mcm2-7 displays *in vitro* helicase activity (**Chapter 5**), many of these questions can and will be examined biochemically.

In vivo, the Mcm2-7 helicase likely has help traveling past histones. It was recently demonstrated that the Ino80 complex, a Swi2/Snf2 family chromatin remodeling complex, is necessary for efficient replication fork progression [225]. It is also known that Asf1, a histone chaperone and assembly factor, associates with stalled forks [226]. One can imagine that these chromatin remodeling factors travel along with Mcm2-7 and replication forks, and when a histone is encountered, Ino80 disassembles it in front of the fork while Asf1 reassembles the

histone behind the fork on newly replicated DNA. It will be interesting to follow this story as it develops and to determine what, if any, roles histone modifications play.

6.5 EPILOGUE – WHY ARE REPLICATIVE HELICASES HEXAMERS?

With few exceptions, replicative helicases are believed to function as toroidal hexamers [35]. However, given the relative abundance of various dimeric (and even monomeric, [227]) helicases that typically function in DNA repair, a hexameric structure is not in itself essential for DNA unwinding. In contrast to most DNA repair helicases, replicative helicases are required to unwind relatively long expanses of DNA without dissociation, and therefore the toroidal nature of these complexes likely decreases the possibility of spontaneous dissociation as previously suggested [35]. However, through the study of homohexameric helicases like the archaeal MCMs, the apparent tight coordinate regulation of the six component ATPase active sites strongly suggests that the hexameric nature of these complexes is mechanistically fundamental to their motor function. The heterohexameric nature of the Mcm2-7 complex provides an illuminating contrast: in the most extreme possibility, evidence suggests that two ATPase active sites may be specialized for DNA unwinding (Mcm3/7 and Mcm7/4), while others may contribute little to DNA unwinding but instead function as a reversible ATP-dependent gate (Mcm2/5). These unique features likely reflect the evolutionary diversification of the single primordial archaeal Mcm gene into six Mcm families early in the ascendance of the first eukaryotes, an event that facilitated the specialization of individual subunits toward different functions.

APPENDIX A

DNA BINDING BY MCM2-7 ATPASE MUTANTS FURTHER SUGGESTS SPECIALIZED ROLES FOR INDIVIDUAL SUBUNITS

A.1 INTRODUCTION

The core enzymatic functions necessary for DNA replication are conserved in all three domains of life (see [74, 108] and references therein). While some structural conservation exists among replication factors from evolutionarily divergent species, the number of proteins required for DNA replication, if not the overall complexity of the process, generally increases from viruses to prokaryotes, archaea to simple eukaryotes, and finally to metazoans [84]. One obvious example of this involves the replicative helicase – the essential enzyme that separates dsDNA into ssDNA templates for DNA polymerases [35].

In viruses and prokaryotes, replicative helicases are homohexameric ring-shaped (d)NTPases typified by the phage T7 gp4 [190], papilloma virus E1 protein [57], and *E. coli* DnaB [50]. The archaea also utilize a homohexamer for DNA unwinding, but it is formed by the MCM protein [143] which has diverged to the point that it is grouped within a AAA+ ATPase superfamily that does not include any of the known replicative helicases from viruses and bacteria [77]. Eukaryotes have taken things one step further; their replicative helicase, the

Mcm2-7 complex, is a heterohexamer composed of six distinct subunits [73, 84]. While evolutionarily related to the archaeal MCM, the divergence into six separate eukaryotic Mcm subunits dates back to the earliest split between archaea and eukarya [77].

The reason for this six-fold increase in complexity is unclear, but one might imagine that it has allowed the six eukaryotic Mcms to evolve specialized functions. Evidence from an analysis of the six Mcm ATPase active sites (see **Chapter 4**) seems to support this notion. In order to gain further insight on the matter, the ssDNA binding activity of ATPase mutant Mcm complexes was investigated. It was once again demonstrated that the Mcm3/7 and 7/4 active sites are important for ssDNA binding. Additionally, the active sites flanking the Mcm2/5 gate may be important for communicating the status of the gate to the rest of the Mcm2-7 complex.

A.2 RESULTS

A.2.1 ssDNA binding by single DENQ and RA mutant hexamers

The ability of the single DENQ (Figure 33A) and single RA (Figure 33B) mutant Mcm2-7 complexes to bind a short, mixed-sequence, radiolabeled ssDNA probe was examined. Of the Walker B mutants, Mcm4DENQ was the most impaired having activity only slightly higher than the sextuple (6XDENQ) mutant. The Mcm2DENQ and 5DENQ complexes retained essentially wild type levels of ssDNA binding, while the 3DENQ and 6DENQ complexes initially display decent binding that then decreased with increasing protein concentration. This effect is likely due to the low concentration of these preparations and represents inhibition (by chloride ions in the protein dialysis/storage buffer) caused by the large volumes of protein used. The

Mcm7DENQ hexamer was not tested as preparations were either too dilute or in limiting amounts.

Of the arginine finger mutants, the Mcm3RA and 7RA complexes displayed the most reduced levels of ssDNA binding. Mcm4RA behaves as wild type, and 6RA behaves essentially as the 3DENQ and 6DENQ complexes (above). Interestingly, the 6XRA preparation displayed low but measurable ssDNA binding that increased with increasing protein concentrations. This is in stark contrast to the 6XKA (Figure 14B) and 6XDENQ complexes (Figure 33A) which are essentially devoid of the activity. The Mcm2RA and 5RA hexamers were not tested in this experiment due to the same limitations as the 7DENQ complex above. It should also be noted that the extent of ssDNA binding by the RA mutant complexes is increased in the presence of ATPγS relative to ATP (not shown). A similar effect was observed for the KA mutant complexes (Figure 14C).

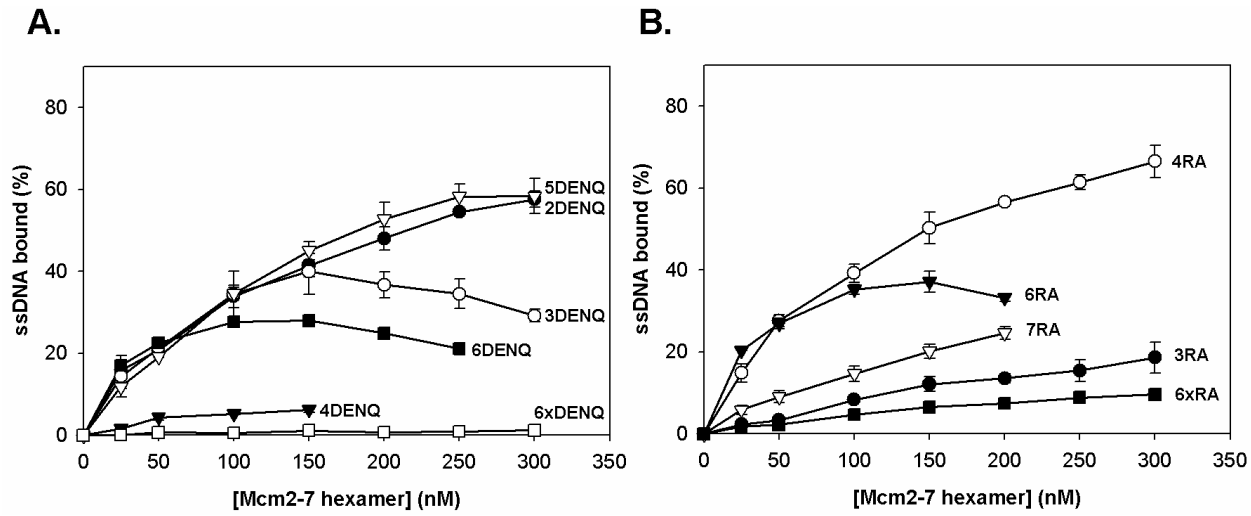

Figure 33. ssDNA binding by the DENQ and RA mutant Mcm2-7 complexes.

ssDNA binding by single and sextuple (6x) A) Walker B (DENQ) and B) arginine finger (RA) mutant hexamers.

A.2.2 The Mcm6/2 and 5/3 active sites are defective for the ATP preincubation-dependent on-rate enhancement effect

Wild type Mcm2-7 complexes associate with ssDNA relatively slowly, but this on-rate can be enhanced by preincubating the complex with ATP or ATPγS (**Chapter 3**). To determine if any of the DENQ or RA mutant hexamers (that retained measurable ssDNA binding) perturbed this effect, their on-rates with and without ATPγS preincubation were measured (Table 5). Of the nine complexes tested, many behaved essentially as wild type (this dissertation). However, the remaining complexes either completely lost the on-rate enhancement due to ATPγS preincubation (Mcm2RA and 2DENQ) or the enhancement was considerably reduced (Mcm3DENQ, 5RA, and 6RA; Figure 34). The Mcm2RA complex has already been discussed in detail (**Chapters 3 & 5**). Interestingly, the Mcm2DENQ & 6RA and Mcm3DENQ & 5RA complexes define the Mcm6/2 and 5/3 ATPase active sites, respectively.

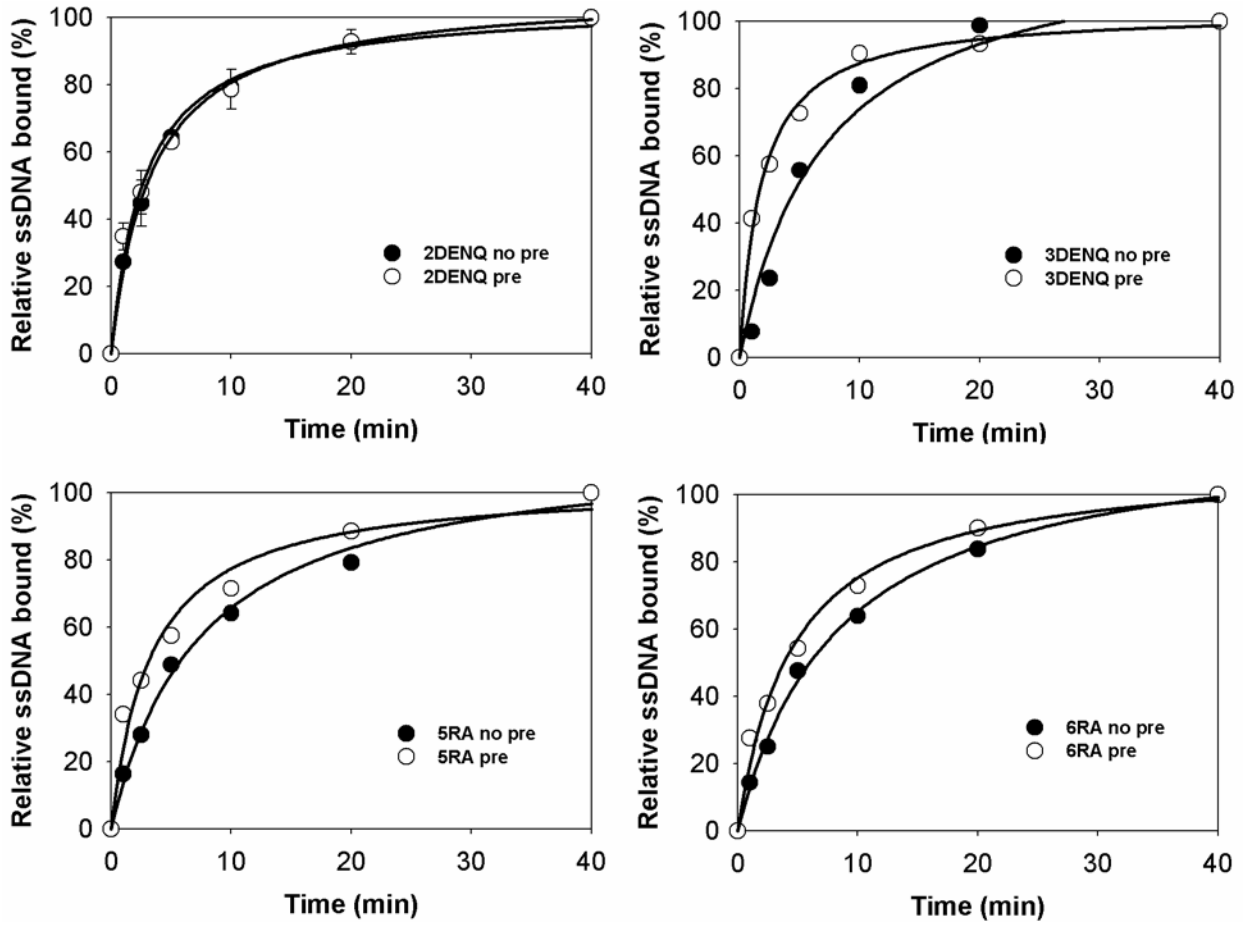

Figure 34. The ssDNA on-rates of mutant hexamers at the Mcm5/3 and 6/2 active sites are largely unaffected by ATPγS preincubation.

The on-rates with (pre) and without (no pre) ATPγS preincubation for the Mcm2DENQ (top left), 3DENQ (top right), 5RA (bottom left), and 6RA (bottom right) hexamers.

A.2.3 The DENQ and RA complexes do not affect circularization

The ability of wild type Mcm2-7 complexes to bind circular ssDNA can be decreased by preincubating the complex with ATP or ATPγS (circularization assay, **Chapter 5**). To determine the contribution of the Walker B and arginine finger motifs to this activity, the DENQ and RA mutant hexamers were examined by the circularization assay (Table 5). The majority of the mutant complexes behaved as wild type with the notable exception of Mcm2RA which has already been discussed (**Chapter 5**). Only a single additional mutant (Mcm3DENQ) had any effect – it appeared to be stuck in the closed position like Mcm467 (**Chapter 5**) – but this result was variable and perhaps an effect of the odd ssDNA binding behavior seen in Figure 33A (discussed below).

Table 5. Biochemical characteristics of ATPase mutant hexamers.[h]

Mutant hexamer	ssDNA binding	dsDNA binding	Ring closure (ATP)[i]	Ring closure (KGlu)	On-rate (ATP)	On-rate (KGlu)	Helicase activity	ATPase activity
2KA	+++++	+++++	WT	WT	WT	WT	++	-
3KA	++++	+	WT	WT	WT	WT	++++	-
4KA	-	+	NA	NA	NA	NA	-	-
5KA	+++	+	Open	Open	Fast	Fast	-	-
6KA	+++++	+++++	WT	WT	WT	WT	-	-
7KA	+++[j]	+	NA	NA	NA	NA	-	-
6XKA	-	-	NA	NA	NA	NA	-	-
2DENQ	++++	++++	WT	ND	Fast	ND	+++	+++
3DENQ	+++(+)[k]	ND	Closed[l]	ND	Fast	ND	+	++++
4DENQ	+	ND	NA	NA	NA	NA	-	-
5DENQ	++++	ND	WT	ND	WT	ND	++++	++
6DENQ	+++(+)[k]	++	WT	ND	WT	ND	-	++++
7DENQ	ND	ND	ND	ND	ND	ND	-	-
6XDENQ	-	ND	NA	NA	NA	NA	-	-
2RA	ND	ND	Closed	Closed	Fast	Fast	-	+++
3RA	+	ND	NA	NA	NA	NA	+++	-
4RA	++++	++++	WT	ND	WT	ND	-	+++
5RA	ND	ND	WT	ND	Fast	ND	++	++++
6RA	+++(+)[k]	++++	WT	ND	Fast	ND	-	++++
7RA	++(+)[k]	ND	WT	ND	WT	ND	-	+++
6XRA	+	ND	NA	NA	NA	NA	-	-

[h] ++++, wild type levels of activity; -, lacks measurable activity; ND, not determined; NA, not applicable (*i.e.*, doesn't bind ssDNA); WT, behaves like wild type Mcm2-7 in the assay; Fast, the on-rate is unaffected by preincubation.

[i] Not all of these circularization assays were done under the same conditions (shorter preincubation time). The reagent listed in parenthesis was used in the preincubation step.

[j] 7KA has high ATP-independent background binding, is hardy stimulated by ATP, and only slightly stimulated by ATPγS (**Chapter 3**).

[k] These preparations are less concentrated and binding likely suffers from chloride inhibition. The (+) is an estimate of the ssDNA binding activity of the preps if they were more concentrated.

[l] This result is difficult to repeat and likely due to the low concentration of the protein.

A.2.4 ATPase mutations have variable effects on helicase activity

Finally, the effects of the DENQ and RA mutations on *in vitro* helicase activity were investigated (Figure 35). Two curious facts emerged from this analysis: 1) many ATPase mutations which are lethal *in vivo* (Mcm2KA, 3KA, 3DENQ, 3RA, 5DENQ, and 5RA) retained some level of DNA unwinding ability *in vitro*; and 2) the two completely viable mutants (Mcm4RA and 6DENQ) display absolutely no helicase activity in this assay. These apparent discrepancies between the *in vivo* and *in vitro* data are discussed elsewhere (Appendix B). Unsurprisingly, the Mcm2DENQ hexamer, which grows very slowly and is partially defective for ATP hydrolysis, could unwind DNA but at reduced levels.

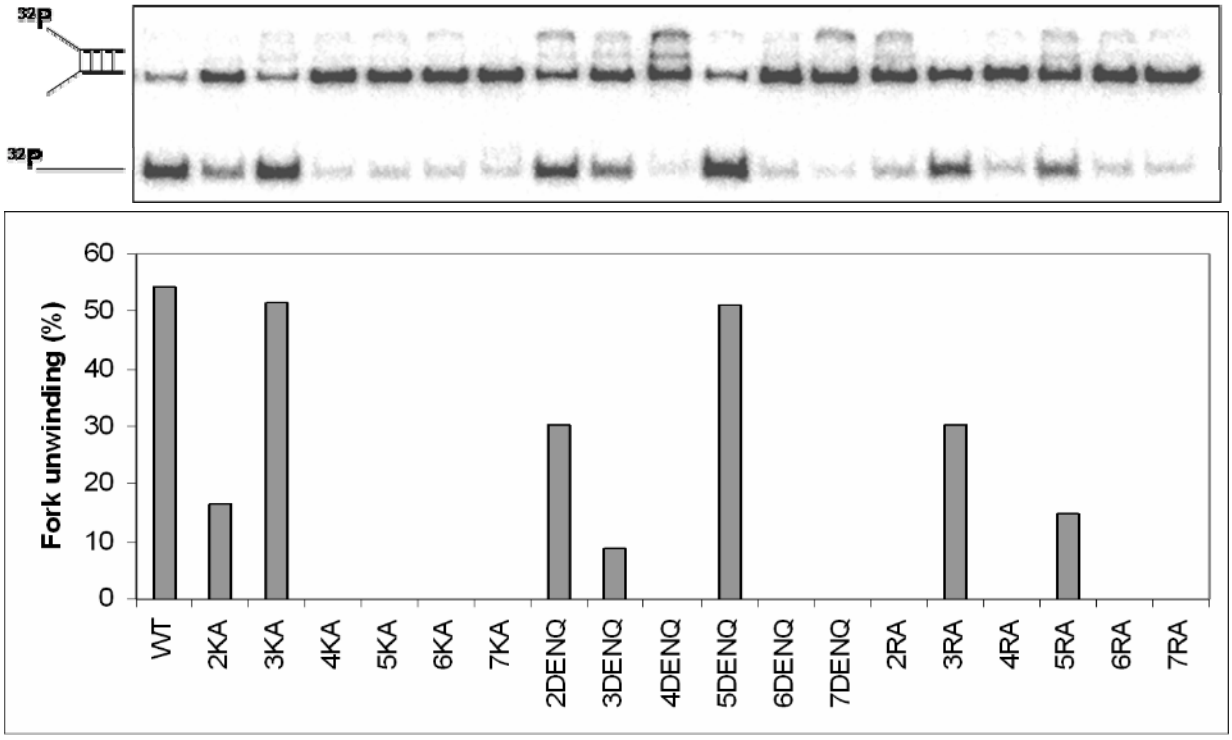

Figure 35. Helicase activity of ATPase mutant hexamers.

The helicase activity (top) of equimolar amounts of wild type (WT) and single ATPase mutant hexamers was examined and quantified (bottom).

A.3 DISCUSSION

This initial biochemical examination of Mcm2-7 complexes containing single DENQ or RA mutant subunits further supports the notion that the six Mcm ATPase active sites have evolved specialized functions. These mutations have variable effects on ssDNA binding and helicase activity that are somewhat predictable when analyzed in the context of the affected active site(s). The data add weight to the hypothesis that the Mcm3/7 and 7/4 active sites are the main "motor" portion of Mcm2-7 and indicate putative roles for the Mcm5/3 and 6/2 active sites. The importance of Mcm3 is also highlighted.

A.3.1 The Mcm3/7 and 7/4 active sites are the ATP-fueled motor of the Mcm2-7 helicase

It has already been suggested that the bulk of Mcm2-7 ATP hydrolysis likely occurs at the Mcm3/7 and 7/4 ATPase active sites ([102, 104]; **Chapter 4**). Their importance in ssDNA binding has also previously been highlighted by examination of the KA mutant complexes (**Chapter 3**). Here, the Mcm2-7 DENQ and RA mutant hexamers lend credence to this claim. Of the mutants tested, the most severe ssDNA binding defects are displayed by Mcm4DENQ, 3RA, and 7RA (Figure 33) which, with the KA mutants, partially (Mcm3/7) or completely (7/4) define these important active sites. The remaining piece of the Mcm3/7 site, Mcm7DENQ, has unfortunately not yet been tested, but is predicted to be defective for ssDNA binding as well.

A.3.2 Do the Mcm5/3 and 6/2 sites communicate gate status?

The Mcm2RA and 5KA mutants are unique because they interfere with the known effects of ATP-preincubation on Mcm2-7 (ssDNA on-rate enhancement and circularization), and thus it was hypothesized that the Mcm2/5 active site forms an ATP-regulated gate in the hexamer (**Chapter 5**). DENQ and RA mutations at the sites flanking the gate (Mcm5/3 and 6/2) have no effect on circularization of Mcm2-7. Conversely, however, their on-rates are already fast regardless of ATP-preincubation which mimics the effects of the Mcm2RA and 5KA mutations. These facts argue against the involvement of the Mcm5/3 and 6/2 active sites in closure of the 2/5 gate, but do hint at the possibility that they may communicate the status (open or closed) of the gate to the rest of the Mcm2-7 complex via conformational changes. It would be interesting to determine (by limited proteolysis) if these mutant hexamers exist in a conformation similar to wild type Mcm2-7 that has been preincubated with ATP or glutamate.

A.3.3 The Mcm3 subunit is special

It has already been discussed that Mcm7 seems to have particular importance with the Mcm2-7 complex (**Chapter 4**). As an active site partner of Mcm7, biochemistry has also shown that Mcm4 plays a prominent role. However, the other neighboring subunit of Mcm7, Mcm3, has been overlooked. I believe it may also be a very important cog in the molecular machine.

First, Mcm2-7 complexes containing mutations in <u>any</u> of the Mcm3 ATPase motifs retain measurable helicase activity (Figure 35). What this exactly means is unclear, but it does make Mcm3 unique among the six Mcm2-7 subunits. It is also somewhat surprising considering that the Mcm3 arginine finger is a vital piece of the Mcm3/7 active site. As described above, Mcm3

may help to communicate the status of the Mcm2/5 gate to Mcm7 and 4. Finally, there is some indication that the Mcm3DENQ complex may be locked in a "closed" conformation (see Table 5 footnote) much like the 2RA mutant. However, this could not be adequately verified due to the low concentration of the protein preparation. If new Mcm3DENQ preparations do confirm this observation, it could indicate that Mcm3 (likely as part of the Mcm5/3 active site) is a "hinge" for the Mcm2/5 gate.

APPENDIX B

GENETIC SCREENS

Genetic analysis of the Mcm2-7 complex has been hampered by the essential nature of the six genes encoding the Mcm subunits [228, 229] and the lack of good conditional mutants. While degron alleles have been made for 5 of the 6 *MCM*s (the *MCM5* degron allele is nonviable; [87]), they require special strain backgrounds and have seen limited use. Unfortunately, most of the *MCM* ATPase mutants that have been well characterized *in vitro* are also lethal *in vivo* (see Table 4; [104, 182]).

As the number of available *in vitro* tools for studying Mcm2-7 has increased in recent years (this dissertation), it has become apparent that the biochemical and *in vivo* data (concerning the same mutation, for instance) don't always align. These discrepancies have fueled a renewed interest in using genetics to tease apart the mysteries of Mcm2-7. In that vein, three screens were undertaken to: 1) search for Mcm ssDNA binding mutants; 2) link specific Mcm ATPase active sites to replication checkpoint responses; and 3) explain why some Mcm ATPase mutants retain *in vitro* helicase activity but are lethal *in vivo*. The results are presented below.

B.1 SCREEN 1: *IN VIVO* ANALYSIS OF MCM4 β-HAIRPIN FINGER MUTANTS

B.1.1 Introduction

In early 2003, Fletcher *et al.* published the crystal structure of the N-terminal half of the MthMCM complex [58]. MthMCM formed a dumbbell-shaped dodecomeric structure composed of two head-to-head MCM hexamers. Interestingly, the structure showed that each subunit in the hexamer contained a β-hairpin "finger" (the anti-parallel beta strands 9 and 10 connected by a loop) that pointed towards the center of the channel in the MthMCM complex and contained positively charged residues at the tip (Figure 3). Alanine substitution mutations were used to neutralize the charged residues, and defects in DNA binding were observed. Using the MthMCM crystal structure and a structure-guided alignment of other archaeal MCMs, DNA binding mutants were also made in the SsoMCM [59].

Bioinformatic analysis suggested that the eukaryotic Mcm2-7 subunits also contained conserved β-hairpin fingers of varying length with one or more positively charged residues that could be important for DNA binding (Figure 36; [58]). In order to test these predictions, four residues (R445, N447, H465, and K467) in the putative β-hairpin finger of *S. cerevisiae* Mcm4 (the eukaryotic Mcm most closely related to MthMCM) were mutated to alanine. Similarly, Mcm4 mutants containing a deletion of the hypothesized finger (amputation allele) and extensions of the "finger tip" (constipation alleles) were also generated. The *mcm4*^{H465A,K467A} mutant was found to be temperature sensitive, and the implications are discussed below.

A. Alignment of β-fingers

```
Mcm5p GTRVTIVGIYSIY NSKNGA------------------GSGRSGGGNGGSGVAIRTP YIKILGIQSD
Mcm3p GDRVNVVGVFKSL G-----------------------AGGMNQSNSNTLIGFKTL ILGNTVYPLH
Mcm2p GEEVEVTGIYKNN ----------------------YDGNLNAKNGFPVFATIIE ANSIKRREGN
Mcm7p GDIVDVTGIFLPA P--------------------------------YTGFKALKAG LLTETYLEAQ
Mcm6p GDRCKFTGVEIVV PDVTQLGLPGVKPSSTLDTRGISKTTEGLNSGVTGLRSLGVRDL TYKISFLACH
Mcm4p GDRIEVTGTFRSI PIRANS------------------RQRVLKSLYKTYVDVVHVK KVSDKRLDVD
```

B. Evolutionary relationship between the Mcm2-7 subunits

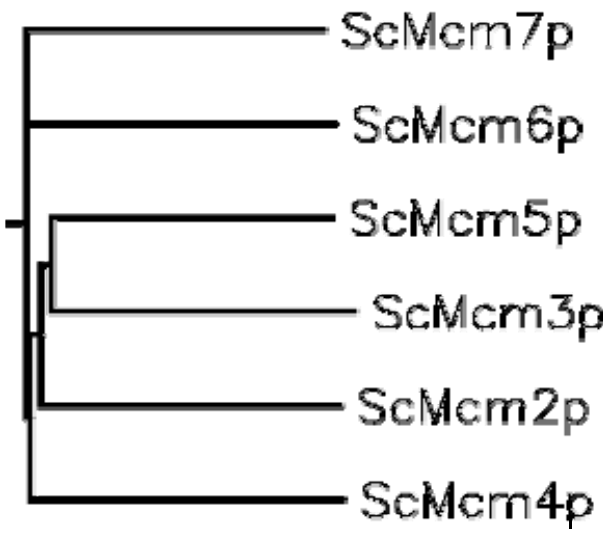

Figure 36. Putative β-hairpin fingers of the *S. cerevisiae* Mcms.

A) Multiple sequence alignment of the putative β-hairpin fingers of Mcm2-7. The proteins were aligned in their entirety by CLUSTALW [79], but only the portions corresponding to β9-loop-β10 of MthMCM [58] are shown. The loop (*i.e.*, fingertip) is separated from β9 (left, underlined) and β10 (right, underlined) by spaces. The Mcm4 residues in bold (R445, N447, H465, and K467) are discussed in the Results section. B) Rooted tree of Mcm subunit relatedness. The tree was generated from the CLUSTALW alignment using the Phylogeny Inference Package (http://seqtool.sdsc.edu/CGI/BW.cgi#!).

B.1.2 Results

Phenotypes of the *mcm4* point mutations

Megaprimer PCR mutagenesis [177] was used to generate the *mcm4*^{R445A,N447A}, *mcm4*^{H465A,K467A}, *mcm4*^{R445A,N447A,H465A,K467A} alleles (herein referred to as the *mcm4RANA*, *HAKA*, and *Quad* mutants, respectively). These genes were cloned into a *TRP1*-marked low copy vector under the control of the *MCM5* promoter and transformed into a *S. cerevisiae MCM4* "swapper strain" (a strain used for plasmid shuffling that contains a chromosomal deletion of the gene of interest and a wild type copy on a *URA3*-marked plasmid). Transformants were then plated on 5-FOA media to select against *MCM4*, and viability was assessed (Figure 37A).

The *mcm4RANA* strain has no apparent growth defect at 22, 30, or 37°C, nor is it cold sensitive (data not shown). The *mcm4HAKA* strain on the other hand grows slowly at 22 and 30°C and is highly temperature sensitive at 37°C. Paradoxically, the *mcm4Quad* stain, which contains the *HAKA* mutation, displays no growth defect or temperature sensitivity. Implications of this result are discussed below.

Phenotypes of the *mcm4* amputation and constipation mutants

An "amputation" allele of *MCM4* (containing a deletion corresponding to residues 445-467 (replaced by AAGPAA) of Mcm4p) and three libraries of "constipation" alleles were also made by megaprimer PCR. The oligos for the "constipation PCR" were designed 1) to make insertions in *MCM4* corresponding to 10 random amino acids at 3 different points in the β-hairpin finger tip, and 2) to be biased against stop codons in their random portions (see Table 1). The resulting mutated genes were cloned into a *LEU2*-marked integrating vector under the control of the *GAL*

promoter and transformed into a wild type *S. cerevisiae* strain (UPY323). It was assumed that a dominant negative phenotype would correspond to *mcm4* alleles that encoded proteins that were capable of oligomerizing with the other Mcms and defective for DNA binding. Integrants that were not dominant negative should encompass wild type *MCM4* and rare alleles containing stop codons in the β-hairpin finger that made it into the constipation libraries.

Transformants were initially plated on media to select for integration of the plasmids and then patched onto media containing galactose for dominant negative testing (data not shown). After sifting through a muddle of *trp1* revertants, it was found that the *mcm4Amputation* mutant was not lethal, but many of the *mcm4Constipation* mutants did indeed display a dominant lethal phenotype. Unfortunately, sequencing of many of the constipation plasmids revealed that the PCR primers introduced stop codons in the β-hairpin despite the design having a bias against them.

Regardless, one constipation clone retained an intact β-hairpin finger, and it was tested for complementation in the *MCM4* swapper strain. As expected, the dominant negative mutant failed to complement a chromosomal deletion of *MCM4* (Figure 37B). Emboldened, *mcm4Constipation* was cloned into a baculovirus for expression in insect cells [104, 126], but a truncated protein was produced. Further sequencing of the clone revealed that a stop codon had been introduced in-frame downstream of the β-finger *in vivo* by dubious means. At this point, the project was abandoned in favor of more well-behaved *in vitro* assays.

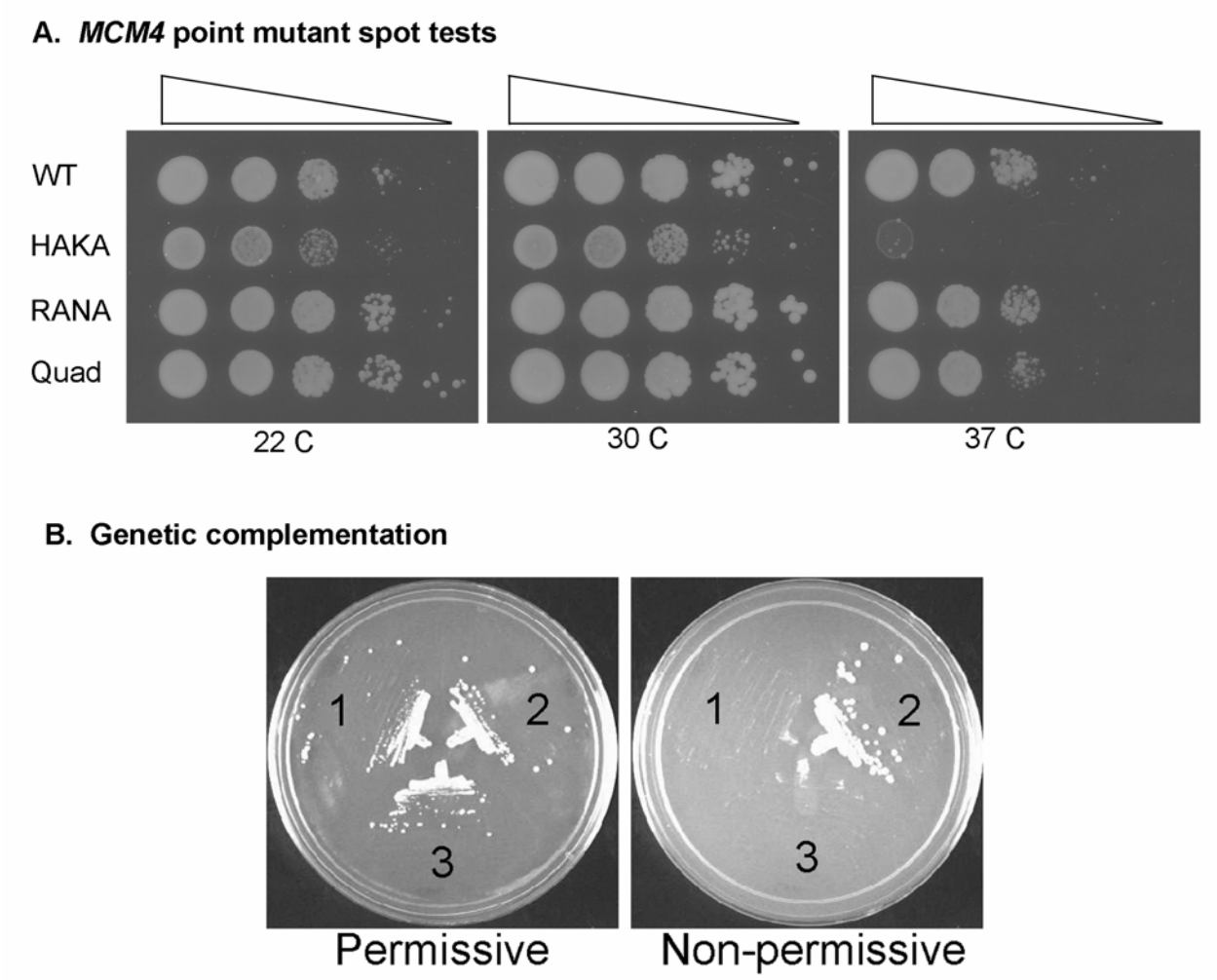

Figure 37. Phenotypes of the putative β-hairpin finger mutants.

A) The *mcm4HAKA* mutant is temperature sensitive. 10-fold serial dilutions of strains encoding *MCM4* (WT), *mcm4*^{H465A,K467A} (HAKA), *mcm4*^{R445A,N447A} (RANA), and *mcm4*^{R445A,N447A,H465A,K467A} (Quad) were spotted on rich media after dilution to the same cell density as the HAKA strain and incubated at the three temperatures indicated. B) The *mcm4Constipation* mutant cannot complement a *Δmcm4* strain. Cells were streaked for single colonies on selective media (permissive) and 5-FOA (non-permissive). Strain 1 carries the constipation mutant on a *TRP1*-marked plasmid; strain 2 carries wild type *MCM4* on the same plasmid; strain 3 contains empty vector. All strains carried a copy of *MCM4* on a *URA3*-marked plasmid.

B.1.3 Conclusions

This screen was largely a cross between a comedy of errors and a Greek tragedy. Positively-charged residues at the tip of the putative Mcm4 β-hairpin finger were neutralized, but the mutants had conflicting phenotypes. Worse yet, attempts to remove and elongate the finger in the form of amputation and constipation alleles met with problems every step of the way.

While it appears that the *mcm4HAKA* mutant grows slowly and is temperature sensitive, the *mcm4Quad* mutant containing both the R445A,N447A and H465A,K467A mutations displays no growth defect. Both constructs will need to be fully sequenced to rule out second site mutations, *etc*. as the cause of the confusion. In any event, the slow growth of *mcm4HAKA* is reminiscent of the *mcm2DENQ* allele (see Screen 2 below) and could indicate a *bona fide* defect in DNA replication.

The experiments with the *mcm4Amputation* and *mcm4Constipation* alleles never panned out. Deletion of the Mcm4 finger had no effect on viability and thus likely has no DNA binding defect. Most of the constipation mutants also had no effect on viability, and this suggests that the 10 amino acid insertion wasn't enough to block the entry of DNA into the central channel of the Mcm2-7 complex. Larger inserts should be tested for their effects. Of the dominant lethal constipation mutants examined, all included a stop codon somewhere in the *MCM4* sequence at or downstream of the putative β-finger region. Aside from the fact that the primers need to be redesigned to totally negate the possibility of inserting a premature stop, the dominant negative phenotype along with co-immunoprecipitation data (not shown) did demonstrate that the N-terminal half of Mcm4 can still oligomerize with one or more of the Mcms.

This project was something of a long shot to begin with because each of the eukaryotic Mcms is thought to possess a β-hairpin finger, and disturbing one out of the six may not be enough to produce the desired DNA binding defect. The situation was further complicated by the eventual publication of a manuscript hypothesizing that each Mcm may actually have two fingers (N- and C-terminal) pointing towards the center of the toroid [145]. Despite these potential obstacles, others have observed interesting effects by mutating the putative β-hairpin fingers of the Mcms individually and in combination. For instance, a *mcm5*^{K304A,R311A,R324A} allele is hypomorphic (although the protein stably interacts with Mcm2) and synthetically lethal with a temperature sensitive *mcm4*^{R445A,K454A,K458A,H465A} mutation (R. Sclafani, personal communication). Two of the alanine substitutions in this allele match those described above (R445A and H465K), but unfortunately in both cases, none of the substitutions were made singly. Single mutations will have to be made to determine if the temperature sensitivity phenotype is related to neutralization of one residue or is the result of multiple mutations.

B.2 SCREEN 2: ARE SPECIFIC MCM ATPASE ACTIVE SITES LINKED TO THE DNA DAMAGE RESPONSE?

B.2.1 Introduction

During DNA replication, chromosomal lesions must be sensed and repaired prior to being replicated to ensure faithful duplication of the genome. Cellular "checkpoints" exist during the initiation and elongation phases of replication that serve as safeguards against replication of damaged DNA by slowing or pausing fork progression when damage is sensed [230-235]. Two well characterized players in these events are Mrc1, which acts in the replication stress response pathway [236], and Rad9, which is involved in the DNA damage response [237].

As the vanguard of the replication fork, the replicative Mcm2-7 helicase is a logical regulatory target of these checkpoint responses, and indeed, the Mcm2-7 complex has been linked to many of the checkpoint pathways (reviewed in [238]). Intriguingly, it was recently discovered that a DE–>NQ mutation in the Walker B box of Mcm2 (Mcm2DENQ) was synthetically lethal with a deletion of *MRC1* in *S. cerevisiae* (Elbakri, Tsai, and Schwacha, unpublished). Evidence is mounting for a Mcm-DNA damage connection because strains encoding *mcm2DENQ* accumulate double-strand breaks at a high frequency (E. Tsai and A. Schwacha, unpublished). To determine if any other *mcm* ATPase alleles may be involved in the replication stress or DNA damage checkpoints, a directed screening of ATPase mutants in *Δmrc1* and *Δrad9* backgrounds was undertaken. The results are presented below.

B.2.2 Results

S. cerevisiae MCM swapper strains with wild type, *Δmrc1*, or *Δrad9* backgrounds (Table 6) were transformed with a low-copy *TRP1*-marked plasmid encoding either a wild type or ATPase mutant *MCM* allele under the control of the endogenous *MCM5* promoter and plated on selective media. The *MCM* swap was completed by patching clones on 5-FOA media to select against the *URA3*-marked plasmid carrying the wild type *MCM*, and viability was assessed.

Table 6. Parental strains used in this screen.

Swapper strain	Genotype [m]
Wild type	*MATa, ade2-1, ura3-11, his3-11,15, leu2-3,12, can-100, trp1-1, ΔMCMX::hisG/pAS404 (ARS/CEN URA+ MCM5 promoter-MCMX)*
Δmrc1	*MATa, ade2-1, ura3-11, his3-11,15, leu2-3,12, can-100, trp1-1, ΔMCMX::hisG/pAS404 (ARS/CEN URA+ MCM5 promoter-MCMX) ΔMRC1::HIS-lox*
Δrad9	*MATa, ade2-1, ura3-11, his3-11,15, leu2-3,12, can-100, trp1-1, ΔMCMX::hisG/pAS404 (ARS/CEN URA+ MCM5 promoter-MCMX), ΔRAD9::HIS-lox*

The results of the screen are collected in Table 7. The slow growth of the *mcm2DENQ* strain (Tsai, Poth, and Schwacha, unpublished), synthetic lethality of the *mcm2DENQ Δmrc1* strain were recapitulated (Tsai, Elbakri, and Schwacha, unpublished), and viability of the *mcm4RA* and *mcm6DENQ* strains (see **Chapter 4**) were recapitulated. In all other cases, the growth phenotype of the wild type background matched that of the *Δmrc1* and *Δrad9* backgrounds. It was noticed however that the *mcm3RA Δrad9*, *mcm7DENQ*, and *mcm7DENQ Δrad9* strains accumulate suppressor mutations at a relatively high frequency (7-10% of transformants).

[m] X = one of the *MCM2-7* genes; a swapper strain for each of the six *MCM*s was made in all three strain backgrounds (WT, *Δmrc1*, and *Δrad9*) for a total of 18 tester strains.

Table 7. Viability of *mcm* alleles.

		Genetic Background		
		Wild type	***Δmrc1***	***Δrad9***
Allele[n]	**(plasmid)**			
		UPY110	UPY428.1	UPY421
Empty vector	(pUP169)	-	-	-
MCM2	(pUP197)	+	+	+
mcm2KA	(pUP198)	-	-	-
mcm2DENQ	(pUP199)	+/-	-	+/-
mcm2RA	(pUP200)	-	-	-
		UPY112	UPY458	UPY425
Empty vector	(pUP169)	-	-	-
MCM3	(pUP201)	+	+	+
mcm3KA	(pUP202)	-	-	-
mcm3DENQ	(pUP203)	-	-	-
mcm3RA	(pUP776)	-	-	-[o]
		UPY114	UPY438	UPY412
Empty vector	(pUP169)	-	-	-
MCM4	(pUP745)	+	+	+
mcm4KA	(pUP205)	-	-	-
mcm4DENQ	(pUP206)	-	-	-
mcm4RA	(pUP207.2)	+	+	+
		UPY116	UPY435	UPY423
Empty vector	(pUP169)	-	-	-
MCM5	(pUP208)	+	+	+
mcm5KA	(pUP210)	-	-	-
mcm5DENQ	(pUP211)	-	-	-
mcm5RA	(pUP212)	-	-	-
		UPY117	UPY452	UPY427
Empty vector	(pUP169)	-	-	-
MCM6	(pUP213)	+	+	+
mcm6KA	(pUP214)	-	-	-
mcm6DENQ	(pUP215)	+	+	+
mcm6RA	(pUP216)	-	-	-
		UPY118	UPY436	UPY424
Empty vector	(pUP169)	-	-	-
MCM7	(pUP217)	+	+	+
mcm7KA	(pUP218)	-	-	-
mcm7DENQ	(pUP219)	-[o]	-	-[o]
mcm7RA	(pUP220)	-	-	-

[n] The "Allele" column denotes the only copy of the particular *MCM* gene in question remaining in the strain after selection on 5-FOA media. +, viable; +/-, slow growth; -, inviable.
[o] These strains pick up suppressors at a higher frequency (7-10%) than the others.

B.2.3 Discussion

This screen served to confirm previous results obtained by past and present members of our research group. Unfortunately, no new synthetically lethal combinations of *mcm* ATPase mutant and *Δmrc1* or *Δrad9* were discovered. Though disappointing, the results underscore the uniqueness of the *mcm2DENQ* allele and its connection to the replication stress response pathway. Additional work will be necessary to fully elucidate the cause of the *mcm2DENQ Δmrc1* synthetic lethality. Similarly, the high rate of spontaneous suppressor mutations in the *mcm3RA Δrad9*, *mcm7DENQ*, and *mcm7DENQ Δrad9* strains warrants further investigation. It will be interesting to determine what these second site suppressors are and if they have any connection to the checkpoint pathways.

B.3 SCREEN 3: SUPPRESSORS OF LETHAL *MCM* ATPASE MUTATIONS

This screen was largely carried out by the talented undergraduate team of Britney Fedor and Dalton Paluzzi.

B.3.1 Introduction

To determine the importance of the Walker A motif, the Walker B motif, and arginine finger of each Mcm subunit, they were all individually mutated, and their effects on viability (Table 4; [104]), ATPase activity (**Chapter 4**; [104]), ssDNA binding (**Appendix A**; [126]), and helicase activity (**Appendix A**; [211]) were examined. Despite the fact that the Mcm2-7 complex is the eukaryotic replicative helicase, it was observed that several Mcm ATPase mutants (Mcm2KA, 3KA, 3DENQ, 3RA, 5DENQ, and 5RA) retained measurable levels of helicase activity *in vitro* but were lethal *in vivo*. If the main cellular function of Mcm2-7 is to unwind DNA at replication forks, then why would mutant complexes that retain this activity (even at reduced levels) cause cell death?

It is possible that the *in vitro* helicase reaction conditions do not mimic physiological conditions closely enough to gauge the true defects of these mutant Mcm complexes. Perhaps under more stringent conditions in the nucleus, the complexes would be completely dead. However, it is also possible that the mutations serve to disrupt interactions between Mcm2-7 and one or more essential partners *in vivo*. Therefore, a high copy suppressor screen was undertaken

to identify genetic interactions between Mcm ATPase mutants and other replication factors. Although this is a work in progress, the current results are presented below.

B.3.2 Results and discussion

In total, over 150,000 transformants were screened between the Mcm2KA, 3KA, 3DENQ, 3RA, 5DENQ, and 5RA strains, and 28 putative suppressors were recovered a high copy genomic DNA library (a gift from K. Arndt). Of these, six have been sequenced so far; the results are presented in Table 8. None of the plasmids have been re-screened to confirm suppression, but the current candidates are nonetheless intriguing (speculation below).

Table 8. Initial suppressor screen results.

	2KA	**3KA**	**3DENQ**	**3RA**	**5DENQ**	**5RA**
# clones screened	16,419	8,893	32,309	36,354	5,346	55,221
# suppressors (%)	4 (0.02)	6 (0.07)	1 (0.003)	3 (0.008)	5 (0.09)	9 (0.02)
Gene(s) on plasmids	*ATP20*[p] *BOR1* *MCM4*[o] *SPC1*[q] *TEL1* *YJR011c*[p]	In progress	In progress	*TEL1;* in progress	*MCM5;* in progress	In progress

[p] These genes are encoded by the same library plasmid.
[q] These genes are encoded by the same library plasmid.

TEL1, a homologue of the human gene mutated in the disease ataxia telangiectasia (ATM) [239], encodes a protein kinase involved in telomere length [240], cell cycle checkpoint control, and responding to DNA damage [241, 242]. The plasmid containing *TEL1* was independently recovered as a suppressor of both the *mcm2KA* and *mcm3RA* mutations. It is interesting to speculate that these two mutant strains may accumulate double-strand breaks (like the *mcm2DENQ* strain; E. Tsai and A. Schwacha, unpublished) at a sufficiently high frequency to cause lethality. Overexpressing *TEL1* may then bolster the DNA damage response to compensate for the increased damage and rescue the cells.

MCM4 encodes a part of the Mcm2-7 motor, but unlike *MCM5*, which was unsurprisingly found to suppress the *mcm5DENQ* mutation, *MCM4* may suppress the *mcm2KA* mutation. This was an unexpected result and begs the question: Can overexpressing other *MCM*s also rescue lethal *MCM* mutations. Experiments are currently under way to test this.

BOR1 encodes a plasma membrane protein that binds and exports HCO_3^-, I^-, Br^-, NO_3^-, and Cl^- from the cell. *In vitro*, these anions are inhibitors of helicase activity (Figure 28, M. Bochman, unpublished). Could changing the ionic make-up of the cell produce conditions that are favorable for helicase activity by *MCM* mutants? This will be tested by assaying for growth under non-permissive conditions (5-FOA) in media supplemented with various anions (glutamate, acetate, chloride, *etc.*).

YJR011c is an uncharacterized ORF. It encodes a putative protein of unknown function, but expression of a Yjr011c/GFP-fusion protein is induced by DNA damage [243]. Experiments will have to be carried out to determine what the role of Yjr011c is during the DNA damage response and if it physically interacts with the Mcms.

ATP20 and *SPC1* encode a subunit of the F1F0 ATP synthase [244] and a subunit of the signal peptidase complex [245], respectively. These have no obvious connection with DNA replication and are found on the same plasmids as *MCM4* and *YJR011c*, respectively. It is therefore doubtful that they are true suppressors.

Currently, the remaining 24 putative suppressors are being sequenced. When their identities are known, they will be re-tested for suppression, as well as tested for suppression in the strains from which they were not isolated. *Bona fide* suppressors can then be further examined for physical interaction with Mcm2-7, *etc.*

APPENDIX C

INITIAL *IN VITRO* CHARACTERIZATION OF THE GINS COMPLEX

Much of this work was either confirmed by or completed with the help of Kristin Klucevesek.

C.1 INTRODUCTION

DNA replication is a fundamental process of life, and therefore it's not surprising that much of the core machinery (*e.g.*, helicases and polymerases) is conserved – enzymatically if not at a sequential level – through all three domains of life. However, just as evolution has resulted in an increase in complexity in organisms from single cells to humans, DNA replication has increased in complexity from prokaryotes to eukaryotes [84]. One obvious layer of complexity is represented by an increase in the sheer number of proteins that are necessary for replication in eukaryotes. For instance, many enzymatic functions (*e.g.*, helicase activity) are accomplished by a single protein in bacteria [181] and viruses [33, 57, 212] but are performed by multiprotein complexes in eukaryotes [84].

Another level of complexity comes from the recent identification of novel replication factors in eukaryotes. One such player is the heterotetrameric GINS complex (Go, Ichi, Nii, and

San; Japanese for five, one, two, and three) which consists of Sld5, Psf1, Psf2, and Psf3 (reviewed in [246]). GINS was first identified in *S. cerevisiae* (ScGINS; [247]), but its four subunits are highly conserved in all eukaryotes. It was later discovered that the archaeal organism *S. solfataricus* encodes a GINS homologue made of two subunits with weak homology to the eukaryotic GINS subunits [248]. Sequence alignments indicate the presence of GINS homologues in other archaea as well.

Like the Mcm2-7 complex (reviewed in [84]) and Cdc45 [97], GINS is necessary for both the initiation and elongation phases of DNA replication [94], but its function(s) during replication are unclear. *In vivo*, GINS seems to be important for the recruitment of DNA polymerases [221, 247, 249]. It also associates with Cdc45 and the Mcms, possibly helping to tether them to the replisome [94-96].

In vitro, the human GINS (HsGINS) complex binds to and stimulates DNA polymerase α-primase, but has no effect on other replicative polymerases [250]. HsGINS was also found to bind ss- and dsDNA by EMSAs, with higher affinity for partially duplex substrates containing one or more ssDNA tails [251]. Transmission electron microscopy (TEM) of the *Xenopus* GINS (XlGINS) complex indicated that it formed a ring-shaped structure with a central channel [221], but a 3-D reconstruction of negatively-stained TEM images suggested that the complex formed a horseshoe-shaped structure [251]. Subsequently and almost simultaneously, three crystal structures of the HsGINS complex were solved [222, 252, 253], but only the structure composed of all four full length subunits yielded a ring-shape with a small central pore [222].

An intriguing recent finding was that Cdc45, Mcm2-7, and GINS form a stable super-complex (CMG complex) in *Drosophila* that has *in vitro* helicase activity [105]. Due to its central role in DNA replication, interaction with Mcm2-7, and possible role as a cog in the

replicative helicase machine, we set out to purify and biochemically characterize the GINS complex from *S. cerevisiae*. We found that yeast GINS forms a stable toroidal heterotetramer. It preferentially binds forked DNA substrates and appears to interact with several Mcms *in vitro.* The implications of this will be discussed below.

C.2 RESULTS

C.2.1 The GINS complex forms a toroidal heterotetramer

SLD5, PSF1, PSF2, and *PSF3* were PCR-amplified from *S. cerevisiae* genomic DNA and cloned into a polycistronic vector [254] for overexpression in *E. coli* (R. Elbakri and A. Schwacha, unpublished). Intact ScGINS complexes were purified by metal-affinity chromatography and contain all four subunits in near-stoichiometric amounts (Figure 38A). The subunits maintained association as a tetramer after purification as demonstrated by native gradient gel electrophoresis (Figure 38B). Low resolution TEM also indicates that 1) the preparation is comprised largely of homogeneous particles (not shown), and 2) GINS appears to form a ring-shaped structure, possibly with a central channel (Figure 38C).

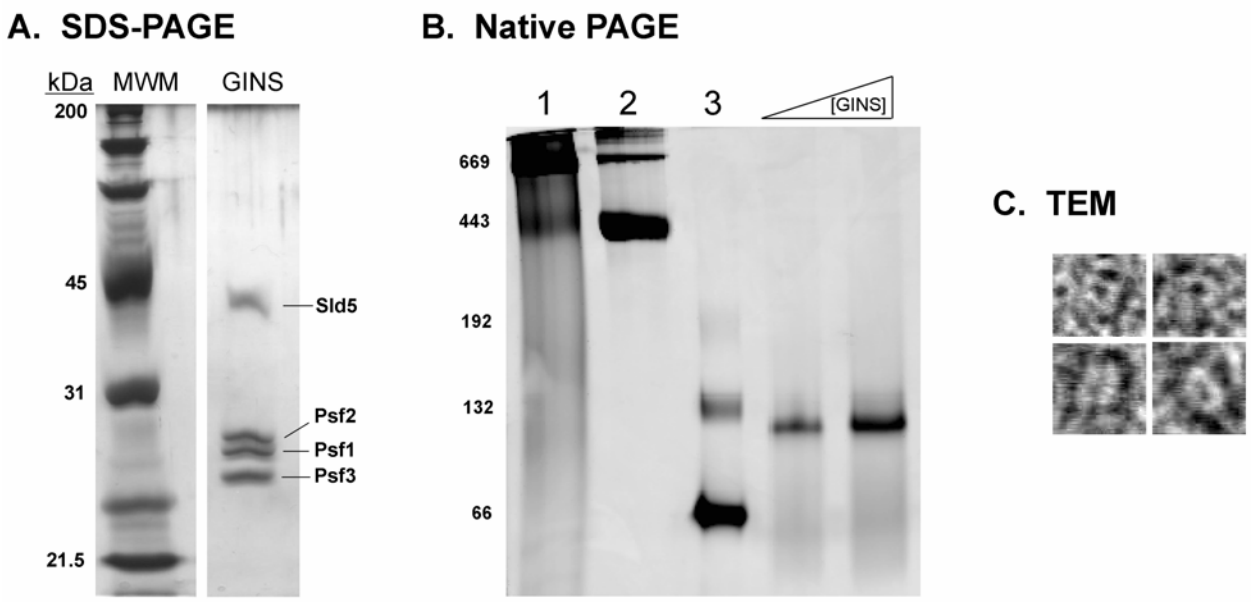

Figure 38. ***In vitro*** **characterization of purified GINS complex.**

A) Denaturing gel electrophoresis of the GINS preparation. A 5 μg sample of the GINS complex (subunits listed on the right) was analyzed by SDS-PAGE through a 12% gel. MWM = molecular weight marker; the sizes of the standards are listed on the left. B) Native gradient gel analysis of the GINS complex. Increasing concentrations (2.3 and 5.8 μg) of purified GINS were subjected to electrophoresis through a 3-12% native gradient gel. Lanes 1-3 contain molecular weight standards: 1, thyroglobulin; 2, apoferritin; 3, BSA. At elevated concentrations, the BSA standard (66 kDa) formed apparent dimers and trimers. C) Transmission electron micrographs of single GINS particles. The high levels of background are due to the small size of the complex and large grain size of the uranyl acetate stain. Magnification = 140,000x.

C.2.2 GINS binds forked DNA substrates

To determine if ScGINS binds DNA like its human homologue [251], EMSAs were conducted with a variety of radiolabeled DNA substrates (Figure 39). Consistent with its localization at replication forks, ScGINS binds forked DNA substrates. This binding appears to be structure-specific; no gel shift was seen with ss- or dsDNA substrates which correspond to the ssDNA tails and duplex region of the fork. The K_d of GINS/fork binding was ~11 nM, indicating either a 2:1 GINS:fork binding stoichiometry or 50% specific activity of the preparation. The binding was stable at moderate concentrations of KCl (~250 mM; data not shown). Competition with a variety of unlabeled homopolymers also revealed that ScGINS preferentially binds poly(dT) substrates and can also bind RNA (poly(U); data not shown).

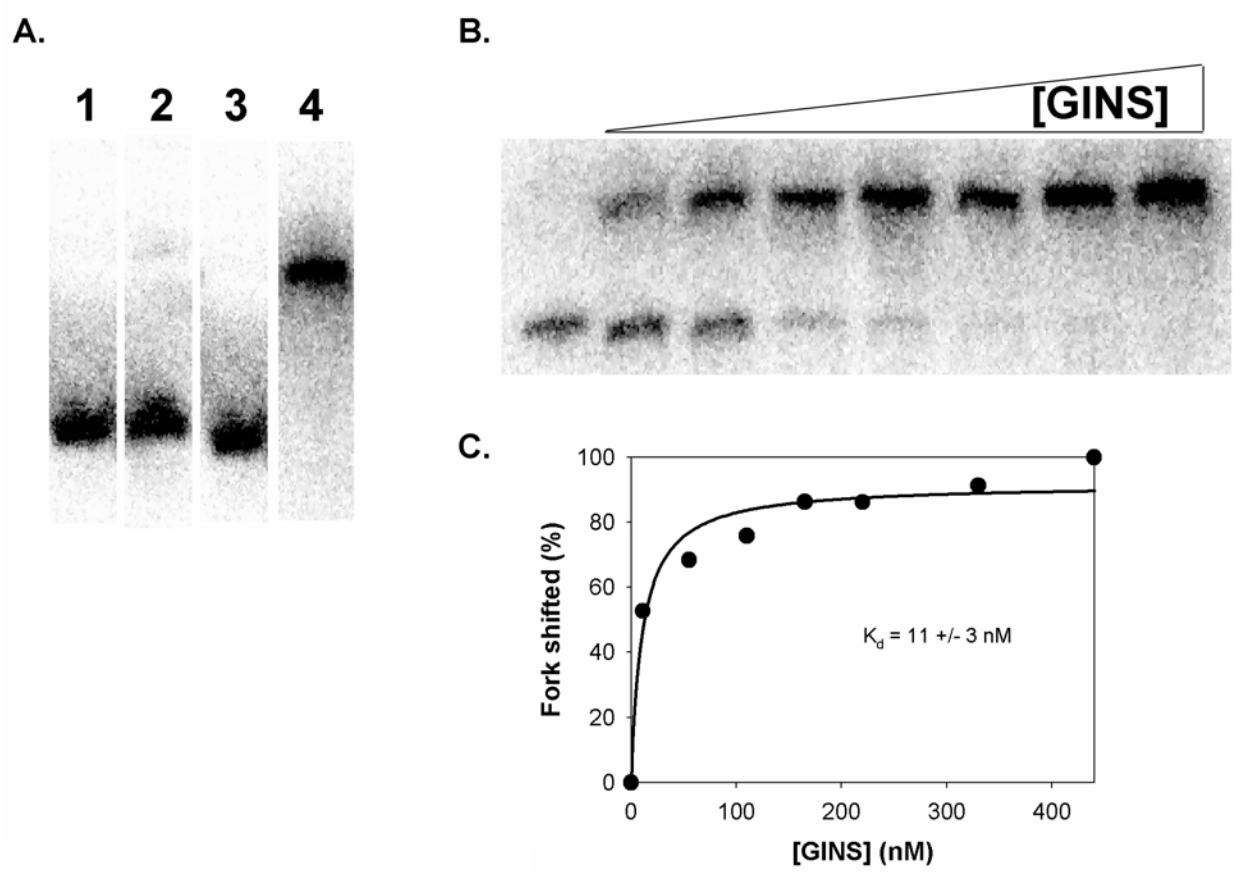

Figure 39. The GINS complex binds DNA forks.

A) GINS/DNA binding is structure specific. Lane 1, 50 nM radiolabeled ssDNA probe; lanes 2-3, 400 nM GINS complex was incubated with 50 nM ssDNA (2), dsDNA (3), or fork (4) probe. The pores in the gel are so large and the acrylamide percentage so low that small (less than 100 nt or bp) substrates migrate at the same position. B) GINS titration. Increasing concentrations of the GINS complex were incubated with 50 nM fork, and binding was quantified by EMSA analysis and phosphoimaging. C) Saturation binding curve. The data from B) were plotted using SigmaPlot and fit with to a hyperbolic curve. The binding constant is noted.

C.2.3 GINS interacts with multiple Mcm2-7 subunits

To begin to determine how the GINS complex might contact and interact with Mcm2-7, southwestern analysis was used to probe GINS binding to Mcm peptide arrays (**Section 2.11**). A positive GINS signal is evident on the arrays for each Mcm subunit, but the strongest binding occurred with Mcm3 and the N-terminus of Mcm5 (Table 9). When the stringency of the wash steps was increased by doubling the salt concentration of the TBS buffer (280 mM NaCl), binding to some individual peptides was lost, decreased, or in some cases increased, but the overall pattern generally remained the same.

Table 9. Putative contacts between the GINS complex and Mcm2-7.

Subunit	Peptides bound[r]
Mcm2	RRRQYEDLENSD
	RELRESNLSSLV
	EGNTANEGEEGL
	RFDILCVVRDLV
	SFPITVRHLESI
	LRRSFAIYTLGH
Mcm3	KAASSTSLNILPHRIIISLDD
	SLVRPKLIRSVHYAAKTGRFHYRDYTDDATTTLTTRIPTP
	EYGYSTFIDHQRITVQEMPEM
	PRSIDVILDDDL
	KSQLLRFVLNTASLAIATTGR
	KLVTIPFLRKYVQYAKERVIPQLTQEAINV
	SLFERINEELPE
Mcm4	SPRRIVDFDTRS
	ILQYVHKITPRG
	YITRDVDTKQLV
	ATTRQLESMIRL
Mcm5	IKSFKNFILEFRLDSQFIYRDQLRNNILVKNYSLTVNME
	RISILSRAQSAN
	RYLTNKVIPGTRVTIVGIYSI
	REFYLEGGAMVL
Mcm6	LLRQSIIRVDVD
Mcm7	DDVLDVILNQRRLRNERMLSDRTNEIRSEN

[r] The peptides are listed N–>C terminal; longer peptides represent sequential 12mers that were bound by GINS.

C.3 DISCUSSION

Our preparation of *S. cerevisiae* GINS has similar biochemical properties as its *Xenopus* and human homologues purified by others [221, 222, 251]. The four subunits, Sld5 and Psf1-3, oligomerize into a toroidal heterotetramer that binds synthetic DNA replication fork substrates and interacts with the Mcm2-7 complex. Although this work is preliminary and must be revisited in a more rigorous and extensive manner, the initial results are intriguing.

The GINS complex is part of the larger replisome progression complex found at replication forks [94]. It is not surprising therefore that ScGINS binds synthetic replication forks *in vitro*. This is similar to the high affinity binding of forks by the HsGINS complex [251], but no direct binding to simple ss- or dsDNA substrates was observed. This may be a species-specific characteristic of ScGINS, but attempts to verify binding by a double filter binding assay [126] failed to demonstrate any DNA binding activity (data not shown). Interestingly, GINS appears to bind poly(dT) DNA with high affinity. This is similar to the Mcm2-7 complex's preference for binding polypyrimidine tracts [126] and could correspond to loading at origins of replication which are often A/T-rich [152-155] and contain stretches of poly(dT) sequence [191, 192].

It remains to be seen if the central channel in the GINS complex houses its DNA binding domain or if binding occurs somewhere on the surface of the molecule. A ring-shaped architecture is exceptionally common among proteins involved in DNA metabolism [16, 255, 256], and in most cases the DNA passes through the central channel of the protein. It's interesting to speculate that perhaps GINS acts as a sliding clamp during replication to tether one

or more polymerases to Mcm2-7 and/or Cdc45. The archetypal eukaryotic sliding clamp PCNA plays a similar role in recruiting and connecting several replication factors that each interact with particular faces of the ring (reviewed in [257]).

In the context of the CMG complex (reviewed in [183]), GINS is necessary for stability of the complex and helicase activity, but it is dispensable for *in vitro* helicase activity of the isolated Mcm2-7 complex (**Chapter 5**). Whether or not GINS forms a necessary piece of the replicative helicase under physiological conditions has yet to be determined. As a step toward elucidating this, we attempted to discover which Mcm subunit(s) GINS interacts with using a Mcm peptide array. It's formally possible that GINS could make contacts with each Mcm subunit *in vivo*, but it seems more likely that it contacts a subset of the Mcms based on the relative sizes of the two complexes. The data indicate that this link might be through Mcms 3 and 5 which are believed to be positioned next to one another and form an ATPase active site within the Mcm2-7 ring (**Chapter 4**; [102]). The N-terminal region of Mcm5 contacted by GINS is also close to the location of the *mcm5-bob1* mutation that obviates the need for the Cdc7/Dbf4 kinase [199]. If the predicted Mcm2/5 gate is a regulatory feature of the Mcm2-7 complex and Cdc7 phosphorylation plays a role in this regulation, then the interaction of the GINS complex with Mcm5 could indicate that GINS also aids in the regulation of the helicase. Testing this will minimally require pinpointing the interacting residues on Mcm2-7 and/or GINS, making targeted mutations to specifically disrupt the interaction, and assaying the consequences on Mcm2-7 ring closure *in vitro* and DNA replication *in vivo*.

BIBLIOGRAPHY

1. Watson, J.D. and F.H. Crick, The structure of DNA. *Cold Spring Harb Symp Quant Biol*, 1953. **18**: 123-31.

2. Watson, J.D. and F.H. Crick, Molecular structure of nucleic acids; a structure for deoxyribose nucleic acid. *Nature*, 1953. **171**(4356): 737-8.

3. Lehman, I.R., et al., Enzymatic synthesis of deoxyribonucleic acid. I. Preparation of substrates and partial purification of an enzyme from Escherichia coli. *J Biol Chem*, 1958. **233**(1): 163-70.

4. Kornberg, A., DNA replication. *J Biol Chem*, 1988. **263**(1): 1-4.

5. Alba, M., Replicative DNA polymerases. *Genome Biol*, 2001. **2**(1): REVIEWS3002.

6. Kawasaki, Y. and A. Sugino, Yeast replicative DNA polymerases and their role at the replication fork. *Mol Cells*, 2001. **12**(3): 277-85.

7. Deutscher, M.P. and A. Kornberg, Enzymatic synthesis of deoxyribonucleic acid. XXIX. Hydrolysis of deoxyribonucleic acid from the 5' terminus by an exonuclease function of deoxyribonucleic acid polymerase. *J Biol Chem*, 1969. **244**(11): 3029-37.

8. Garcia-Diaz, M. and K. Bebenek, Multiple functions of DNA polymerases. *CRC Crit Rev Plant Sci*, 2007. **26**(2): 105-122.

9. Kogoma, T., Two types of temperature sensitivity in DNA replication of an Escherichia coli dnaB mutant. *J Mol Biol*, 1976. **103**(1): 191-7.

10. LeBowitz, J.H. and R. McMacken, The Escherichia coli dnaB replication protein is a DNA helicase. *J Biol Chem*, 1986. **261**(10): 4738-48.

11. Arai, K. and A. Kornberg, Mechanism of dnaB protein action. II. ATP hydrolysis by dnaB protein dependent on single- or double-stranded DNA. *J Biol Chem*, 1981. **256**(10): 5253-9.

12. McMacken, R., K. Ueda, and A. Kornberg, Migration of Escherichia coli dnaB protein on the template DNA strand as a mechanism in initiating DNA replication. *Proc Natl Acad Sci U S A*, 1977. **74**(10): 4190-4.

13. Kornberg, A.a.B., T.A., *DNA Replication*. 2nd ed ed. 1992, New York: Freeman.

14. Sekimizu, K., D. Bramhill, and A. Kornberg, ATP activates dnaA protein in initiating replication of plasmids bearing the origin of the E. coli chromosome. *Cell*, 1987. **50**(2): 259-65.

15. Erzberger, J.P., M.L. Mott, and J.M. Berger, Structural basis for ATP-dependent DnaA assembly and replication-origin remodeling. *Nat Struct Mol Biol*, 2006. **13**(8): 676-83.

16. Davey, M.J. and M. O'Donnell, Replicative helicase loaders: ring breakers and ring makers. *Curr Biol*, 2003. **13**(15): R594-6.

17. Kelman, Z. and M. O'Donnell, DNA polymerase III holoenzyme: structure and function of a chromosomal replicating machine. *Annu Rev Biochem*, 1995. **64**: 171-200.

18. McInerney, P., et al., Characterization of a triple DNA polymerase replisome. *Mol Cell*, 2007. **27**(4): 527-38.

19. Kim, S., et al., Coupling of a replicative polymerase and helicase: a tau-DnaB interaction mediates rapid replication fork movement. *Cell*, 1996. **84**(4): 643-50.

20. Mok, M. and K.J. Marians, The Escherichia coli preprimosome and DNA B helicase can form replication forks that move at the same rate. *J Biol Chem*, 1987. **262**(34): 16644-54.

21. Stano, N.M., et al., DNA synthesis provides the driving force to accelerate DNA unwinding by a helicase. *Nature*, 2005. **435**(7040): 370-3.

22. Bujalowski, W., M.M. Klonowska, and M.J. Jezewska, Oligomeric structure of Escherichia coli primary replicative helicase DnaB protein. *J Biol Chem*, 1994. **269**(50): 31350-8.

23. Reha-Krantz, L.J. and J. Hurwitz, The dnaB gene product of Escherichia coli. I. Purification, homogeneity, and physical properties. *J Biol Chem*, 1978. **253**(11): 4043-50.

24. Arai, K., S. Yasuda, and A. Kornberg, Mechanism of dnaB protein action. I. Crystallization and properties of dnaB protein, an essential replication protein in Escherichia coli. *J Biol Chem*, 1981. **256**(10): 5247-52.

25. San Martin, M.C., et al., A structural model for the Escherichia coli DnaB helicase based on electron microscopy data. *J Struct Biol*, 1995. **114**(3): 167-76.

26. Yu, X., et al., The hexameric E. coli DnaB helicase can exist in different Quaternary states. *J Mol Biol*, 1996. **259**(1): 7-14.

27. San Martin, C., et al., Three-dimensional reconstructions from cryoelectron microscopy images reveal an intimate complex between helicase DnaB and its loading partner DnaC. *Structure*, 1998. **6**(4): 501-9.

28. Bailey, S., W.K. Eliason, and T.A. Steitz, Structure of hexameric DnaB helicase and its complex with a domain of DnaG primase. *Science*, 2007. **318**(5849): 459-63.

29. Wang, G., et al., The structure of a DnaB-family replicative helicase and its interactions with primase. *Nat Struct Mol Biol*, 2008. **15**(1): 94-100.

30. Biswas, T. and O.V. Tsodikov, Hexameric ring structure of the N-terminal domain of Mycobacterium tuberculosis DnaB helicase. *Febs J*, 2008. **275**(12): 3064-71.

31. Jezewska, M.J., U.S. Kim, and W. Bujalowski, Interactions of Escherichia coli primary replicative helicase DnaB protein with nucleotide cofactors. *Biophys J*, 1996. **71**(4): 2075-86.

32. Walker, J.E., et al., Distantly related sequences in the alpha- and beta-subunits of ATP synthase, myosin, kinases and other ATP-requiring enzymes and a common nucleotide binding fold. *Embo J*, 1982. **1**(8): 945-51.

33. Koonin, E.V., A common set of conserved motifs in a vast variety of putative nucleic acid-dependent ATPases including MCM proteins involved in the initiation of eukaryotic DNA replication. *Nucleic Acids Res*, 1993. **21**(11): 2541-7.

34. Biswas, S.B. and E.E. Biswas-Fiss, Quantitative Analysis of Binding of Single-Stranded DNA by Escherichia coli DnaB Helicase and the DnaB.DnaC Complex. *Biochemistry*, 2006. **45**(38): 11505-11513.

35. Patel, S.S. and K.M. Picha, Structure and function of hexameric helicases. *Annu Rev Biochem*, 2000. **69**: 651-97.

36. Bujalowski, W. and M.M. Klonowska, Negative cooperativity in the binding of nucleotides to Escherichia coli replicative helicase DnaB protein. Interactions with fluorescent nucleotide analogs. *Biochemistry*, 1993. **32**(22): 5888-900.

37. Rajendran, S., M.J. Jezewska, and W. Bujalowski, Multiple-step kinetic mechanism of DNA-independent ATP binding and hydrolysis by Escherichia coli replicative helicase DnaB protein: quantitative analysis using the rapid quench-flow method. *J Mol Biol*, 2000. **303**(5): 773-95.

38. Bujalowski, W. and M.J. Jezewska, Kinetic mechanism of nucleotide cofactor binding to Escherichia coli replicative helicase DnaB protein. stopped-flow kinetic studies using

fluorescent, ribose-, and base-modified nucleotide analogues. *Biochemistry*, 2000. **39**(8): 2106-22.

39. Bujalowski, W. and M.J. Jezewska, Interactions of Escherichia coli primary replicative helicase DnaB protein with single-stranded DNA. The nucleic acid does not wrap around the protein hexamer. *Biochemistry*, 1995. **34**(27): 8513-9.

40. Jezewska, M.J., U.S. Kim, and W. Bujalowski, Binding of Escherichia coli primary replicative helicase DnaB protein to single-stranded DNA. Long-range allosteric conformational changes within the protein hexamer. *Biochemistry*, 1996. **35**(7): 2129-45.

41. Jezewska, M.J., et al., Does single-stranded DNA pass through the inner channel of the protein hexamer in the complex with the Escherichia coli DnaB Helicase? Fluorescence energy transfer studies. *J Biol Chem*, 1998. **273**(17): 10515-29.

42. Jezewska, M.J. and W. Bujalowski, Global conformational transitions in Escherichia coli primary replicative helicase DnaB protein induced by ATP, ADP, and single-stranded DNA binding. Multiple conformational states of the helicase hexamer. *J Biol Chem*, 1996. **271**(8): 4261-5.

43. Bujalowski, W. and M.J. Jezewska, Kinetic mechanism of the single-stranded DNA recognition by Escherichia coli replicative helicase DnaB protein. Application of the matrix projection operator technique to analyze stopped-flow kinetics. *J Mol Biol*, 2000. **295**(4): 831-52.

44. Berry, R.S., Rice, S. A. & Ross, J., *Chemical kinetics*, in *Physical Chemistry*. 1980, J. Wiley & Sons: New York.

45. Jezewska, M.J., S. Rajendran, and W. Bujalowski, Strand specificity in the interactions of Escherichia coli primary replicative helicase DnaB protein with a replication fork. *Biochemistry*, 1997. **36**(33): 10320-6.

46. Jezewska, M.J., S. Rajendran, and W. Bujalowski, Complex of Escherichia coli primary replicative helicase DnaB protein with a replication fork: recognition and structure. *Biochemistry*, 1998. **37**(9): 3116-36.

47. Galletto, R., M.J. Jezewska, and W. Bujalowski, Unzipping mechanism of the double-stranded DNA unwinding by a hexameric helicase: the effect of the 3' arm and the stability of the dsDNA on the unwinding activity of the Escherichia coli DnaB helicase. *J Mol Biol*, 2004. **343**(1): 101-14.

48. Galletto, R., M.J. Jezewska, and W. Bujalowski, Unzipping mechanism of the double-stranded DNA unwinding by a hexameric helicase: quantitative analysis of the rate of the dsDNA unwinding, processivity and kinetic step-size of the Escherichia coli DnaB helicase using rapid quench-flow method. *J Mol Biol*, 2004. **343**(1): 83-99.

49. Eoff, R.L. and K.D. Raney, Helicase-catalysed translocation and strand separation. *Biochem Soc Trans*, 2005. **33**(Pt 6): 1474-8.

50. Kaplan, D.L. and M. O'Donnell, DnaB drives DNA branch migration and dislodges proteins while encircling two DNA strands. *Mol Cell*, 2002. **10**(3): 647-57.

51. Bujalowski, W., Expanding the physiological role of the hexameric DnaB helicase. *Trends Biochem Sci*, 2003. **28**(3): 116-8.

52. Kaplan, D.L. and M. O'Donnell, Twin DNA pumps of a hexameric helicase provide power to simultaneously melt two duplexes. *Mol Cell*, 2004. **15**(3): 453-65.

53. Takahashi, T.S., D.B. Wigley, and J.C. Walter, Pumps, paradoxes and ploughshares: mechanism of the MCM2-7 DNA helicase. *Trends Biochem Sci*, 2005. **30**(8): 437-44.

54. Gai, D., et al., Mechanisms of conformational change for a replicative hexameric helicase of SV40 large tumor antigen. *Cell*, 2004. **119**(1): 47-60.

55. Enemark, E.J. and L. Joshua-Tor, Mechanism of DNA translocation in a replicative hexameric helicase. *Nature*, 2006. **442**(7100): 270-5.

56. Borowiec, J.A., et al., Binding and unwinding--how T antigen engages the SV40 origin of DNA replication. *Cell*, 1990. **60**(2): 181-4.

57. Schuck, S. and A. Stenlund, Assembly of a double hexameric helicase. *Mol Cell*, 2005. **20**(3): 377-89.

58. Fletcher, R.J., et al., The structure and function of MCM from archaeal M. Thermoautotrophicum. *Nat Struct Biol*, 2003. **10**(3): 160-7.

59. Pucci, B., et al., Amino acids of the Sulfolobus solfataricus mini-chromosome maintenance-like DNA helicase involved in DNA binding/remodeling. *J Biol Chem*, 2004. **279**(47): 49222-8.

60. Li, D., et al., Structure of the replicative helicase of the oncoprotein SV40 large tumour antigen. *Nature*, 2003. **423**(6939): 512-8.

61. Abbate, E.A., J.M. Berger, and M.R. Botchan, The X-ray structure of the papillomavirus helicase in complex with its molecular matchmaker E2. *Genes Dev*, 2004. **18**(16): 1981-96.

62. Shen, J., et al., The roles of the residues on the channel beta-hairpin and loop structures of simian virus 40 hexameric helicase. *Proc Natl Acad Sci U S A*, 2005. **102**(32): 11248-53.

63. Kaplan, D.L., M.J. Davey, and M. O'Donnell, Mcm4,6,7 uses a "pump in ring" mechanism to unwind DNA by steric exclusion and actively translocate along a duplex. *J Biol Chem*, 2003. **278**(49): 49171-82.

64. Hingorani, M.M. and S.S. Patel, Cooperative interactions of nucleotide ligands are linked to oligomerization and DNA binding in bacteriophage T7 gene 4 helicases. *Biochemistry*, 1996. **35**(7): 2218-28.

65. Patel, S.S. and M.M. Hingorani, Nucleotide binding studies of bacteriophage T7 DNA helicase-primase protein. *Biophys J*, 1995. **68**(4 Suppl): 186S-189S; discussion 189S-190S.

66. Moir, D., et al., Cold-sensitive cell-division-cycle mutants of yeast: isolation, properties, and pseudoreversion studies. *Genetics*, 1982. **100**(4): 547-63.

67. Hennessy, K.M., et al., A group of interacting yeast DNA replication genes. *Genes Dev*, 1991. **5**(6): 958-69.

68. Maine, G.T., P. Sinha, and B.K. Tye, Mutants of S. cerevisiae defective in the maintenance of minichromosomes. *Genetics*, 1984. **106**(3): 365-85.

69. Maiorano, D., M. Lutzmann, and M. Mechali, MCM proteins and DNA replication. *Curr Opin Cell Biol*, 2006. **18**(2): 130-6.

70. Takahashi, K., H. Yamada, and M. Yanagida, Fission yeast minichromosome loss mutants mis cause lethal aneuploidy and replication abnormality. *Mol Biol Cell*, 1994. **5**(10): 1145-58.

71. Chong, J.P., P. Thommes, and J.J. Blow, The role of MCM/P1 proteins in the licensing of DNA replication. *Trends Biochem Sci*, 1996. **21**(3): 102-6.

72. Chong, J.P. and J.J. Blow, DNA replication licensing factor. *Prog Cell Cycle Res*, 1996. **2**: 83-90.

73. Forsburg, S.L., Eukaryotic MCM proteins: beyond replication initiation. *Microbiol Mol Biol Rev*, 2004. **68**(1): 109-31.

74. Kelman, L.M. and Z. Kelman, Archaea: an archetype for replication initiation studies? *Mol Microbiol*, 2003. **48**(3): 605-15.

75. Grabowski, B. and Z. Kelman, Archeal DNA replication: eukaryal proteins in a bacterial context. *Annu Rev Microbiol*, 2003. **57**: 487-516.

76. McGeoch, A.T. and S.D. Bell, Eukaryotic/archaeal primase and MCM proteins encoded in a bacteriophage genome. *Cell*, 2005. **120**(2): 167-8.

77. Iyer, L.M., et al., Evolutionary history and higher order classification of AAA+ ATPases. *J Struct Biol*, 2004. **146**(1-2): 11-31.

78. Erzberger, J.P. and J.M. Berger, Evolutionary relationships and structural mechanisms of AAA+ proteins. *Annu Rev Biophys Biomol Struct*, 2006. **35**: 93-114.

79. Thompson, J.D., D.G. Higgins, and T.J. Gibson, CLUSTAL W: improving the sensitivity of progressive multiple sequence alignment through sequence weighting, position-specific gap penalties and weight matrix choice. *Nucleic Acids Res*, 1994. **22**(22): 4673-80.

80. Johnson, R.T. and P.N. Rao, Mammalian cell fusion: induction of premature chromosome condensation in interphase nuclei. *Nature*, 1970. **226**(5247): 717-22.

81. Johnson, R.T., P.N. Rao, and H.D. Hughes, Mammalian cell fusion. 3. A HeLa cell inducer of premature chromosome condensation active in cells from a variety of animal species. *J Cell Physiol*, 1970. **76**(2): 151-7.

82. Rao, P.N. and R.T. Johnson, Mammalian cell fusion: studies on the regulation of DNA synthesis and mitosis. *Nature*, 1970. **225**(5228): 159-64.

83. Rao, P.N. and R.T. Johnson, Mammalian cell fusion. IV. Regulation of chromosome formation from interphase nuclei by various chemical compounds. *J Cell Physiol*, 1971. **78**(2): 217-23.

84. Bell, S.P. and A. Dutta, DNA replication in eukaryotic cells. *Annu Rev Biochem*, 2002. **71**: 333-74.

85. Bell, S.P., Eukaryotic replicators and associated protein complexes. *Curr Opin Genet Dev*, 1995. **5**(2): 162-7.

86. Wyrick, J.J., et al., Genome-wide distribution of ORC and MCM proteins in S. cerevisiae: high-resolution mapping of replication origins. *Science*, 2001. **294**(5550): 2357-60.

87. Labib, K., J.A. Tercero, and J.F. Diffley, Uninterrupted MCM2-7 function required for DNA replication fork progression. *Science*, 2000. **288**(5471): 1643-7.

88. Nguyen, V.Q., et al., Clb/Cdc28 kinases promote nuclear export of the replication initiator proteins Mcm2-7. *Curr Biol*, 2000. **10**(4): 195-205.

89. Rowles, A., S. Tada, and J.J. Blow, Changes in association of the Xenopus origin recognition complex with chromatin on licensing of replication origins. *J Cell Sci*, 1999. **112 (Pt 12)**: 2011-8.

90. Hua, X.H. and J. Newport, Identification of a preinitiation step in DNA replication that is independent of origin recognition complex and cdc6, but dependent on cdk2. *J Cell Biol*, 1998. **140**(2): 271-81.

91. Randell, J.C., et al., Sequential ATP hydrolysis by Cdc6 and ORC directs loading of the Mcm2-7 helicase. *Mol Cell*, 2006. **21**(1): 29-39.

92. Bowers, J.L., et al., ATP hydrolysis by ORC catalyzes reiterative Mcm2-7 assembly at a defined origin of replication. *Mol Cell*, 2004. **16**(6): 967-78.

93. Aparicio, O.M., D.M. Weinstein, and S.P. Bell, Components and dynamics of DNA replication complexes in S. cerevisiae: redistribution of MCM proteins and Cdc45p during S phase. *Cell*, 1997. **91**(1): 59-69.

94. Gambus, A., et al., GINS maintains association of Cdc45 with MCM in replisome progression complexes at eukaryotic DNA replication forks. *Nat Cell Biol*, 2006. **8**(4): 358-66.

95. Kanemaki, M. and K. Labib, Distinct roles for Sld3 and GINS during establishment and progression of eukaryotic DNA replication forks. *Embo J*, 2006. **25**(8): 1753-63.

96. Pacek, M., et al., Localization of MCM2-7, Cdc45, and GINS to the site of DNA unwinding during eukaryotic DNA replication. *Mol Cell*, 2006. **21**(4): 581-7.

97. Tercero, J.A., K. Labib, and J.F. Diffley, DNA synthesis at individual replication forks requires the essential initiation factor Cdc45p. *Embo J*, 2000. **19**(9): 2082-93.

98. Chong, J.P., et al., A double-hexamer archaeal minichromosome maintenance protein is an ATP-dependent DNA helicase. *Proc Natl Acad Sci U S A*, 2000. **97**(4): 1530-5.

99. Kelman, Z., J.K. Lee, and J. Hurwitz, The single minichromosome maintenance protein of Methanobacterium thermoautotrophicum DeltaH contains DNA helicase activity. *Proc Natl Acad Sci U S A*, 1999. **96**(26): 14783-8.

100. Shechter, D.F., C.Y. Ying, and J. Gautier, The intrinsic DNA helicase activity of Methanobacterium thermoautotrophicum delta H minichromosome maintenance protein. *J Biol Chem*, 2000. **275**(20): 15049-59.

101. Ishimi, Y., A DNA helicase activity is associated with an MCM4, -6, and -7 protein complex. *J Biol Chem*, 1997. **272**(39): 24508-13.

102. Davey, M.J., C. Indiani, and M. O'Donnell, Reconstitution of the Mcm2-7p heterohexamer, subunit arrangement, and ATP site architecture. *J Biol Chem*, 2003. **278**(7): 4491-9.

103. Lee, J.K. and J. Hurwitz, Processive DNA helicase activity of the minichromosome maintenance proteins 4, 6, and 7 complex requires forked DNA structures. *Proc Natl Acad Sci U S A*, 2001. **98**(1): 54-9.

104. Schwacha, A. and S.P. Bell, Interactions between two catalytically distinct MCM subgroups are essential for coordinated ATP hydrolysis and DNA replication. *Mol Cell*, 2001. **8**(5): 1093-104.

105. Moyer, S.E., P.W. Lewis, and M.R. Botchan, Isolation of the Cdc45/Mcm2-7/GINS (CMG) complex, a candidate for the eukaryotic DNA replication fork helicase. *Proc Natl Acad Sci U S A*, 2006. **103**(27): 10236-41.

106. Edgell, D.R. and W.F. Doolittle, Archaea and the origin(s) of DNA replication proteins. *Cell*, 1997. **89**(7): 995-8.

107. Olsen, G.J. and C.R. Woese, Archaeal genomics: an overview. *Cell*, 1997. **89**(7): 991-4.

108. Kelman, Z. and M.F. White, Archaeal DNA replication and repair. *Curr Opin Microbiol*, 2005. **8**(6): 669-76.

109. Matsunaga, F., et al., In vivo interactions of archaeal Cdc6/Orc1 and minichromosome maintenance proteins with the replication origin. *Proc Natl Acad Sci U S A*, 2001. **98**(20): 11152-7.

110. Matsunaga, F., et al., Genomewide and biochemical analyses of DNA-binding activity of Cdc6/Orc1 and Mcm proteins in Pyrococcus sp. *Nucleic Acids Res*, 2007. **35**(10): 3214-22.

111. Carpentieri, F., et al., Physical and functional interaction between the mini-chromosome maintenance-like DNA helicase and the single-stranded DNA binding protein from the crenarchaeon Sulfolobus solfataricus. *J Biol Chem*, 2002. **277**(14): 12118-27.

112. Poplawski, A., et al., The zinc finger domain of the archaeal minichromosome maintenance protein is required for helicase activity. *J Biol Chem*, 2001. **276**(52): 49371-7.

113. Grainge, I., S. Scaife, and D.B. Wigley, Biochemical analysis of components of the pre-replication complex of Archaeoglobus fulgidus. *Nucleic Acids Res*, 2003. **31**(16): 4888-98.

114. Haugland, G.T., et al., Stimulation of MCM helicase activity by a Cdc6 protein in the archaeon Thermoplasma acidophilum. *Nucleic Acids Res*, 2006. **34**(21): 6337-44.

115. Liu, W., et al., Structural analysis of the Sulfolobus solfataricus MCM protein N-terminal domain. *Nucleic Acids Res*, 2008. **36**(10): 3235-43.

116. Yu, X., et al., The Methanobacterium thermoautotrophicum MCM protein can form heptameric rings. *EMBO Rep*, 2002. **3**(8): 792-7.

117. Pape, T., et al., Hexameric ring structure of the full-length archaeal MCM protein complex. *EMBO Rep*, 2003. **4**(11): 1079-83.

118. Gomez-Llorente, Y., et al., Polymorphism and double hexamer structure in the archaeal minichromosome maintenance (MCM) helicase from Methanobacterium thermoautotrophicum. *J Biol Chem*, 2005. **280**(49): 40909-15.

119. Costa, A., et al., Structural studies of the archaeal MCM complex in different functional states. *J Struct Biol*, 2006.

120. Costa, A., et al., Structural basis of the Methanothermobacter thermautotrophicus MCM helicase activity. *Nucleic Acids Res*, 2006.

121. Chen, Y.J., et al., Structural polymorphism of Methanothermobacter thermautotrophicus MCM. *J Mol Biol*, 2005. **346**(2): 389-94.

122. You, Z., Y. Komamura, and Y. Ishimi, Biochemical analysis of the intrinsic Mcm4-Mcm6-mcm7 DNA helicase activity. *Mol Cell Biol*, 1999. **19**(12): 8003-15.

123. Lee, D.G., et al., Regulation of origin recognition complex conformation and ATPase activity: differential effects of single-stranded and double-stranded DNA binding. *Embo J*, 2000. **19**(17): 4774-82.

124. Sato, M., et al., Electron microscopic observation and single-stranded DNA binding activity of the Mcm4,6,7 complex. *J Mol Biol*, 2000. **300**(3): 421-31.

125. Yabuta, N., et al., Mammalian Mcm2/4/6/7 complex forms a toroidal structure. *Genes Cells*, 2003. **8**(5): 413-21.

126. Bochman, M.L. and A. Schwacha, Differences in the single-stranded DNA binding activities of MCM2-7 and MCM467: MCM2 and 5 define a slow ATP-dependent step. *J Biol Chem*, 2007.

127. Adachi, Y., J. Usukura, and M. Yanagida, A globular complex formation by Nda1 and the other five members of the MCM protein family in fission yeast. *Genes Cells*, 1997. **2**(7): 467-79.

128. Lee, J.K. and J. Hurwitz, Isolation and characterization of various complexes of the minichromosome maintenance proteins of Schizosaccharomyces pombe. *J Biol Chem*, 2000. **275**(25): 18871-8.

129. Ying, C.Y. and J. Gautier, The ATPase activity of MCM2-7 is dispensable for pre-RC assembly but is required for DNA unwinding. *Embo J*, 2005. **24**(24): 4334-44.

130. Yu, Z., D. Feng, and C. Liang, Pairwise interactions of the six human MCM protein subunits. *J Mol Biol*, 2004. **340**(5): 1197-206.

131. Sherman, D.A., S.G. Pasion, and S.L. Forsburg, Multiple domains of fission yeast Cdc19p (MCM2) are required for its association with the core MCM complex. *Mol Biol Cell*, 1998. **9**(7): 1833-45.

132. Sakwe, A.M., et al., Identification and Characterization of a Novel Component of the Human MCM complex. *Mol Cell Biol*, 2007.

133. Bochkareva, E., et al., Structure of the origin-binding domain of simian virus 40 large T antigen bound to DNA. *Embo J*, 2006. **25**(24): 5961-9.

134. Meinke, G., P.A. Bullock, and A. Bohm, Crystal structure of the simian virus 40 large T-antigen origin-binding domain. *J Virol*, 2006. **80**(9): 4304-12.

135. Meinke, G., et al., The crystal structure of the SV40 T-antigen origin binding domain in complex with DNA. *PLoS Biol*, 2007. **5**(2): e23.

136. Benight, A.S., et al., Dynamic light scattering investigations of RecA self-assembly and interactions with single strand DNA. *Biochimie*, 1991. **73**(2-3): 143-55.

137. Skordalakes, E. and J.M. Berger, Structural insights into RNA-dependent ring closure and ATPase activation by the Rho termination factor. *Cell*, 2006. **127**(3): 553-64.

138. Fletcher, R.J. and X.S. Chen, Biochemical activities of the BOB1 mutant in Methanobacterium thermoautotrophicum MCM. *Biochemistry*, 2006. **45**(2): 462-7.

139. Fletcher, R.J., et al., Double hexamer disruption and biochemical activities of Methanobacterium thermoautotrophicum MCM. *J Biol Chem*, 2005. **280**(51): 42405-10.

140. Kasiviswanathan, R., et al., Biochemical characterization of the Methanothermobacter thermautotrophicus minichromosome maintenance (MCM) helicase N-terminal domains. *J Biol Chem*, 2004. **279**(27): 28358-66.

141. Jenkinson, E.R. and J.P. Chong, Minichromosome maintenance helicase activity is controlled by N- and C-terminal motifs and requires the ATPase domain helix-2 insert. *Proc Natl Acad Sci U S A*, 2006. **103**(20): 7613-8.

142. Shin, J.H. and Z. Kelman, The replicative helicases of bacteria, archaea and eukarya can unwind RNA-DNA hybrid substrates. *J Biol Chem*, 2006.

143. Barry, E.R., et al., Archaeal MCM has separable processivity, substrate choice and helicase domains. *Nucleic Acids Res*, 2007. **35**(3): 988-998.

144. Pucci, B., et al., Modular organization of the Sulfolobus solfataricus mini-chromosome maintenance protein. *J Biol Chem*, 2007. **282**(17): 12574-82.

145. McGeoch, A.T., et al., Organization of the archaeal MCM complex on DNA and implications for the helicase mechanism. *Nat Struct Mol Biol*, 2005. **12**(9): 756-62.

146. Moreau, M.J., et al., ATPase Site Architecture and Helicase Mechanism of an Archaeal MCM. *Mol Cell*, 2007. **28**(2): 304-14.

147. You, Z., et al., Thymine-rich single-stranded DNA activates Mcm4/6/7 helicase on Y-fork and bubble-like substrates. *Embo J*, 2003. **22**(22): 6148-60.

148. Biswas-Fiss, E.E., S.M. Khopde, and S.B. Biswas, The Mcm467 complex of Saccharomyces cerevisiae is preferentially activated by autonomously replicating DNA sequences. *Biochemistry*, 2005. **44**(8): 2916-25.

149. Sakakibara, N., et al., Coupling of DNA binding and helicase activity is mediated by a conserved loop in the MCM protein. *Nucleic Acids Res*, 2008. **36**(4): 1309-20.

150. De Felice, M., et al., A CDC6-like factor from the archaea Sulfolobus solfataricus promotes binding of the mini-chromosome maintenance complex to DNA. *J Biol Chem*, 2004. **279**(41): 43008-12.

151. Rothenberg, E., et al., MCM forked substrate specificity involves dynamic interaction with the 5'-tail. *J Biol Chem*, 2007. **282**(47): 34229-34.

152. Aladjem, M.I., et al., Genetic dissection of a mammalian replicator in the human beta-globin locus. *Science*, 1998. **281**(5379): 1005-9.

153. Boulikas, T., Common structural features of replication origins in all life forms. *J Cell Biochem*, 1996. **60**(3): 297-316.

154. Spradling, A.C., ORC binding, gene amplification, and the nature of metazoan replication origins. *Genes Dev*, 1999. **13**(20): 2619-23.

155. Stanojcic, S., et al., In Xenopus egg extracts DNA replication initiates preferentially at or near asymmetric AT sequences. *Mol Cell Biol*, 2008.

156. Kasiviswanathan, R., J.H. Shin, and Z. Kelman, DNA binding by the Methanothermobacter thermautotrophicus Cdc6 protein is inhibited by the minichromosome maintenance helicase. *J Bacteriol*, 2006. **188**(12): 4577-80.

157. Shin, J.H., et al., Regulation of minichromosome maintenance helicase activity by Cdc6. *J Biol Chem*, 2003. **278**(39): 38059-67.

158. De Felice, M., et al., Biochemical characterization of a CDC6-like protein from the crenarchaeon Sulfolobus solfataricus. *J Biol Chem*, 2003. **278**(47): 46424-31.

159. De Felice, M., et al., Modular organization of a Cdc6-like protein from the crenarchaeon Sulfolobus solfataricus. *Biochem J*, 2004. **381**(Pt 3): 645-53.

160. De Felice, M., et al., Biochemical characterization of two Cdc6/ORC1-like proteins from the crenarchaeon Sulfolobus solfataricus. *Extremophiles*, 2006. **10**(1): 61-70.

161. Shin, J.H., et al., Archaeal minichromosome maintenance (MCM) helicase can unwind DNA bound by archaeal histones and transcription factors. *J Biol Chem*, 2007. **282**(7): 4908-15.

162. Marsh, V.L., A.T. McGeoch, and S.D. Bell, Influence of chromatin and single strand binding proteins on the activity of an archaeal MCM. *J Mol Biol*, 2006. **357**(5): 1345-50.

163. Shin, J.H., et al., Substrate requirements for duplex DNA translocation by the eukaryal and archaeal minichromosome maintenance helicases. *J Biol Chem*, 2003. **278**(49): 49053-62.

164. Ross, P.D., et al., A free energy cascade with locks drives assembly and maturation of bacteriophage HK97 capsid. *J Mol Biol*, 2006. **364**(3): 512-25.

165. Harris, J.R., Negative staining of thinly spread biological samples. *Methods Mol Biol*, 2007. **369**: 107-42.

166. Harris, J.R. and D. Scheffler, Routine preparation of air-dried negatively stained and unstained specimens on holey carbon support films: a review of applications. *Micron*, 2002. **33**(5): 461-80.

167. Baschong, W., C. Baschong-Prescianotto, and E. Kellenberger, Reversible fixation for the study of morphology and macromolecular composition of fragile biological structures. *Eur J Cell Biol*, 1983. **32**(1): 1-6.

168. Baschong, W. and N.G. Wrigley, Small colloidal gold conjugated to Fab fragments or to immunoglobulin G as high-resolution labels for electron microscopy: a technical overview. *J Electron Microsc Tech*, 1990. **14**(4): 313-23.

169. Baschong, W. and J. Roth, Lyophilization of protein-gold complexes. *Histochem J*, 1985. **17**(10): 1147-53.

170. Baschong, W., J.M. Lucocq, and J. Roth, "Thiocyanate gold": small (2-3 nm) colloidal gold for affinity cytochemical labeling in electron microscopy. *Histochemistry*, 1985. **83**(5): 409-11.

171. Hainfeld, J.F., A small gold-conjugated antibody label: improved resolution for electron microscopy. *Science*, 1987. **236**(4800): 450-3.

172. Wrigley, N.G., E.B. Brown, and J.J. Skehel, Electron microscopic evidence for the axial rotation and inter-domain flexibility of the Fab regions of immunoglobulin G. *J Mol Biol*, 1983. **169**(3): 771-4.

173. Wong, I. and T.M. Lohman, A double-filter method for nitrocellulose-filter binding: application to protein-nucleic acid interactions. *Proc Natl Acad Sci U S A*, 1993. **90**(12): 5428-32.

174. Riggs, A.D., S. Bourgeois, and M. Cohn, The lac repressor-operator interaction. 3. Kinetic studies. *J Mol Biol*, 1970. **53**(3): 401-17.

175. Winter, R.B., O.G. Berg, and P.H. von Hippel, Diffusion-driven mechanisms of protein translocation on nucleic acids. 3. The Escherichia coli lac repressor--operator interaction: kinetic measurements and conclusions. *Biochemistry*, 1981. **20**(24): 6961-77.

176. Wright, C.M., et al., Pyrimidinone-peptoid hybrid molecules with distinct effects on molecular chaperone function and cell proliferation. *Bioorg Med Chem*, 2008. **16**(6): 3291-301.

177. Sarkar, G. and S.S. Sommer, The "megaprimer" method of site-directed mutagenesis. *Biotechniques*, 1990. **8**(4): 404-7.

178. Thomas, B.J. and R. Rothstein, Elevated recombination rates in transcriptionally active DNA. *Cell*, 1989. **56**(4): 619-30.

179. Messer, W., The bacterial replication initiator DnaA. DnaA and oriC, the bacterial mode to initiate DNA replication. *FEMS Microbiol Rev*, 2002. **26**(4): 355-74.

180. Myllykallio, H. and P. Forterre, Mapping of a chromosome replication origin in an archaeon: response. *Trends Microbiol*, 2000. **8**(12): 537-9.

181. McMacken, R., Silver, L., and Georgopoulos, C., *Escherichia coli and Salmonella typhimirium*. DNA Replication, ed. F. Neidhardt. 1987: American Society for Microbiology.

182. Gomez, E.B., M.G. Catlett, and S.L. Forsburg, Different phenotypes in vivo are associated with ATPase motif mutations in Schizosaccharomyces pombe minichromosome maintenance proteins. *Genetics*, 2002. **160**(4): 1305-18.

183. Aparicio, T., A. Ibarra, and J. Mendez, Cdc45-MCM-GINS, a new power player for DNA replication. *Cell Div*, 2006. **1**: 18.

184. You, Z. and H. Masai, DNA binding and helicase actions of mouse MCM4/6/7 helicase. *Nucleic Acids Res*, 2005. **33**(9): 3033-47.

185. Claycomb, J.M., et al., Visualization of replication initiation and elongation in Drosophila. *J Cell Biol*, 2002. **159**(2): 225-36.

186. Traut, T.W., Physiological concentrations of purines and pyrimidines. *Mol Cell Biochem*, 1994. **140**(1): 1-22.

187. Coue, M., et al., Evidence for different MCM subcomplexes with differential binding to chromatin in Xenopus. *Exp Cell Res*, 1998. **245**(2): 282-9.

188. Edwards, M.C., et al., MCM2-7 complexes bind chromatin in a distributed pattern surrounding the origin recognition complex in Xenopus egg extracts. *J Biol Chem*, 2002. **277**(36): 33049-57.

189. Saenger, W., *Principles of Nucleic Acid Structure*. 1984, New York: Springer-Verlag.

190. Picha, K.M., P. Ahnert, and S.S. Patel, DNA binding in the central channel of bacteriophage T7 helicase-primase is a multistep process. Nucleotide hydrolysis is not required. *Biochemistry*, 2000. **39**(21): 6401-9.

191. Okuno, Y., et al., Clustered adenine/thymine stretches are essential for function of a fission yeast replication origin. *Mol Cell Biol*, 1999. **19**(10): 6699-709.

192. Dai, J., R.Y. Chuang, and T.J. Kelly, DNA replication origins in the Schizosaccharomyces pombe genome. *Proc Natl Acad Sci U S A*, 2005. **102**(2): 337-42.

193. Cha, R.S. and N. Kleckner, ATR homolog Mec1 promotes fork progression, thus averting breaks in replication slow zones. *Science*, 2002. **297**(5581): 602-6.

194. Arlt, M.F., A.M. Casper, and T.W. Glover, Common fragile sites. *Cytogenet Genome Res*, 2003. **100**(1-4): 92-100.

195. Laskey, R.A. and M.A. Madine, A rotary pumping model for helicase function of MCM proteins at a distance from replication forks. *EMBO Rep*, 2003. **4**(1): 26-30.

196. Garrett, N.E. and H.S. Penefsky, Interaction of adenine nucleotides with multiple binding sites on beef heart mitochondrial adenosine triphosphatase. *J Biol Chem*, 1975. **250**(17): 6640-7.

197. Hackney, D.D., Kinesin ATPase: rate-limiting ADP release. *Proc Natl Acad Sci U S A*, 1988. **85**(17): 6314-8.

198. Ishimi, Y., et al., Binding of human minichromosome maintenance proteins with histone H3. *J Biol Chem*, 1996. **271**(39): 24115-22.

199. Hardy, C.F., et al., mcm5/cdc46-bob1 bypasses the requirement for the S phase activator Cdc7p. *Proc Natl Acad Sci U S A*, 1997. **94**(7): 3151-5.

200. Lei, M., et al., Mcm2 is a target of regulation by Cdc7-Dbf4 during the initiation of DNA synthesis. *Genes Dev*, 1997. **11**(24): 3365-74.

201. Masai, H. and K. Arai, Dbf4 motifs: conserved motifs in activation subunits for Cdc7 kinases essential for S-phase. *Biochem Biophys Res Commun*, 2000. **275**(1): 228-32.

202. Bochman, M.L., S.P. Bell, and A. Schwacha, Subunit organization of Mcm2-7 and the unequal role of active sites in ATP hydrolysis and viability. *Mol Cell Biol*, 2008.

203. Hanson, P.I. and S.W. Whiteheart, AAA+ proteins: have engine, will work. *Nat Rev Mol Cell Biol*, 2005. **6**(7): 519-29.

204. Crevel, G., et al., Nearest neighbour analysis of MCM protein complexes in Drosophila melanogaster. *Nucleic Acids Res*, 2001. **29**(23): 4834-42.

205. Tsao, C.C., C. Geisen, and R.T. Abraham, Interaction between human MCM7 and Rad17 proteins is required for replication checkpoint signaling. *Embo J*, 2004. **23**(23): 4660-9.

206. Cortez, D., G. Glick, and S.J. Elledge, Minichromosome maintenance proteins are direct targets of the ATM and ATR checkpoint kinases. *Proc Natl Acad Sci U S A*, 2004. **101**(27): 10078-83.

207. Sterner, J.M., et al., Negative regulation of DNA replication by the retinoblastoma protein is mediated by its association with MCM7. *Mol Cell Biol*, 1998. **18**(5): 2748-57.

208. Boyer, P.D., The binding change mechanism for ATP synthase--some probabilities and possibilities. *Biochim Biophys Acta*, 1993. **1140**(3): 215-50.

209. Guenther, B., et al., Crystal structure of the delta' subunit of the clamp-loader complex of E. coli DNA polymerase III. *Cell*, 1997. **91**(3): 335-45.

210. Jeruzalmi, D., M. O'Donnell, and J. Kuriyan, Crystal structure of the processivity clamp loader gamma (gamma) complex of E. coli DNA polymerase III. *Cell*, 2001. **106**(4): 429-41.

211. Bochman, M.L. and A. Schwacha, The Mcm2-7 complex has in vitro helicase activity. *Mol Cell*, 2008. **31**(2): 287-93.

212. Reynisdottir, I., et al., Phosphorylation and active ATP hydrolysis are not required for SV40 T antigen hexamer formation. *J Biol Chem*, 1993. **268**(33): 24647-54.

213. Hofmeister, F., On the understanding of the effects of salts. Second report. On regularities in the precipitating effect of salts and their relationship to their physiological behavior. *Naunyn-Schmiedebergs Archiv fuer Experimentelle Pathologie und Pharmakologie*, 1888. **24**: 247-260.

214. Record, M.T., Jr., C.F. Anderson, and T.M. Lohman, Thermodynamic analysis of ion effects on the binding and conformational equilibria of proteins and nucleic acids: the roles of ion association or release, screening, and ion effects on water activity. *Q Rev Biophys*, 1978. **11**(2): 103-78.

215. Ellison, V. and B. Stillman, Opening of the clamp: an intimate view of an ATP-driven biological machine. *Cell*, 2001. **106**(6): 655-60.

216. Leirmo, S., et al., Replacement of potassium chloride by potassium glutamate dramatically enhances protein-DNA interactions in vitro. *Biochemistry*, 1987. **26**(8): 2095-101.

217. Coury, L.A., et al., The yeast Saccharomyces cerevisiae does not sequester chloride but can express a functional mammalian chloride channel. *FEMS Microbiol Lett*, 1999. **179**(2): 327-32.

218. Geraghty, D.S., et al., Premature structural changes at replication origins in a yeast minichromosome maintenance (MCM) mutant. *J Biol Chem*, 2000. **275**(24): 18011-21.

219. You, Z., et al., Roles of Mcm7 and Mcm4 subunits in the DNA helicase activity of the mouse Mcm4/6/7 complex. *J Biol Chem*, 2002. **277**(45): 42471-9.

220. Lue, N.F. and R.D. Kornberg, Accurate initiation at RNA polymerase II promoters in extracts from Saccharomyces cerevisiae. *Proc Natl Acad Sci U S A*, 1987. **84**(24): 8839-43.

221. Kubota, Y., et al., A novel ring-like complex of Xenopus proteins essential for the initiation of DNA replication. *Genes Dev*, 2003. **17**(9): 1141-52.

222. Chang, Y.P., et al., Crystal structure of the GINS complex and functional insights into its role in DNA replication. *Proc Natl Acad Sci U S A*, 2007. **104**(31): 12685-90.

223. Siderovski, D.P. and F.S. Willard, The GAPs, GEFs, and GDIs of heterotrimeric G-protein alpha subunits. *Int J Biol Sci*, 2005. **1**(2): 51-66.

224. Lin, D.I., P. Aggarwal, and J.A. Diehl, Phosphorylation of MCM3 on Ser-112 regulates its incorporation into the MCM2-7 complex. *Proc Natl Acad Sci U S A*, 2008. **105**(23): 8079-84.

225. Papamichos-Chronakis, M. and C.L. Peterson, The Ino80 chromatin-remodeling enzyme regulates replisome function and stability. *Nat Struct Mol Biol*, 2008. **15**(4): 338-45.

226. Aguilera, A. and B. Gomez-Gonzalez, Genome instability: a mechanistic view of its causes and consequences. *Nat Rev Genet*, 2008. **9**(3): 204-17.

227. Wu, L. and I.D. Hickson, DNA helicases required for homologous recombination and repair of damaged replication forks. *Annu Rev Genet*, 2006. **40**: 279-306.

228. Dutta, A. and S.P. Bell, Initiation of DNA replication in eukaryotic cells. *Annu Rev Cell Dev Biol*, 1997. **13**: 293-332.

229. Kelly, T.J. and G.W. Brown, Regulation of chromosome replication. *Annu Rev Biochem*, 2000. **69**: 829-80.

230. Osborn, A.J., S.J. Elledge, and L. Zou, Checking on the fork: the DNA-replication stress-response pathway. *Trends Cell Biol*, 2002. **12**(11): 509-16.

231. Hartwell, L.H. and T.A. Weinert, Checkpoints: controls that ensure the order of cell cycle events. *Science*, 1989. **246**(4930): 629-34.

232. Lopes, M., et al., The DNA replication checkpoint response stabilizes stalled replication forks. *Nature*, 2001. **412**(6846): 557-61.

233. Paulovich, A.G. and L.H. Hartwell, A checkpoint regulates the rate of progression through S phase in S. cerevisiae in response to DNA damage. *Cell*, 1995. **82**(5): 841-7.

234. Santocanale, C. and J.F. Diffley, A Mec1- and Rad53-dependent checkpoint controls late-firing origins of DNA replication. *Nature*, 1998. **395**(6702): 615-8.

235. Weinert, T.A. and L.H. Hartwell, The RAD9 gene controls the cell cycle response to DNA damage in Saccharomyces cerevisiae. *Science*, 1988. **241**(4863): 317-22.

236. Szyjka, S.J., C.J. Viggiani, and O.M. Aparicio, Mrc1 is required for normal progression of replication forks throughout chromatin in S. cerevisiae. *Mol Cell*, 2005. **19**(5): 691-7.

237. Lieberman, H.B., Rad9, an evolutionarily conserved gene with multiple functions for preserving genomic integrity. *J Cell Biochem*, 2006. **97**(4): 690-7.

238. Forsburg, S.L., The MCM helicase: linking checkpoints to the replication fork. *Biochem Soc Trans*, 2008. **36**(Pt 1): 114-9.

239. Morrow, D.M., et al., TEL1, an S. cerevisiae homolog of the human gene mutated in ataxia telangiectasia, is functionally related to the yeast checkpoint gene MEC1. *Cell*, 1995. **82**(5): 831-40.

240. Ritchie, K.B. and T.D. Petes, The Mre11p/Rad50p/Xrs2p complex and the Tel1p function in a single pathway for telomere maintenance in yeast. *Genetics*, 2000. **155**(1): 475-9.

241. Craven, R.J., et al., Regulation of genome stability by TEL1 and MEC1, yeast homologs of the mammalian ATM and ATR genes. *Genetics*, 2002. **161**(2): 493-507.

242. Nakada, D., et al., The ATM-related Tel1 protein of Saccharomyces cerevisiae controls a checkpoint response following phleomycin treatment. *Nucleic Acids Res*, 2003. **31**(6): 1715-24.

243. Lee, M.W., et al., Global protein expression profiling of budding yeast in response to DNA damage. *Yeast*, 2007. **24**(3): 145-54.

244. Arnold, I., et al., Yeast mitochondrial F1F0-ATP synthase exists as a dimer: identification of three dimer-specific subunits. *Embo J*, 1998. **17**(24): 7170-8.

245. Fang, H., et al., The homologue of mammalian SPC12 is important for efficient signal peptidase activity in Saccharomyces cerevisiae. *J Biol Chem*, 1996. **271**(28): 16460-5.

246. Labib, K. and A. Gambus, A key role for the GINS complex at DNA replication forks. *Trends Cell Biol*, 2007. **17**(6): 271-8.

247. Takayama, Y., et al., GINS, a novel multiprotein complex required for chromosomal DNA replication in budding yeast. *Genes Dev*, 2003. **17**(9): 1153-65.

248. Marinsek, N., et al., GINS, a central nexus in the archaeal DNA replication fork. *EMBO Rep*, 2006. **7**(5): 539-45.

249. Kanemaki, M., et al., Functional proteomic identification of DNA replication proteins by induced proteolysis in vivo. *Nature*, 2003. **423**(6941): 720-4.

250. De Falco, M., et al., The human GINS complex binds to and specifically stimulates human DNA polymerase alpha-primase. *EMBO Rep*, 2007. **8**(1): 99-103.

251. Boskovic, J., et al., Molecular architecture of the human GINS complex. *EMBO Rep*, 2007. **8**(7): 678-84.

252. Kamada, K., et al., Structure of the human GINS complex and its assembly and functional interface in replication initiation. *Nat Struct Mol Biol*, 2007. **14**(5): 388-96.

253. Choi, J.M., et al., Crystal structure of the human GINS complex. *Genes Dev*, 2007. **21**(11): 1316-21.

254. Tan, S., A modular polycistronic expression system for overexpressing protein complexes in Escherichia coli. *Protein Expr Purif*, 2001. **21**(1): 224-34.

255. Hingorani, M.M. and M. O'Donnell, Toroidal proteins: running rings around DNA. *Curr Biol*, 1998. **8**(3): R83-6.

256. Hingorani, M.M. and M. O'Donnell, A tale of toroids in DNA metabolism. *Nat Rev Mol Cell Biol*, 2000. **1**(1): 22-30.

257. Moldovan, G.L., B. Pfander, and S. Jentsch, PCNA, the maestro of the replication fork. *Cell*, 2007. **129**(4): 665-79.